Fault zone architecture, deformation conditions, and kinematics of the Camp Lake and Offset faults of the Lac des Iles Mine, Northwestern Ontario, Canada

Jordan Peterzon

A thesis presented to Lakehead University in partial fulfillment of the requirements for the degree of Master of Science (Geology)

Lakehead University Department of Geology

Thunder Bay, Ontario

Abstract

Faults and their associated damage zones are important geologic structures that serve as permeable pathways through the upper crust. The development of fault cores and damage zones is typically controlled by the strength and composition of the protolith, conditions of deformation, and fluid chemistry. The effect of host lithology on fault core development and damage zone structure is currently poorly constrained. This study uses the Lac des Iles palladium mine in northwestern Ontario, Canada as a natural laboratory to study how faults behave in different lithologies. The Lac des Iles mine is hosted in the 2.689 Ga ± 1.0 Ma Lac des Iles mafic-ultramafic intrusion with current reserves of ~5 Moz of 3E (Pd+Pt+Au) at an average grade of 2.6 g/t. The intrusion hosts numerous mineralized zones, most notably the Roby, Offset, and Camp Lake zones, divided by faults. The Camp Lake and Offset faults are two major structures that offset blocks of the ore body within the Lac des Iles mine, with displacements of ~500 and ~275 m, respectively. The faults crosscut gabbronorite and tonalite, often with these rock units in fault contact with each other.

We studied the variation in fracture density surrounding the Camp Lake and Offset faults to quantify how damage zone structure changes with respect to the host lithology. Fracture density decay rates within damage zones (with distance from the fault core) show that fractures in tonalite decay at a faster rate than gabbronorites, irrespective of whether they are in the hanging wall or footwall. The fault cores in gabbronorites are characterized by chlorite-rich gouges whereas tonalite fault cores are composed of silica-rich cataclasites. It is hypothesized that the development of a frictionally weak, chlorite-rich fault core impeded the development of a more fracture-dense damage zone in the gabbronorite. Results from whole-rock geochemistry show variations in major elements that correlate with the largest zones of visible alteration and

deformation within the damage zone, and no significant rare earth element variation that can be attributed directly to the faulting. Electron microprobe analysis of chlorite was conducted on fault core and host rock samples to constrain the temperatures of deformation. Three notable clusters in the temperature data were observed, interpreted to represent periods of chlorite formation that were pre-, syn- and post-faulting (290°C, 236°C, and 110 – 175°C, respectively).

A combination of structural and geochemical data shows that the Camp Lake and Offset faults have undergone multiple deformation events, with pulses of hydrothermal fluids altering the mineralogy and geochemical signature of the surrounding rocks in the Lac des Iles mine. Palladium mineralization is depleted within the fault core and damage zones. It is hypothesized that hydrothermal fluids associated with faulting are the cause of stripped palladium mineralization.

This research highlights the interplay of the geological processes associated with faulting and fluid migration and how they have affected the distribution of palladium within the Lac des Iles mine. Understanding the relationship between faulting and economic mineralization can improve exploration strategies and guide mining efforts for the future.

Acknowledgments

I would like to express my deepest gratitude to Dr. Noah Phillips and Dr. Pete Hollings for the endless support and invaluable feedback throughout the entirety of this thesis. Without either of your guidance this thesis would not have been possible, and I am profoundly thankful for your contributions. Your patience and wisdom over these last few years have been a constant source of encouragement, and for that, I am truly grateful.

I would also like to thank Impala Canada for funding this study, and for allowing me to conduct research and providing employment during the summers of 2022 and 2023. Thank you also to the Impala Canada Geology and Exploration Team who I spent much time with over the last few years. Thank you also to the NSERC Alliance Grant for making this thesis possible.

Thank you to the organizers and donors of the Bernie Schieders Memorial Award, the Dr. Melville Bartley Memorial CESME Award, the GSA Executive Award, the Mining Industry Resources Council Award, the Faculty of Science & Environmental Studies Award, the Lakehead Graduate Bursary Program, and the ILSG Eisenbrey Student Award. Your generosity made this thesis possible.

Thank you to Dr. Tobias Stephan, Dr. James Tolley and Dr. Moses Angombe for your support with all things thesis related and for the great chats and vent sessions in the lab.

Thank you to the Lakehead Geology staff who have assisted with this thesis in one way or another. All the work you have done to support this project has not gone unnoticed.

An additional thank you to the reviewers of this thesis, Dr. Moses Angombe and Dr. James Kirkpatrick. Your edits and critiques are much appreciated and have made this a better piece of work.

Thank you to my friends and family who have stood by me during this thesis. It has not been easy, but I am eternally grateful for your patience, kindness, and laughs that have kept me going. A special thanks to Cal, Cassandra, Justin, Dan, Vlad, and Kevin.

A last thank you to my partner and best friend, Paige. Thank you for listening to me vent, complain, and yap about everything under the sun. Thank for believing in me when I didn't, and for your unwavering support and motivation during the hard times. This thesis certainly would not have been possible without you by my side.

Table of Contents

List of Figures

List of Tables

Chapter 1: Introduction

Studying how rocks deform is critical to understanding processes related to earthquakes and mineral systems (Cheng et al., 2022). Faults influence the mechanical and fluid flow properties of the crust and affect the behaviour of earthquakes within the crust (Faulkner et al., 2010). The physical and chemical attributes of exhumed fault rocks hold valuable information for understanding both the long-term and short-term behaviour of active faults and earthquakes (Yang et al., 2020).

A fault is a planar discontinuity with an observable displacement across a lithological body (Figure 1.1; Caine et al., 1996; Faulkner et al., 2010). Typically, a fault has three zones or components: 1) an unaltered protolith, only affected by pre-existing regional structures and metamorphism; 2) a damage zone, where most of the fracturing and faulting has been accommodated with increased permeability, and in turn, is strongly to intensely fluid altered; and 3) a fault core, where most of strain has been accommodated and slip has been localized. (Caine et al., 1996; Caine & Forster, 1999).

Fault cores can be differentiated from damage zones. Fault cores and damage zones have different permeabilities; while damage zones are areas of high permeability from increased fracturing, fault cores typically act as low to impermeable zones (Knipe, 1989; Billi et al., 2003). The fault core consists of cataclastic rocks and very fine-grained gouges, where the pre-existing structures are obliterated, whereas damage zones consist of rock volumes that are fractured during the faulting processes (Billi et al., 2003). In damage zones, the pre-faulting structures and fabrics are often preserved.

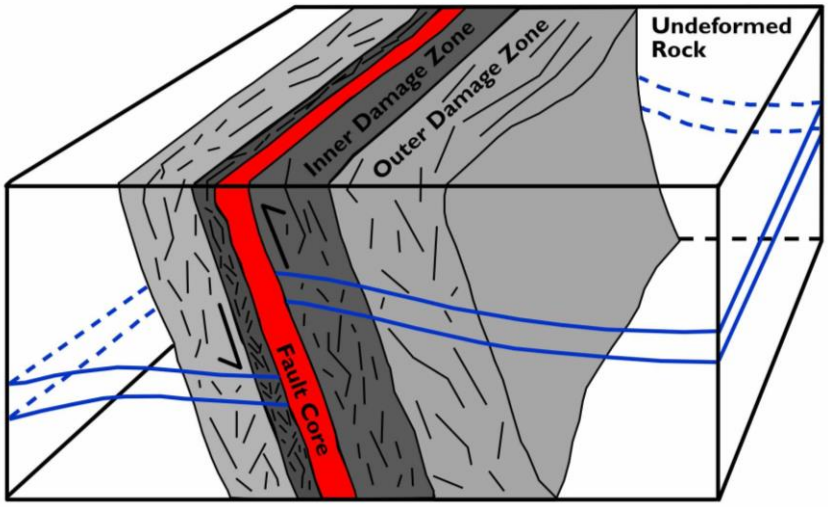

Figure 1.1 Conceptual model of a fault zone, adapted from Ma et al., 2023.

Structural controls of ore deposits is a popular theme in both literature and industry, as structures, such as faults, often act as pathways and barriers for mineralized fluids (Sheldon & Micklethwaite, 2007; Faulkner et al., 2010). Most of the literature surrounding fault structure and mineralization focuses on their implications for mineralization, as they are important when targeting exploration programs (Sheldon & Micklethwaite, 2007; Cheng et al., 2022). However, we still lack a detailed understanding on late faults and their effect on pre-existing ore bodies. This thesis examines late faults cutting a mineralized area which appear to have locally diminished or entirely depleted the metal content.

The Lac des Iles Mine is primarily producing Pt-Pd and located approximately 85 km north of Thunder Bay Ontario, Canada. It's hosted within mafic to ultramafic intrusive bodies and tonalitic country rock near the contact between the granite greenstone terrane of the western Wabigoon subprovince and the northwestern margin of the Quetico subprovince (Barnes & Gomwe, 2011). The Lac des Iles mine has been a producing Pt-Pd mine since 1993, and as of 2020, has produced 4 million ounces (Moz) Pd from 70 million tons (Mt) of ore, mined at an average grade of ~2.3 grams per ton (g/t) (Implats, 2022). As of 2022, mineral reserves include

40.4 Mt of Pd at 1.90 g/t, 0.18 g/t Pt, 0.14 g/t Au, and 0.12% Ni and Cu (Implats, 2022), and since June 2024, 5.8 Moz of 3E (Pt+Pd+Au) has been estimated at a grade of 2.60 g/t (Implats, 2024). The two principal ore zones at the Lac des Iles mine are the Roby Zone and the Offset Zone, separated by the Offset fault (Implats, 2022). The Camp Lake Zone, Impala's newest exploration target is separated from the Offset Zone by the Camp Lake fault.

For all types of faulting, fault slip is driven by the release of elastic strain that has been built up in the surrounding rocks via frictional dissipation; however, the mode of frictional dissipation varies depending on the rheology of the fault zone (Tesei et al., 2012). It is important to understand the mechanical and physical processes involved in brittle and ductile deformation of rocks and how they are impacted by change in rock types. While much work has focused on understanding the mechanics, hydraulic and seismic properties of fault zones (Olgaard & Brace, 1983; Chester et al., 1993; Isaacs, 2005), the effect of protolith variation (from mafic to felsic) has not seen the same level of investigation (Evans, 1990; Savage & Brodsky, 2011; Savage et al., 2021). Understanding the processes which develop fault zones and how they vary with lithology is important for constraining the hydrogeochemical processes that influence mineralization. The Lac des Iles mine is an excellent natural laboratory to study the effect of lithology on fault structure for three reasons:

1) The ore body, offset by late faults, is hosted within mafic-ultramafic rocks and is in contact with the felsic tonalite country rocks.
2) There is an abundance of drill core available which intercept the faults and mineralized zones.

3) A depletion in Pd mineralization occurs surrounding the damage zone of each respective fault, making it possible to investigate how late faults can impact pre-existing mineralization.

This thesis examined two late faults (Offset and Camp Lake) that crosscut the ore body at the Lac des Iles mine.

The objectives of this thesis were to:

1) Constrain the kinematics, micromechanics, and deformation conditions of the Camp Lake fault, and Offset fault.
2) Analyze the variation in the alteration geochemistry of protoliths with proximity to faulting.
3) Examine the offset and relative motions of the ore bodies.
4) Compare the fault zone architecture of the faults in mafic protoliths to those of felsic protoliths.

Together, this study provides evidence for lithological control on the variation in fault zone structure, the alteration geochemistry, the kinematics and conditions of deformation of the Camp Lake and Offset faults at the Lac des Iles mine. This study highlights the critical role of lithology in controlling fault zone architecture, deformation conditions, and the hydrothermal alteration at the Lac des Iles mine. These findings can aid our understanding of fault-impacted ore systems and aid in exploration strategies in similar geological settings.

Chapter 2: Regional and Local Geology

2.1 Geology of the Superior Province

The Superior Province makes up approximately 70% of the Canadian Shield in Ontario and is the largest craton in the world covering ~1,572,000 km^2 of Canada and the northern United States (Figure 2.1; Thurston, 1991; Percival & Easton, 2007). It forms the core of the North American continent and is surrounded by provinces of Paleoproterozoic age on the west, north, and east, and Mesoproterozoic age (Grenville Province) on the southeast. It has been tectonically stable since the late Archean (~2.5 Ga) with the exception of Proterozoic rifting and faulting (Card & Ciesielski, 1986; Card, 1990; Percival & Easton, 2007). The western, northern, and southeastern boundaries of the Superior Province have been described as fault contacts, marked by thrusting, whereas the southeastern boundary is unconformably in contact with the Mesoproterozoic Grenville Province (Card, 1990).

The Superior Province is a collage of Meso- to Neoarchean continental, arc and oceanic fragments (Card, 1990; Tomlinson et al., 2003), that show roughly linear east-west trending subprovinces which have been traditionally divided by lithology (Card & Ciesielski, 1986). Subprovince boundaries in the Superior Province are observed as transition zones of metamorphism, structure, or lithological transition, that are often masked by late, Neoarchean to early Paleoproterozoic faulting or igneous activity (Card & Ciesielski, 1986). Lithologies of the Superior Province are dominantly (~75%) gneissic and plutonic rocks, with lesser (~25%) low to medium grade supracrustal and metasedimentary rocks (Card, 1990). Gneissic rocks show a concentration in the north and southwest Superior Province, whereas the central Superior dominantly consists of low-grade granite-greenstones and metasedimentary rocks (Card, 1990). Metasedimentary rocks as old as 2.48 Ga uncomformably overlie basement crustal rock, allowing for the interpretation that most erosion had occurred before that time (Percival, 2007).

The Superior Province has been subdivided into four litho-tectonic domains by Card and Ciesielski (1986) primarily based on lithology, structure, geophysics and geochronology: volcano-plutonic (granite-greenstone) subprovinces, metasedimentary subprovinces, plutonic subprovinces, and high-grade gneisses. The subprovince boundaries may be placed along faults, where both low- and high-grade metamorphic rocks have been observed, with contrasting structural characteristics making precise subprovince geographical and geological divisions challenging.

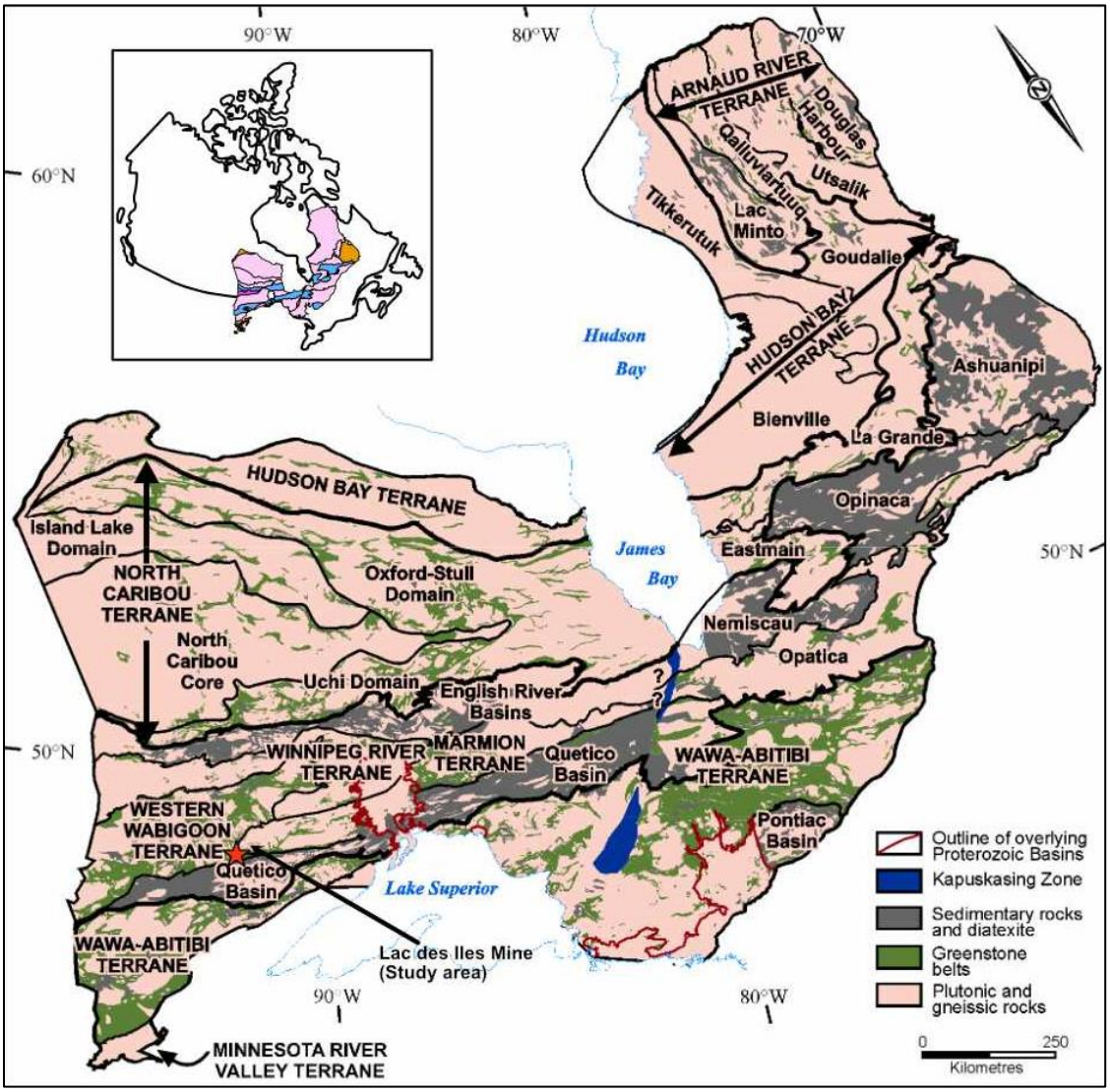

Figure 2.1 Superior Province in Canada with terranes. Modified from Stott et al. (2010).

An alternative classification scheme for the Superior Province has been proposed in recent years, with an emphasis on new age dates and results from lithological mapping and geophysical results and interpretations providing more precise subdivisions (Stott et al., 2010). The new subdivisions follow a hierarchy in terms of their nomenclature, including: "superterranes", "terranes", "domains" and "tectonic assemblages" (Percival, 2007; Stott et al., 2010). These subdivisons can be defined as such:

Superterrane – An amalgamation of two or more terranes before Neoarchean assembly of the Superior Province.

Terrane – A tectonically bounded region with internal characteristics distinct from those in adjacent regions.

Domain – A younger, lithologically distinct part of a terrane, either with juvenile crust or sharing a common basement.

Tectonic or Tectonostratigraphic Assemblage – Distinct in lithology, time tectonic setting, and composed of one or more stratigraphic groups or formations.

This thesis will predominantly use the new classification scheme, however when appropriate, subprovinces will be referred to as such. A map of subprovinces within the southwestern Superior Province can be seen in Figure 2.2.

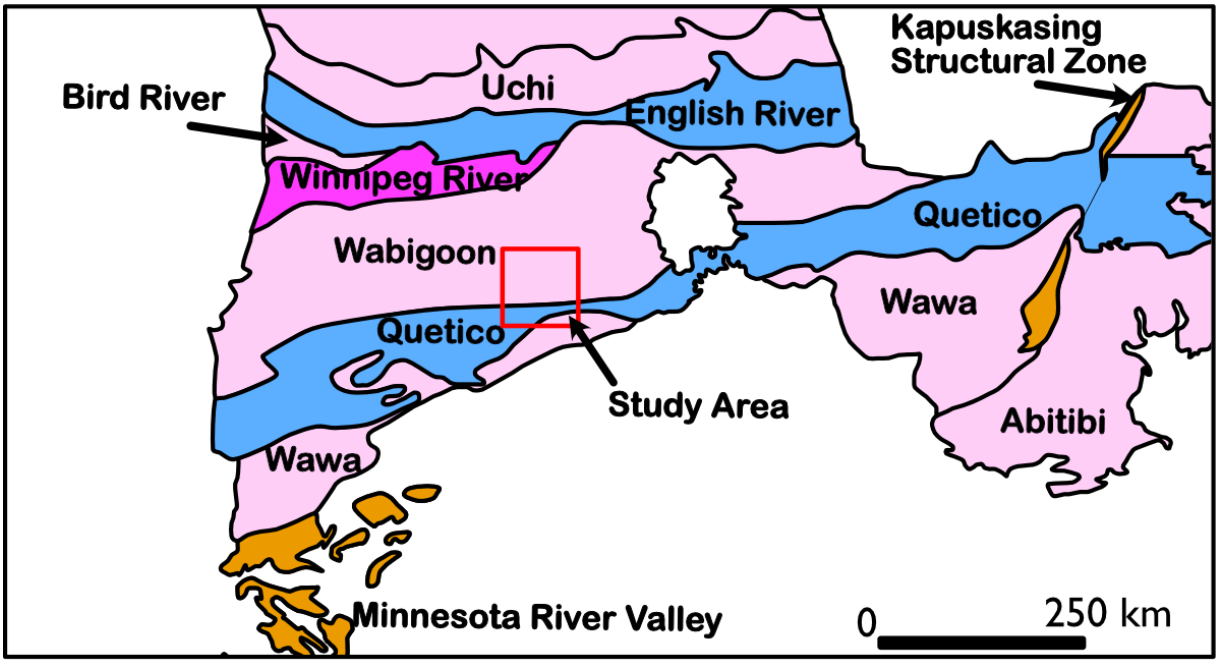

Figure 2.2 Map of the Superior Province and subprovinces with study area highlighted. Adapted from Card (1990).

The Superior Province has a complex history of assembly and tectonic evolution until 2.60 Ga, including craton assembly during the Kenoran Orogeny from 2.72 – 2.68 Ga (Percival et al., 2006). Five distinct accretional events occurred during the Kenoran Orogeny, each including separate events of magmatism, sedimentation, deformation, metamorphism and plutonism (Thurston, 1991; Percival et al., 2006). The cratonic evolution of the Superior Province has been recorded back to ~3.9 Ga via detrital zircon ages in granitic and gneisses in the northern Superior Province (Percival et al., 2006), which have been reworked by granitoid magmatism sporadically from 3.2 – 2.71 Ga (Percival & Easton, 2007). The evolution of the northern Superior Province is believed to represent a continental magmatic arc setting, followed by amphibolite-facies metamorphism between 2.68 and 2.1 Ga (Percival & Easton, 2007). The Superior Province is now surrounded by early Proterozoic (2.5 – 1.6 Ga) orogens (Card, 1990). Activity in the Superior Province during the Proterozoic (and after) is limited to rifting, mafic dyke swarms, and large-scale rotation at 1.9 Ga, followed by failed rifting at 1.1 Ga (Percival, 2007).

2.2 Wabigoon and Quetico Subprovinces

The volcano-plutonic Wabigoon subprovince is located in the southwestern Superior Province and is a key area for understanding the development of the western Superior Province (Tomlinson et al., 2003). It is characterized by ~900 km long and 150 km wide east-west trending granite-intruded greenstone belt hosting mafic to felsic volcanic rocks with minor komatiites and metasedimentary rocks ranging from 3.0 – 2.71 Ga, crosscut by ~3.0 – 2.69 Ga mafic sills and stocks (Blackburn et al., 1991). Mafic volcanic rocks range from tholeiitic to calc-alkaline whereas felsic tonalitic rocks are predominantly calc-alkaline (Blackburn et al., 1991). The Wabigoon subprovince is bordered to the northwest by the dominantly granitoid Winnipeg River subprovince, to the northeast by the migmatitic metasedimentary English River subprovince, and to the south by the metasedimentary Quetico subprovince (Blackburn et al., 1991). The Wabigoon subprovince is subdivided into tonalitic basement rocks (~3.0 Ga), tonalite-trondhjemite-granodiorite (TTG) complexes (2.732 – 2.708 Ga), and post-tectonic granitoid stocks 2.709 – 2.685 Ga (Blackburn et al., 1991; Bain et al., 2023). Mafic-ultramafic complexes intrude the granitoid country rocks of the Wabigoon subprovince (~ 2.69 Ga) including the Lac des Iles intrusive suite (Pettigrew & Hattori, 2001; Bain et al., 2023). Tomlinson et al. (2004) subdivided the Wabigoon subprovince into crustal blocks including the Winnipeg River terrane, Marmion terrane and Western Wabigoon terrane (Stone et al., 2003; Tomlinson et al., 2004). The south-central Wabigoon, hereby referred to as the Marmion terrane hosts the Marmion batholith and is overlain by mafic volcanic sequences with ages of 3.0 – 2.9, 2.83, and 2.73-2.72 Ga (Tomlinson et al., 2004). The structural geology of the Wabigoon subprovince has a complex style that distinguishes it from the bordering Quetico and English River subprovinces. The northern and southern margins of the Wabigoon comprise linear belts of

supracrustal rocks, with long meandering shear zones hosting both brittle and ductile deformation structures (Blackburn et al., 1991).

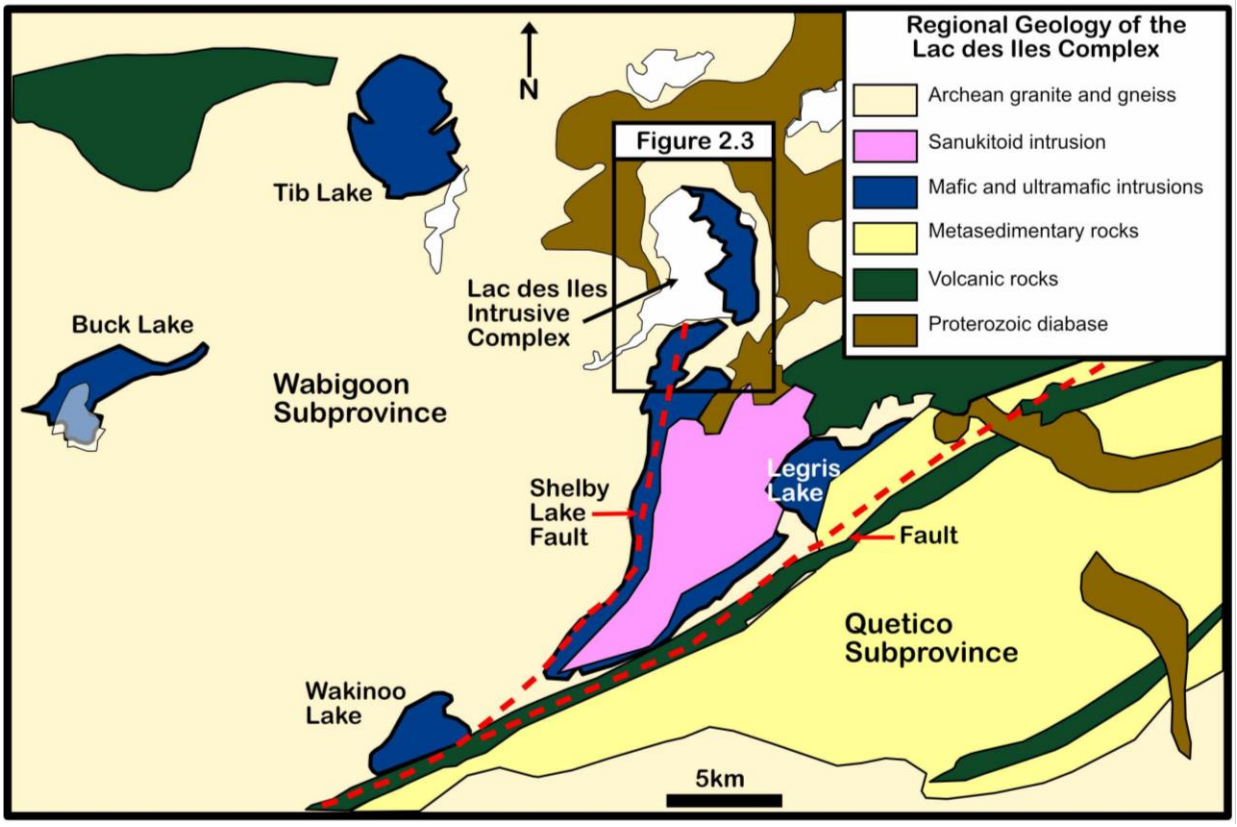

Figure 2.3 Geology of the Wabigoon and Quetico subprovinces with Lac des Iles Intrusive Suite. Modified from Djon et al. (2018).

The 10-100 km wide Quetico subprovince is a belt-like strip of predominantly metasedimentary rocks (primarily bedded greywacke, siltstones, conglomerates and minor iron formation), that extends along the southern boundary of the Wabigoon subprovince (~1200 km) from the Phanerozoic cover in Minnesota in the west, to east of the Kapuskasing Structural Zone (Card, 1990; Williams, 1991; Pettigrew & Hattori, 2001; Stone, 2010; Bain et al., 2023). The Quetico subprovince is also characterized by greenschist-facies metavolcanic rocks of basaltic composition (Bain et al., 2023). The metasedimentary rocks are commonly interbedded or crosscut by the mafic metavolcanic rocks (Figure 2.3; Pettigrew & Hattori, 2001). The Quetico

was likely formed as an accretionary wedge during collision of the Wawa-Abitibi and Wabigoon terranes at ~2.696 Ga (Percival & Williams, 1989). Detrital zircons from the Quetico have yielded ages from 3009 to 2698 Ma, indicating that Quetico sediments are younger than any igneous activity in the Wabigoon or Wawa subprovinces (Card, 1990).

The northern boundary of the Quetico subprovince with the Wabigoon subprovince is observed as a structural feature, referred to as the Quetico fault (Figure 2.3; Card, 1990). The regional structural trend of the Quetico subprovince varies from east-west in the north to northeast-southwest in the south (Kehlenbeck, 1976). The Quetico fault is a regional-scale right-lateral east-west trending fault that transects the Wabigoon-Quetico subprovince boundary (Fumerton, 1982; Thurston, 1991; Williams, 1991), and serves as the boundary between the Wabigoon and Quetico subprovinces in Kashabowie and 45 km west of Atikokan (Williams, 1991). There is evidence of the Quetico fault splaying into the Wabigoon subprovince east of Kashabowie (Sawyer, 1983; Williams, 1991) and from Calm Lake to Rainy Lake (~120 km) the Quetico fault is completely within the Wabigoon subprovince (Fumerton, 1982). The Seine River fault appears to be a splay of the original Quetico fault system and when the Quetico fault is completely in the Wabigoon subprovince, the Seine River fault appears to act as the transitional zone or boundary between the Wabigoon and Quetico (Fumerton, 1982). The presence of cataclasites from Dog Lake eastward to Highway 800 provides some implications for a possible extension of the Quetico fault west of Thunder Bay (Kehlenbeck, 1976). Based on field observations from Kehlenbeck (1976), a transition zone between recognizable Quetico and Wabigoon lithologies is denoted by the presence of metapelites, implying that the boundary between the two subprovinces is more complex than expected.

2.3 Marmion terrane

The Marmion terrane is a relatively geographically small (100 km x 30 km) section of the western Superior Province, formerly included as part of the south-central Wabigoon subprovince (Tomlinson et al., 2004; Percival & Easton, 2007). It predominantly consists of a 3.003 to 2.999 Ga granitoid batholiths (tonalite to tonalitic gneiss) referred to as the Marmion batholith followed by plutonism (tonalite to granites) overlain by 2.703 – 2.695 Ga greenstone sequences from the western Wabigoon terrane (Tomlinson et al., 2004; Percival, 2007; Stone, 2010). Average ^{207}Pb / ^{206}Pb ages from Tomlinson (2003) suggest an age of 3.001 Ga +/- 1.7 Ma for the Marmion batholith, based on zircon U-Pb ages. Recent work has led to the interpretation of the Marmion terrane as a discrete crustal block, supported by Nd ages and a 3.293 Ga inherited zircon likely representing material from the Winnipeg River terrane north of the Marmion (Tomlinson et al., 2004; Stone, 2010). Tomlinson et al. (2004) described the Marmion terrane as variably influenced by 3.0 Ga plutonic and supracrustal sequences of the south-central Wabigoon subprovince area. Neodymium isotopes from the southern boundary between the Marmion and western Wabigoon terrane reflect the transition from oceanic rocks in the western Wabigoon to continental rocks of the Marmion (Tomlinson et al., 2004). The interior of the south-central Wabigoon subprovince is dominated by greenschist to sub-greenschist facies metamorphism and progresses to amphibolite grade at the margins (Tomlinson et al., 2004). Magmatic activity in the Neo-Archean (2.745 – 2.72 Ga) was minimal, if existent at all in the Marmion terrane in contrast to the Wabigoon in the east and west (Percival & Easton, 2007). Tomlinson (2003 & 2004) hypothesized that Marmion terrane was allochthonous with respect to the Winnipeg River, and the accretion of the Marmion terrane onto the Winnipeg River took place between 2.93 – 2.87 Ga (Tomlinson et al., 2003, 2004; Percival & Easton, 2007), followed by collision with the western Wabigoon at 2.710 Ga (Percival & Easton, 2007).

2.4 Lac des Iles Intrusive Suite

The Lac des Iles Intrusive Suite (LDIS) is a series of Neoarchean mafic to ultramafic intrusions hosting significant Pd and Pt mineralization within a ~35 x 40 km sub-circular area of the Marmion Terrane and parallels the boundary between the Wabigoon and Quetico subprovinces (Watkinson & Dunning, 1979; Sutcliffe et al., 1989; Lavigne et al., 2005; Djon et al., 2018). The suite consists of several mafic to ultramafic intrusive bodies emplaced into gneissic tonalites and granodiorites (Stone, 2010; Barnes & Gomwe, 2011). The Lac des Iles Complex (LDIC), Tib Lake, Demars Lake, Wakinoo Lake, Tomle Lake, Buck Lake, Taman Lake, and Dog River intrusions comprise the LDIS, several of which host Pd mineralization (Sutcliffe, 1986; Bain et al., 2023). Mafic rocks ranging from various types of gabbros and gabbronorites (leucogabbro, hornblende gabbro, gabbronorite and norite) form the Lac des Iles Intrusive suite, alongside some ultramafic rocks (Sutcliffe et al., 1989). The rocks of the LDIS intrude tonalitic gneiss of the Wabigoon and Quetico subprovinces, but appear to be coeval with the biotite and hornblende tonalite plutons that intrude the tonalitic gneiss of the Wabigoon subprovince (Sutcliffe, 1989; Sutcliffe et al., 1989; Brügmann et al., 1996).

Considerable geochronological research has been conducted on the LDIS. Samples from the mafic intrusions show a narrow range of ages from 2.699 – 2.671 Ga in the Lac des Iles area (Stone, 2010). The Mine Block Intrusion of the Lac des Iles Complex has a reported age of 2689.0 +/- 1.0 Ma and the Tib Lake Complex has yielded an age of 2685.9 +/- 1.6 Ma (Stone, 2010), consistent with the U-Pb zircon ages from Bain et al. (2023) of 2690.59 +/- 0.77 Ma for the Legris Lake Complex.

There is some debate on the formation of the Lac des Iles suite. It was proposed by Percival and Williams (1989) that the rocks of the LDIC formed during subduction of oceanic lithosphere beneath the Wabigoon subprovince (Boudreau et al., 2014). It is also suggested by

Bain et al. (2023) that the LDIS was emplaced during subduction of the Wawa-Abitibi and formation of the Quetico subprovince following accretion with the Wabigoon at 2.696 – 2.690 Ga (Percival & Williams, 1989; Williams, 1991; Pettigrew & Hattori, 2001; Stone, 2010; Percival et al., 2012). It is currently favoured that the intrusive complexes of the LDIS formed in an Archean arc-like setting (Bain et al., 2023). It is also noteworthy that there is an association between mafic-ultramafic intrusions within the LDIS and faults. For example, Stone et al. (2003) argued that the Shelby Lake fault was a likely conduit for magma emplacement, preceding the intrusions and subsequent mineralization. It is suggested that gabbro bodies could represent early mafic phases of the sanukitoid intrusion that have been compressed against the rim of the batholith by emplacement of later a core phase – or that the gabbro bodies represent one or more Lac des Iles intrusions disrupted by the Shelby Lake batholith (Stone et al., 2003; Stone, 2010).

2.5 Lac des Iles Complex

The Lac des Iles Complex is the largest and economically most important member of the Lac des Iles Suite and is classified as a structurally-controlled magmatic sulfide deposit (Stone, 2010; Peck & Djon, 2020). Mineral exploration in the LDIC has been on-going for over 50 years and been mined for over 25 (Peck & Djon, 2020). As of 2019, the Lac des Iles mine has produced almost 4 million ounces of Pd mined at an average grade of ~2.3 g/t, and as of June 2020, contained 79.9 million tonnes of measured, indicated and inferred resources grading at 2.66 g/t 3E (Pd + Pt +Au) (Peck & Djon, 2020; Implats, 2022). The LDIC is subdivided into two distinct subcomplexes or intrusive bodies, typically referred to as the ultramafic North Lac des Iles Complex and the mafic (gabbroic) south Lac des Iles Complex; the latter hosts the zones of economic Pd-Pt mineralization (Figure 2.4; Stone et al., 2003; Djon et al., 2018).

The complex is situated along the NE-trending Shelby Lake fault, which is interpreted to be a splay of the E-W trending Quetico fault, and is a possible feeder structure for the complex (Stone et al., 2003; Maxwell & Benson, 2020). The immediate country rocks that the Lac des Iles Complex has intruded include the ~3.0 Ga tonalites and the 2732 – 2708 Ma granitoid complexes of the Wabigoon subprovince. These rocks include foliated tonalitic gneisses that lie at the north end of the Shelby Lake fault and range in age from 2775 to 2722 Ma, with coeval plutons of hornblende tonalite and biotite tonalite dated at 2727.8 +/- 1.5 Ma and 2685 +/- 1.6 Ma, respectively (Stone et al., 2003; Barnes & Gomwe, 2011; Bain et al., 2023). The rocks of the LDIC are generally cumulates, and discriminating between different mafic units based on incompatible trace element concentrations has proven to be a challenge (Smith, 2023).

The North LDI (NLDI) complex is composed of cyclically layered ultramafic cumulates that consists of two major intrusive centers, the northern ultramafic center and the southern ultramafic centre covering an area of ~4.5 x 6 km (Barnes & Gomwe, 2011; Djon et al., 2018). The North Lac des Iles contains PGE-bearing sulfide mineralization associated with pyrrhotite, chalcopyrite, and pentlandite; but no significant or economically feasible occurrences have been found (Barnes & Gomwe, 2011). The predominant rock type in the NLDI is clinopyroxenite, which forms 80 m thick layers that have gradational contacts with peridotite cumulates (Barnes & Gomwe, 2011). These units are cut by hornblende gabbro and diorite (Stone, 2010). Djon et al. (2017) proposed that the NLDI Complex postdates the SLDI Complex.

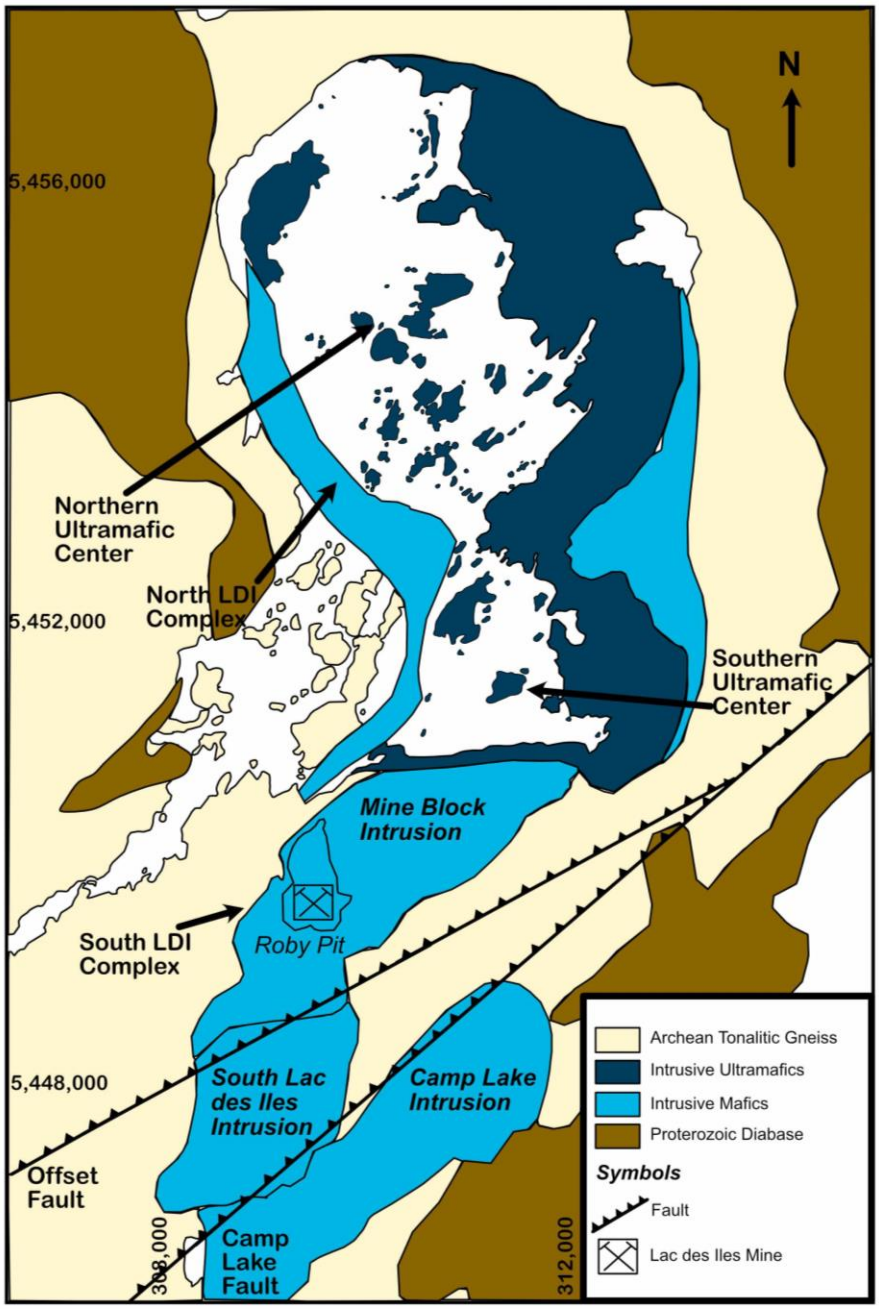

Figure 2.4 Lac des Iles Intrusive Complex with Lac des Iles Mine. Modified from Djon et al. (2018). The Camp Lake and Offset faults are interpreted to be reverse faults.

The SLDI is divided into three discrete bodies, including the Mine Block Intrusion, South LDI, and the Camp Lake Intrusion, all of which are separated by tonalitic country rock (Lavigne & Michaud, 2001; Boudreau et al., 2014; Djon et al., 2018). The SLDI Complex is an arcuate, multi-phase intrusive body, contemporaneous with a regional magmatic event and during

regional collision with the Wabigoon-Marmion terrane in the north and the Abitibi-Wawa in the south (Peck & Djon, 2020). Geochemical data from the SLDI record at least two discrete magmatic episodes, but has been hypothesized that many magmas fluxed through the LDIC changing their geochemistry progressively (Smith, 2023). Four intrusive phases (domains) make up the SLDI complex including gabbronorite, norite, breccia, and diorites (Implats, 2022). It is suggested that the gabbronorite domain formed first, followed by the norite and breccia domains, and lastly the diorite domain (Peck & Djon, 2020). The main LDI deposit is lenticular in shape, expanding upwards and striking to the north with a dip to the south; the ore body is subvertical and is offset along two major NNW trending structures, the Camp Lake and Offset faults (Peck & Djon, 2020). Economic mineral resources in the LDIC are exclusively hosted within the SLDI complex, with the vast majority of Ni-Cu-PGE reserves found in the Roby and Offset zones (~80 Mt and ~55 Mt, respectively) in the western part of the Mine Block Intrusion (Implats, 2022). All of the known Pd mineralization is hosted by orthopyroxene +/- plagioclase cumulate rocks including melanorite, norite and leuconorite (Djon et al., 2018) and commonly have an intrusive breccia structure with a matrix of varitextured leuconorite. A series of pre- to syn- and post magmatic regional structures have been identified in the South LDI complex and are thought to have strongly influenced the emplacement of intrusive mafic rocks and the distribution of PGE sulfide mineralization (Implats, 2022). The majority of the Pd mineralization in the western Mine Block Intrusion occurs within an interpreted N-striking and subvertically oriented feeder structure that hosts both the Roby and Offset zone deposits (Stone et al., 2003; Djon et al., 2018). Grade distribution in the LDIC moves west from the sharp hanging wall contact in the east to the more diffuse footwall contact in the west.

2.5.1 Mine Block Intrusion

The Mine Block Intrusion (MBI) occurs directly south of the Northern Ultramafic Intrusion (Figure 2.4). It is predominantly a gabbroic body roughly elliptical in plan view trending to the north-east (Stone et al., 2003). The MBI hosts economic palladium, platinum, and gold mineralization. The MBI has been described as a gabbroic to gabbronoritic intrusion with variable lithologies, including anorthosite, leuco- to melanogabbro, chlorite-actinolite schist, and oxide-rich gabbronorite, most of the rocks are plagioclase-orthopyroxene cumulates (Barnes & Gomwe, 2011; Duran et al., 2016). The MBI is zoned with a gabbro rim and a largely gabbronorite core and is mineralized with Pd and lesser Pt, Au, Cu and Ni within three main zones characterized by brecciated and pegmatitic gabbro (Stone, 2010). The majority of the Pd mineralization in the western Mine Block occurs within an interpreted N-striking and subvertically oriented feeder structure that hosts both the Roby and Offset zones (Stone et al., 2003; Djon et al., 2018), referred to as the Shelby Lake fault. The Roby and Offset zones both host discrete subzones and satellite mineralized bodies (*i.e.*, Upper and Lower B2, C-Zone, Twilight, etc.; Implats, 2022) and include the Roby Northwest, Sheriff, Sheriff South, Roby SW Wall, Roby South and B zones. The Roby and Offset zones consist of irregularly shaped footwall zones with average grades of 1 – 2 g/t Pd and a semi-tabular 10 – 80m thick hanging-wall zone with average grades of 4 – 6 g/t Pd that occur with several meter-thick subintervals having average grades in excess of 10 g/t Pd (Peck et al., 2015). The domains of the MBI are concentrically zoned with a rim of varitextured gabbro and a complex core zone composed of gabbronorite breccia, massive medium-grained gabbro, heterolithic gabbro breccia, and magnetite gabbronorite (Stone et al., 2003). Mineralization was likely introduced to the MBI by late pulses of fertile primitive magma (Hinchey et al., 2005; Barnes & Gomwe, 2011). These late magmas were introduced energetically and affected by magmatic fluids leading to the complex

breccia textures and alteration seen in the MBI (Hinchey et al., 2005). The northern margin of the MBI is interpreted to be intruded locally by the ultramafic North LDI complex (Rankin, 2013). Both the northern and southern contacts of the MBI appear to dip approximately 60 degrees southeast (Rankin, 2013).

2.5.2 Camp Lake Target

Impala Canada Ltd. has documented a hornblende gabbro south of the Lac des Iles intrusion at the Camp Lake, Wakinoo Lake, Legris and Towel Lakes (Peck & Djon, 2020; Implats, 2022) suggesting that the gabbro bodies of the LDIS are dispersed along the rim of the Shelby Lake batholith (Stone, 2010). The Camp Lake Zone (CLZ) is an ongoing target for Impala Canada, situated approximately 1.5 km beneath surface down-plunge from the Offset Zone (Peck & Djon, 2020; Implats, 2022). Currently it is unknown whether the Camp Lake Zone (CLZ) is an extension of the Offset Zone at greater depth (Figure 2.5), which has been displaced by the Camp Lake fault, however, all presently characterized Offset sub-zones have downward extensions that are likely to be observed at depth alongside the Camp Lake Zone (Smith, 2023). While the relationship between the Offset and Camp Lake Zones is still being studied, the connection between the mineralization of the two zones may indicate that they are related. Smith (2023) showed that the rocks from the Camp Lake Zone are the most lithologically diverse of the LDIC with compositional affinities of two discrete chemical groups – one aligning with the Offset Block, and one the East Mine Block (Smith, 2023). Smith (2023) hypothesized that there is no obvious lithological control on high-grade Pd mineralization, rather it appears to be confined to structures and the cores of cylindrical ore zones. Additionally, there are a series of additional minor faults that crosscut the ore body in the south LDIC, however they remain

unstudied in detail and do not appear to be offsetting major ore bodies unlike the Offset and Camp Lake faults.

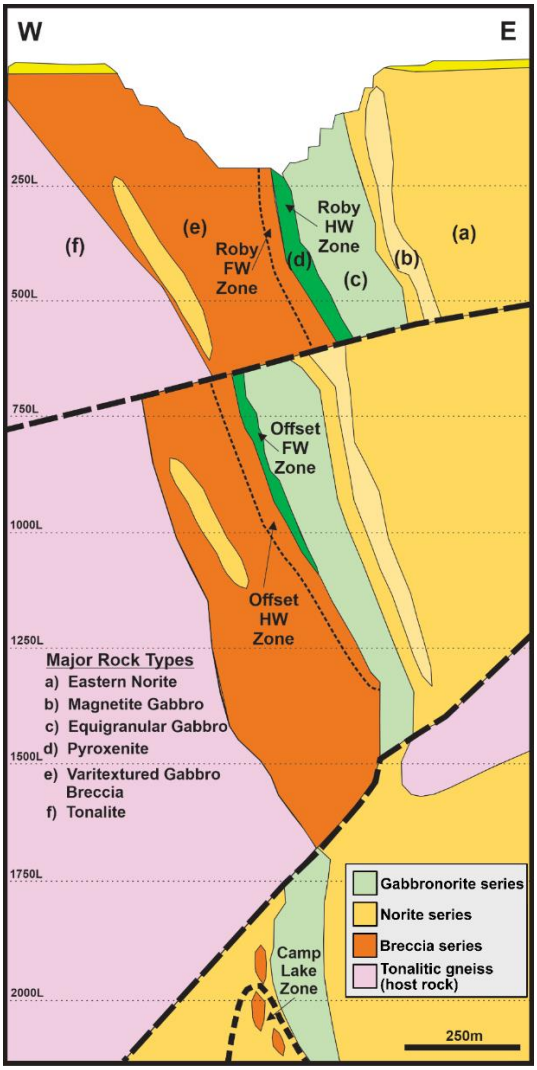

Figure 2.5 Cross section of geology within the Mine Block Intrusion (Roby and Offset Zones) with exposed Camp Lake Target at depth. Image from Impala Canada (2020).

2.5.3 Faulting in the Lac des Iles Complex

Two major sets of Neoarchean subvertical, transcurrent faults transect the Lac des Iles area (Stone, 2010). The east- to northeast-trending dextral Quetico fault and Shelby Lake fault extend along the Quetico-Wabigoon boundary (Figure 2.3) and are marked by zones of schist and mylonite up to 1 km wide, with sporadically developed mylonite where faults crosscut the felsic plutons within the Quetico (Stone, 2010). Cataclastic rocks and pseudotachylites are also

observed indicating some form of brittle deformation has occurred (Stone, 2010). The Shelby Lake fault, hypothesized to be a splay of the Quetico fault, is characterized by a broad zone of mylonite with associated high-shear strain only a few kilometers south of the last exposure of the Quetico fault (Stone, 2010). The north-south feeder structure for the LDIC has been interpreted to be an extension of the Shelby Lake fault (Stone et al., 2003; Djon et al., 2018).

The south LDIC has been affected by syn- to post-magmatic faulting that has complicated the primary ore forming processes and the pre-faulting configuration of ore zones (Peck & Djon, 2020). Two structures referred to as the Offset and Camp Lake faults divide the Roby-Offset deposit into three structural blocks referred to as the Roby, Offset and Camp Lake blocks (Peck & Djon, 2020; Implats, 2022). The Offset and Camp Lake faults are subparallel, northeast-striking and moderate to steeply northwest-dipping (249/50 W & 239/59 W, respectively). The inferred sense of movement of the Offset fault has primarily been based on the Pd grade and equigranular gabbro (EGAB) intercepts. Based on this information, the Offset fault has been classified as a reverse right-lateral oblique fault (Vektore, 2021). Similarly, the EGAB, norite, and tonalite units logged by Impala Canada geologists and the variations in Pd grade were used in a similar manner to interpret the movement of the Camp Lake fault. The Camp Lake fault has a sub-parallel slip direction and similar kinematic style to that of the Offset fault (i.e., high angle reverse faulting; Vektore, 2021).

Chapter 3: Methods

3.1 Core Logging and Macroscopic Observations

Detailed core logging was completed on eight unoriented drill holes: four that intersect the Camp Lake fault and four that intersect the Offset fault. The goals were to: 1) quantify micro- and macroscopic damage within fault cores and associated damage zones and, 2) to characterize the geochemical alteration associated with fluid flow along the fault. Drill core observations were supplemented with underground visits to key localities of the Camp Lake and Offset faults to collect oriented samples. Drill hole logs were variable lengths, as many were collared in different areas of the mine, resulting in different fault intercepts. Core logging initially was conducted to establish a background fracture density. We attempted to have a minimum of 100 meters on either side of the fault for fracture density counting purposes. Core logs are found in Appendix 1.

Fracture densities (linear) were determined by counting the number of fractures intersecting the drill core across a given interval and converting to per unit length. Macrofractures visible to the unaided eye were counted, while microfractures (only visible in thin section) were not. As fracture density is known to decrease with distance from the fault core (Savage & Brodsky, 2011 and references therein). Measurements were made every 25 m at distances greater than 100 m from the fault core, 5–10 m at distances 10–100 m from the fault core, and every meter within 10 m of the fault core. Measured intervals were 2 m in length at distances greater than 100m from the fault core, 1 m in length at distances 10-100 m from the fault core, and 50 cm in length at distances less than 10 m from the fault core. Measured distances from fault core were converted to true distances from the fault core using the average orientation of the fault and the orientation of the drillhole. Alteration, orientations of fractures

(alpha-angles as core was unoriented), and mineralogy of the fracture fill were noted. Alpha angles are the acute angle between the core axis and some planar feature.

Fracture density in units per meter can be fit by the power law function:

$$D = cr^{-n}, \qquad (1)$$

where c is a fault specific constant, r is distance from fault, n is an exponent describing the rate of decay (slope of the line in log-log space). Power law fits are plotted in log-log space where the slope of the linear regression is n. Standard errors for fracture density counting were calculated via a linear regression in log-log space. During the data collection process, precautions were taken to minimize sampling errors. Fractures that crosscut the drill core and filled fractures were counted, whereas fractures from the drilling process were not counted. A horizontal line drawn down the core axis was used to reduce double counting of fractures.

Table 3.1 Orientations of drill holes and intercepted faults with calculated angle between drill hole and fault.

Fault	Strike / Dip	Drill Hole	DDH Orientation	Angle between drill hole and fault
Camp Lake	239 / 59 W	22-905	099 → -44	38.8
Camp Lake	239 / 59 W	22-750	096 → -45	40.8
Camp Lake	239 / 59 W	21-700	191 → -64	43.4
Camp Lake	239 / 59 W	21-503	088 → -28	49.7
Offset	249 / 50 W	22-682	176 → -11	69.9
Offset	249 / 50 W	21-603	202 → -11	47.9
Offset	249 / 50 W	21-600	185 → -10	37.9
Offset	249 / 50 W	18-602	355→ -70	69.7

Samples were systematically collected from each drill hole and from the underground exposures for microstructural analysis. Drill core samples were collected approximately 1, 2, 5, and 10 m from the fault core, and approximately every 25 m from then on, from the interface between the fault core and damage zones on both the hanging wall and footwall side. Oriented

samples from the underground exposures of the Camp Lake (5 samples; Figure 3.1) and Offset (3 samples) faults were also collected. Friable fault core samples were cured with epoxy in place (prior to sampling) to better preserve microstructures during sampling and were further vacuum impregnated with epoxy in the lab prior to thin section preparation. Samples were collected with the intention of analyzing and quantifying alteration intensity and geochemistry with proximity to faulting in both zones. Alteration was quantified observationally as weak, moderate, intense, and extreme, and was classified based on the percentage of primary mineral replacement. In total 88 samples were taken and analyzed for whole rock geochemistry, 51 from the Camp Lake Zone drill hole 22-750, and 37 from the Offset Zone drill hole 21-603. Samples taken ranged from quarter-cut to full NQ (47.6mm) drill core. Two samples were removed from the study as they contained dike material in the samples.

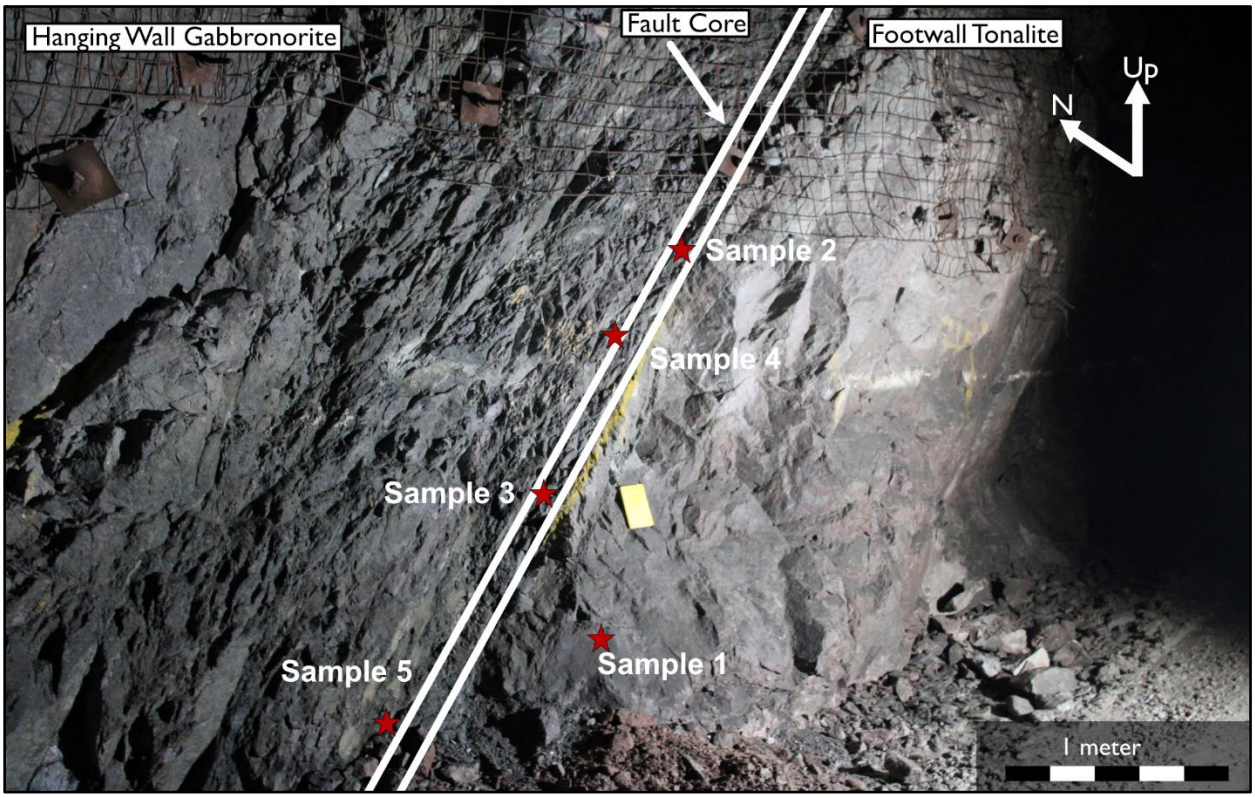

Figure 3.1 Underground sample locations from Camp Lake fault

3.2 Microstructural Analysis

Microstructural observations and petrographic analysis of polished thin sections were conducted on an Olympus BX 51 microscope with an Olympus SC180 camera and a Zeiss Axioscope 7 at Lakehead University under transmitted and reflected light. Samples from the Camp Lake and Offset faults were analyzed to observe mineralogical, textural, and alteration changes with proximity to the respective fault core.

3.2.1 Scanning Electron Microscopy

Scanning electron microscopy (SEM) was conducted at Lakehead University on a Hitachi SU-70 Schottky Field Emission SEM equipped with an Oxford Aztec 80mm/124ev EDX detector. Carbon coated samples were analyzed using a working distance of 15mm and an accelerating voltage of 20kV. The SEM was used to analyze the microstructures and geochemical composition of slip surfaces and fault gouge. Internal lab standards were used before data collection to establish a baseline chemistry of minerals analyzed under the SEM.

3.3 Whole Rock Geochemistry

One drill hole intersecting the Camp Lake and Offset fault was sampled for lithogeochemistry. Eighty-eight samples were sent to ALS Labs in Thunder Bay, ON for whole rock geochemical analysis. Samples were prepared for analysis by crushing 70% of materials to <2mm, then pulverizing to 250 grams of the material until 85% could pass through a 75um sieve (ALS package PREP 31). A combination of base metals analysis via 4-acid digest, major element analysis via ICP-AES, trace element analysis via ICP-MS and lithium borate fusion ICP-MS were used for each sample (ALS package: CCP-PKG01). Total carbon, sulphur, and loss on ignition (LOI) were also completed via induction by furnace, for the complete characterization to obtain the complete suite of elements. Full results of geochemical analyses are provided in Appendix 2.

We assessed element mobility in the fault zones by comparing the fault rock composition to the local protolith (in this case, the least altered or most distal sample). Element mobility was calculated by subtraction of the original sample (sample A, or protolith) from the sample of interest (sample B), divided by the concentration of the element within sample A, or:

$$\Delta C_i = B - A$$

And:

$$\text{Weight percent change} = \Delta C_i / \Delta C_iO$$

Where C_i is the difference between a concentration of an element in the most distal sample (sample A) and the sample in question (sample B), and C_iO is the initial concentration of the element in question of sample A. QA/QC for the samples was assured via lab standards, duplicates and blank standards into the sequence. The measured values of standards and blanks were found to be within the allowed instrumental error for the certified values.

3.4 X-Ray Diffraction

X-ray diffraction was conducted at Lakehead University Instrumentation Laboratory to analyze mineralogy of clays and clay-sized particles. Samples were preferentially chosen based on proximity to the fault core with an emphasis on damage zone (less than 10 m from fault core) and fault core samples. The limitations of XRD include the detection limit in samples with multiple components, which is approximately 2%. Samples containing multiple components which are more difficult to analyze through a Reitveld analysis were made into oriented clay slides and analyzed under dry and glycolated conditions.

3.4.1 Random Powder XRD

Nineteen randomly oriented powders for XRD were prepared and analyzed at Lakehead University using a PAN analytical Expert Pro Diffractometer. Samples were crushed with mortar

and pestle in 30 second intervals followed by sieving to avoid amorphization of clays, and this process was repeated until the entire sample could be passed through a 150μm mesh. Powders were run under the following parameters: 5–96 degrees 2 theta, a step size of 0.02 degrees, and 37.74 seconds / step. Data collected was analyzed with the PDXL2 software. Mineral phases were assigned based on spectrum peak position and intensity.

3.4.2 Oriented and Glycolated Clay XRD

Sixteen oriented clay slides were prepared and analyzed at Lakehead University. Aggregate mounts were prepared from the powders produced above and placed into vials filled with 50mL of distilled water, and a small amount (< 0.5g) of sodium hexametaphosphate. The samples were loaded into a centrifuge and run at 500 rpm for 1 minute to separate clays from silt. Silt was removed from the vials and disposed while clays were returned to the cleaned vial. This process was repeated 1-4 times until the fluid was clear and free of silt. The liquid samples with particulate were vacuum filtered to separate light particles from solution and to orient particles parallel to the filter paper (Poppe et al., 2001). Filtered material was carefully transferred to a glass slide and run under the following parameters: 2–35 degrees 2 theta, a step size of 0.01 degrees, and 200 seconds / step. Once collected, XRD spectra were analyzed using the PDXL2 software. The 16 oriented clay slides used were then glycolated overnight in a sealed container of ethylene glycol. Slides were then run a second time under the same conditions. The Kübler index was used to determine diagenetic and very-low grade metamorphic zones.

3.5 Chlorite Thermometry via Electron Microprobe

Representative chlorites from six samples were analyzed using a JEOL JXA8230 5-WDS electron microprobe at the University of Toronto. Analyses were conducted using a 15 kV accelerating voltage, a 20 nA current, and a working distance of 11 mm. Each analysis was

conducted for a duration of 3.5 minutes with a 10-micron unfocused beam. Samples were analyzed for major elements Si, Ti, Al, Cr, Fe, Mn, Mg, Ca, Na and K. All data obtained from EMPA analysis and standards used in this study are available in Appendix 3. Samples totalling over 100 or under 98 wt % oxides were removed, and samples where K+Na+Ca > 0.1 apfu were considered contaminated and were removed.

Of the analyses performed on the selected thin sections, 352 spots from the protolith and 214 spots from the fault core samples were deemed usable after the removal of analyses that did not conform to a chlorite chemistry. Internal lab standards were used before and after the data collection process to ensure an accurate analysis of the chlorite chemistry was conducted. See Appendix 3 for raw data and chlorite standards.

Chapter 4: Results

4.1 Overview of Fault Structure

This section summarizes the field-based observations at the mesoscopic scale; details regarding microstructural observations can be found in section 4.3.4. Observations from underground exposures of the Camp Lake and Offset faults show that both are discrete faults with an average orientation of 259/59 W and 249/50 W, respectively (Figure 4.1).

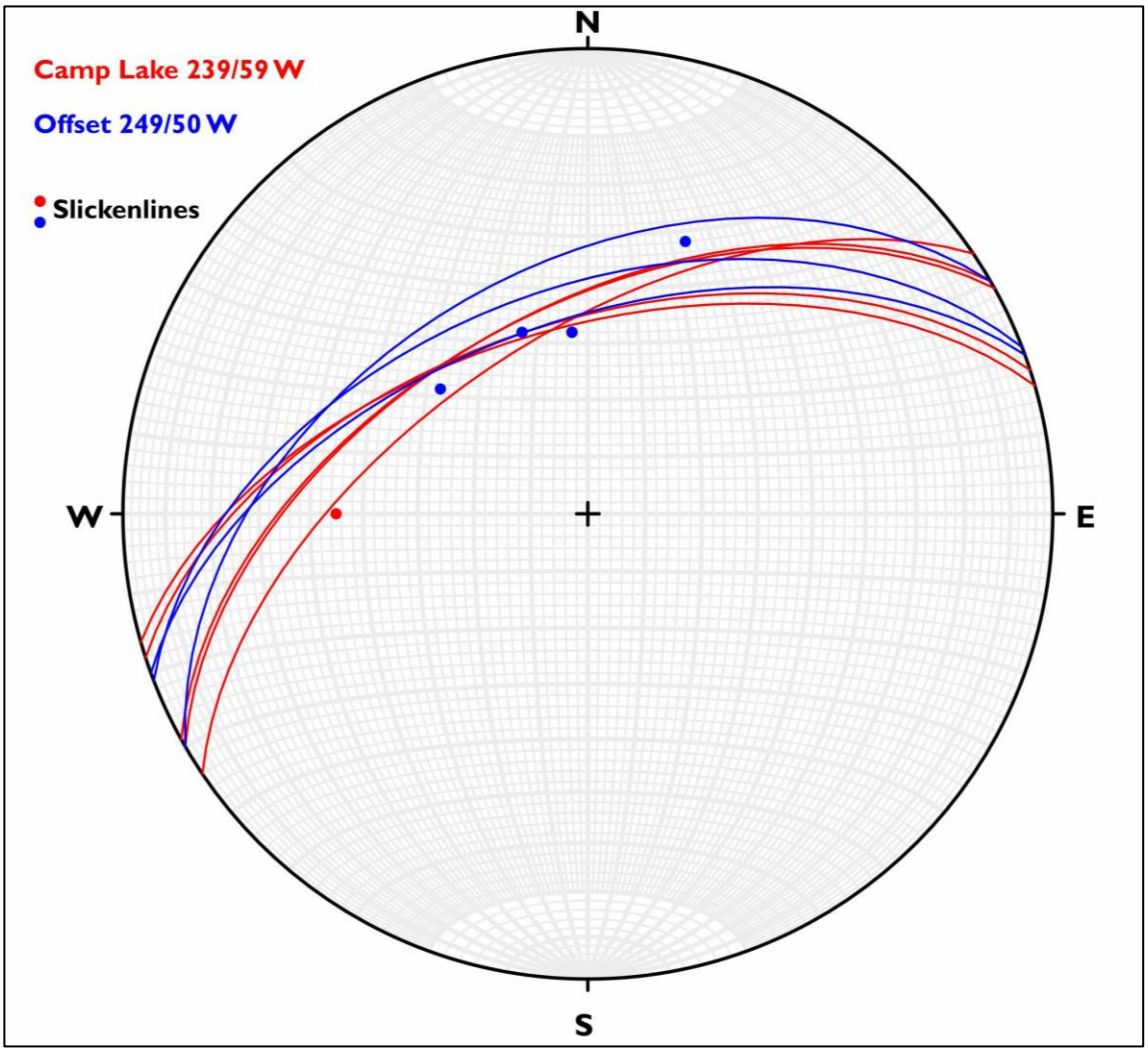

Figure 4.1 Stereonet of average orientations of Camp Lake and Offset faults and their respective slickenline orientations.

Each studied fault has a well-developed damage zone and fault core, with an increase in alteration and fracture density with proximity to the fault core. The fault core for each fault

typically exhibits a clay-rich fault gouge in mafic fault cores and a silicified cataclasite in felsic fault cores. Fault gouges in drill core and underground exposures vary in thickness from less than 10 cm to 25 cm.

In the studied drill holes, there is often a change in lithology when crossing either fault (tonalite juxtaposed against gabbronorite, or vice versa). Drill holes in this study that intercept the Offset fault typically are collared in the Roby Zone and drill into the Offset Zone, whereas drill holes that intercept the Camp Lake fault typically are collared in the Offset Zone and drill into the Camp Lake Zone. Drill holes in the Offset Zone collar in a swarm of mafic dikes, then intercept tonalite with sporadic mafic and felsic dikes. The hanging wall tonalite is intercepted by the Offset fault then after fault core a variably altered and textured gabbronorite unit is observed. This is the case for all studied drill holes apart from 18-602 where the gabbronorite unit is observed in both the hanging wall and footwall. Drill holes used in this study that intercept the Camp Lake fault often collar in gabbronorite, except for one drill hole which collars in tonalite. The drill holes intercept various mafic and felsic dikes in the hanging wall and tonalite in the footwall.

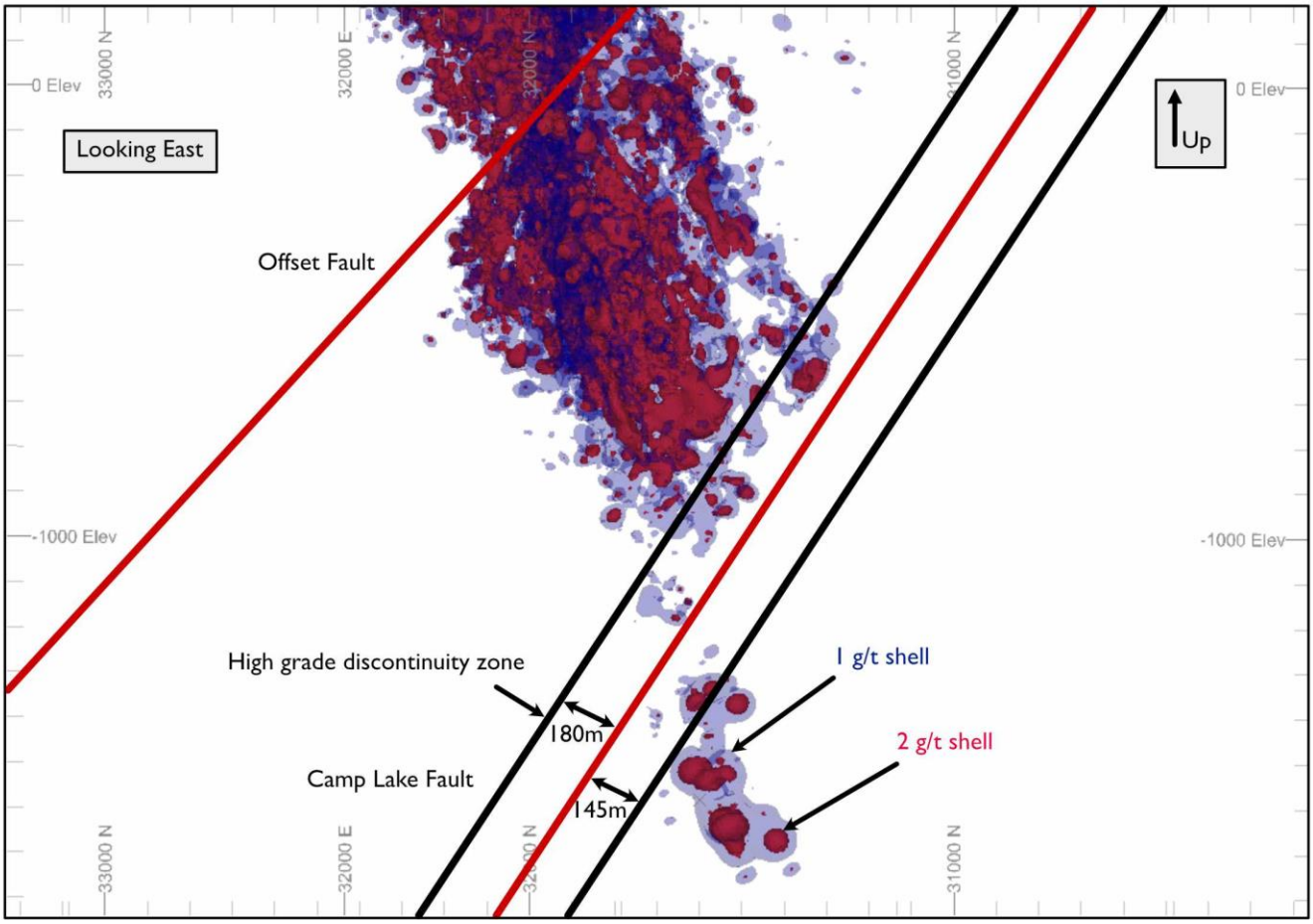

Figure 4.2 Model of ore shells and average grades of Pd. Camp Lake and Offset faults are highlighted with high-grade discontinuity zone and damage zones (Impala, 2022).

4.1.1 Camp Lake Fault Zone

External consultants produced a report on the Camp Lake fault in 2020 and determined the displacement to be greater than 500 meters based off displaced mineral envelopes where Pd is > 0.4ppm and the intercepts of the equigranular gabbro unit "EGAB" (Vektore, 2020). The sense of shear in both the Camp Lake and Offset faults are hypothesized and modelled to be reverse. Underground exposure of the Camp Lake fault shows the relationships between the main protoliths found in the hanging wall and footwall of the fault zone. Observations from underground samples and mapping show the hanging wall of the Camp Lake fault gabbronorite unit is often in contact with the tonalite footwall (Figure 4.3), however the lithology of the

hanging wall and footwall can change along strike. The hanging wall gabbronorite is predominantly grey-dark green, medium to very fine-grained and displays strong, pervasive chlorite alteration with quartz and plagioclase phenocrysts. The fault core consists of a quartz-chlorite gouge approximately 10 cm thick with a 1cm wide principal slip surface. Slickenlines plunge 38° towards 200°. The footwall tonalite on the north side of the fault is highly fractured, fine-grained, with strong potassic (potassium feldspar, quartz, white mica) alteration. Physically, the tonalite is much more cohesive than the gabbronorite and remains intact on the cut face. Microcracks are visible in both the hanging wall and footwall and display a dark red colour, caused by hematite infill from iron precipitation. Chlorite and gouge filled slip surfaces were observed within the fault core. The underground exposure of the Camp Lake fault shows strongly foliated gabbronorite 1-2 meters into the hanging wall from the fault core (Figure 4.4). Within the gouges of the fault core, chlorite appears to be the dominant mineral phase with associated quartz-calcite nodules and dark red fracture infill of unknown mineralization. R- and Y- shears were observed in, and outside the fault core in the gabbronorites (Figure 4.4).

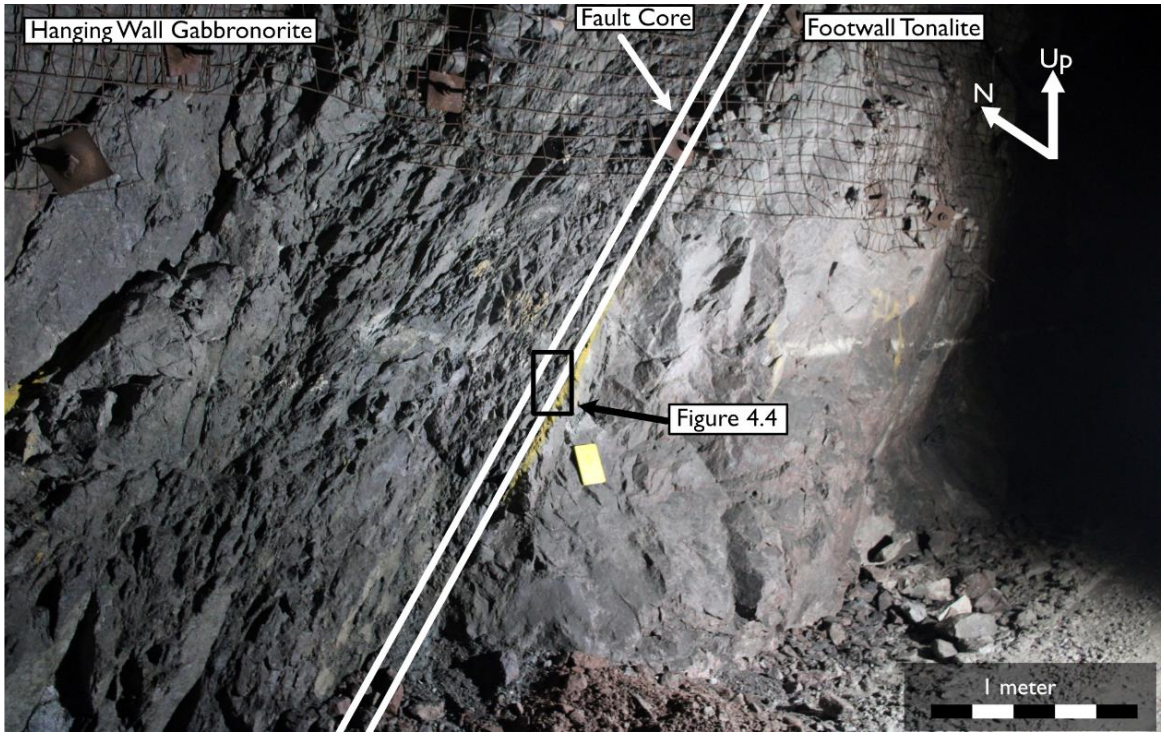

Figure 4.3 Photo of the underground exposure of the Camp Lake fault exemplifying the primary lithologies of the study in fault contact with each other.

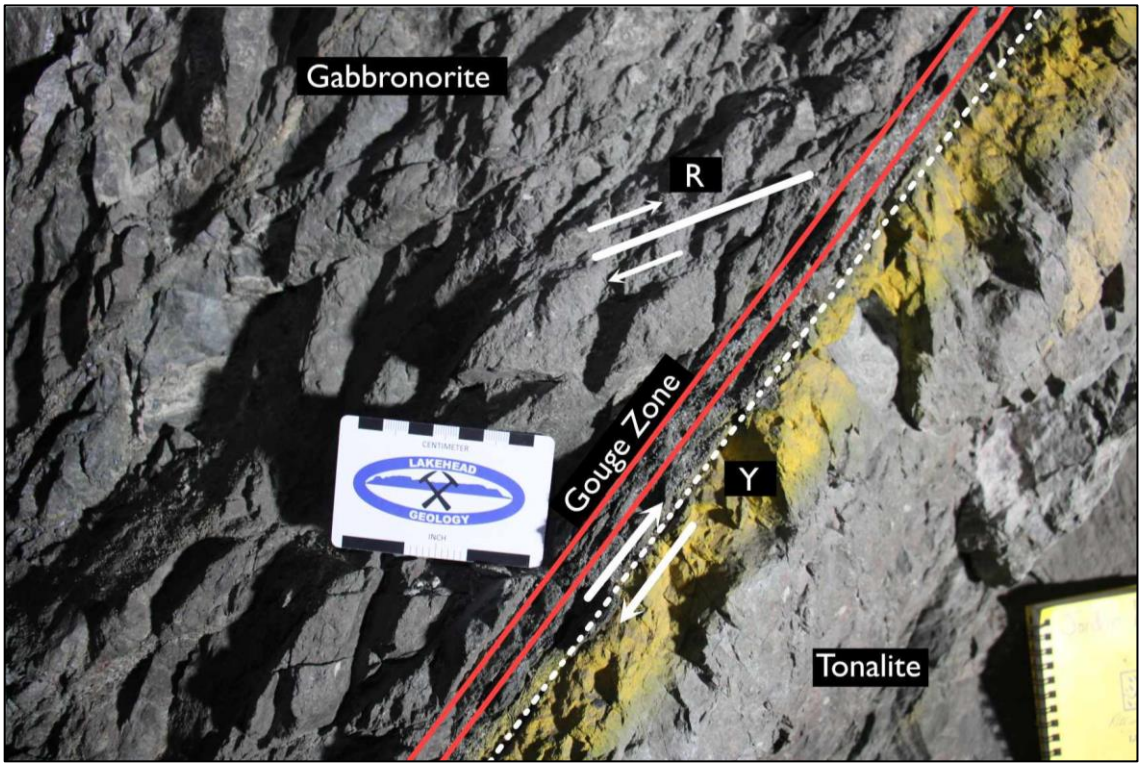

Figure 4.4 Close up photo of underground exposure of Camp Lake fault core with R- and Y- shears in gabbronorite.

4.1.2 Offset Fault Zone

The Offset fault strikes 249° and dips 50° degrees to the northwest. It has been noted by Impala Canada geologists and external consultants that the relative right-lateral horizontal displacement is approximately 250 meters with 100 meters of vertical displacement based off displaced mineral envelopes (where Pd is > 0.4 ppm) and the intercepts of the equigranular gabbro unit "EGAB" (Vektore, 2021). Observations from underground samples show a strongly altered gabbronorite in both the hanging wall and footwall in underground exposures (Figure 4.5). The gabbronorite is dark grey to green, with strong chlorite and silica alteration, and weak potassic staining. Slickenlines are visible on the underside of the hanging wall and plunge 45° towards 270°. A fault core is observed in the Offset fault exposures, approximately 10 cm thick, and is composed of gouge and a visible principal slip surface cutting the gouge. The underground exposure of the Offset fault shows the fault cross-cutting gabbronorite as opposed to a fault contact between gabbronorite and tonalite (Figures 4.4 & 4.5).

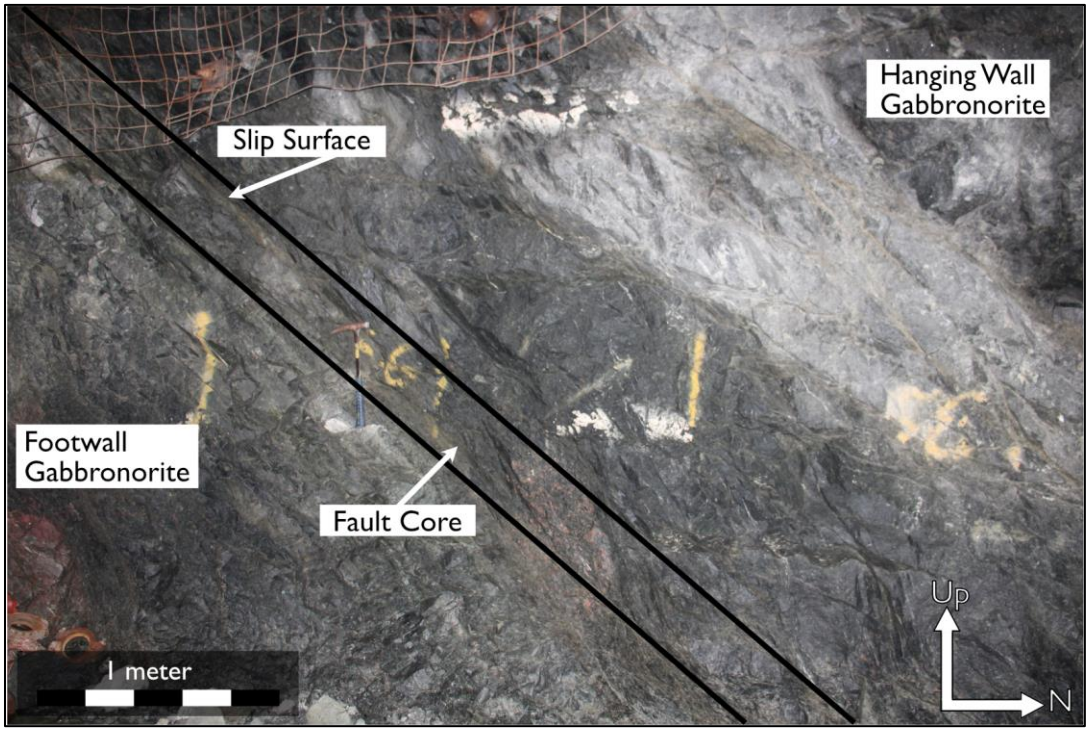

Figure 4.5 Photo of the Offset fault cross-cutting gabbronorite body.

4.2 Core Logging Observations and Principal Lithologies

An increase in alteration was observed in both tonalites and gabbronorites with proximity to the fault core. Potassium feldspar, epidote, and sericite alteration are the dominant alteration minerals in the tonalites, whereas chlorite, tremolite, actinolite, and minor sericite alteration occur in the gabbronorites.

In the studied holes, the observed lithologies include: gabbronorites to norites, chlorite-actinolite schist, and variably altered and foliated tonalite. These lithologies occur primarily in sharp contacts when transitioning from gabbronorite to tonalite, and in gradational contacts when transitioning from gabbronorites to norites or the chlorite-actinolite schist. In the unaltered to least-altered zones observed in drill core, the gabbronorites are commonly medium grained, variably altered, and are composed of > 90% pyroxene and plagioclase in variable quantities with trace amounts of sulfides (pyrite, chalcopyrite, pyrrhotite, pentlandite; Figure 4.6 A). Tonalites observed at the Lac des Iles mine are made up of > 60% quartz and plagioclase, potassium feldspar, minor accessory mafic minerals (biotite and hornblende), and trace pyrite. They are typically medium grained, grey/white to pink or green, and are locally foliated (Figure 4.6 B). The tonalites vary strongly in terms of alteration and structure. Least altered samples are mainly grey to white with a weak to moderately developed foliation defined by biotite. Highly altered and deformed (damage zone) gabbronorite samples show veinlets and a moderately developed foliation defined by chlorite (Figure 4.6 C). Highly altered/deformed tonalite samples show a reduced grain size, and either are strongly foliated, fractured, or brecciated (Figure 4.6 D, F). Alteration assemblages in the tonalites are dominantly epidote, sericite, and potassium feldspar, with minor calcite. Green and pink staining observed are due to epidote and potassium feldspar alteration. Fault core style varies primarily with protolith. Fault cores which crosscut gabbronorite are typically dark to medium grey and can be characterized by medium to very

fine-grained plagioclase + chlorite +/- quartz unconsolidated clay-rich gouge, or strongly altered and weakly consolidated gabbronorite with chlorite infill. Slickenlines (unoriented) are visible on some fault surfaces and can be observed in drill core. Angular to sub-rounded clasts of quartz-carbonate were observed in both hand sample and thin section. Gabbronorite fault core samples are typically clay-rich incohesive gouges (Figure 4.6 E). The primary mafic mineral assemblage in the gabbronorites begin to be partly or entirely replaced by chlorite and sericite as alteration increases and is predominantly visible in thin section (See section 4.3). Sericite replaces plagioclase and occurs within veinlets in the damage zone. Tonalite fault core samples are typically brecciated. They vary from matrix supported to clast supported breccias, and are strongly altered by epidote, quartz-carbonate, and various feldspar group minerals. Mineral grains are typically fragmented and highly fractured and are most often angular with occasional sub-rounded grains visible. Tonalite cataclasites in fault cores appear to be re-silicified gouges (Figure 4.6 F). Approaching the fault core, the breccias change from clast supported to matrix supported, until they are composed entirely of re-silicified clay sized fragments.

The chlorite-actinolite schist is a relatively uncommon unit observed in drill core. The dominant mineral assemblage is > 90% chlorite and actinolite, with trace hornblende, plagioclase and sulfides (pyrite, chalcopyrite). A well-developed schistose fabric is the dominant identifier for this unit, with fine to medium-grained, green to black chlorite and actinolite visible in drill core. Medium- to fine-grained chlorite, tremolite, and actinolite are the dominant minerals in the lithology and are observed in both schistose bands and medium-sized grains which appear to be replacing pyroxene. Minor, very fine-grained plagioclase can be seen in between chlorite and actinolite bands.

Fractures in gabbronorites are predominantly chlorite-actinolite filled and are less obvious in hand sample compared to the epidote-sericite-quartz-calcite filled fractures observed in the tonalites. Within the Lac des Iles Mine the gabbronorites are split into separate sub-lithologies such as vari-textured gabbro (GABVT), norite, leucocratic gabbro and melanocratic gabbro. These lithologies are subdivided based on grain size, textures, and pyroxene-plagioclase ratios, but based on geochemistry can be grouped as gabbronorites to norites. The most notable zones of alteration are within the damage zone and fault core. This is observed both in drill core and hand samples from the underground exposures. There is a correlation between the increased frequency of fracturing (see section 4.6) and the observable alteration in drill core. As fracture density increases towards the fault core, alteration intensity of the host rock increases.

During the data collection process, potential sources of error were identified. These sources of error include human error and analytical/logging errors. To ensure the data collection was conducted in a way to minimize these errors, photos were taken before and during the core logging process.

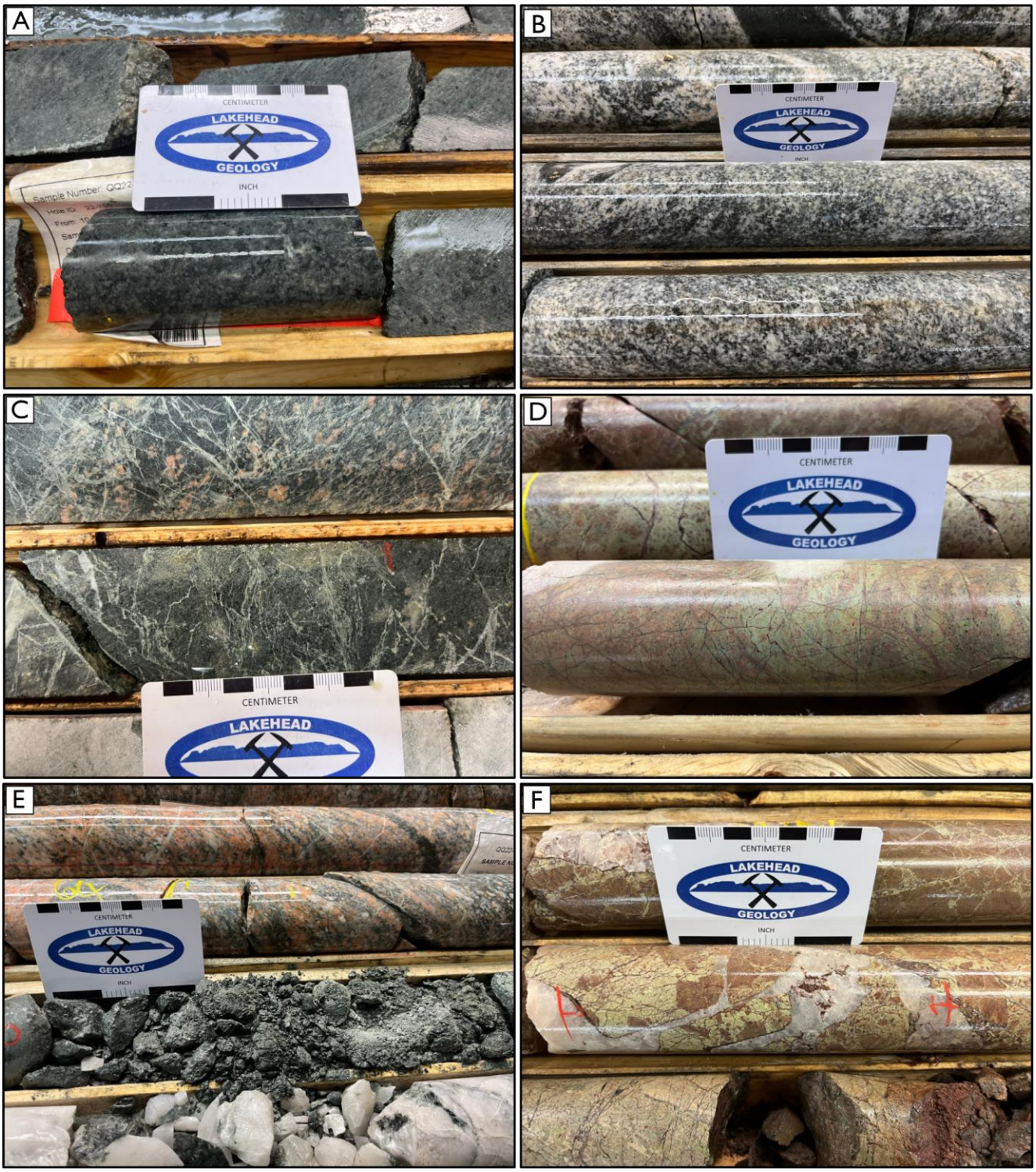

Figure 4.6 A) Typical least altered gabbronorite unit in drill core, ~200 meters from fault. B) Moderately foliated and least altered tonalite unit, ~95 meters from fault. C) Strongly altered and fractured gabbronorite in damage zone, ~5 meters from fault. D) Strongly altered and fractured tonalite damage zone, ~10 meters from fault. E) Fault core / gouge in gabbronorite. F) Silicified cataclasite / breccia, a typical tonalite-hosted fault core.

4.3 Petrography and Microstructures

4.3.1 Petrography of Major Lithologies

Samples from the Camp Lake and Offset fault zones are predominantly composed of variably altered gabbronorites (n=48) and tonalites (n=29). Due to the strong alteration of the damage zone and fault core samples, determining the pre-alteration species of pyroxene was not possible and they are generally grouped as pyroxene unless truly discernable. As expected, all samples regardless of lithology exhibit stronger alteration towards the fault core.

Camp Lake Gabbros

Samples from the Camp Lake drill holes are composed of gabbronorites and chlorite-actinolite schists. Typical gabbronorite samples are composed of 40-60% plagioclase, 10-40% pyroxene, 5-30% chlorite, trace quantities of sulfides, typically pyrite, magnetite and chalcopyrite, and occasional relic olivine grains. Plagioclase is medium to very fine-grained, euhedral to anhedral, typically randomly oriented, and altered primarily by sericite with variable degrees of replacement. Plagioclase can be identified by polysynthetic twinning (Figure 4.7 A, B) and sericite alteration. Pyroxene is medium to very fine-grained, anhedral to subhedral, bladed and acicular, and altered to tremolite-actinolite, with alteration ranging from unaltered to extremely altered. Chlorite is typically very fine-grained, fibrous, frequently infilling fractures and partially replacing pyroxenes and biotite. Sulfides are very fine-grained and blebby or fracture filling.

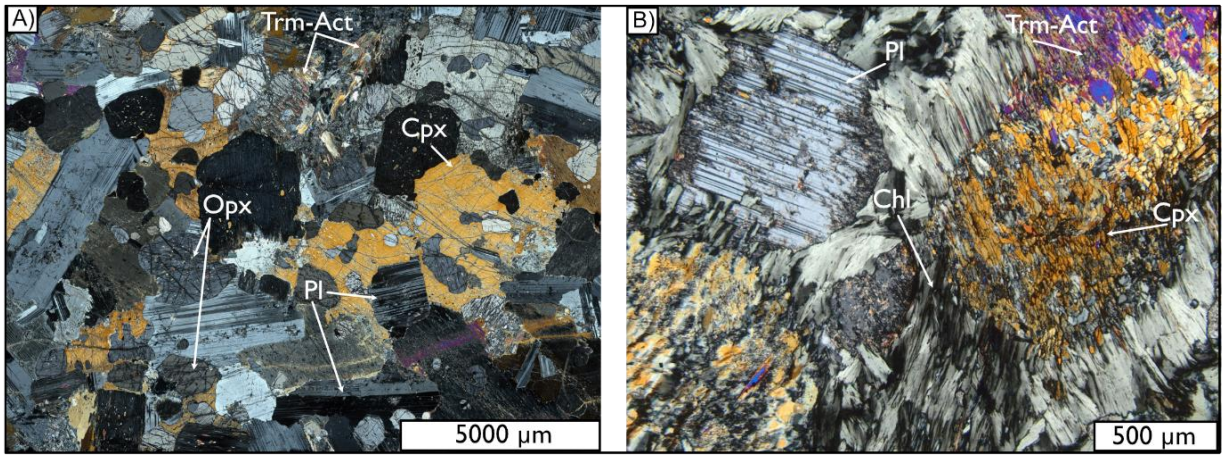

Figure 4.7 Cross polarized photomicrographs of least altered gabbronorites. A) Sample 22-750-07 displaying primary textures and least altered pyroxene and plagioclase. B) Most distal gabbronorite sample with weak to moderate alteration of plagioclase and chlorite. Abbreviations: Trm-Act- tremolite-actinolite, Opx- orthopyroxene, Cpx- clinopyroxene, Pl- plagioclase, Chl- chlorite.

Alteration of plagioclase is most evident in samples proximal to the fault core (~25m). Of the thin sections selected from the Camp Lake fault drill holes, only one (22-750-07) appears to exhibit primary magmatic textures and displays little to no alteration and deformation (Figure 4.7 A). The remainder of the samples are altered to some extent and show a weak to moderate foliation. Alteration of plagioclase appears to be pervasive, however in many samples where quartz surrounds plagioclase, the alteration is not as intense, and plagioclase retains its original shape (Figure 4.8 A, B).

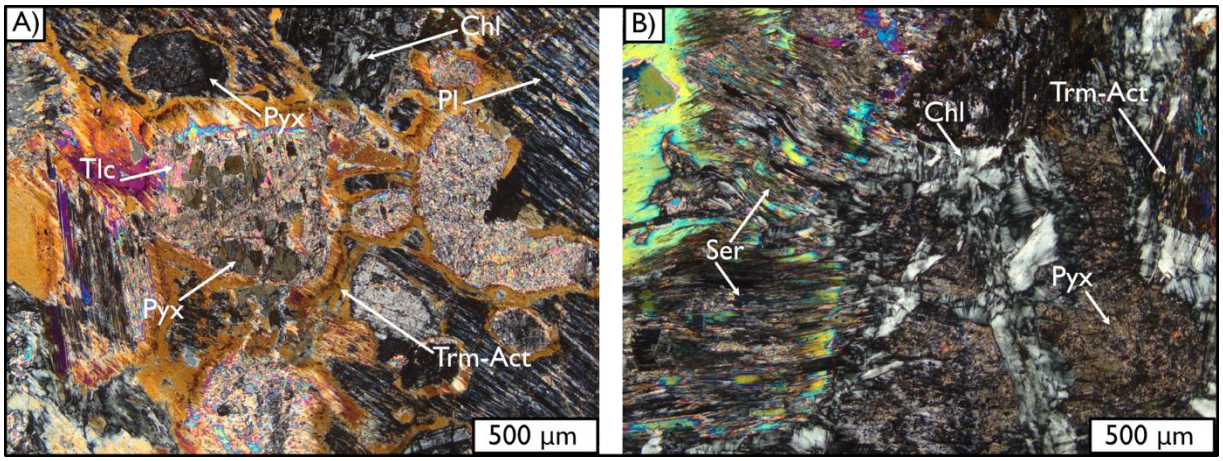

Figure 4.8 Cross polarized photomicrographs of damage zone gabbronorite samples. A) Sample 22-750-15 displaying alteration of pyroxene and plagioclase. B) Sample 22-750-14 with strong sericite and chlorite alteration of plagioclase with relic pyroxene grains. Abbreviations: Trm-Act- tremolite-actinolite, Tlc- talc, Pyx- pyroxene, Pl- plagioclase, Chl- chlorite, Ser- sericite.

Camp Lake Tonalites

Thin sections from the Camp Lake fault tonalites are composed of 30-60% quartz, 20-60% plagioclase feldspar (albite), 5-10% biotite, and up to 10% sulfides (pyrite) +/- variable quantities of chlorite, epidote, sericite, tremolite-actinolite, calcite, and alkali feldspar (Figure 4.9 A, B). Samples are typically medium to very fine-grained and exhibit variable intensities of alteration. Quartz is typically anhedral, medium to very fine-grained, and is occasionally aligned to form a shape preferred orientation. Epidote alteration is the most pervasive alongside sericite. Calcite is present in the most altered samples and fills large fractures.

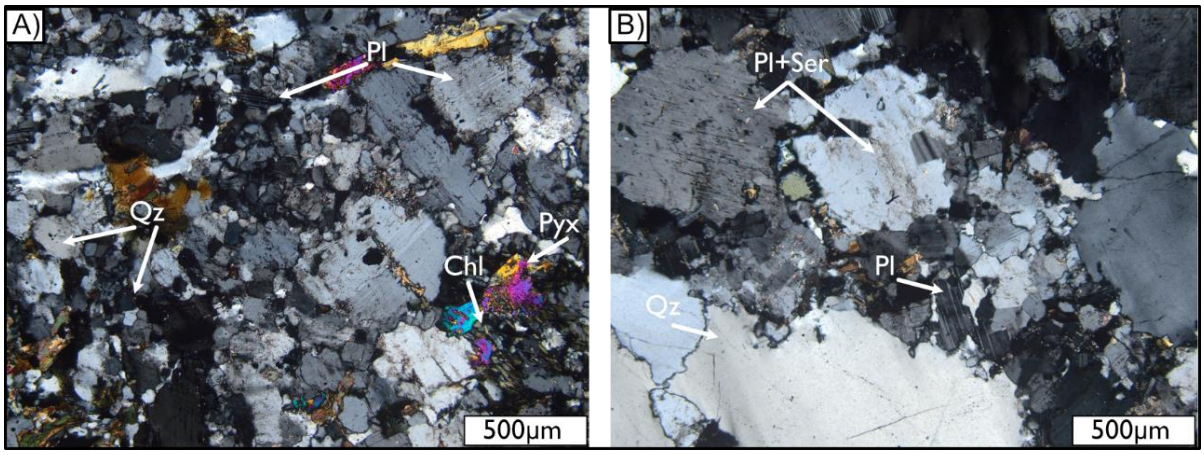

Figure 4.9 Cross polarized photomicrographs of representative tonalite samples. A) Moderately altered tonalite with fractured quartz and plagioclase. B) Weakly altered tonalite. Quartz grain boundaries are still intact and have not been comminuted. Plagioclase is weakly altered to fresh. Abbreviations: Pl- plagioclase, Qz- quartz Pyx- pyroxene, Chl- chlorite, Ser- sericite.

Offset Gabbros

Gabbroic samples from the Offset fault drill hole are composed of 30-50% plagioclase, 30-40% pyroxene, and potentially 0-10% relic olivine that has been completely altered from the original rock. Plagioclase feldspar (albite) ranges from coarse to very fine-grained and is variably altered (from 0-100%) to sericite and tremolite-actinolite (Figure 4.10 A). Plagioclase is most often euhedral to subhedral, with occasional anhedral grains present in strongly deformed samples, and is easily identified by polysynthetic twinning. Trace amounts of alkali feldspar can be found in some samples and are discernable via tartan and Carlsbad twinning, and perthite unmixing (Figure 4.10 B). Pyroxene is medium to very fine-grained and is often replaced entirely by tremolite-actinolite +/- talc. The most distal gabbronorite sample from the Offset samples is medium to coarse grained and is weakly altered. Pyroxene shows stronger alteration compared to the neighbouring plagioclase grains, but alteration is variable. Microfractures are present across both pyroxene and plagioclase. Gabbroic samples also contain sulfide mineralization from 0-5%. Sulfide assemblages are typically pyrite + ilmenite +/- magnetite +/- chalcopyrite. Sulfides are predominantly disseminated.

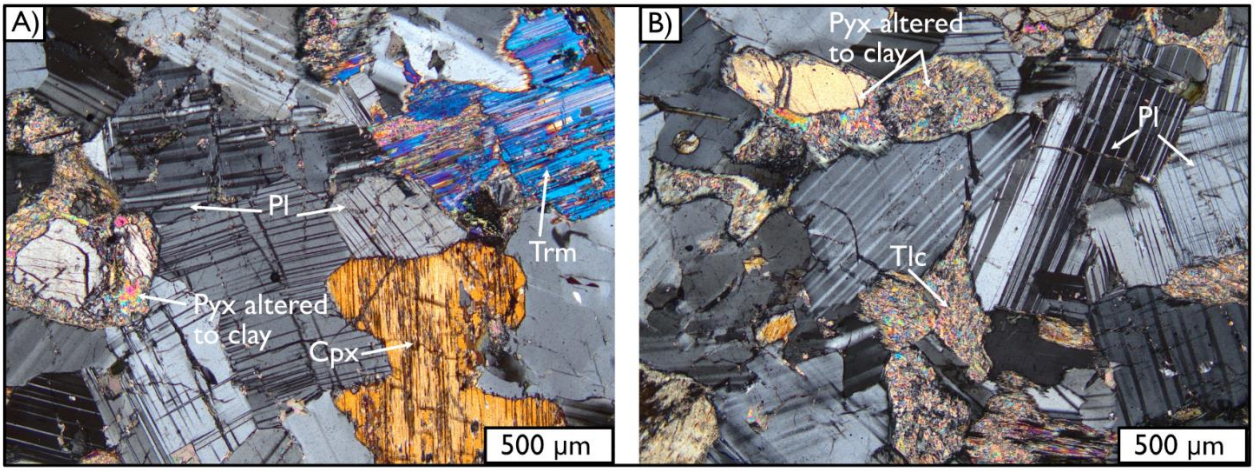

Figure 4.10 Distal (50 meters from fault) cross polarized photomicrographs of gabbronorites from the Offset drill hole. A) Weakly altered plagioclase with minor microfracturing and kinking. Clinopyroxene (Cpx) with almost no alteration and orthopyroxene (Opx) altering to clay and tremolite. B) Talc alteration of pyroxenes and unaltered plagioclase. Abbreviations: Trm- tremolite, Pl- plagioclase, Pyx- pyroxene, Cpx- clinopyroxene, Tlc- talc.

In highly altered samples, distinguishing orthopyroxene from clinopyroxene is not possible due to the strong deformation and alteration (Figure 4.11 A). The original textures are not always observable within the samples. Occasionally, relic and less altered pyroxene grains are visible in less deformed samples and determining clinopyroxene from orthopyroxene is possible (Figure 4.11 A, B).

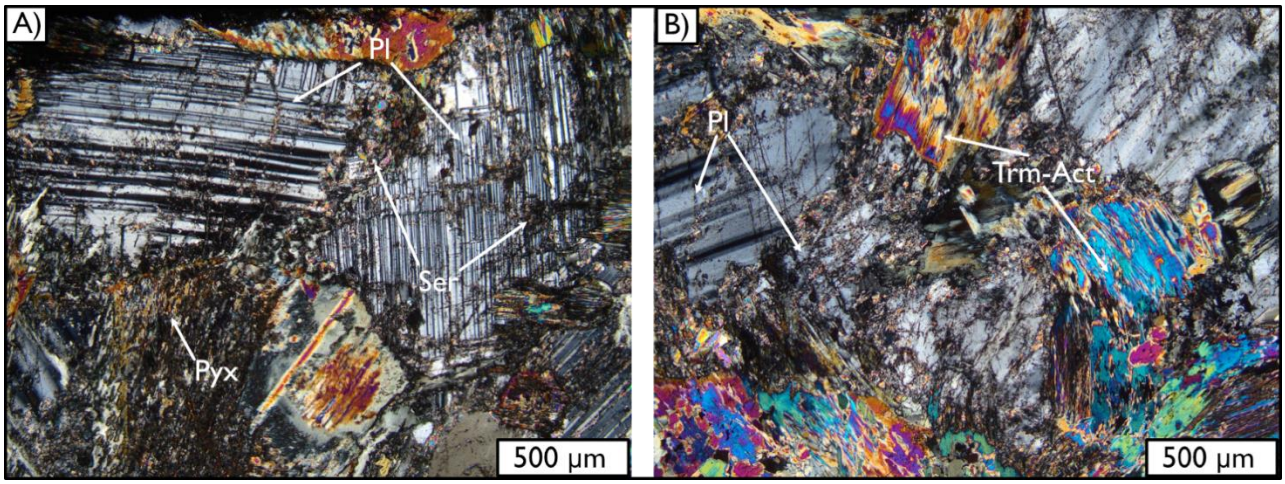

Figure 4.11 Cross polarized photomicrographs of damage zone sample of gabbronorite from the Offset drill hole. A) Altered plagioclase and remnant pyroxene grains showing alteration increasing with proximity to fault core. B) Plagioclase altered by sericite and pyroxene altered by tremolite-actinolite. Abbreviations: Pl- plagioclase, Ser- sericite, Pyx- pyroxene, Trm-Act- tremolite-actinolite.

Offset Tonalites

Thin sections of the Offset fault drill hole tonalite are composed of 30-65% quartz, 20-60% plagioclase feldspar (typically albite), and up to 10% biotite, +/- alkali feldspar, pyroxene, chlorite, and epidote, with sulfides ranging from 0 to < 5%. The least altered, or most distal, tonalite sample from the Offset fault has weakly foliated quartz, plagioclase that has not been or is only partially altered by sericite, primary biotite that has not been entirely replaced by chlorite, and trace amounts of pyroxene, pyrite, and alkali feldspar (Figure 4.12 A, B). Quartz grains are medium to very fine-grained, anhedral to subhedral, and often have undulatory extinction. Plagioclase is typically medium to fine-grained and subhedral to euhedral and exhibits polysynthetic twinning. Sericite dominantly alters plagioclase and increases in intensity with proximity to the fault core. Chlorite replaces biotite completely and epidote is present in trace quantities.

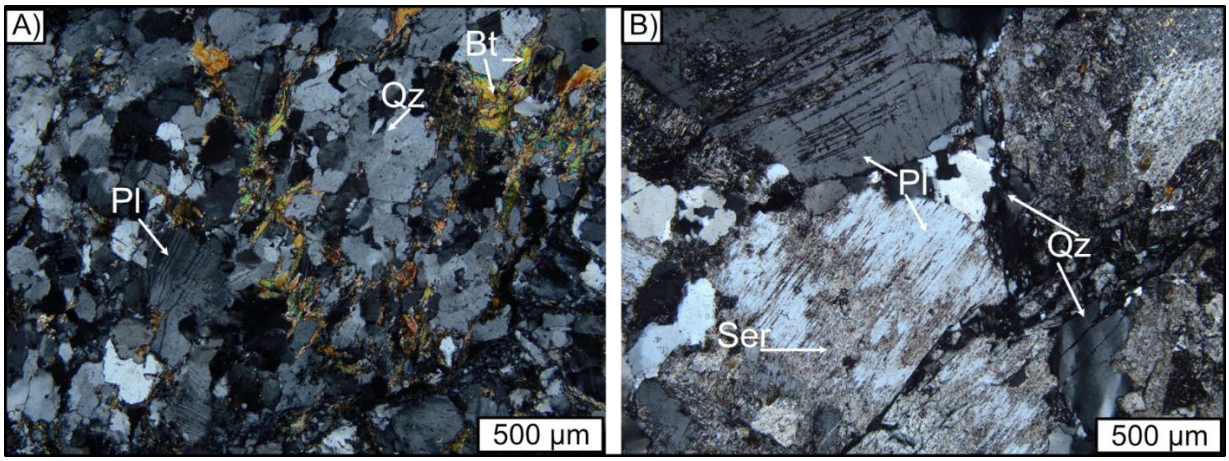

Figure 4.12 Cross polarized photomicrographs of distal (least altered) tonalite samples from the Offset drill hole. A) Relatively unaltered quartz, plagioclase and biotite with no strong apparent foliation. B) Moderately sericitized plagioclase and moderately deformed quartz. Abbreviations: Bt- biotite, Qz- quartz, Pl- plagioclase, Ser- sericite.

Damage zone samples of the tonalite unit display strongly sericitized plagioclase, foliated quartz with undulatory extinction, and alteration minerals such as epidote, tremolite, chlorite and calcite (Figure 4.13 A, B).

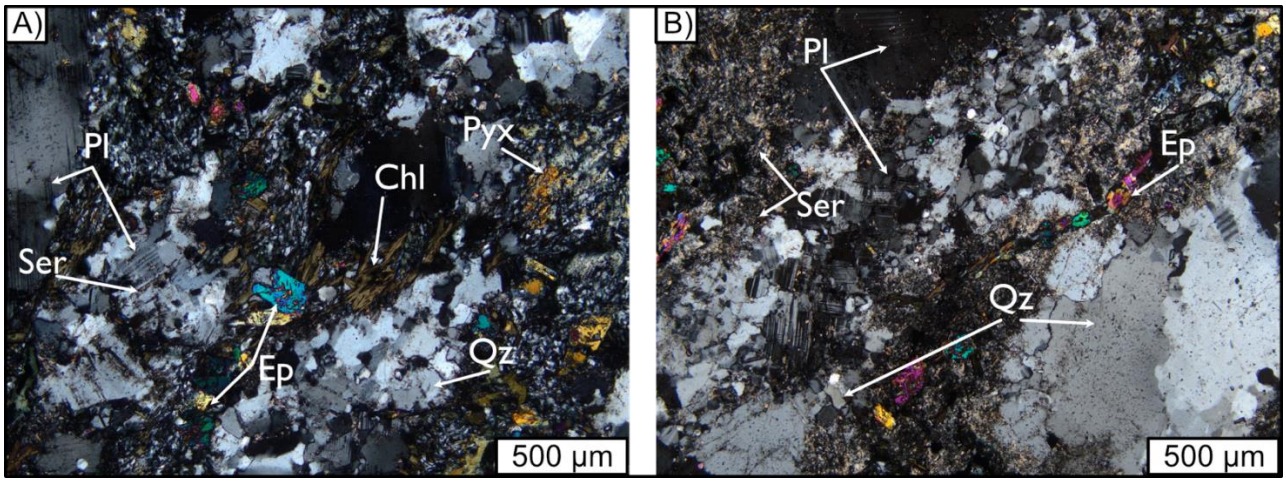

Figure 4.13 Cross polarized photomicrographs of damage zone tonalite samples from the Offset drill hole displaying a strong increase in alteration and deformation of mineral grains. A) Moderate to strongly altered tonalite. Epidote alteration of pyroxenes and sericitized plagioclase. Chlorite replacement of biotite and comminuted quartz and plagioclase grains. Abbreviations: Pl- plagioclase, Ser- sericite, Chl- chlorite, Pyx- pyroxene, Ep- epidote, Qz- quartz.

4.3.2 Fault Core Petrography

Five samples were taken from the underground expression of the Camp Lake fault and used to determine the mineralogy, alteration and deformation. Four samples were taken from the Offset fault. Deformation and alteration show similar intensities when comparing each fault in drill core and in hand sample but are quite different with respect to lithology. The gabbronorite fault core is dominated by fine-grained fibrous chlorite, both blue and dark brown in colour, fine to very fine-grained clasts of quartz and albite, with a very fine-grained groundmass (Figure 4.14 A). Very fine-grained, high birefringent minerals are present within the groundmass but are indiscernible by optical microscopy. In general, the gabbronorite fault core is strongly foliated, chlorite-rich, and very fine-grained (Figure 4.14 A, B). A dark red isotropic mineral is consistent across many of the fault core thin sections and typically has a foliated appearance.

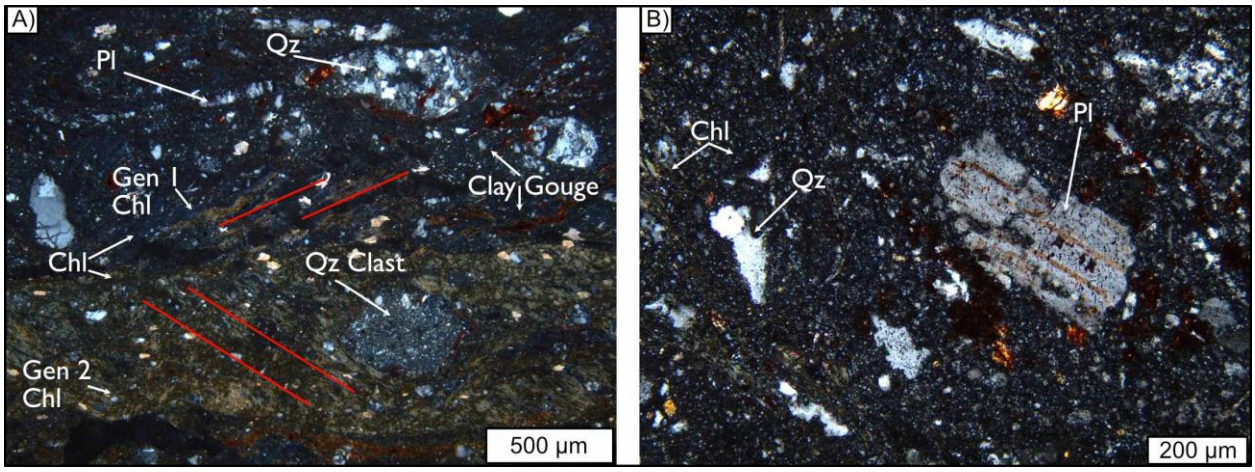

Figure 4.14 Cross polarized photomicrographs of fault core samples of the gabbronorite unit taken from the underground exposure of the Camp Lake fault. A) Strongly foliated (foliation trace highlighted in red) chlorite-rich fault gouge with remnant quartz and plagioclase. Two different generations of chlorite growth are prominent in the thin section and are discernable via the brown-green colour and the rich blue colour. The clay gouge is composed of quartz, plagioclase, pyroxene and chlorite fragments. B) Gouge zone of the fault core samples, with remnant plagioclase that displays a red-brown tinge along twinning planes. The gouge zone of these samples does not display as strong of a foliation as the clay-rich chlorite zones. Abbreviations: Pl- plagioclase, Qz- quartz, Chl- chlorite.

The tonalite fault core is composed of medium to very fine-grained and aphanitic fragments of angular to subrounded quartz (Figure 4.15 A, B). The groundmass is predominantly comminuted quartz and plagioclase grains. Calcite and epidote are present within the tonalite fault core, however on the thin section scale they are inconsistent and not pervasive. Grain size within the tonalite fault core is inconsistent – in samples approaching the fault core, an apparent foliation and grain size reduction is evident, however, in fault core the samples do not follow this trend and range from coarse to very fine-grained (Figure 4.15 B).

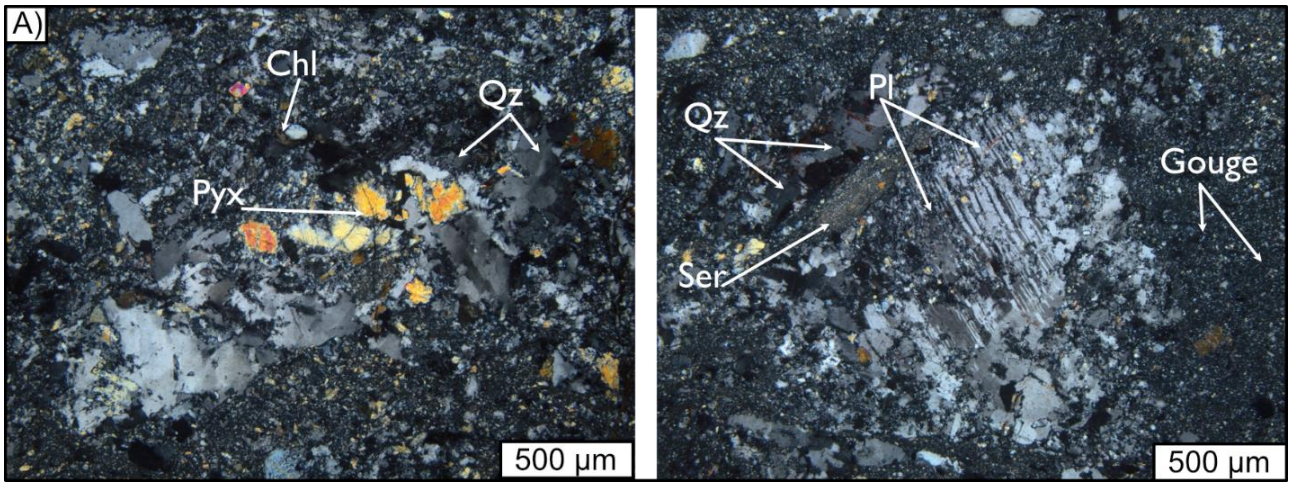

Figure 4.15 Photomicrographs of tonalite fault core samples from the underground expression of the Camp Lake fault. Both microphotographs display comminuted quartz and plagioclase grains surrounded by a pyroxene and quartz matrix. Very little clay is present in the tonalite fault core. A) Quartz clast that has not broken down entirely with remnant pyroxenes. B) Sericite altered remnant plagioclase grain surrounded by a quartz-rich gouge. Abbreviations: Pyx- pyroxene, Chl- chlorite, Qz- quartz, Ser- sericite.

The principal slip surface of the fault core has a dark red to brown colour in both plain and cross polarized light with a glassy-like appearance. In general, the fault cores vary drastically with respect to lithology. Gabbronorites exhibit a very strongly foliated and clay-rich unconsolidated gouge, while tonalites appear to be comminuted, quartz-rich and vary in grain size.

4.3.3 Microstructures of Fault Core

Here we examine the microstructures of the Camp Lake fault core to understand the kinematics of the fault slip direction. The fault core consists of cataclasites and fault gouge, with phyllosilicates infilling fractures which in turn display a ductile overprint, showing that the fault core microstructures are quite complex.

Fault Rock Structures

Fault rocks include gouges and cataclasites from the gabbronorite and tonalite protoliths, with some samples containing both in thin section (Figure 4.16).The nature of the fault core is complex. There are lenses of what appears to be tonalite present within the gouge of the hanging

wall gabbronorite (Figure 4.16). It is apparent that there are two different types of gouge within the fault core, a darker phyllosilicate-rich gouge typically defined by the chlorite foliation, and a lighter quartz and plagioclase dominated gouge with accessory chlorite infilling fractures. A horizontal slip surface separates these two gouges. The gouges do not crosscut one another as they appear to be restricted to the respective protolith, however inclusions of either protolith is observed within each gouge. High resolution scans of fault core thin sections can be found in Appendix 4.

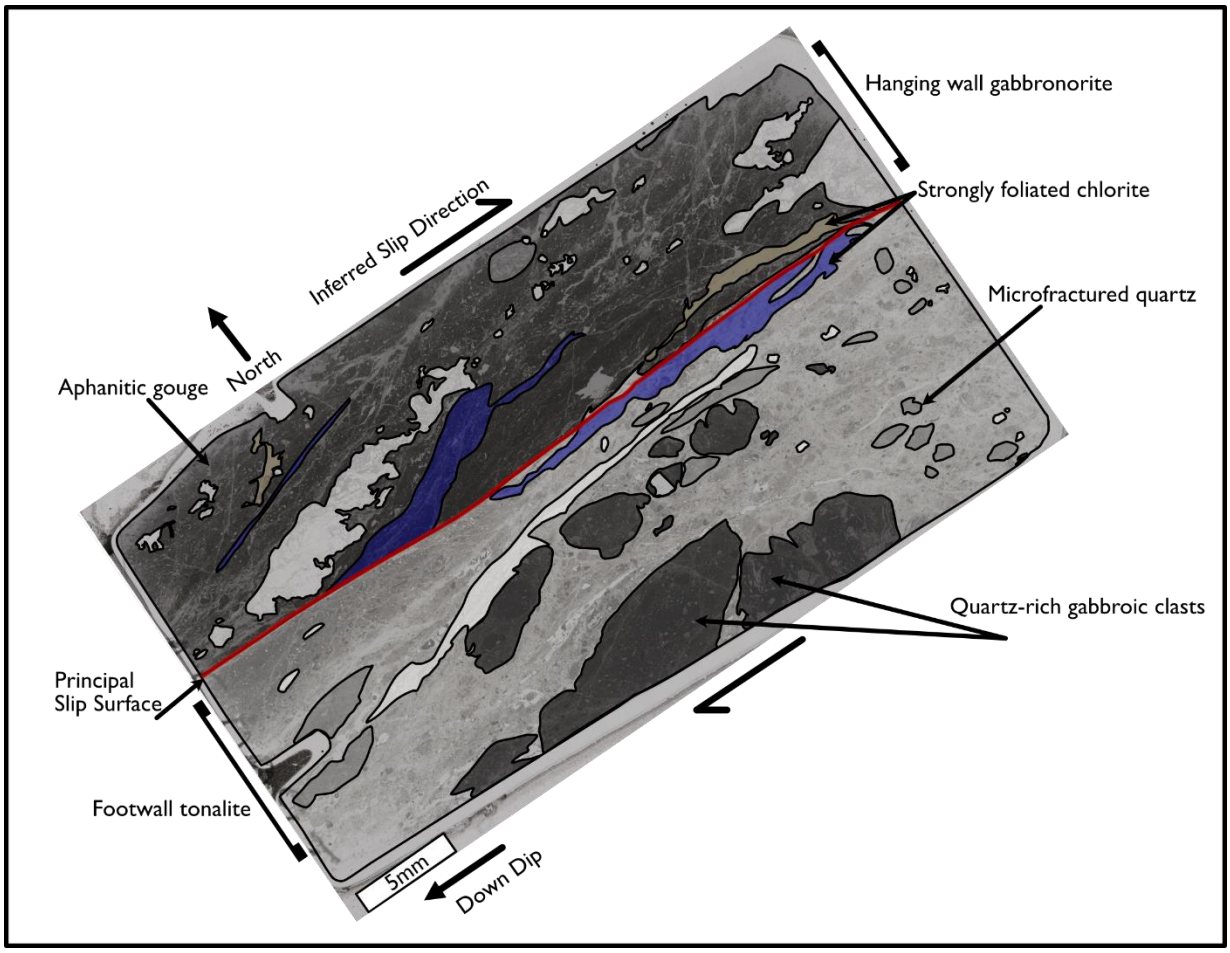

Figure 4.16 Annotated plane polarized photomicrograph of sample JP002A from the Camp Lake fault core. Highlighted are the hanging wall and footwall lithologies and their respective styles of gouge. Inclusions of each lithology inside the neighbouring gouge can be observed by the clasts. Microstructures are consistent with thrust faulting.

The nature of the gabbronorite fault core is quite complex, with more than one generation of fault gouge, and overprinting structures (Figure 4.17 A). Phyllosilicate minerals define the foliation within the gouge, predominantly in the gabbronorites which are strongly foliated (Figure 4.17 B). Fractured quartz clasts are often found within the chlorite-rich gouge. The weakly sheared clasts, ~300 µm, are surrounded by strongly foliated chlorite (Figure 4.17 C) with deflection of foliated chlorite around more rigid bodies. S-C fabrics and C-type shear bands are observable in the gabbronorite fault core. The principal slip surface defines the C-surface while the phyllosilicates are aligned with the S-surfaces (Figure 4.17 A-C). Occasionally,

plagioclase and quartz will follow a preferred orientation that is locally parallel to the chlorite foliation.

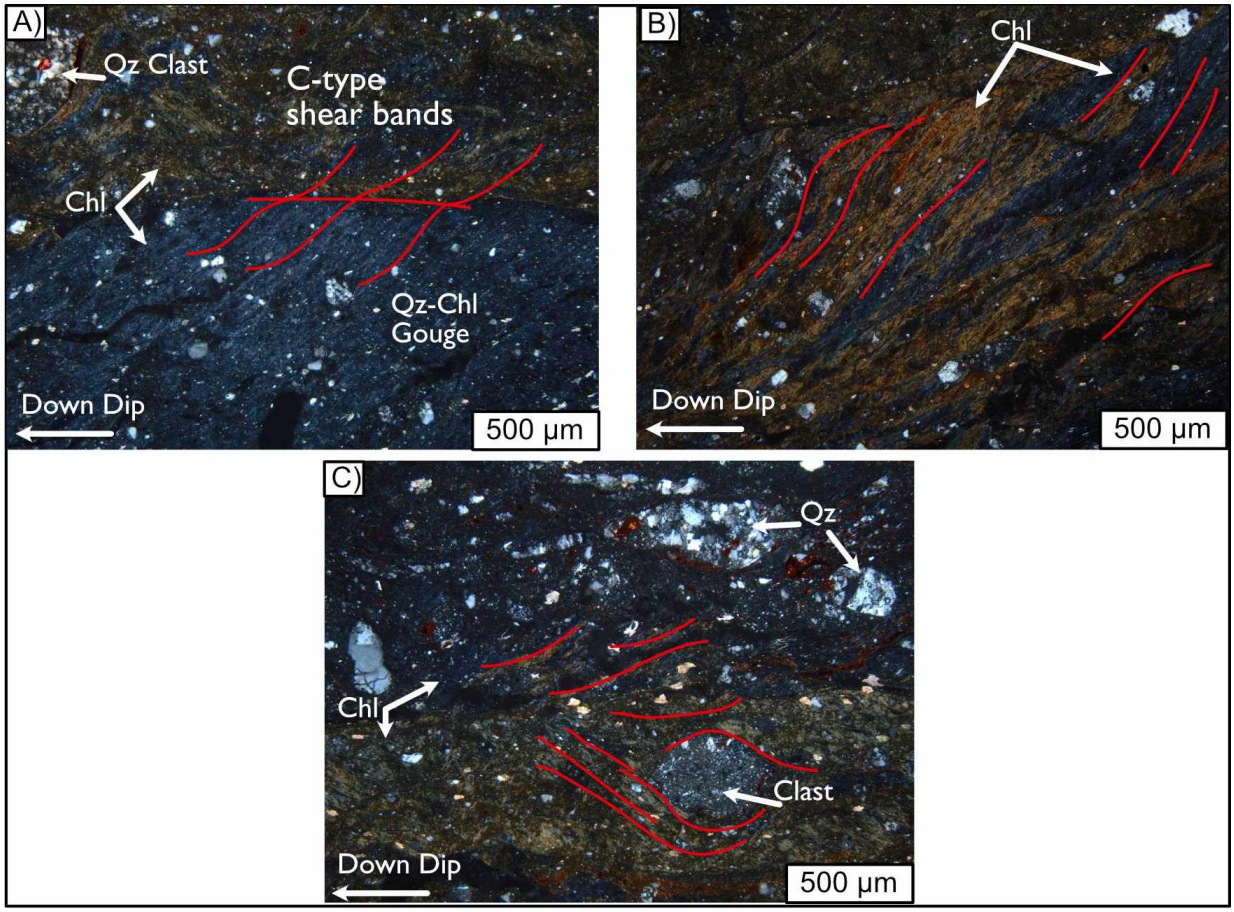

Figure 4.17 Cross polarized photomicrographs of microstructures from the gabbronorite fault core. A) More than one generation of gouge and chlorite species. S-C fabrics present in the gouge. B) Chlorite defining the foliation in the fault core. C) Foliated chlorite wrapping around more rigid quartz clast. Quartz-rich cataclasites (top) occur as clasts within the foliated chlorite. Abbreviations: Qz- quartz, Chl- chlorite.

Tonalite samples display strong evidence of cataclasis with silica infill. As mentioned above, quartz grains are highly variable in size throughout the sample and thin section (Figure 4.18 A). Microcracks are common within quartz grains (Figure 4.18 B). The plagioclase grains display extreme pervasive sericite alteration and are associated with remnant pyroxene grains. The larger quartz grains show evidence for subgrain rotation crystallization (Figure 4.18 B) and are typically surrounded by gouges (Figure 4.14 B). The gouges of the tonalite samples are less complex than the gouges of the gabbronorites, as the orientation is random, and there is not

always a strong foliation or fabric within the gouge. However, it is apparent that within the tonalite there is more than one generation of cataclasite. An original cataclasite fabric featuring the breakdown of quartz grains is apparent by the larger dark brown to black clasts (in PPL), which is surrounded by, and composed of, additional smaller grains of quartz and plagioclase, typically with a lighter brown colour in PPL (Figure 4.18 C). Riedel shears are common in brittle fault zones and can be observed in Figure 4.18 C. The Y-shears are referred to as boundary faults and are parallel to the fault, while R-shears are at an angle to the Y-shears, and P-shears are at a back angle to the Y-shears.

In general, it is apparent that both the gabbronorite and tonalite have undergone brittle deformation during the faulting process, the tonalites exhibit stronger more apparent brittle features (*i.e.,* Riedel shears) whereas the gabbronorites display a combination of brittle and ductile features as defined by the fabrics in the fault core (Figure 4.18 C)

The potential sources of error during the petrography data collection process are minimal. To ensure the thin sections were made in the correct orientation, photos and scans were taken before the billet cutting process and were referenced during and afterwards. During petrographic analysis of the thin sections, these scans were referred to when needed.

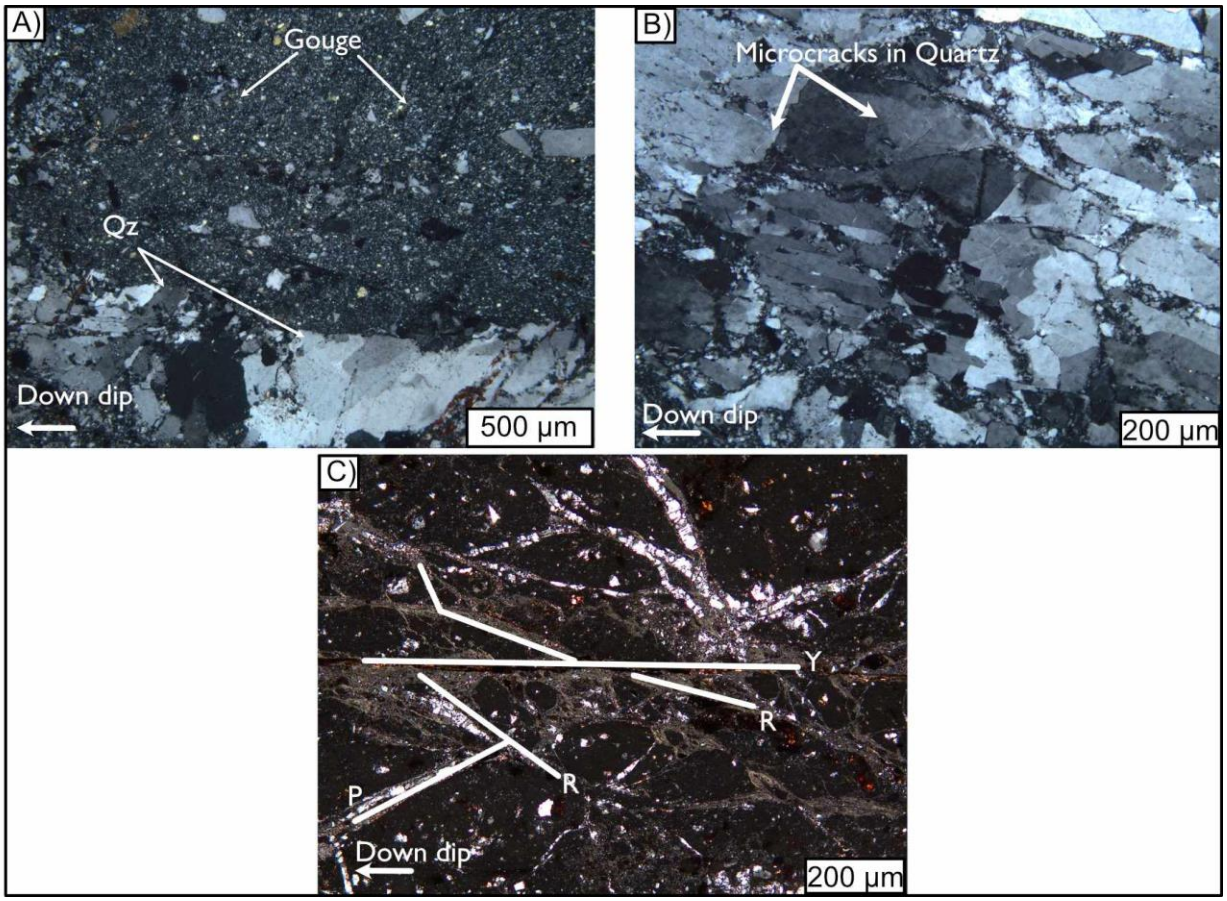

Figure 4.18 Cross polarized photomicrographs of microstructures from the tonalite fault core. A) Quartz-rich gouge surrounded by either late quartz grains from veining, or remnant grains that were not comminuted. B) Microcracks in fractured quartz grains with comminuted quartz grains in between larger grains. C) Riedel shears in the tonalite fault core. Clasts are aphanitic in both XPL and PPL but appear to be composed of chlorite, pyroxene and quartz. Chlorite (brown) is present in fractures along with quartz. Abbreviations: Qz- quartz, Chl- chlorite.

4.4 Scanning Electron Microscopy

Because of the very fine-grained nature of the fault gouges, they were often not distinguishable through optical microscopy. Scanning electron microscopy (SEM) was used to obtain compositions of fault gouges and for analysis of microstructures within the gouge. The microscopic structures, fabrics, and mineralogy were examined in oriented thin sections taken from the exposed fault surfaces.

Observations of fault gouge under the SEM show that fragments range from angular to sub-rounded, are often foliated, and are aligned parallel with the main fabric in the gouge. Clay

minerals, predominantly the preferred orientation of chlorite, along with the fragmented silicate minerals compose and define the fabric within the gouge (Figure 4.19 A & C). Fault surfaces in gabbronorite samples are predominately composed of phyllosilicate minerals, are well foliated, and often contain a principal slip surface. Fault core samples from tonalites are less foliated, more angular and do not appear to follow any general fabric (Figure 4.19 B & D). Foliated gouge compositions are dominated by various chlorite and epidote group minerals (*i.e.*, clinochlore and pumpellyite to epidote) whereas the dominant minerals within the unfoliated gouges appear to be cemented fragments of albite and quartz, with epidote alteration. The principal slip surface under the SEM returns high readings of Ca, S and O (Figure 4.20 A, B) corresponding to a formula of $CaSO_4$, or gypsum.

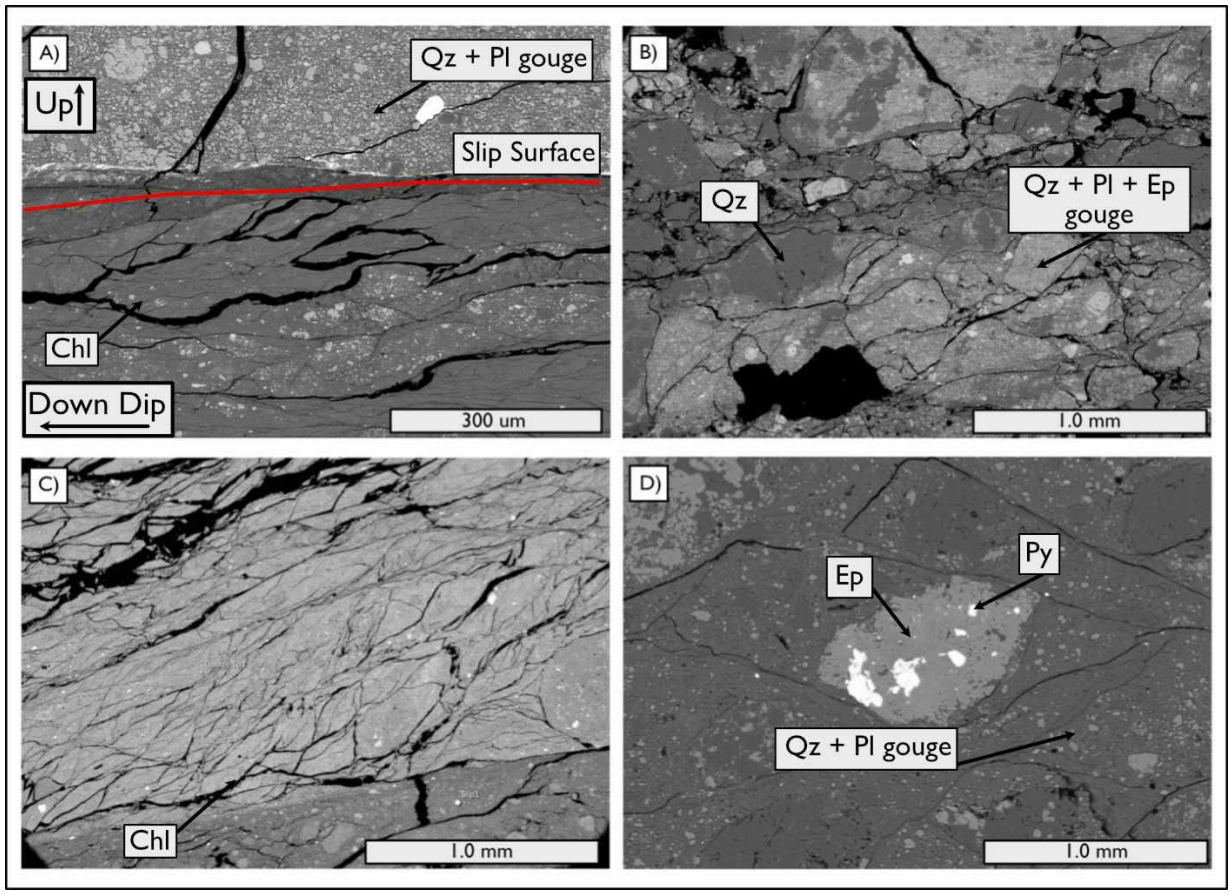

Figure 4.19 A) SEM image of foliated fault gouge displaying the fabric in a chlorite-rich gouge, derived from gabbronorite (bottom) compared to the random nature of the gouges in the tonalites (top). B) Typical SEM image of fault gouge derived from tonalite. C) Phyllosilicate minerals showing preferred alignment in the fault core. D) SEM image of ~1mm sized epidote altered clast within a finer grained matrix. Abbreviations: Qz- quartz, Chl- chlorite, Pl- plagioclase, Ep- epidote.

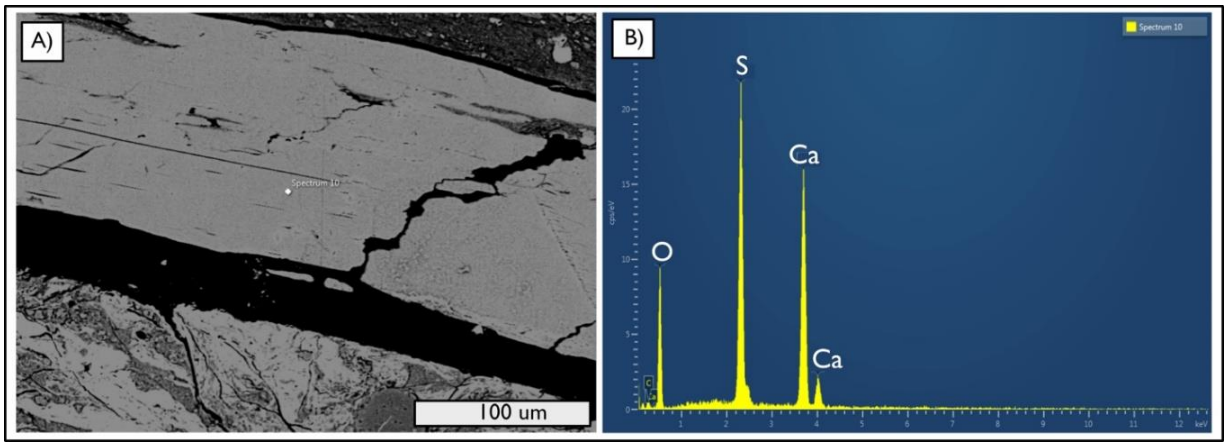

Figure 4.20 A) SEM scan of principal slip surface from the Camp Lake fault. B) Spectra of chemical components from principal slip surface.

4.5 X-Ray Diffraction

XRD of randomly oriented powders gives an approximate bulk mineralogy for the analyzed samples. Samples were taken from damage zones (in the hanging wall and footwall) and the fault core from four Camp Lake fault intercepts and one Offset fault intercept. Samples include highly altered gabbronorites, clay-rich fault gouge, silicified cataclasite, and highly altered tonalite (Figure 4.21). Analyzed samples of the gabbronorites and clay-rich gouges all show elevated (compared to the damage zone samples) quantities of chlorite (up to 37% of the mineral percentage) and quartz (up to 15%) within the fault core, while tonalite fault core samples are dominated by higher quantities of albite (up to 29% of the mineral percentage) and quartz (up to 25%; Figure 4.21 A-F). A generalized trend of changes in mineral percentages can be observed when moving across the fault zone, however, the increase or decrease in mineral percentages is likely related to the surrounding protoliths as the fault is at times, irregular with respect to lithology and alteration.

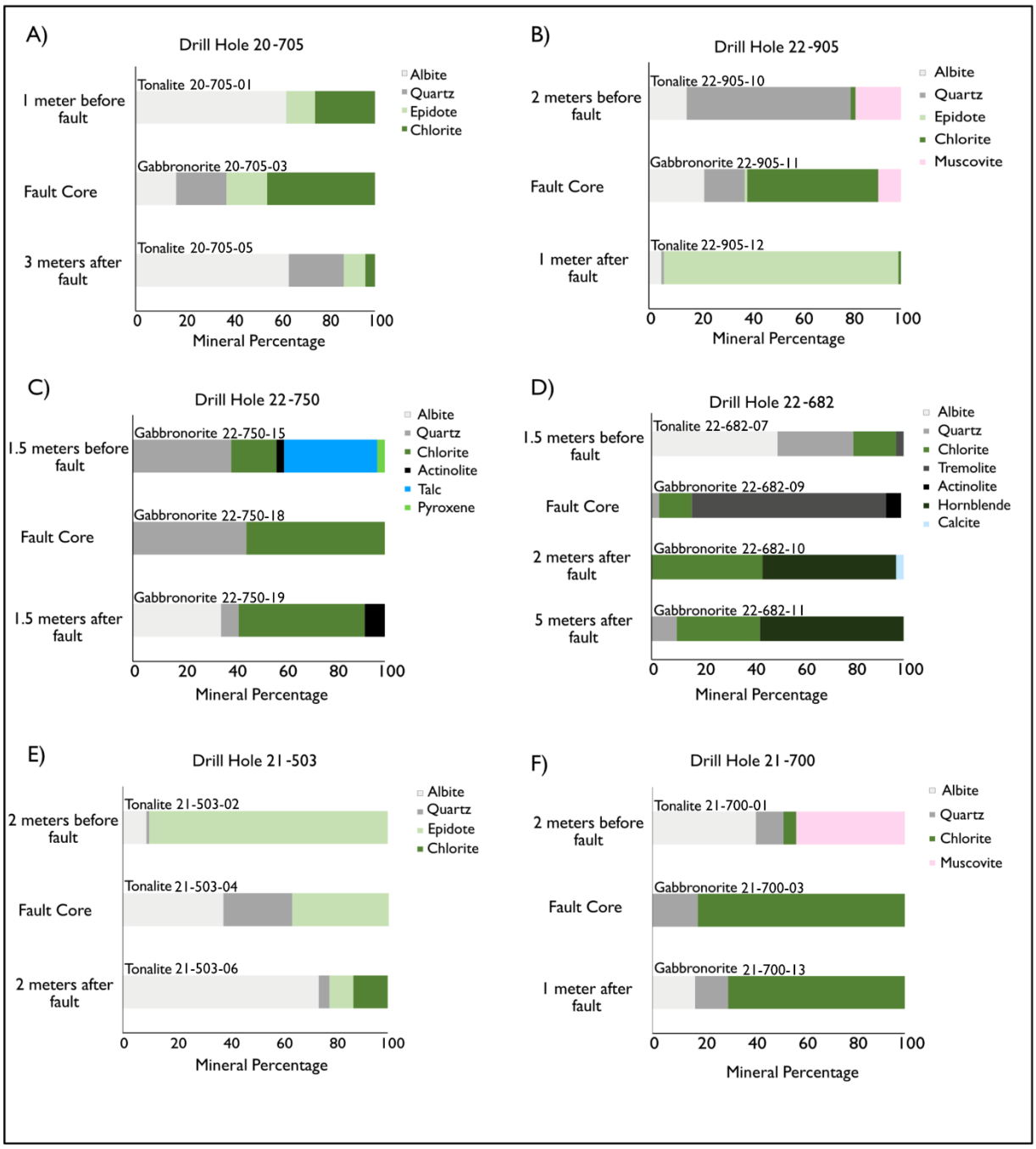

Figure 4.21 Bar charts of mineralogy determined through Rietveld analysis of XRD spectra. Charts A, B, C, E and F belong to the Camp Lake fault drill holes, and chart D belongs to the Offset fault drill hole.

Oriented clay slides were also analyzed. All gabbronorite samples display well developed (001) to (004) peaks for chlorite (Figure 4.22). Albite (002) peaks are also well developed in many samples alongside quartz. Glycolation affected sample 22-682-09, adding a small peak around 4 degrees 2-theta, and sample 22-750-18 were shifted to the left by approximately one

degree 2-theta (Figure 4.22 C), implying there are swelling clays within the fault core of 22-682 from the Offset Block.

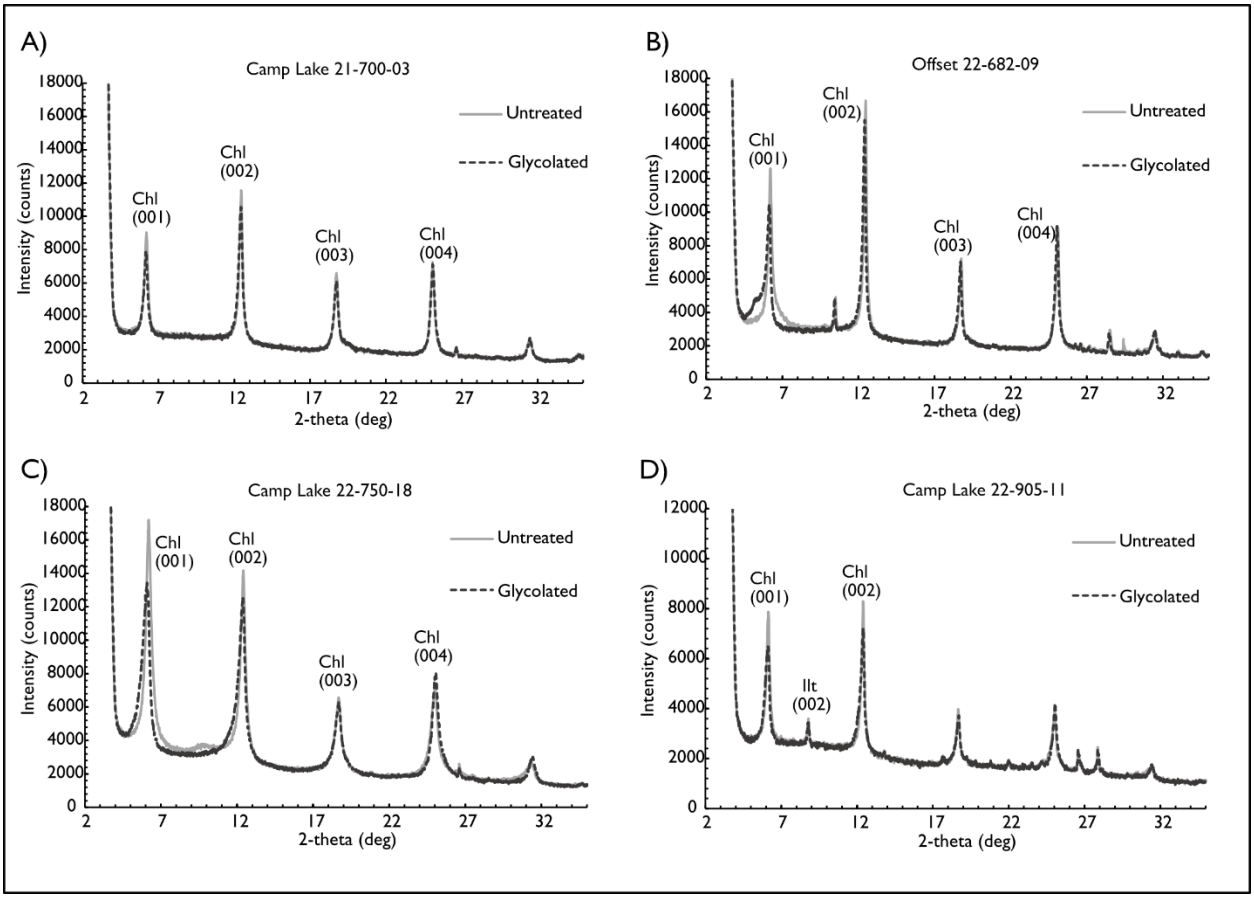

Figure 4.22 Spectra from XRD of oriented clay aggregates from drill hole samples. A) 21-700-03 displays well-defined chlorite peaks. B) 22-682-09 with bump on the Chl (001) peak following glycolation. C) 22-750-18 displaying leftward shift of (002) peak from glycolation. D) 22-905-11 spectra with illite (002) peak.

A (002) reflection of illite is present at 9 degrees 2-theta in sample 22-905-11. Plotting chlorite crystallinity on a single variate Kübler Index (Figure 4.23) displays the fault core samples, as denoted by coloured squares, are of lower metamorphic grades than the surrounding hanging wall and footwall from each drill hole, except for the footwall sample from drill hole 21-503. The remainder of the hanging wall and footwall samples plot in the range from upper to lower epizone. A single variate Kübler index was chosen due to the lack of illite present within

the samples. The low and high anchizone can be defined as the prograde limit of diagenesis and the onset of the epizone (Kisch, 1987; Battaglia et al., 2004) before metamorphism occurs.

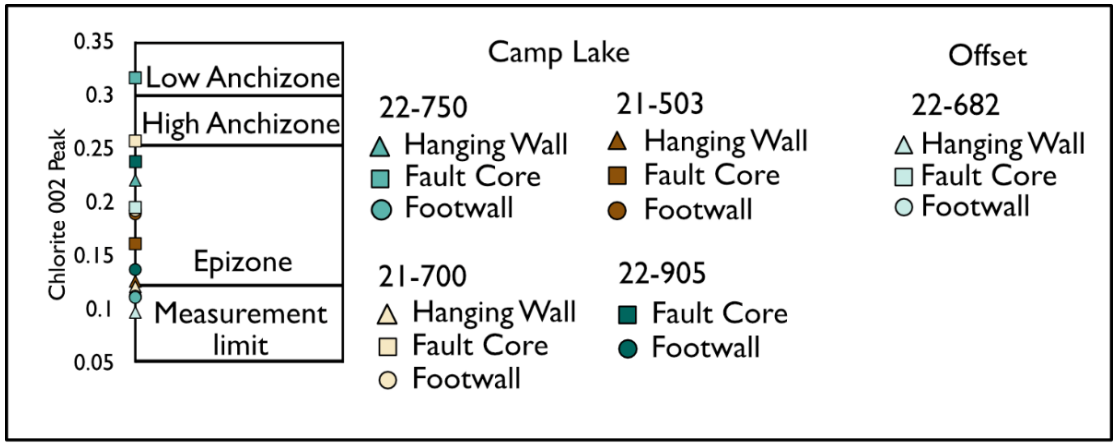

Figure 4.23 Single variate Kübler index results from oriented slides analyzed via XRD.

Contamination of samples may be the largest potential source of error during the data collection process of XRD powders. To ensure the samples were not contaminated with previous sample powder, the mortar and pestle were wiped and cleaned with compressed air to remove any remnant particles or dust that remained from the previously prepared sample.

4.6 Fracture Density

Across all drill holes sampled and analyzed for fracture density a visible trend was observed which is consistent with the idealized fault zone model. Fracture density increased with proximity to the fault core in both the hanging wall and footwall. Both lithologies, gabbronorites and tonalites, display this trend. Tonalite intervals display a greater increase in fracture density with proximity to faulting when compared to the gabbronorite units, as well as a greater decay rate on average (Figures 4.24 and 4.25). Background fracture density in the Camp Lake and Offset gabbronorite and tonalite averages 1-2 fractures per meter, with fracture densities as low as 1 fracture per meter, with the exception of drill hole 22-682, where the tonalite from the

Offset fault does not meet the typical observed background fracture density, due to the intercept of the Offset fault at a shallower level in the drill core.

Drillhole 18-602, which crosscuts the Offset fault, intercepts gabbronorite in both the hanging wall and footwall of the Offset fault (Figure 4.25 D). The fracture density data collected from this drillhole displays a similar trend on both sides of the fault, with the footwall exhibiting a slightly faster decay rate (0.69 compared to the 0.59 of the hanging wall). The width of the damage zone can vary with respect to lithology. The damage zone width on average observed in both lithologies can range from 30 to 60 meters.

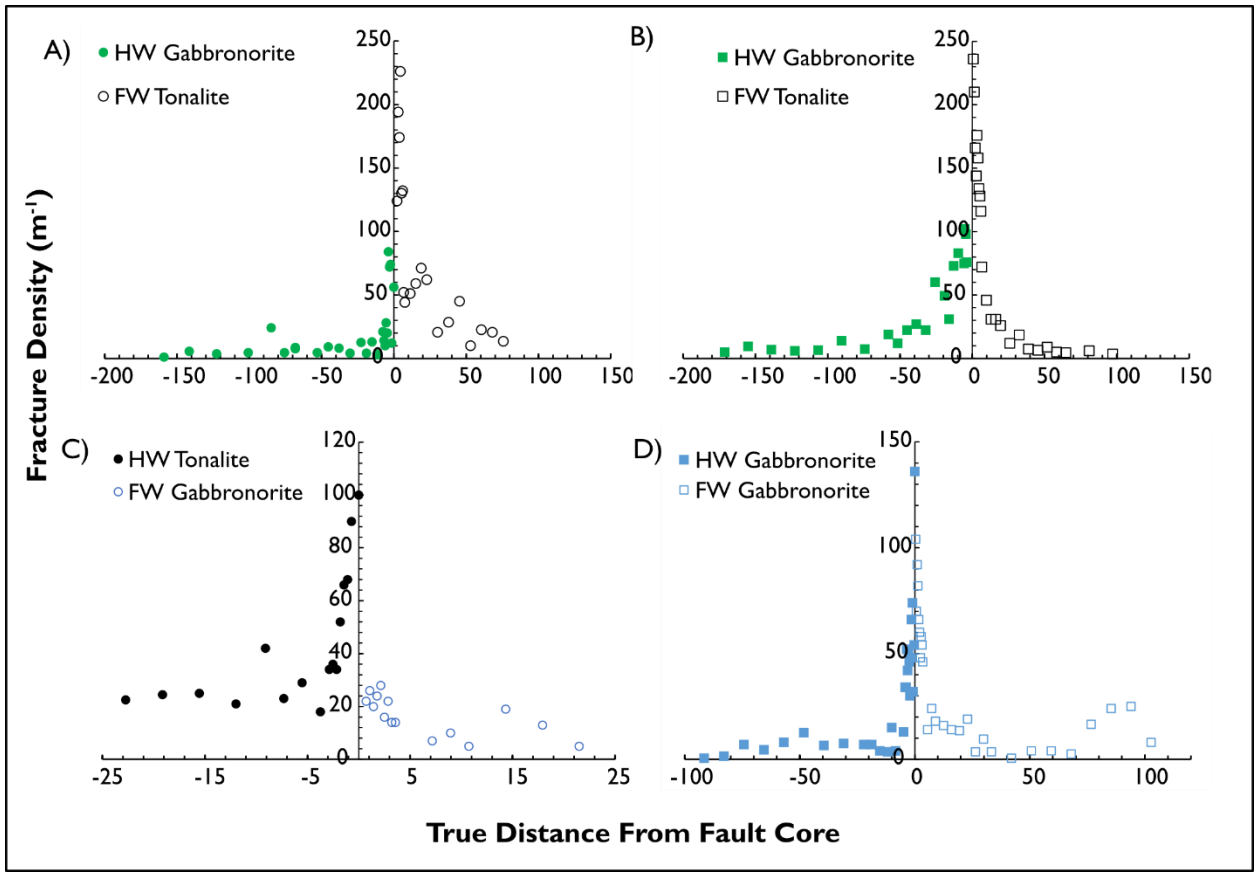

Figure 4.24 Fracture density plots for Camp Lake and Offset drill holes. A) Camp Lake drill hole 22-750 B) Camp Lake drill hole 21-503 C) Offset drill hole 22-682 D) Offset drill hole 18-602, intercepting gabbronorite in hanging wall and footwall. Gabbronorites in the Camp Lake fault zone are coloured green, and gabbronorite in the Offset fault zone are coloured blue. Tonalites are black for both fault zones.

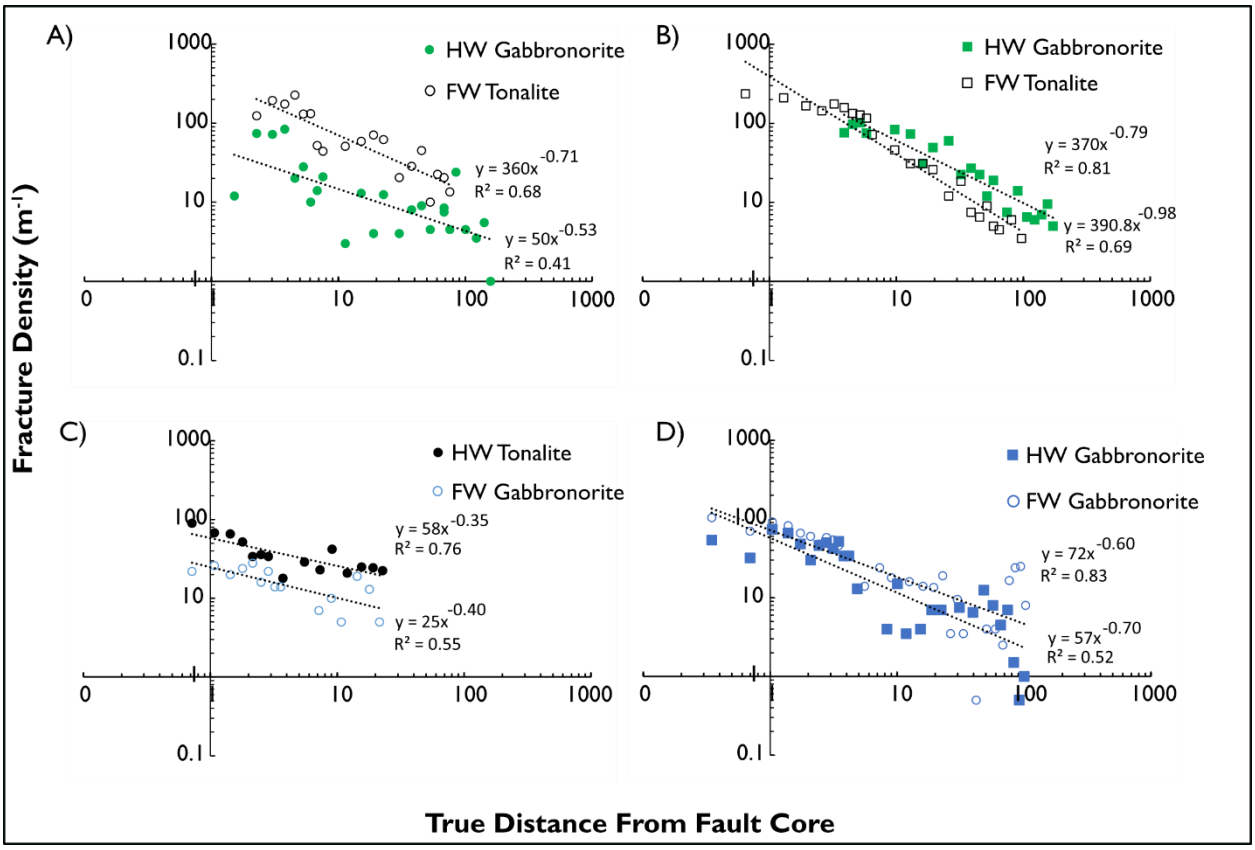

Figure 4.25 Fracture densities of drill holes from Figure 4.24 plotted in log-log space. A) Camp Lake drill hole 22-750 B) Camp Lake drill hole 21-503 C) Offset drill hole 22-682 D) Offset drill hole 18-602.Gabbronorites in the Camp Lake fault zone are coloured green, and gabbronorite in the Offset fault zone are coloured blue. Tonalites are black for both fault zones.

Camp Lake tonalite decay rates range from 0.52 ± 0.06 to 0.98 ± 0.05 while Camp Lake gabbronorite decay rates range from 0.26 ± 0.11 to 0.79 ± 0.06. Similarly, damage decay rates in tonalites from the Offset fault range from 0.35 ± 0.07 to 0.40 ± 0.05 with gabbronorite damage decay rates ranging from 0.39 ± 0.1 to 0.69 ± 0.08 (Figures 4.26 & 4.27). There is potential for analytical and human error when counting fracture densities. We found that during the data collection process, fractures were the most obvious in tonalite, as they were often filled with epidote or sericite and had a high colour contrast, while fractures in gabbronorite were not always as apparent. We logged several drill holes from each fault to reduce uncertainty (See Appendix 5 for fracture density plots).

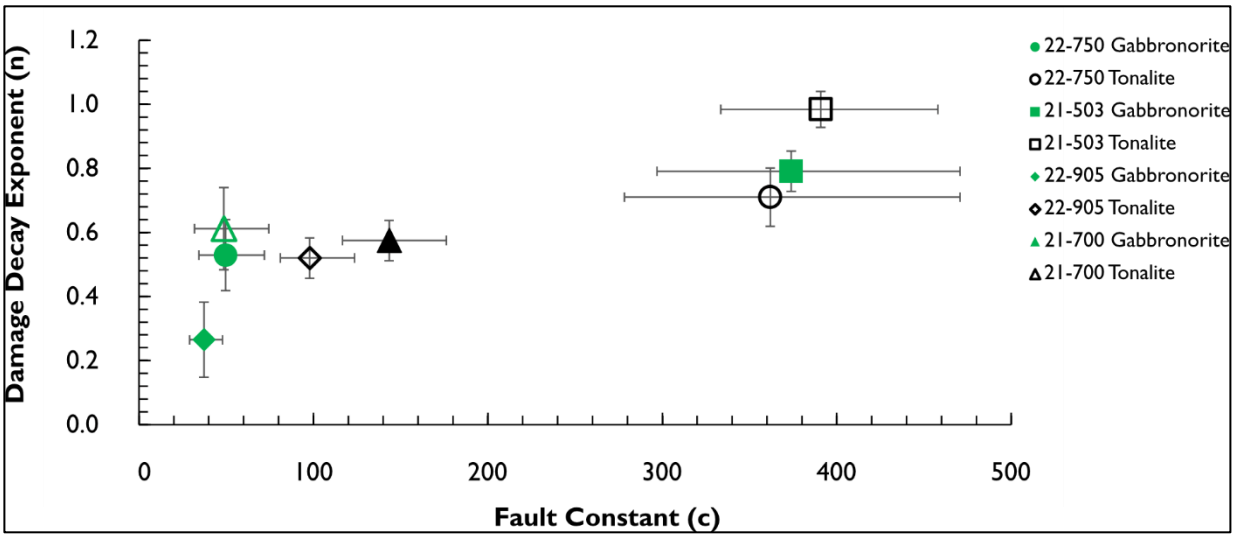

Figure 4.26 Plot of power law fit parameters for Camp Lake fault fracture density measurements.

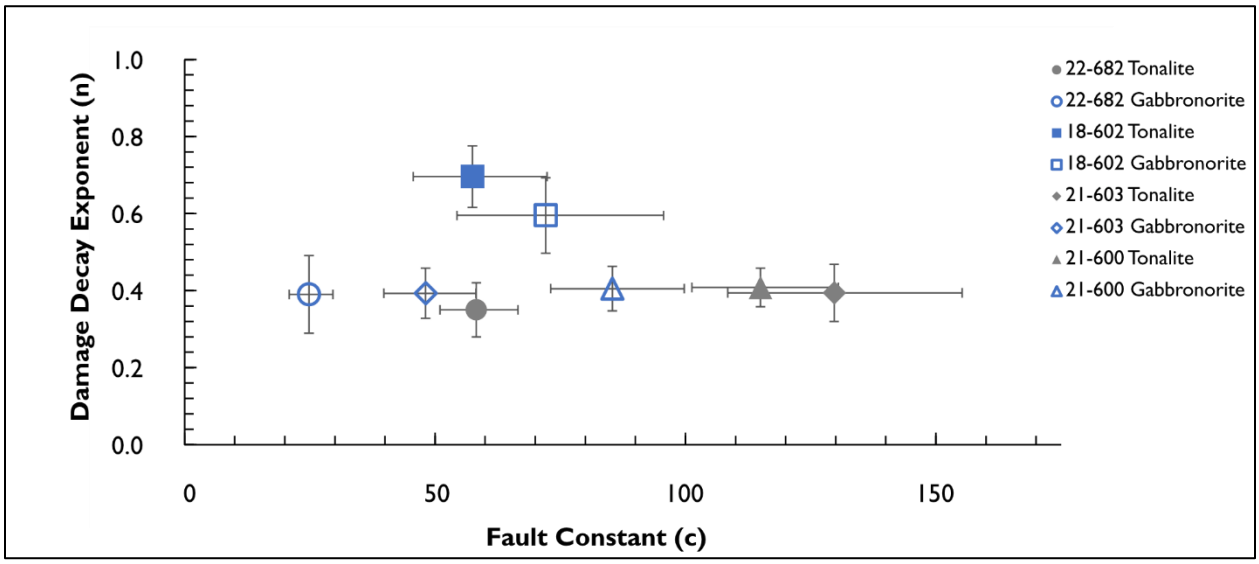

Figure 4.27 Plot of power law fit parameters for Offset fault fracture density measurements.

4.7 Whole Rock Geochemistry

Whole rock geochemistry was used to classify the lithologies present along with petrographic observations and observe how it varies with proximity to the fault core. Geochemical characteristics and trends were observed through major and trace element concentrations to evaluate the genesis and alteration of protoliths with proximity to faulting. Hydrothermal alteration is common in fault zones; thus, it is an important to take alteration into consideration when analyzing geochemical signatures. A complete list of all geochemical data is included in Appendix 3.

Initial rock classifications were conducted during field work and sampling based on textures and mineralogy. Igneous rock classifications are often based on whole-rock major element lithogeochemistry. However, when the original igneous mineralogical assemblages have been altered or destroyed by the faulting process, the use of trace element or immobile element ratios is preferred.

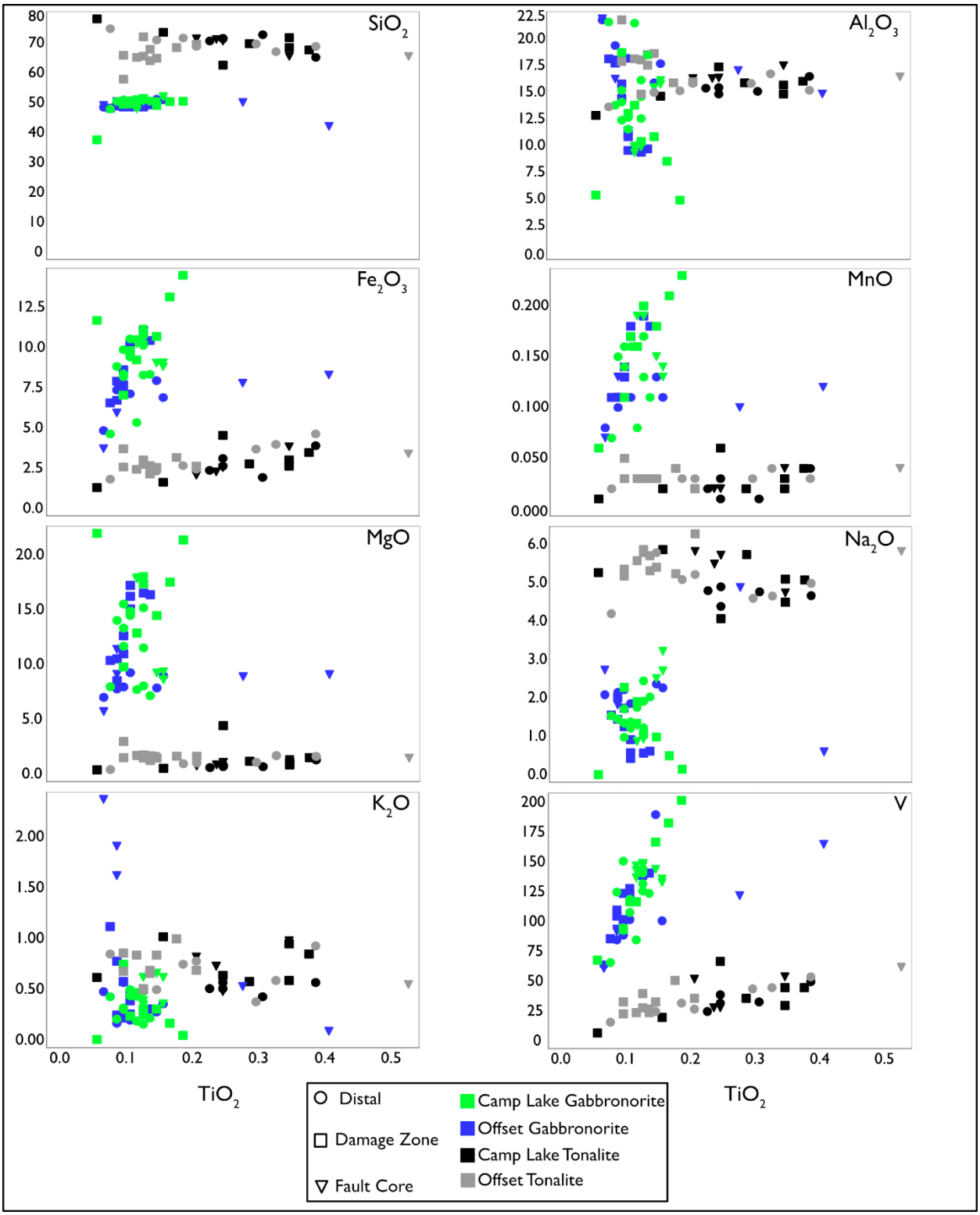

Figure 4.28 Bivariate plots of major elements and vanadium vs TiO_2 for Camp Lake and Offset fault drill holes.

4.7.1 Camp Lake Geochemistry

Of the 51 samples taken from the Camp Lake Zone, 27 were from the hanging wall approaching the fault, with the remaining 24 taken from the footwall extending into the Camp Lake Block. The fault core from this drill hole (22-750) is approximately 20 cm wide. Lithologies range geochemically from gabbro to granodiorite. An increase in alteration intensity is observed with proximity to the fault core. Downhole plots of major element oxides are plotted in Figure 4.29. A general trend observed in the downhole plots from the Camp Lake Zone are the increased variations in major element oxides with proximity to faulting. Damage zone hanging wall and footwall samples near the fault core display the largest variations in abundance.

Trace element concentrations from Camp Lake drill hole 22-750 are plotted on spider diagrams normalized to primitive mantle values of Sun & McDonough, (1989) with distal (to fault), damage zone and fault core samples separated along with lithology (Figures 4.31 & 4.32). The most distal gabbronorite trace element patterns display weakly enriched light rare earth element (LREE) profiles, relatively flat HREE patterns, a moderate negative Nb anomaly, a weakly positive Eu anomaly and a weakly negative Ti anomaly. Zirconium and Hf display weakly negative to positive anomalies. Damage zone gabbronorite samples display a slightly smaller negative Nb anomaly, less La enrichment, a more negative Eu anomaly, and a more widespread, but overall flatter LREE to HREE pattern relative to their distal counterparts (Figure 4.30). Fault core gabbronorite samples have a relatively similar LREE to HREE pattern to that of the distal samples, except for slightly higher Th, Nb, and La concentrations, steeper patterns, and a more pronounced positive Eu anomaly. Tonalite samples have highly variable LREE and trace element concentrations and show a correlation between enrichment and distance from fault core.

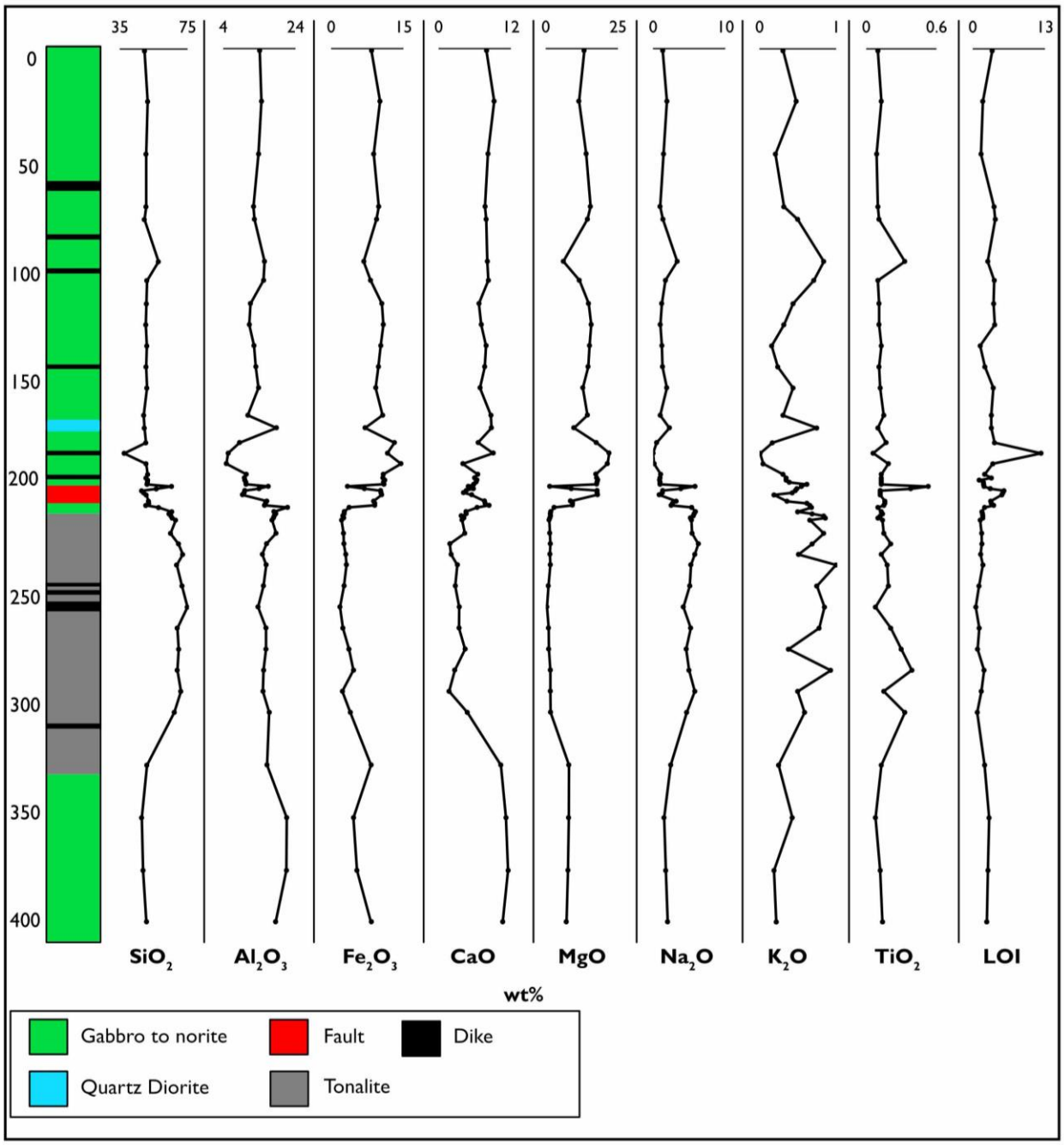

Figure 4.29 Downhole plots and stratigraphic column of major element oxides and LOI for Camp Lake fault drill hole.

Damage zone samples show the weakest positive anomalies, distal samples show stronger positive anomalies, and the fault core shows the strongest positive anomalies of LREEs. Tonalite samples have very weakly negative to very strongly positive Th and Nb anomalies, strong positive La anomalies, and have shallow negative trending primitive mantle normalized HREE

patterns. They all have moderate positive Eu anomalies, and weakly negative to weakly positive Ti anomalies. HREEs are weakly depleted in most samples and are relatively flat.

Gabbronorite samples from this drill hole show some variability in REE patterns in the fault core samples, with Pr, Nd, Zr, Hf, Sm, and Eu showing weakly elevated levels when compared to the most distal samples. Tonalite samples do not display any distinct variations in REE patterns.

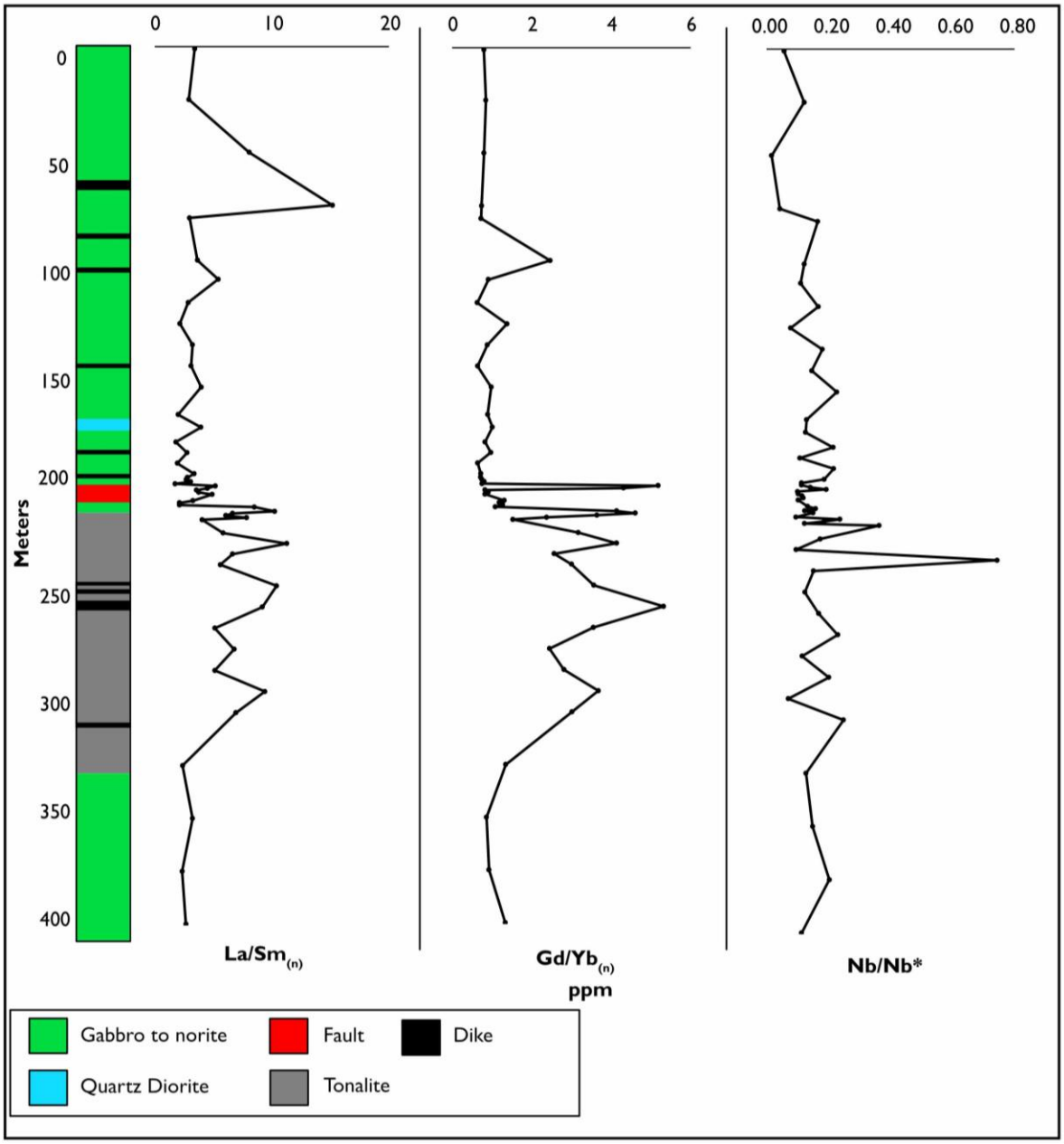

Figure 4.30 Downhole plots and stratigraphic columns for trace element ratios of the Camp Lake drill hole. Normalizing values from Sun & McDonough (1989). $La/Sm_{(n)}$, $Gd/Yb_{(n)}$, and Nb/Nb are trace element ratios normalized to primitive mantle values.*

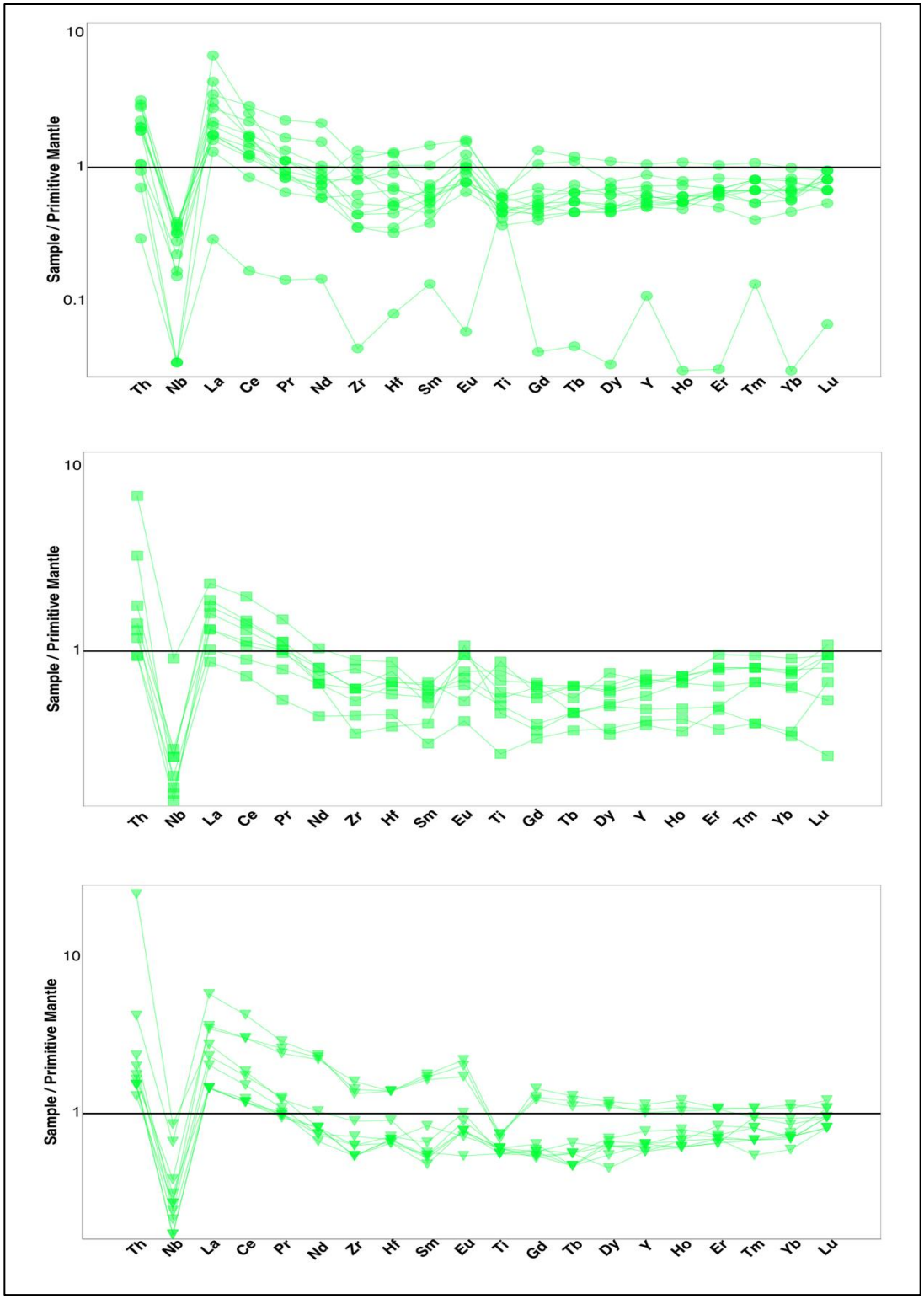

Figure 4.31 Primitive mantle normalized spider diagram for Camp Lake fault drill hole gabbronorite samples. Distal samples are denoted with circles, damage zone with squares, and fault core with triangles. Normalizing values from Sun & McDonough (1989).

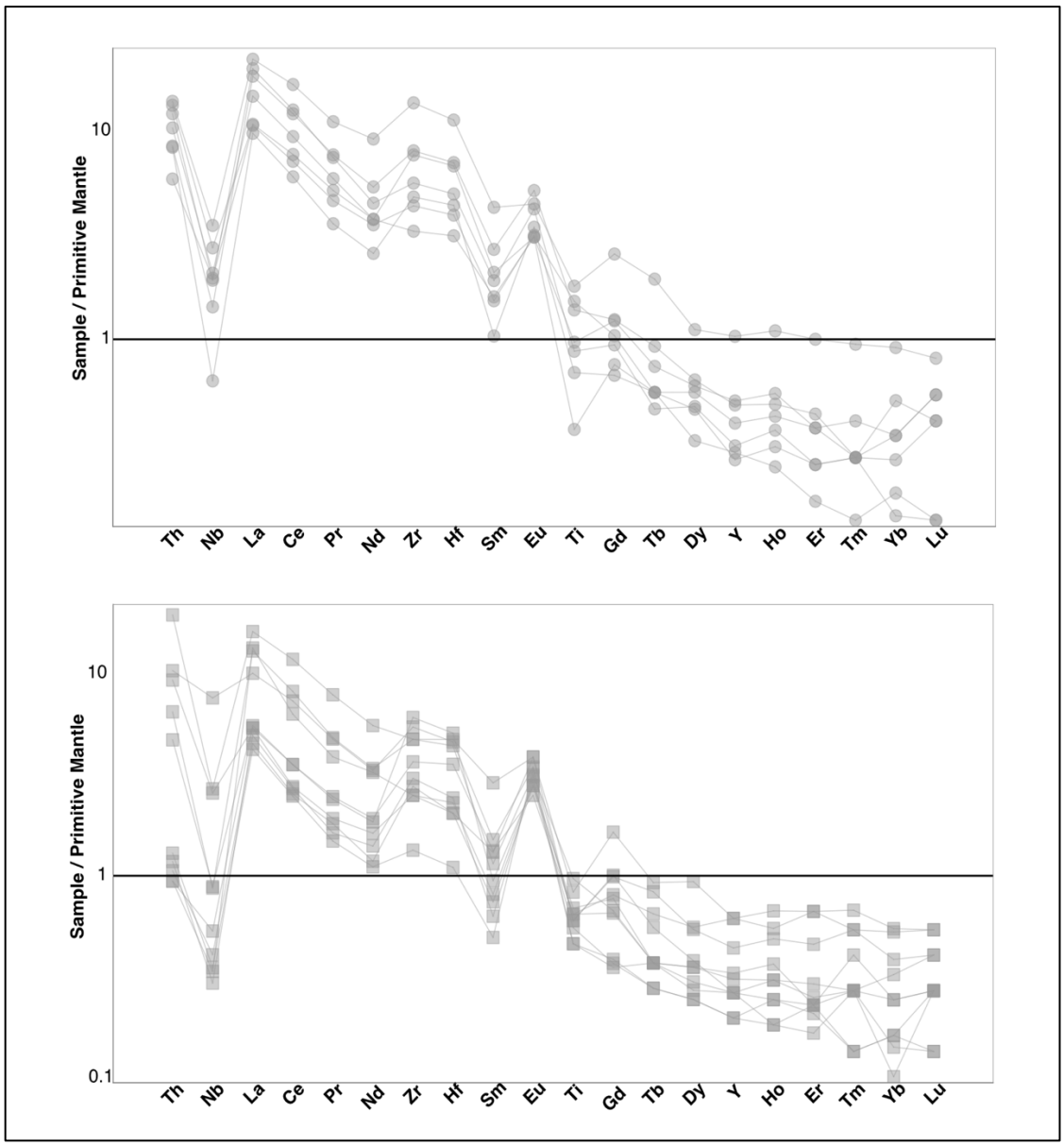

Figure 4.32 Primitive mantle normalized spider diagram for Camp Lake fault drill hole tonalite samples. Distal samples are denoted with circles, damage zone with squares. Normalizing values from Sun & McDonough (1989).

4.7.2 Offset Geochemistry

Thirty-seven samples were taken from Offset drill hole 21-603, 17 from the hanging wall and 20 from the footwall. The lithologies are variably altered gabbronorites and tonalites with fault core gabbroic units displaying a wider variation in total alkali ($Na_2O + K_2O$) composition, and one sample with a significantly lower SiO_2 concentration than their damage zone and least altered equivalents. The remaining gabbro-gabbronorite samples (damage zone and distal) plot in

the gabbro field of the TAS Plutonic diagram from Middlemost (1994; See Appendix 6 for additional plots). Similar to the Camp Lake drill hole, the intercepted lithologies in the Offset drill hole occur in domains with sharp contacts. The degree of alteration, as defined by increased abundance of alteration minerals and increased geochemical variability, increases in the drill hole with proximity to the fault core. Downhole plots of samples taken from this drill hole (Figure 4.33) show variations in major element oxides with most notable variations occurring in the damage zone surrounding the Offset fault (100-140m).

Trace element concentrations from drill hole 21-603 are plotted on a spider diagram normalized to primitive mantle values of Sun and McDonough (1989; Figures 4.35 & 4.36). Tonalites exhibit a moderately evolved signature, with moderate enrichments of LREE and trace elements (Th, Nb, Zr and Hf), and a strong positive Eu anomaly but a weakly positive Ti anomaly in most samples. Curves display moderate negative slopes for LREEs and flat patterns for HREEs. The most distal samples appear to show less variation in LREE concentrations than those of the damage zone and show higher concentrations on average. Damage zone samples also show more variation in HREE concentrations.

Gabbronorite samples display moderately positive Th and negative Nb anomalies, with fault core samples showing the largest positive anomalies compared to the distal and damage zone samples (Figure 4.33). Most samples show relatively flat LREE to HREE patterns, with positive Eu anomalies and negative Ti anomalies. Zr and Hf anomalies range from weakly negative to strongly positive. Distal samples show the least amount of variation and are relatively flat curves. Distal and damage zone samples both display weakly positive La anomalies, whereas some fault core samples have strong positive La anomalies. The enrichments of gabbronorite fault core are similar to the tonalite samples (strong positive La anomaly, weakly positive Ti, and

relatively flat HREEs) but also follows the pattern exhibited by the remaining gabbronorite samples. The samples display some evidence for REE mobility within the fault core.

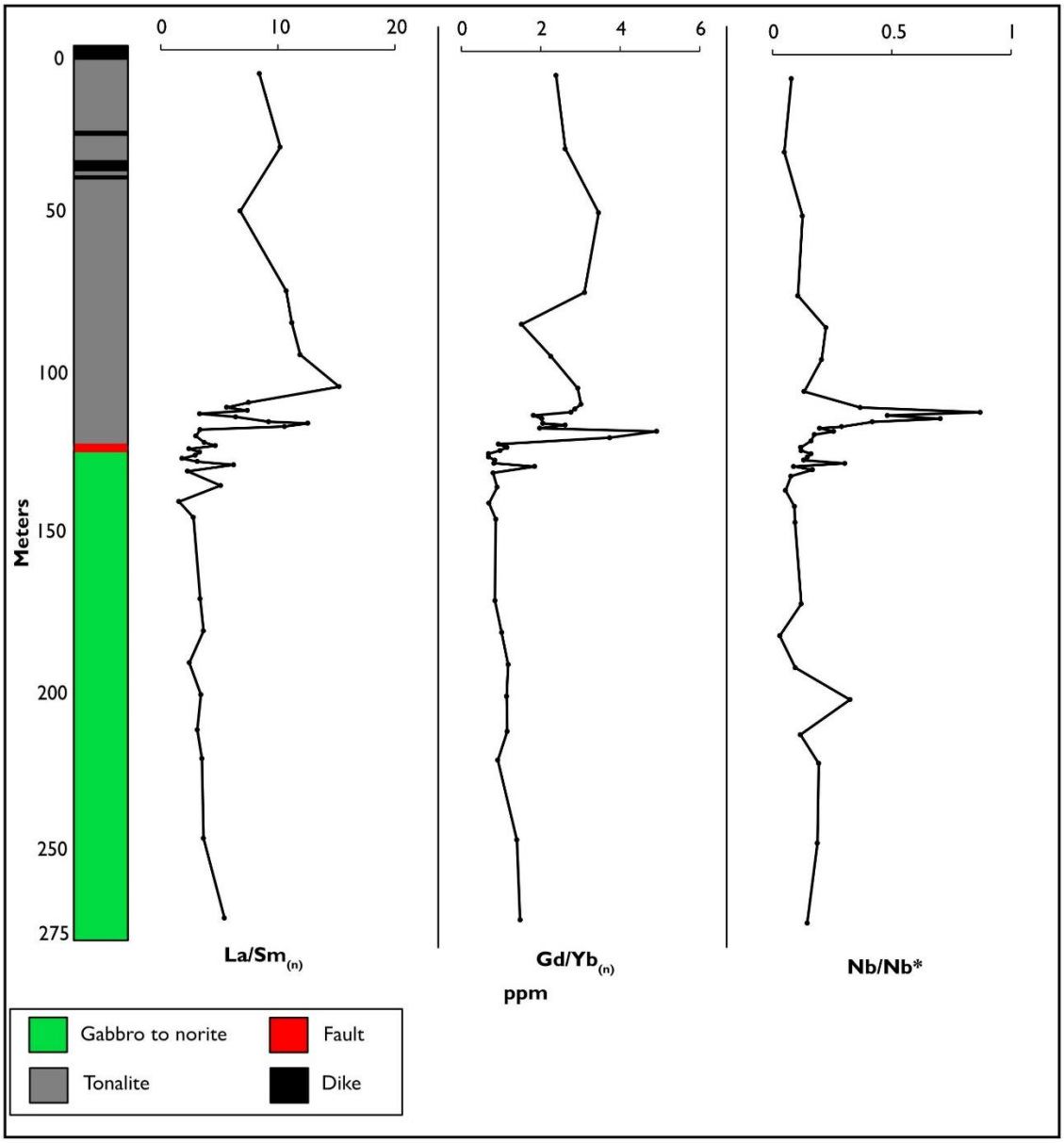

Figure 4.33 Downhole plots and stratigraphic columns for trace element ratios of the Offset fault drill hole. Normalizing values from Sun & McDonough (1989).

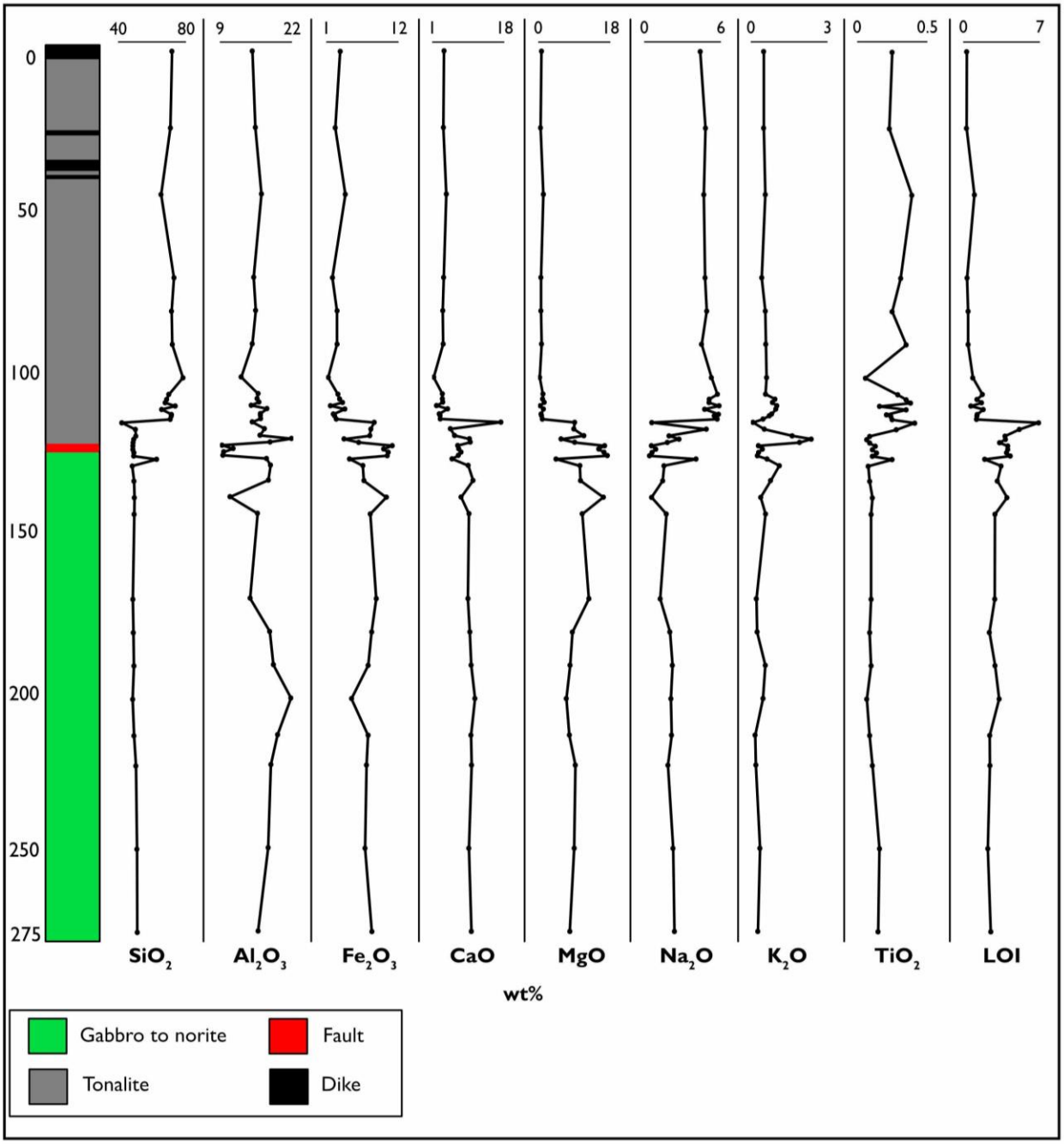

Figure 4.34 Downhole plots and stratigraphic column of major element oxides and LOI for Offset fault drill hole.

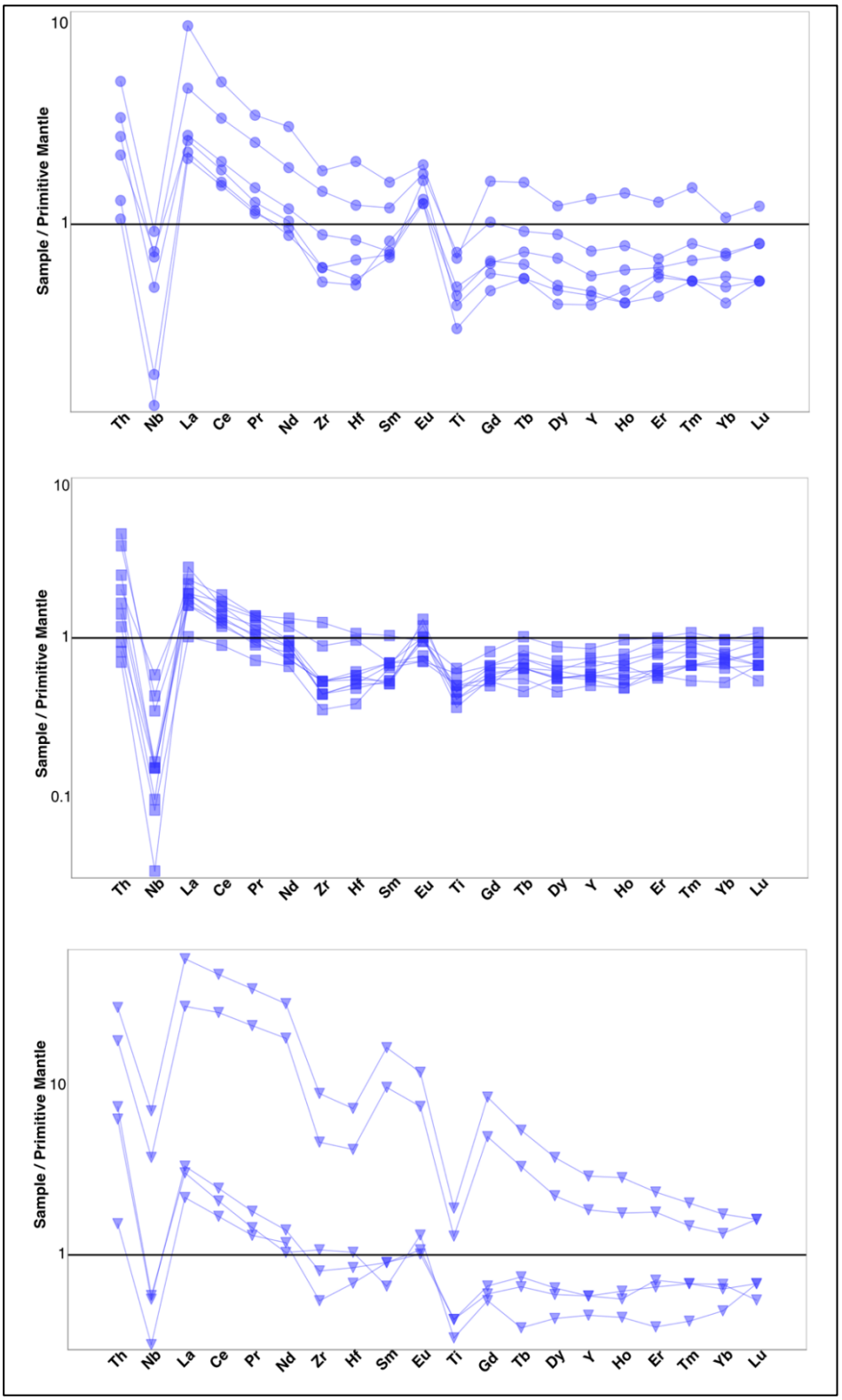

Figure 4.35 Primitive mantle normalized spider diagram for Offset fault drill hole gabbronorites. Distal samples are denoted by circles, damage zone by squares, and fault core by triangles. Normalizing values from Sun & McDonough (1989).

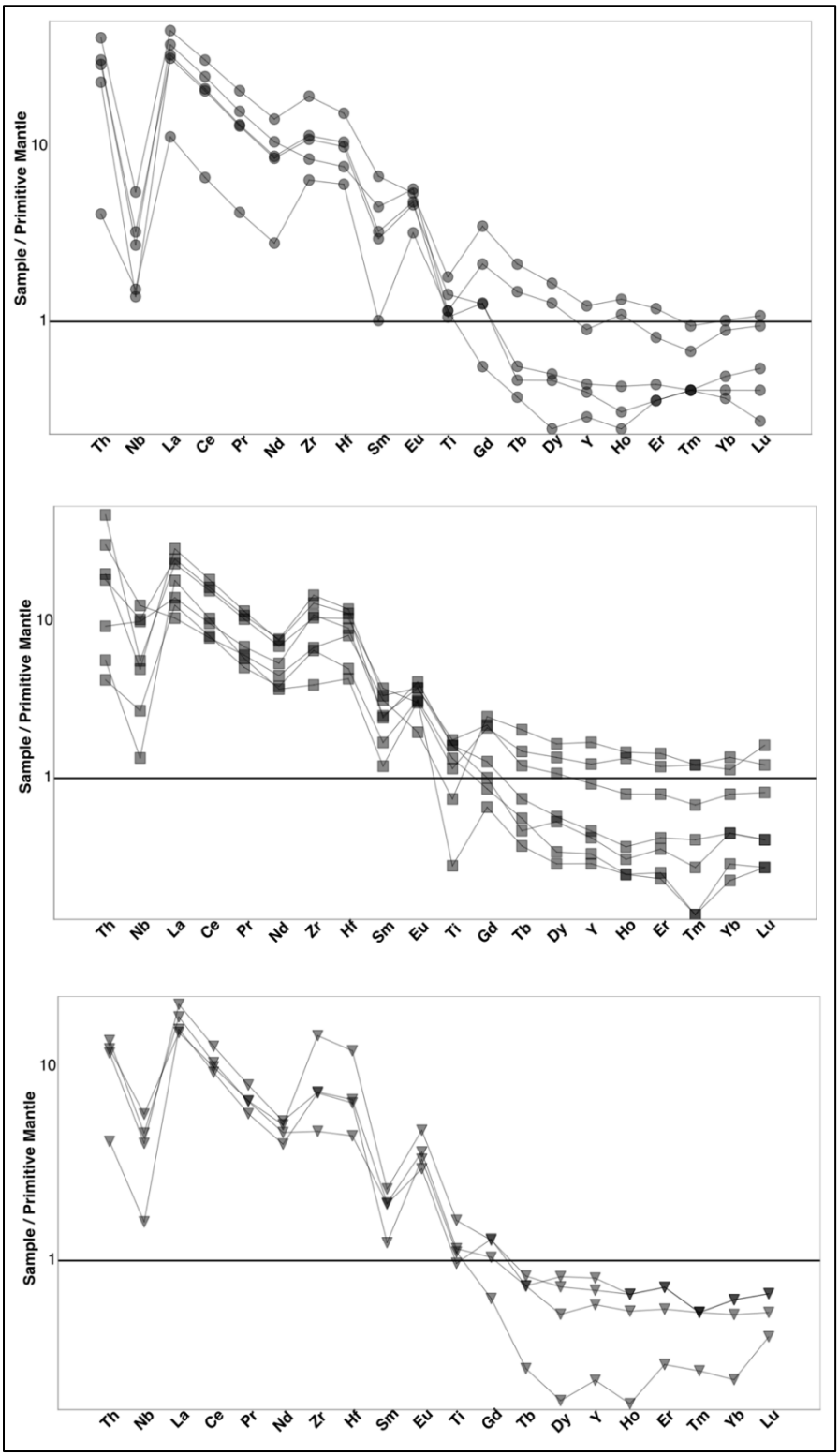

Figure 4.36 Primitive mantle normalized spider diagram for Offset fault drill hole tonalites. Distal samples are denoted by circles, damage zone by squares, and fault core by triangles. Normalizing values from Sun & McDonough (1989).

4.7.3 Alteration Geochemistry

We used geochemical analyses to quantify changes in elemental mass from alteration in the Camp Lake and Offset fault zones. Elemental mass distribution in the samples taken from drill core were plotted against the true distance from fault core (Figure 4.37) to assess a spatial pattern of elemental mass redistribution.

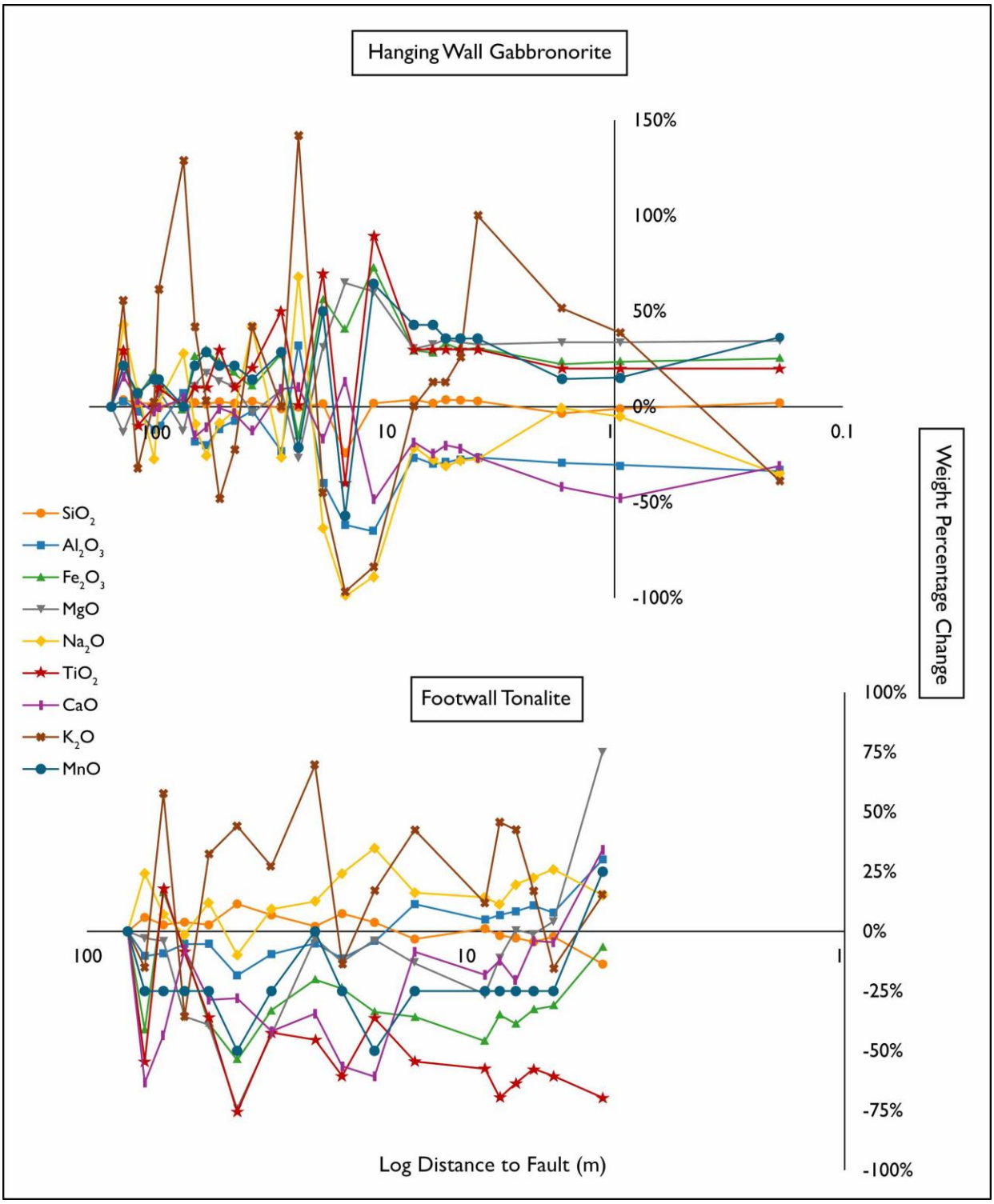

Figure 4.37 Percent enrichment of major element oxides in hanging wall and footwall with log-distance to fault core for the Camp Lake fault drill hole.

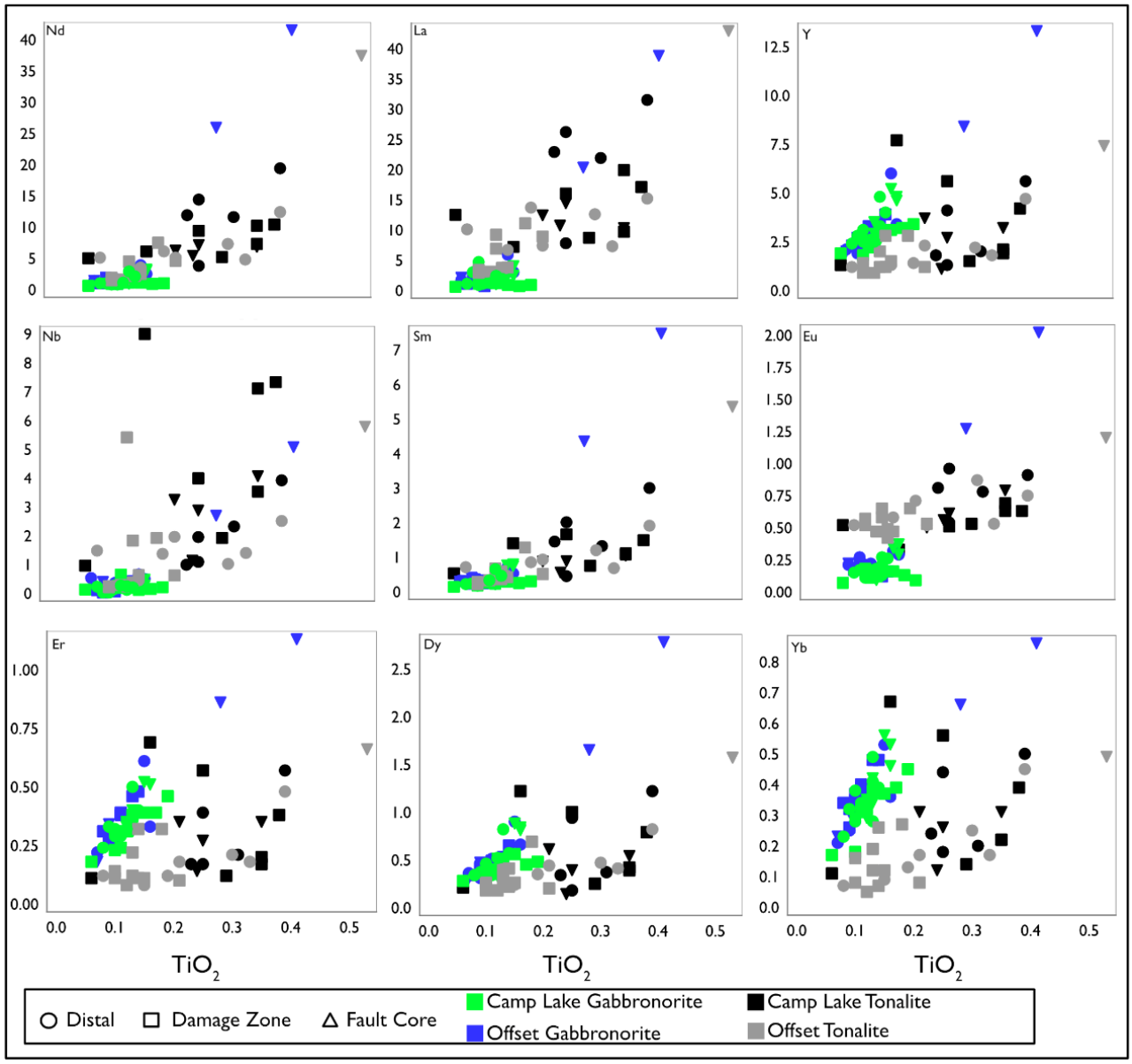

Figure 4.38 Bivariate plots of immobile elements vs TiO_2 from Camp Lake and Offset fault drill holes.

Gabbronorite units in the hanging wall show low to moderate (0-40%) changes in concentration from the least altered to the beginning of the damage zone, with the exception of K_2O (approximately 40 meters from the fault core; Figure 4.37). K_2O at the beginning of the damage zone exhibits greater changes compared to other major element oxides, up to 129% increase in concentration. The damage zone shows the greatest variation in elemental concentration change for the remaining major element oxides. The highest altered zone occurs

from approximately 38 m to 1 m from the fault core based on geochemical variations. K_2O, shows the greatest variation in this section, with an up to 142% increase in concentration. Elements such as TiO_2, MnO, MgO, Fe_2O_3, appear to show, on average, increase in concentration except for a decrease in SiO_2 of -24%. CaO, Na_2O, and Al_2O_3 are variable, but tend to exhibit decrease within the damage zone. K_2O shows rapid positive and negative concentration changes and does not appear to follow any consistent trend. Fault core samples follow a similar trend to those in the damage zone, with K_2O decreasing from 100% to -39% from damage zone to fault core. Percentage change of loss on ignition (LOI) with proximity to fault core for these samples is plotted in Figure 4.39. An original LOI value of 3.53% in the most distal sample was used as the reference for percentage change in the hanging wall samples. Like the major element oxide plots, the most drastic changes in LOI can be observed within the damage zone.

Concentrations in tonalite samples from the footwall follow a similar pattern to those of the hanging wall, with the widest range in variation in the damage zone (Figure 4.37). Elements such as SiO_2 and Na_2O show relatively consistent and positive concentration changes with proximity to the fault core. Al_2O_3, TiO_2, CaO, MgO, and Fe_2O_3 show consistent negative concentrations relative to the most distal sample. Similar to the hanging wall, K_2O exhibits large and sporadic changes throughout the section. Tonalite samples show an increase in LOI within the damage zone, and on average increase with proximity to fault (Figure 4.39).

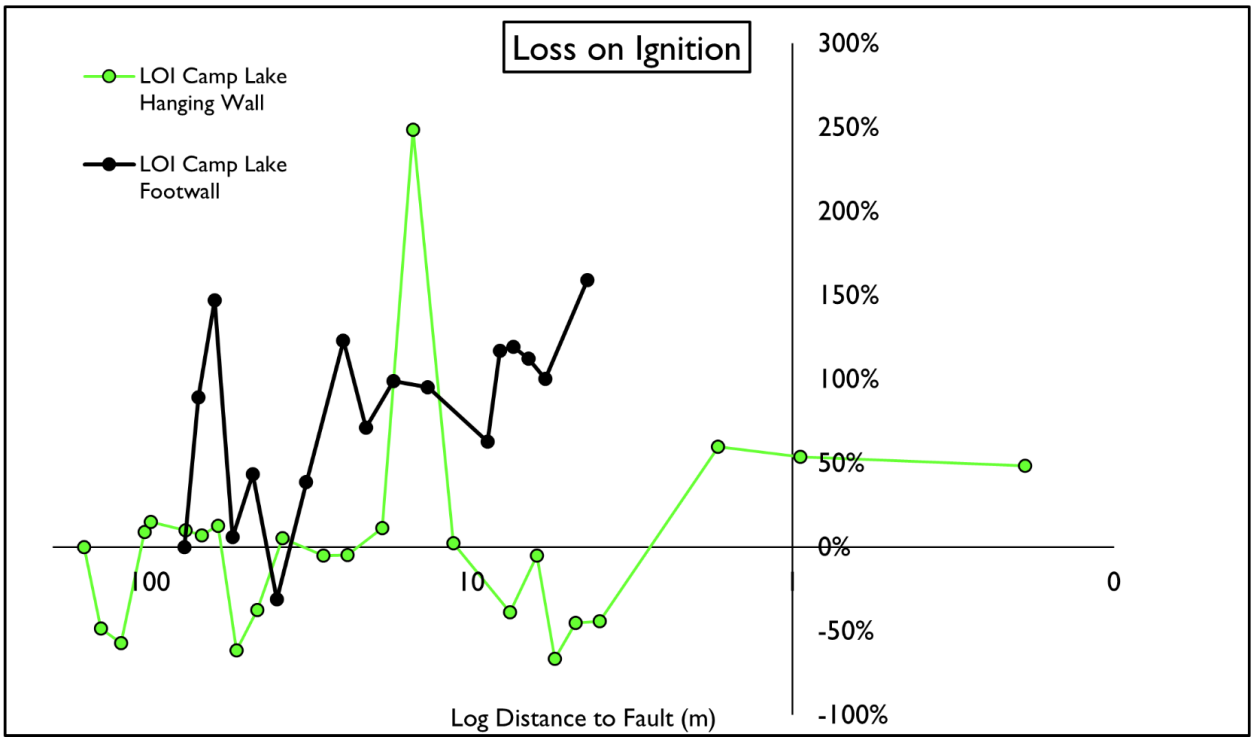

Figure 4.39 Changes in LOI with distance to fault core from Camp Lake fault.

Weight percentage changes in the sampled drill hole from the Offset fault are plotted in Figure 4.40. The hanging wall tonalite follows the trend of largest enrichments/depletions within the damage zone. In this section, TiO_2, Fe_2O_3, MgO, K_2O and MnO exhibit the largest changes in concentrations. These elements are predominantly depleted within 10 meters from the fault core and drastically vary from -80% to 100%. SiO_2, Na_2O, and Al_2O_3 are relatively consistent and display less than 20% concentration changes throughout the section. CaO and K_2O vary sporadically throughout the damage zone into the fault core. Overall, the weight percentage change of major element oxide concentrations appears to be sporadic but follow a trend of largest variations within the damage zone.

K_2O exhibits the largest changes when compared to the most distal sample, with upwards of 700% change, locally (Figure 4.40). SiO_2 appears to be relatively flat and less than 10% change throughout the section. Na_2O, TiO_2, CaO, and Al_2O_3 are consistently depleted throughout

the damage zone and into the fault core, with Al_2O_3 and Na_2O showing moderate enrichments at the core. Fe_2O_3 and MnO are moderately enriched in the damage zone and moderately depleted once into the fault core. MgO and K_2O show the largest but sporadic changes in concentration relative to the most distal sample but are predominantly enriched throughout the damage zone and fault core.

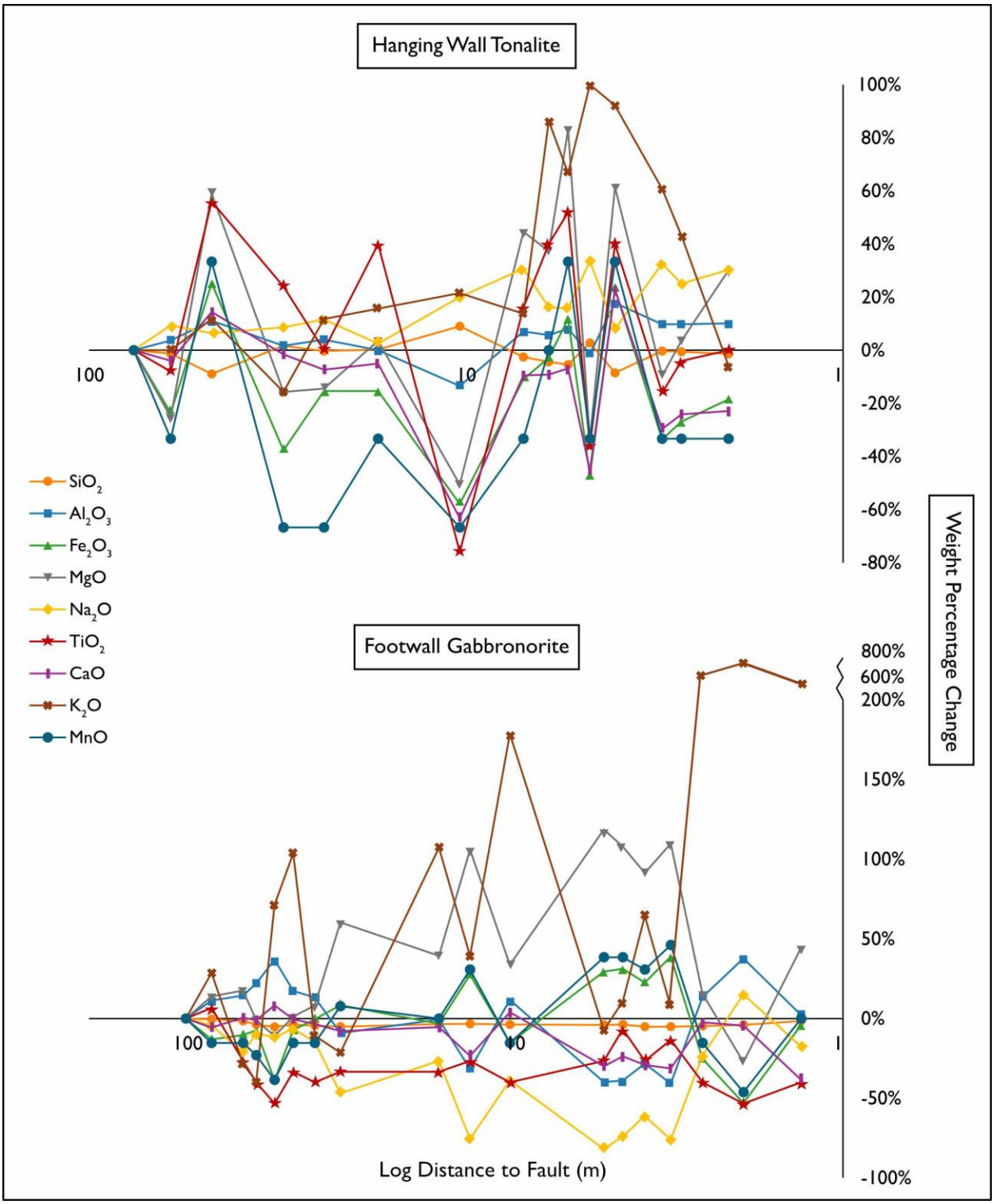

Figure 4.40 Alteration geochemistry plots of major element oxides in hanging wall and footwall with log-distance to fault core for the Offset fault drill hole.

The hanging wall tonalites show a large increase in LOI followed by a steep decrease throughout the damage zone into the fault core, some with as much a 475% increase in LOI, from 0.32% in most distal sample to 1.78% (Figure 4.41). Gabbronorite samples from the footwall of the Offset fault show a relatively flat LOI with proximity to fault core (all less than 80% change). LOI also has the highest percent change in the damage zone approaching the fault core.

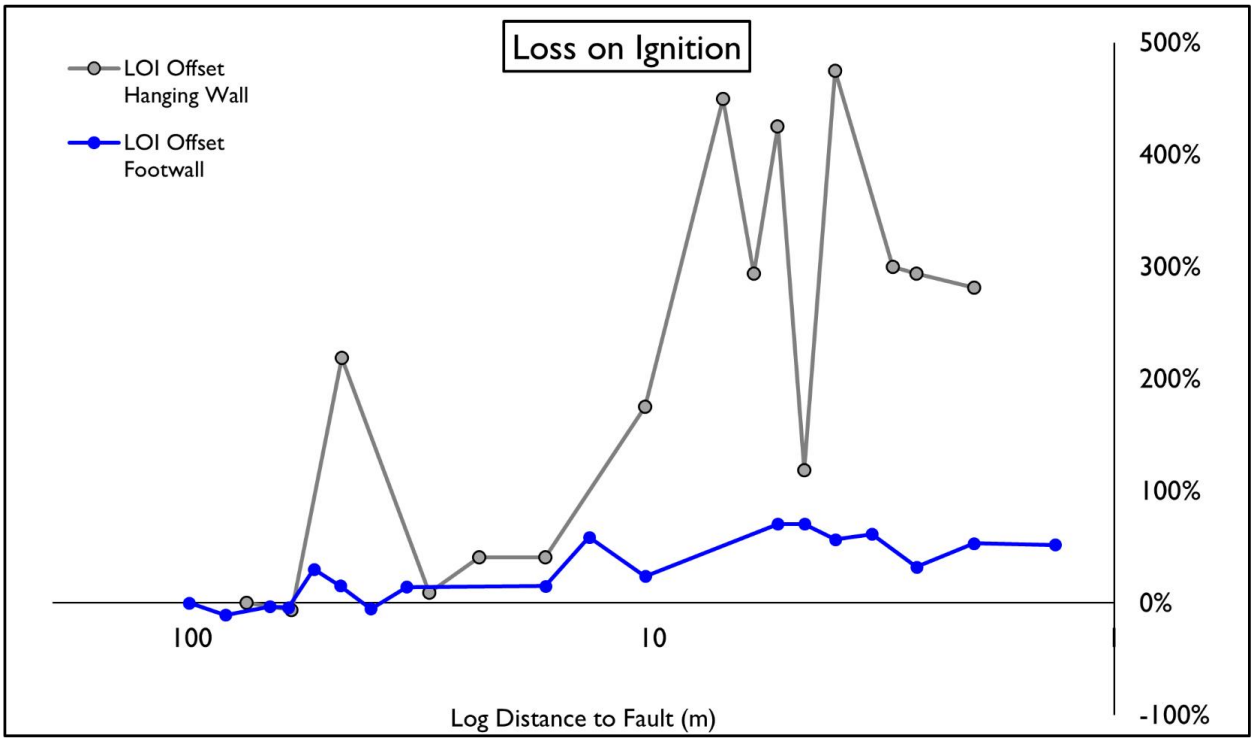

Figure 4.41 Changes in LOI with distance to fault core from Offset fault.

4.8 Electron Microprobe Analysis of Chlorite

Chlorite group minerals can be used as geothermometers due to their non-stoichiometric behaviour as chlorite composition can record information about physiochemical conditions during formation (De Caritat et al., 1993). Of the samples selected, three were protolith samples and three were fault core samples. Clinochlore was the dominant chlorite group mineral found from the electron microprobe analyses, including the Si-rich and Fe-poor clinochlore (pycnochlorite) and the ferroan clinochlore (ripidolite). The dominant chlorite species in the

chlorite-actinolite schist unit (21-503-08) is ripidolite, whereas other protolith samples are dominantly clinochlore. Distal samples are predominantly ripidolite and pycnochlorite, whereas fault core samples are composed of a wider range of chlorites including clinochlore, penninite, pycnochlorite, diabantite and ripidolite (Table 4.1).

Table 4.1: Chlorite species varieties and quantities of samples analyzed via EMPA. Numbers within brackets refer to the number of analyses that fit the composition of each chlorite.

Chlorite Varieties		
Sample	**Protolith**	**Chlorite Varieties**
21-503-08 (Host Rock)	Chlorite-Actinolite Schist	Ripidolite (141) Pycnochlorite (2)
21-700-18 (Host Rock)	Gabbronorite	Ripidolite (34) Pycnochlorite (1)
22-750-28 (Host Rock)	Gabbronorite	Ripidolite (142) Pycnochlorite (14) Diabantite (2)
21-700-02 (Fault Core)	Gabbronorite	Pycnochlorite (63) Clinochlore (22) Penninite (4) Diabantite (2)
21-700-13 (1 meter outside fault core)	Gabbronorite	Penninite (24) Pycnochlorite (21) Ripidolite (9) Clinochlore (1)
22-905-11 (Fault Core)	Gabbronorite	Penninite (62) Clinochlore (43) Pycnochlorite (15) Ripidolite (7)

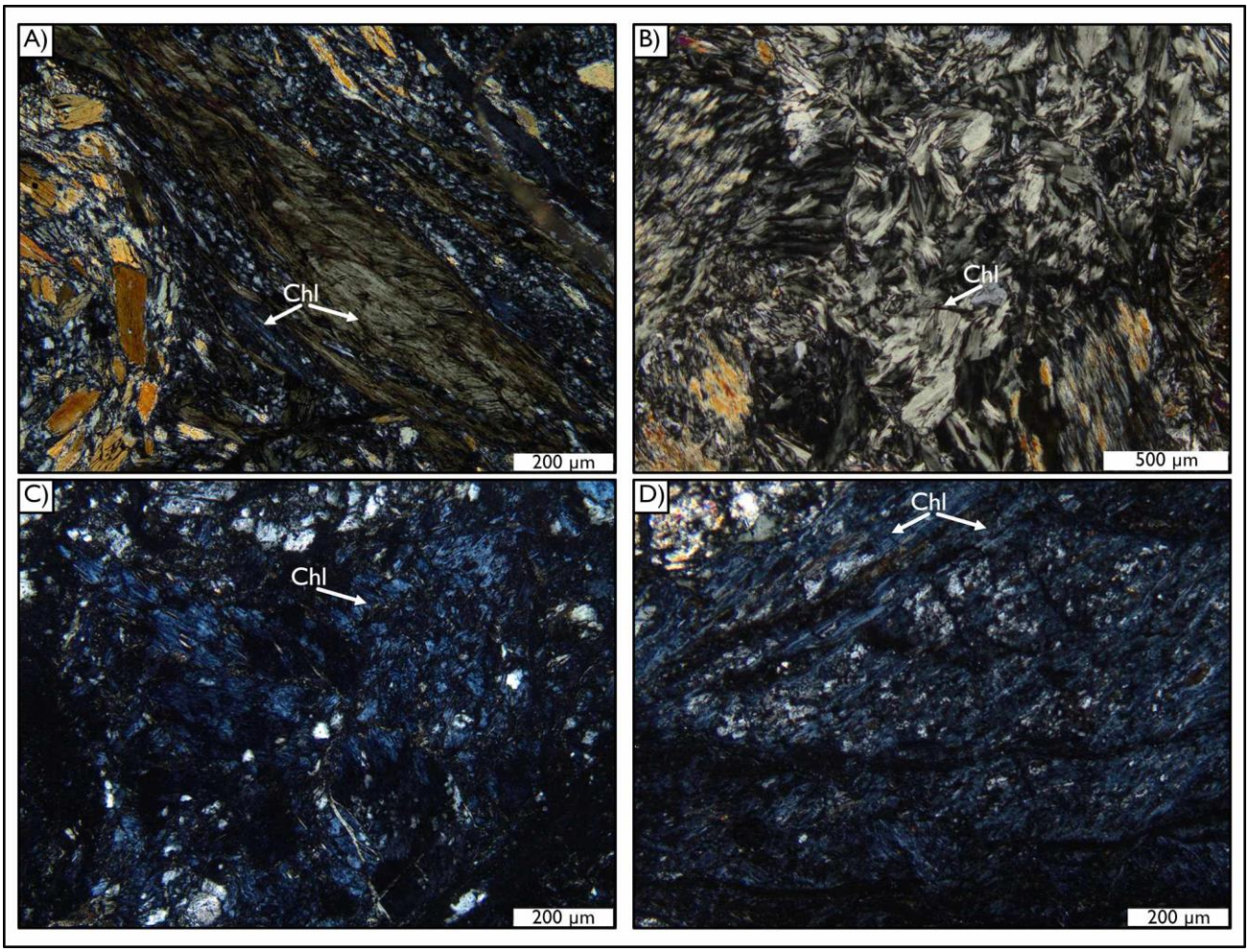

Figure 4.42 A) Thin section photomicrograph of sample 21-503-08 displaying variable chlorites in the chlorite-actinolite schist unit (XPL). B) Distal sample chlorite grains showing a radial texture (XPL). C&D) Fault core chlorite samples photomicrographs in cross polarized light (XPL). Abbreviations: Chl – chlorite.

Chlorite species are dominated by green to brown and grey chlorite grains (Figure 4.42, A, B) whereas fault core chlorites exhibit a berlin-blue like interference colour in cross polarized light photomicrographs (Figure 4.42 C, D). The dominant chlorite species in the chlorite-actinolite schist unit (21-503-08) is ripidolite, whereas other protolith samples are dominantly clinochlore. Fault core chlorite analyses display a wider range of clinochlore. As normalized Si values increase, the Fe/(Fe + Mg) decreases from 0.2 – 0.4 in the host rock chlorites to 0.1 – 0.3 in fault core chlorites (Figure 4.43). Host rock and fault core chlorite show different compositions characterized by Fe/(Fe + Mg) values. The Fe/(Fe + Mg) values vary from 0.22 –

0.36 in the host rock, to 0.16 – 0.21 in the fault core. Lastly, protolith chlorite is present within the fault core, indicating that not all chlorites were either replaced or recrystallized during the faulting process; this is also observable in Table 4.2, as the standard deviations of the chemical compositions are significantly greater in fault core chlorites than the standard deviations observed in the host rock chlorite (Table 4.3).

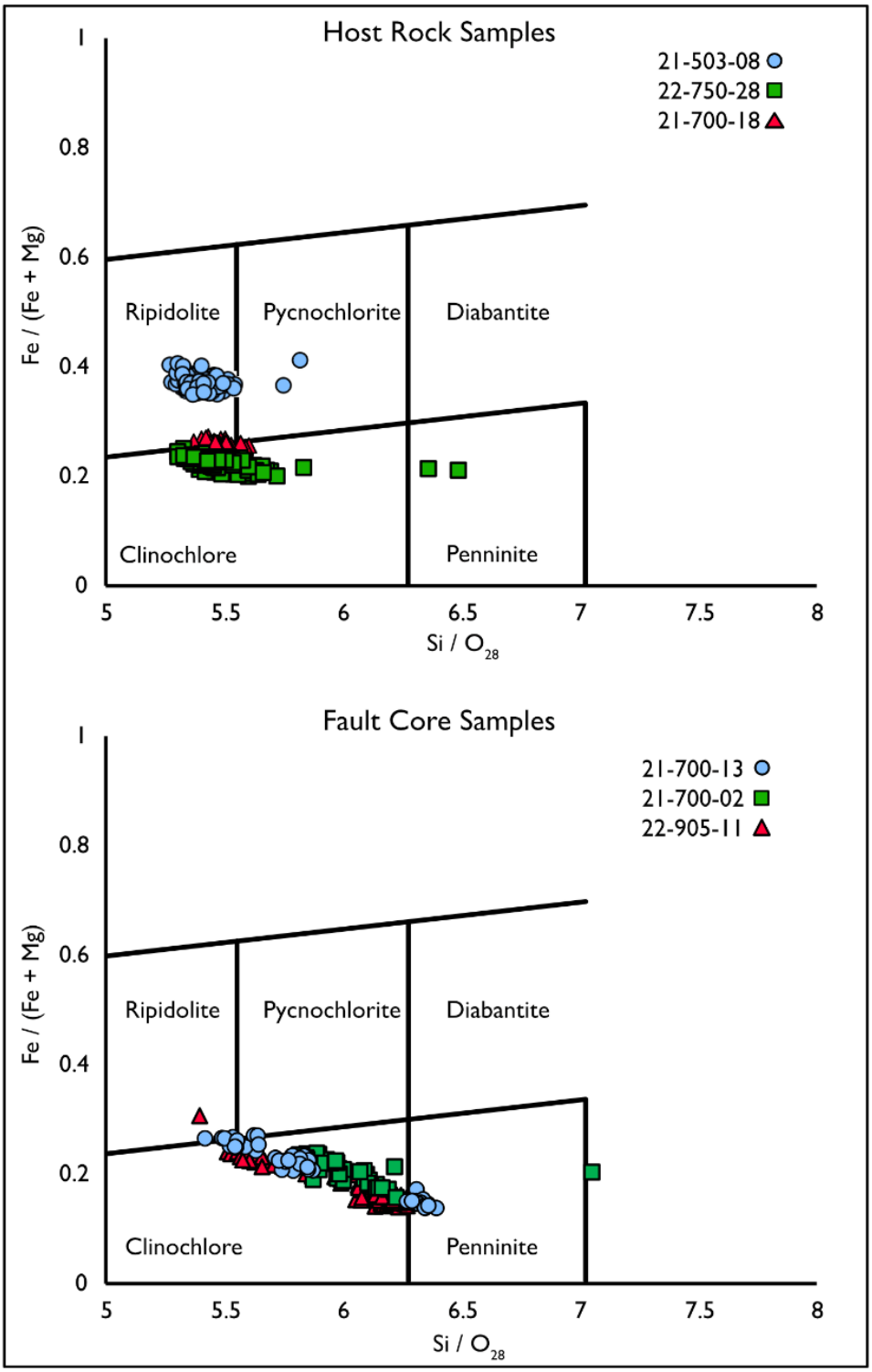

Figure 4.43 Fe/(Fe+Mg) vs SiO_2 normalized to 28 oxygens of protolith and fault core chlorite samples displaying the variation in chlorite species. Adapted from Zang and Fyfe (1995).

Table 4.2: Protolith chlorite EMPA results of major element oxides and respective temperatures

Chlorite – Distal Samples						
Sample #	21-503-08		21-700-18		22-750-28	
	n = 143	SD	n = 35	SD	n = 159	SD
SiO_2	26.91	0.37	28.10	0.27	28.42	1.09
TiO_2	0.05	0.03	0.09	0.07	0.02	0.02
Al_2O_3	21.99	0.51	22.44	0.34	22.60	0.68
FeO	20.35	0.68	14.18	0.39	11.93	0.97
MnO	0.22	0.02	0.13	0.02	0.22	0.02
MgO	19.63	0.47	23.33	0.24	24.74	0.66
Na_2O	0.01	0.03	0	0.01	0.01	0.02
K_2O	0.01	0.04	0.04	0.04	0	0.01
Total	101.30	0.98	101.28	0.38	101.15	0.83
Si	5.40	0.07	5.48	0.05	5.50	0.16
Al iv	2.59	0.06	2.52	0.04	2.50	0.16
Al vi	2.61	0.05	2.65	0.04	2.66	0.08
Ti	0.01	0	0.01	0.01	0	0
Fe^{3+}	0.02	0.03	0.09	0.03	0.09	0.10
Fe^{2+}	3.42	0.11	2.31	0.06	1.93	0.16
Mn	0.04	0	0.02	0	0.04	0
Mg	5.87	0.12	6.78	0.07	7.14	0.19
Na	0.01	0.02	0	0	0	0.02
K	0.01	0.02	0.02	0.02	0	0.01
Fe / (Fe + Mg)	0.36	0.01	0.26	0	0.22	0.01
Temp (°C)	293	7.27	285	4.96	283	16.61
Al Iv Zang & Fyfe Correction	2.57	0.06	2.59	0.04	2.60	0.15
Temp (°C) Zang & Fyfe	290	7.31	292	4.77	294	16.28

Table 4.3: Fault core chlorite EMPA results of major element oxides and respective temperatures

Chlorite – Fault Core Samples						
Sample #	21-700-02		21-700-13		22-905-11	
	n = 91	SD	n = 55	SD	n = 129	SD
SiO_2	31.75	1.57	31.67	2.51	33.21	9.04
TiO_2	0.06	0.19	0.02	0.02	0.01	0.03
Al_2O_3	21.98	1.29	19.86	2.27	18.74	2.75
FeO	8.29	2.78	9.68	3.05	7.74	2.13
MnO	0.18	0.03	0.16	0.06	0.20	0.04
MgO	23.44	1.11	25.83	2.29	26.40	3.61
Na_2O	0.02	0.02	0.01	0.02	0.02	0.02
K_2O	0.10	0.12	0.02	0.04	0.01	0.01
Total	102.26	3.06	101.95	1.20	101.22	3.33
Si	5.97	0.14	6.00	0.37	6.22	0.99
Al iv	2.03	0.14	2	0.36	1.89	0.22
Al vi	2.88	0.27	2.47	0.25	2.36	0.32
Ti	0.01	0.03	0	0	0	0
Fe^{3+}	0.47	0.19	0.27	0.15	0.28	0.07
Fe^{2+}	1.31	0.46	1.54	0.51	1.23	0.35
Mn	0.03	0.01	0.03	0.01	0.03	0.01
Mg	6.57	0.31	7.30	0.56	7.48	1.00
Na	0.02	0.02	0.01	0.02	0.01	0.01
K	0.05	0.06	0.01	0.02	0.01	0.01
Fe / (Fe + Mg)	0.21	0.02	0.19	0.05	0.16	0.03
Temp (°C)	233	14.53	229	38.44	218	23.9
Al Iv Zang & Fyfe Correction	2.14	0.12	2.12	0.33	2.01	0.20
Temp (°C) Zang & Fyfe	245	12.9	243	34.52	234	21.3

Temperatures were calculated using chlorite geothermometers from Cathelineau (1988) and Zang & Fyfe (1995). Figure 4.44 highlights the temperatures from Cathelineau (1988) and Bourdelle & Cathelineau (2015). There is a distinct grouping around 350°C in host rock samples. The fault core samples have two apparent clusters, one around 350°C and another around 125°C – 200°C with a linear trend of analyses originating from each. These temperatures were determined by plotting Si against Fe^{2+} + Mg, both normalized to 14 oxygen atoms per formula unit (apfu).

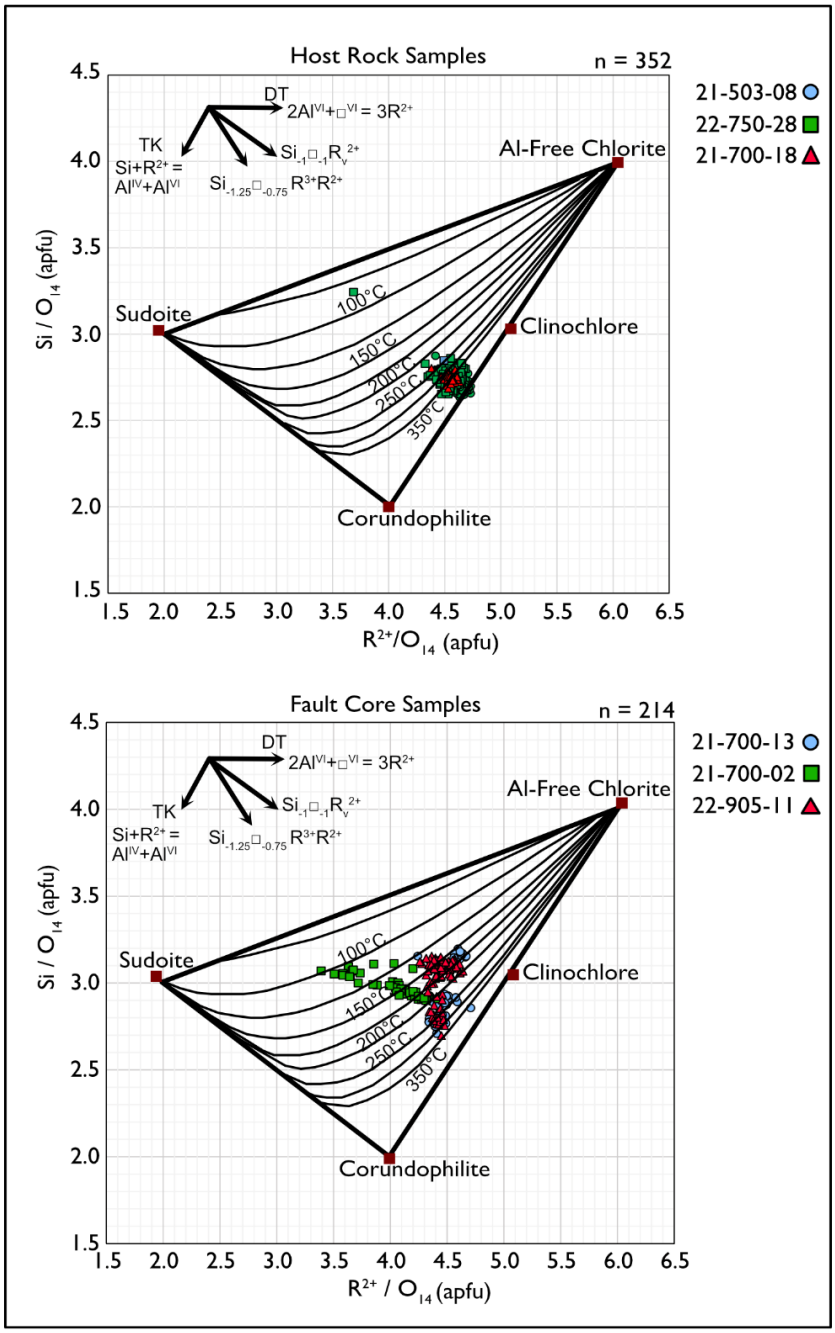

Figure 4.44 Protolith and fault core chlorite analyses plots of Si vs R^{2+} (Fe + Mg) displaying temperatures of chlorite formations (after Wiewióra & Weiss, 1990). TK = Tschermak Substitution (Si + (Mg, Fe^{2+}) = Al^{IV} + Al^{VI}), DT = Di-trioctahedral ($2Al^{VI}$ + $□^{VI}$ = 3 (Mg, Fe^{2+}). Note that □ represents vacancies/empty octahedral sites in the chlorite structure.

The average chlorite temperature for the distal samples is 287°C, and the average chlorite temperature in the fault core samples is 225°C.(Tables 4.2 & 4.3). As noted earlier, the

standard deviation of fault core samples is significantly larger resulting in a skewed average due to the presence of remnant chlorite samples. To combat the skewed averages from the remnant chlorites a k-means cluster analysis was conducted. Three clusters are observable (Figure 4.45), cluster 1, the proto-chlorite averages 291°C (SD = 12.8), cluster 2 averages 236°C (SD = 17.9) and cluster 3 averages 227°C (SD = 18.2). The standard deviations of each cluster represent how widespread the temperatures are and follow the consistent trend of larger degrees of spreading within the samples from the fault.

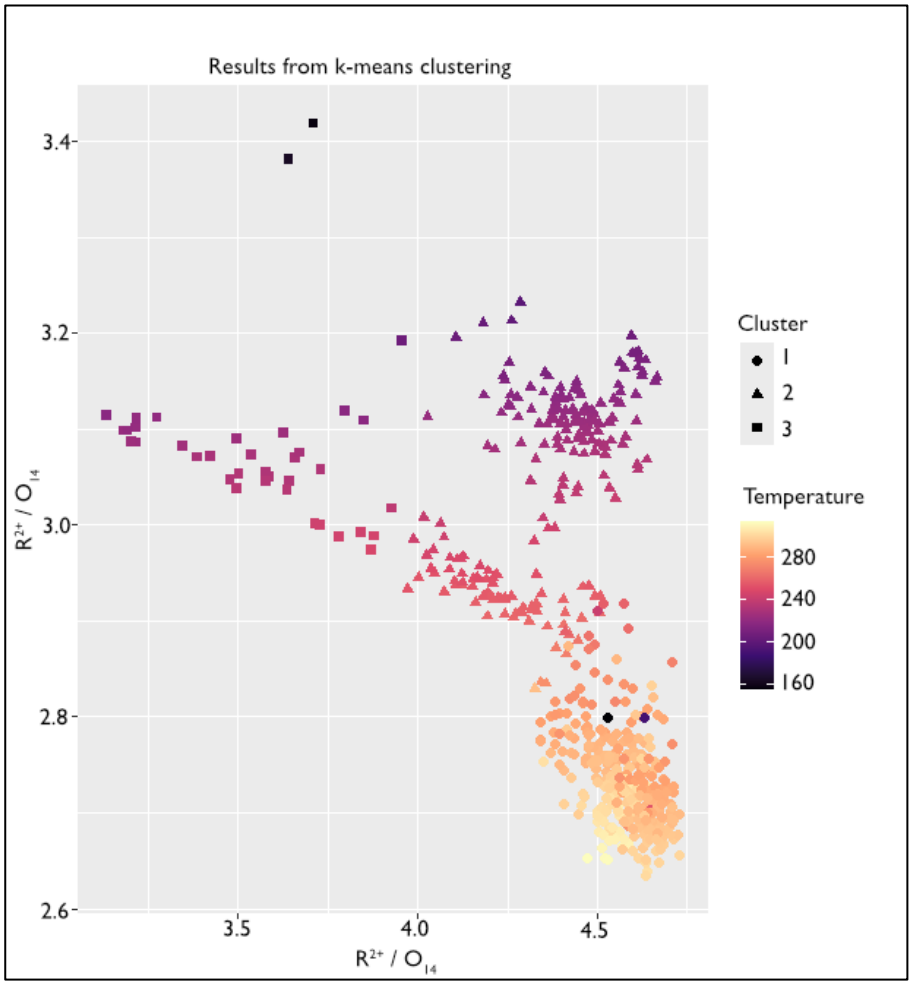

Figure 4.45 Results from k-means cluster analysis. Three clusters are observed indicating three generations of chlorite formation.

Additionally, temperature was calculated using the method of Zang and Fyfe (1995):

$$T\ °C = 106.2 * Al\ (iv) + 17.5$$

Once corrected for the Al (iv) value, the temperature can be recalculated for both distal and fault core chlorites, resulting in an average temperature of 292°C and 239°C, respectively. Comparing the initial temperature to the Al (iv) corrected temperature from Zang and Fyfe (1995), the initial average temperature of 287°C reduces by 5°C in the distal samples, and by 13°C (226°C) in the fault core samples. Tschermak substitution is the dominant substitution mechanism with di-trioctahedral substitution have a minor effect on two of the samples analyzed.

The potential sources of error in the EMPA data collection process were discussed in Section 3.5. Internal lab standards were analyzed before and after unknowns. The largest source of error is analytical errors which were mitigated via the internal standards.

Chapter 5: Discussion

5.1 Deformation conditions, mechanisms, and clay minerals in fault core

Phyllosilicates, or clay minerals, are a large family of minerals characterized by a sheet-like structure and are a major component of fault systems (Sánchez-Roa et al., 2017; Volpe, 2023). Previous studies suggest phyllosilicates play a significant role in controlling fault strength by facilitating shear localization in the frictionally weak, clay-rich matrix as the frictional properties of phyllosilicates have been thought to explain the weakness and creeping behaviour of faults (Schleicher et al., 2012; Tesei et al., 2012; Janssen et al., 2014; Sánchez-Roa et al., 2017). Magnesium bearing phyllosilicates in particular have been suggested to contribute to lowering the strength of active faults (Sánchez-Roa et al., 2017). Chlorite is a major component of the Camp Lake and Offset fault rocks and in the altered host rocks of the Lac des Iles mine, typically forming by alteration of biotite, hornblende, and pyroxene minerals. Chlorite most often is associated with the mafic protoliths (*i.e.,* gabbronorites and the altered equivalents) suggesting chlorite formed after the intrusion and during regional to local metamorphism (Somarin et al., 2009; Barnes & Gomwe, 2011). Within the observed fault zones, chlorite is much more prominent than other alteration minerals and likely has reduced the fault zone strength.

The analyzed chlorite compositions from section 4.8 correspond to three different settings that we interpret to record the chlorite growth at different temperatures and conditions: the distal samples (21-503-08, 21-700-18, and 22-750-28) all appear to cluster in what we hypothesize to be a pre-alteration and pre-faulting phase, grouping with temperatures around 290°C. This is based on the samples being least altered and distal from the fault core. The next cluster (observable in Figure 4.45 and denoted by triangles) is the syn-faulting chlorite, which average ~236°C. This is interpreted to be the temperature when the faulting occurred. These occur in the

fault/slip zone, where chlorite is hypothesized to have induced faulting. The third cluster (Figure 4.45, denoted by squares) with temperatures from ~110 to 175°C is interpreted to be late forming chlorite, related to post-faulting meteoric fluids. Because chlorite is the result of hydrothermal fluid alteration and not a purely diagenetic processes (Braden & Behr, 2021) the temperatures produced from the graphical representation adapted from Bourdelle & Cathelineau (2015) and Zane & Weiss, (1998) for low-temperature chlorite genesis cannot be taken as absolute temperatures, however, the three groups with distinct compositions likely correspond to different deformation conditions and structural domains (*i.e.,* pre-, syn-, and post-faulting). Formation of phyllosilicate minerals during hydrothermal alteration is often associated with the removal or uptake of metals and silica in chlorite (Nimis et al., 2004), as observed in this study, chlorite samples from the fault core display an increase in Si, Mg, and Fe^{3+}, and lesser amounts of Al and Fe^{2+} when compared to the distal chlorite samples, indicating an increase in Si contents in chlorite within the fault core. The Si increase in chlorite can likely be attributed to precipitation of Si-bearing fluids during the alteration of various minerals to chlorite. The Fe_2O_3 values from the distal chlorite samples are all less than 4% (two outliers), and most of the fault core chlorite samples (27 outliers) are less than 4%, implying these are mostly unoxidized chlorites as per Hay (1954). In general, the Fe/(Fe+Mg) ratio for distal chlorites is higher than the fault core chlorite, implying there is less Fe within the fault core. A broad range of chlorite species within a single fault-related sample implies a complex alteration history (Schleicher et al., 2012). The variation in chlorite chemistries seen here is likely the result of repeated influx of fault-related fluids during deformation percolating across the damage zone.

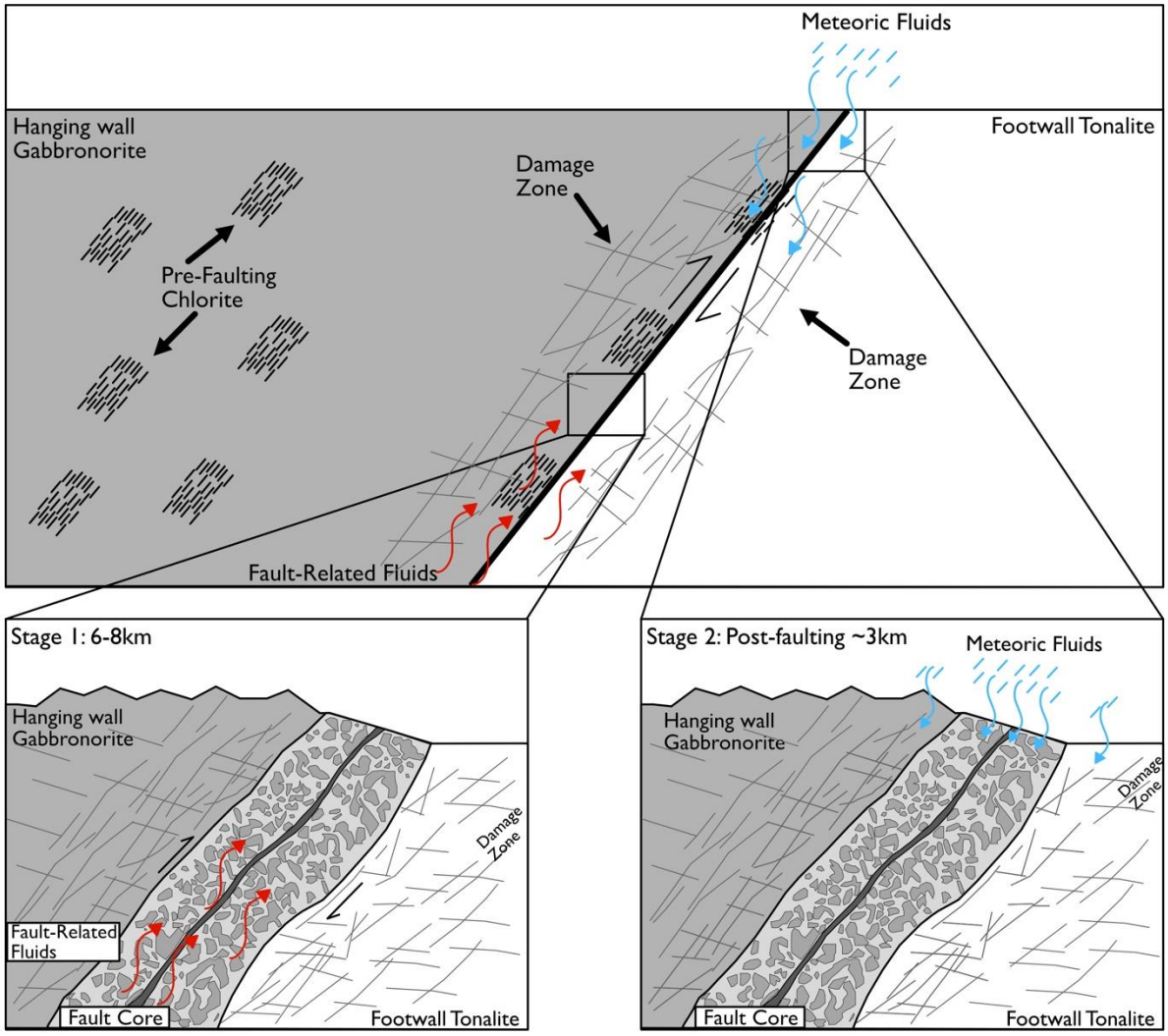

Figure 5.1 Schematic diagram displaying the pre-, syn-, and post- faulting stages of chlorite growth.

During the development of the Camp Lake and Offset faults, the tonalite and gabbronorite were subject to shearing and fragmentation, leading to the development of the schistose fabric and grain size reduction that intensifies toward the fault core. Based on the microstructures and petrographic observations of fault rock samples, we infer five coefficients of friction for the fault rock samples based on their mineralogies and previous workers experiments. These include an unconsolidated clay-rich gouge (μ = ~0.3), strongly foliated chlorite (μ = 0.3), brecciated fault core with tonalite and gabbronorite clasts (μ = 0.6), quartz and plagioclase rich cataclasite (μ = 0.50 – 0.57), and clasts of cataclasite within a cataclasite (μ = 0.5) where μ represents the

coefficient of friction (Byerlee, 1978; Behnsen & Faulkner, 2012; Masuda et al., 2019; Phillips et al., 2020; Braden & Behr, 2021). Foliated gouges and cataclasites (both observed in this study) are commonly interpreted as the product of distributed (aseismic) fault creep. The deformation of quartz by brittle mechanisms has been documented to occur up to ~300 – 350°C, corresponding to crustal depths of 10 – 12 km (assuming a geothermal gradient of 30°C per km), whereas feldspar can deform via brittle mechanisms up to 500°C, corresponding to depths of 20 – 30 km (Masuda et al., 2019). The brittle deformation of quartz and feldspar in the gabbronorite and tonalite units provides evidence that faulting occurred at less than 10 – 12 km. Based on the microstructures and mineralogical results from this study, there are three interpreted phases of deformation involved in the history of the Camp Lake and Offset faults.

1) Regional metamorphism to greenschist facies (290°C) and local hydrothermal alteration leave some rocks unaltered or relatively unaltered. The production of chlorite (ripidolite) through alteration prior to faulting from the breakdown of biotite, pyroxene and amphibole produces the frictionally weak phyllosilicate minerals that could allow for localized deformation.
2) Fracturing of the host rocks initiating the first faulting event. This would have included brecciation of the gabbronorite and tonalite units, alongside cataclasis. The presence of multiple generations of cataclasite suggests more than one faulting event. During this period, hydrothermal fluids (T = ~230°C) would have moved across the fault zone producing the main alteration signature in the damage zone and fault core. Chlorite (clinochlore) would have precipitated during this stage. This event produced a shear fabric/foliated chlorite within the gabbronorites.

3) Post-faulting, the precipitation of low temperature chlorite, likely from meteoric fluids would be the last stage of the process. This may have occurred in the absence of slip in the fault once exhumation brought the fault to the surface. The temperatures of this stage (~110° C) indicate ~3 km depth (assuming a geothermal gradient of ~30°C per km).

Byerlee's law states that when the tectonically derived shear stress acting on a plane (T) is higher than the stress resisting sliding along the fault (μ_s), then frictional sliding will occur (Coulomb, 1776; Byerlee, 1978). Experiments on the frictional strength of intact mafic volcanic rocks (unaltered and altered basalt, gabbro, and gabbro gouge) are estimated to have coefficients of friction of $\mu = 0.6 – 0.7$ at temperatures from 100 – 400°C consistent with Byerlee's law (Braden & Behr, 2021 and references therein). However, components of gouges when wet (i.e., chlorite) have lower coefficients of friction ($\mu = \sim 0.3$). Experiments from He et al. (2007) display an increasing coefficient of friction with increasing temperature in gabbro gouges, along with displaying evidence for velocity weakening behaviour when subject to temperatures below 310°C. The sliding response is likely a reflection of the gouge material (i.e chlorite-rich) while the bounding units (i.e., tonalite and gabbronorite) influence the mechanical response through their elastic or inelastic response, but not by their frictional properties (Logan et al., 1992). Observable in the damage zone and fault core, in grains of plagioclase that have not entirely been replaced by sericite, the spacing of microfractures within plagioclase grains appears to decrease with increasing distance from the fault core. Intracrystalline fractures are observable in many plagioclase grains alongside mechanical twinning, providing evidence for both brittle and ductile deformation across the fault zones (Brown & Macaudiére, 1984).

5.2 Fracture density and fault zone architecture

The fault zone architecture of the Camp Lake and Offset faults are similar in that both fault zones comprise fault cores composed of cataclasites to fault breccia in tonalite, and clay-rich gouge in the gabbronorites. Additionally, both faults follow a typical fault zone architecture of a damage zone with increasing fracture density and alteration, and a fault core. Based on the observations from drill core logging and whole rock geochemistry showing an increase in alteration in the damage zone, both faults can be classified as a "combined conduit-barrier" fault system after Caine et al. (1996) due to the well-developed damage zone and fault core (Figure 5.2).

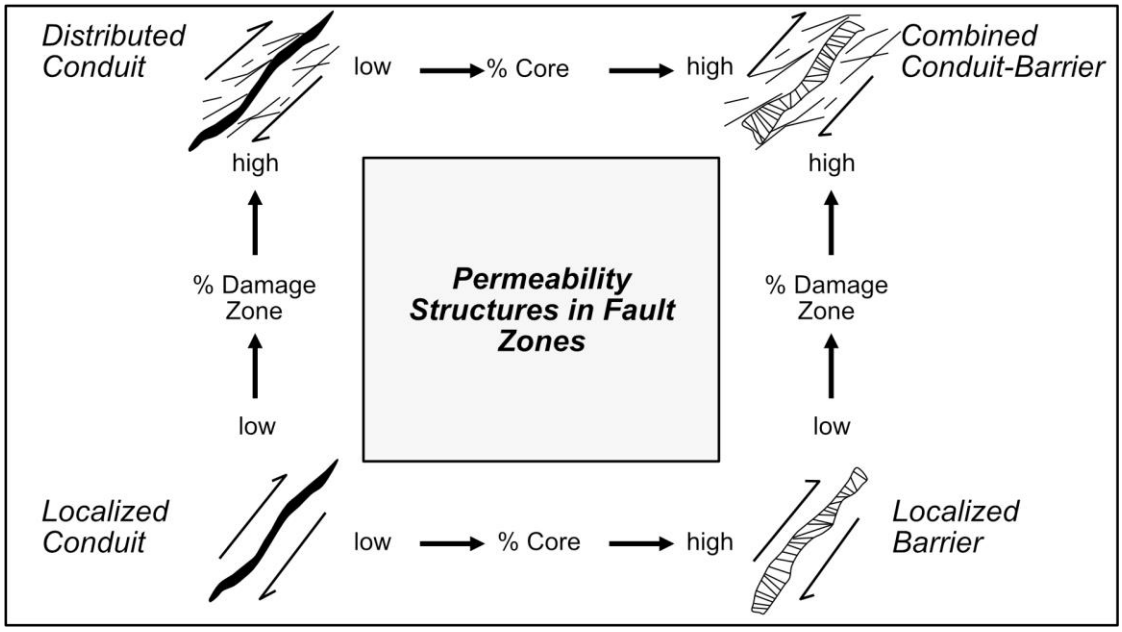

Figure 5.2 Conceptual model of permeability structures in fault zones modified from Caine et al. (1996).

There are some differences between the Camp Lake and Offset faults. The first notable difference between the Camp Lake and Offset faults are the relative displacements. The Camp Lake fault has an inferred displacement of more than 500 meters, whereas the Offset fault has an observed displacement of 275 meters (Vektore, 2021). Secondly, the gabbronorites behave similarly in both the Camp Lake and Offset faults, with damage decay rates ranging from 0.27 –

0.79 and 0.39 – 0.69, respectively. The tonalite damage decay rate is higher in the Camp Lake fault (0.52 – 0.98) compared to the Offset fault (0.35 – 0.40) which could be due to greater displacement on the Camp Lake fault. Additionally, the width of the gouge zone from Camp Lake intercepts from drill core (>10cm) and underground exposure (~20cm) is wider compared to the Offset fault (<10cm and ~10cm), providing more evidence for larger displacement (Evans, 1990; Savage & Brodsky, 2011).

Damage decay (of macrofractures) provides insight into how stress decayed with distance from the fault. Savage & Brodsky (2011) showed that the decay of damage is a function of distance from the fault, and less dependent on the local lithology, but rather the absolute number of fractures (Figure 5.3 A). The former is likely true; however, we argue that the controls on the absolute number of fractures is not only displacement dependent but likely has a strong lithological control. Evans (1990) suggested that there is a linear correlation between the thickness and the displacement of fault zones (in logarithmic space), however some authors (Jamison & Stearns, 1982; Blenkinsop & Rutter, 1986; Woodward et al., 1988) argued that thickness evolves depending on the orientation of Riedel, and conjugate Riedel and Y-shears. The results from this study, compiled with other fault zones of varying lithologies, show that fault zone width does increase with displacement but only up until a certain point. After that point, fault zone width can be considered saturated after a few hundred kilometers of displacement (Savage & Brodsky, 2011; Thomas et al., 2017) and no longer correlates (Figure 5.3 B). The faults observed in this study are consistent with the trend of damage zone width correlating to displacement, implying that both have not reached the saturation point.

The hanging wall and footwall damage zones of the Camp Lake and Offset faults vary in width, fracture decay rate and fracture density. Fracture decay rate and fracture density are likely

lithologically controlled in the study area. Different rock types have been shown to affect the development of fault zones (Evans, 1990; Savage & Brodsky, 2011). In our study (see section 4.6), felsic lithologies (tonalites) display a greater fracture density than mafic lithologies (gabbronorites) within the same drill hole irrespective of whether the tonalite is in the hanging wall or footwall of the fault (Figures 4.24 and 4.25).

Heterogenous fault zones have a more complex mechanical behaviour than homogenous fault zones. Rheological heterogeneities within fault zones can arise from juxtaposing rocks with different mechanical and physical properties (Volpe, 2023). Damage zones develop due to fault zone propagation, wear, and plasticity accompanying earthquake ruptures, and are closely linked to other factors such as displacement, deformation history, roughness and the mechanical properties of the protolith (Keren & Kirkpatrick, 2016). Granular materials such as quartz and feldspar deform predominantly by cataclastic processes and therefore are generally considered frictionally strong, with a coefficient of friction of 0.6 – 0.7 (wet and dry) compared to the coefficient of friction of phyllosilicate minerals (clays and micas) of 0.22 – 0.44 (dry) and 0.12 – 0.38 (wet) (Higgins, 1971; Byerlee, 1978; Behnsen & Faulkner, 2012; Masuda et al., 2019). We hypothesize that the lower coefficient of friction in chlorite-rich gouges impeded the development of a fracture-rich damage zone.

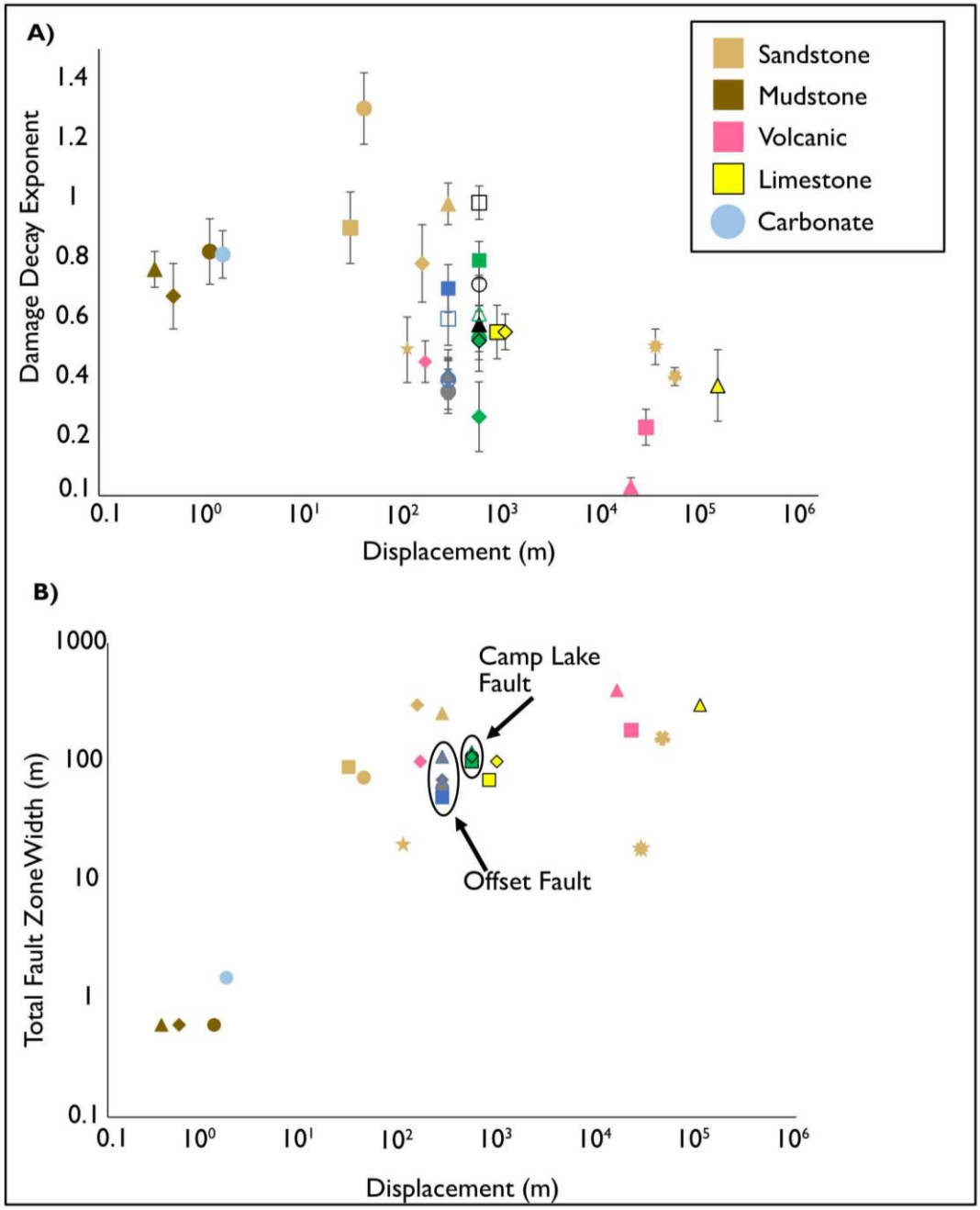

Figure 5.3 A) Damage decay exponent vs displacement of variable lithologies and faults (data from Savage and Brodsky, 2011) compared to data from this study. B) Total fault zone width vs displacement with data from Savage and Brodsky (2011).

Fluid flow in the crust is largely controlled by the physical and mechanical properties of rocks and heterogeneities such as faults and shear zones (Caine et al., 1996; Faulkner et al., 2010; Mitchell & Faulkner, 2012). As mentioned earlier, damage zones surrounding faults

contain pervasively fractured rocks, and fault cores typically contain fine-grained, low-permeability clays and gouges. The increased density in fractures was likely responsible for the observed increase in alteration and hypothesized fluid flow in the damage zone of the Camp Lake and Offset faults. The fault core in the gabbronorite intervals is dominantly chlorite-rich and likely acts as some form of barrier resistant to fluid flow.

5.3 Geochemistry and element mobility

Here we examine the role of fault related fluids on major and trace element chemistry, which reflects the permeability structure of the damage zone and implications for the distribution of Pd around late faults. When analyzing the geochemical data in rocks from fault zones, it is important to consider any alteration or metamorphism that may have taken place prior to faulting. As we examine the rocks from the Lac des Iles Complex which have undergone regional metamorphism, it is necessary to establish a pre-faulting signature. To distinguish between fault-related alteration and pre-faulting signature, we need to compare samples from this study, which appear to have all been altered to some extent, to those from previous researchers (Brügmann et al., 1996; Jonsson, 2023; Smith et al., 2024). This can help us discern the pre-faulting signature of trace and major elements in the host lithologies.

Gabbronorites

Previous work on the Lac des Iles intrusion suggests that the LDIC was formed in a continental arc setting (Brügmann et al., 1996; Djon et al., 2018; Smith et al., 2024). Samples from different domains across the intrusion have similar trace-element chemistry, including enriched LILE/LREE patterns, flat to negatively sloping HREE patterns, and prominent negative Nb/Nb* anomalies (Jonsson, 2023; Smith et al., 2024). Gabbronorite samples from both fault zones show similar trace element patterns. Distal samples display enriched LREEs with

relatively flat MREE to HREE trends, with positive Eu and negative Ti anomalies. One sample from the Camp Lake zone exhibits a positive Zr-Hf anomaly, which could be cause by REE loss, however, as this sample is distal from the fault core and damage zone, it is likely not related to faulting. The damage zone samples from the Camp Lake and Offset faults show relatively flat LREE to HREE patterns, with minor variations in the relative concentration. Negative Niobium anomalies are present like those of the distal samples. A positive Eu anomaly is present in some of the Offset fault samples, but not as pronounced in the Camp Lake samples. Two samples from the Offset fault show positive Zr-Hf anomalies, which again, could be due to REE loss. Negative Ti anomalies are present in all samples. HREEs in both are quite flat but show some spread in the Camp Lake samples unlike the distal samples. Fault core samples from both faults exhibit the widest variations in concentration of trace elements, consistent with greater alteration intensity in the area.

Tonalites

Tonalite trace element patterns from the LDIC have relatively high LILE concentrations, negative Nb/Nb* anomalies, positive Eu/Eu* anomalies, and low HREE concentrations with moderately high Zr, Hr concentrations (Smith et al., 2024). In general, comparing the trace element data from this study to the average composition of tonalites presented in Smith et al. (2024; Figure 5.4A), the distal tonalite samples from both faults are similar to average patterns for regional samples, specifically, the slightly positive Nb anomalies, and overall slope/concentration of LREE's. Damage zone samples (Figure 5.4B) follow a similar pattern to the average tonalite composition except for larger positive Nb anomalies and a wider spread HREE. The fault core samples all display stronger positive Nb anomalies, Zr-Hf anomalies, and a sag in HREEs (Figure 5.4C). The trace element patterns amongst distal, damage zone and fault

core samples of the tonalites, and comparison to the average tonalite sample from Smith et al. (2024) show a broad range of values implying that the unit is heterogeneous in composition.

The variations in LREE and most trace elements across the diagrams relative to the primitive mantle standard, and when compared to average samples from previously researched datasets, display a range of compositions from more primitive to more evolved, leading to the belief that the changes in LREE and trace elements are likely a petrogenetic factor as opposed to metasomatism or alteration from fault-related fluids.

Heavy rare earth element concentrations in the tonalite samples on occasion show saggy patterns but are not consistent with proximity to faulting. Figure 5.4 shows distal, damage zone, and fault core samples all with variable HREE patterns. The mobility of trace elements, specifically HREE's in low temperature alteration systems is debated amongst researchers (Yongliang & Yusheng, 1991). McLennan & Taylor (1979) argued that HREE are preferentially retained in hydrothermal solutions and only removed in late stage or low temperature deposits.

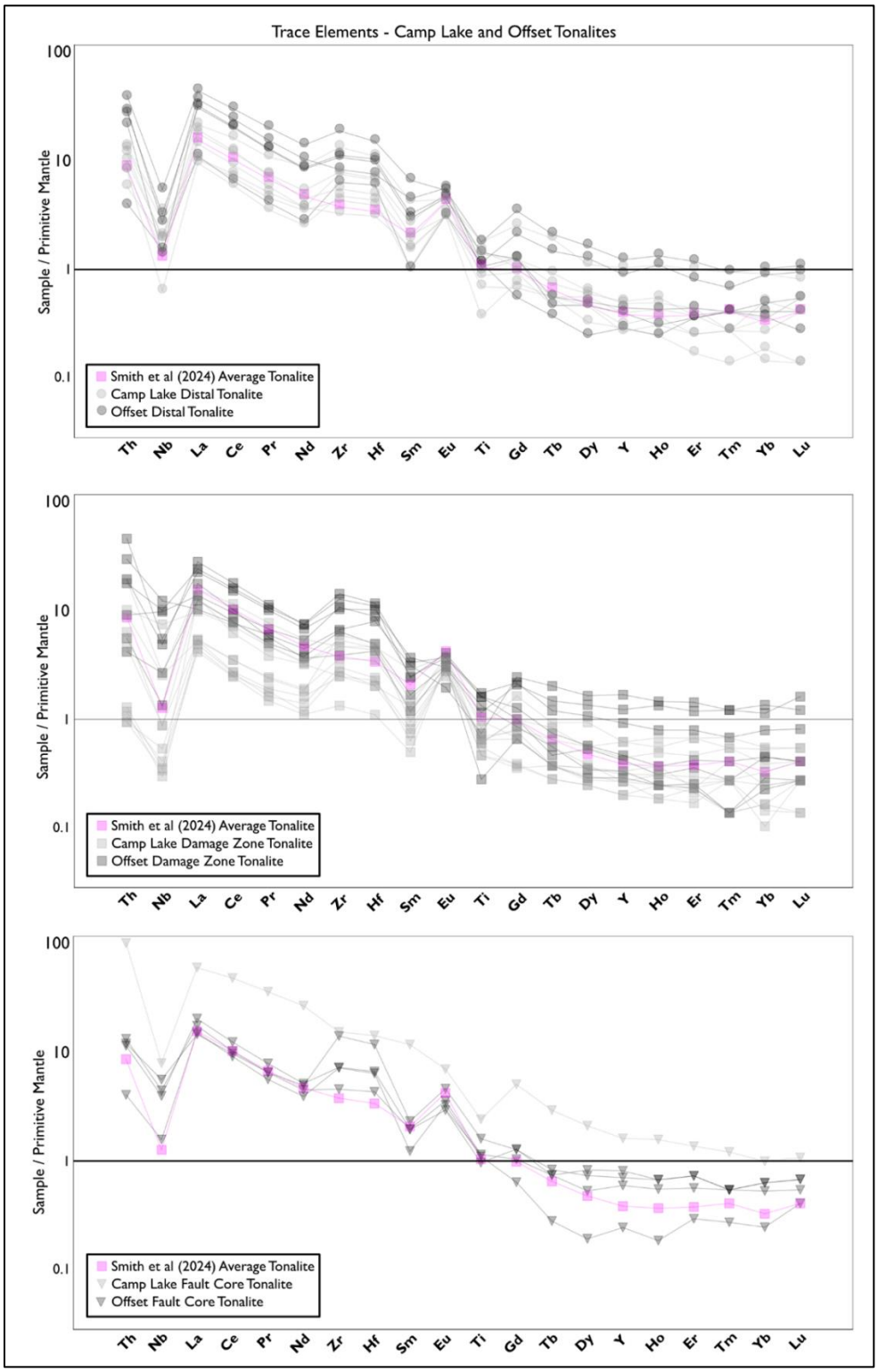

Figure 5.4 Trace element spiderplot diagrams of LDI tonalites from this study compared to the average tonalite from Smith et al. (2024). Normalized to primitive mantle from Sun & McDonough (1989).

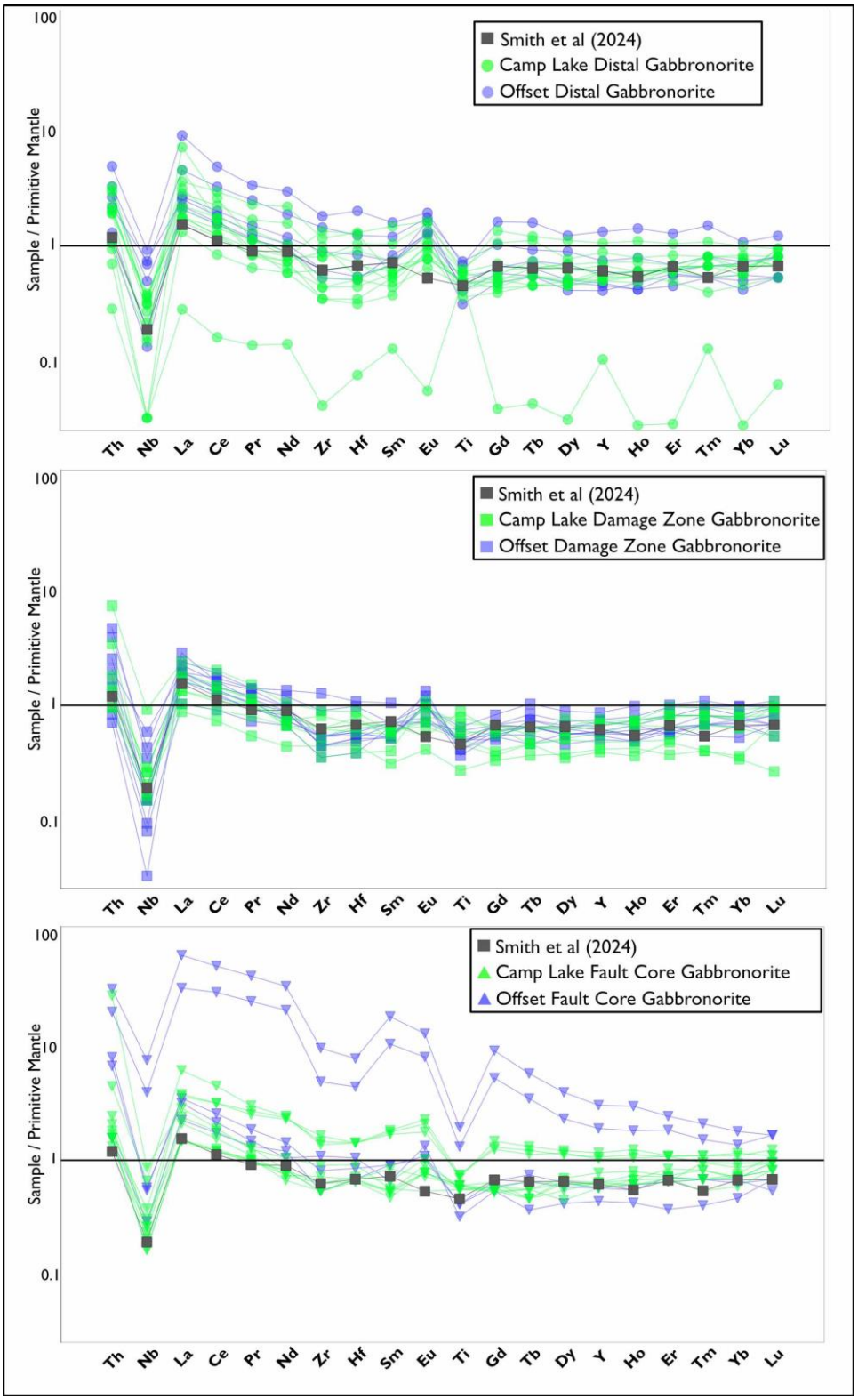

Figure 5.5 Trace element spiderplot diagrams of LDI gabbronorites from this study compared to the average olivine-bearing sample from Smith et al. (2024). Normalized to primitive mantle from Sun & McDonough (1989).

The chemical and mineralogical changes of major elements observed in the Camp Lake and Offset fault zones likely result from hydrothermal alteration introduced during faulting. The alteration of both fault zones appears to be dominated by different alteration styles, but dominated by chloritization, sericitization, and propylitic alteration. Prior to the faulting events, high-temperature conditions likely produced mineral assemblages that are observable in other domains of the Lac des Iles mine (i.e. chlorite-actinolite schist; Hinchey et al., 2005). When comparing the Camp Lake fault and Offset fault drill holes, the SiO_2 shows the least variation in both the gabbronorite and tonalite and can be considered generally immobile in this system, similar to the findings of Somarin (2007) who showed that SiO_2 and P_2O_5 were immobile within the North Roby Zone of the Lac des Iles mine.

The alteration plots from Chapter 4 (Figures 4.33 and 4.36) indicate that the most mobile elements in the system are K_2O and Na_2O. Replacement of plagioclase by sericite is commonly observed in the fault and damage zone rocks of the Camp Lake and Offset faults, and would explain the variations in the K_2O within both protoliths (Somarin et al., 2009).. The alteration of Fe-rich biotite consumes Mg^{2+}, releases K^+, and H^+ and produces Mg-rich chlorite, silica and oxidized Fe (Dorsey et al., 2021), consistent with the higher Mg chlorite in the fault core samples. Loss on ignition (LOI) has also been used to quantify alteration in the Lac des Iles mine as the development of hydrous minerals can be linked to elevated LOI (Somarin et al., 2009; Jonsson, 2023).

Previous studies (Goddard & Evans, 1995; Bradbury et al., 2015; Duan et al., 2016; Dorsey et al., 2021) have examined the changes in geochemical signature in rocks that have been subject to faulting. Results from these studies commonly show that alteration signature is

typically lithologically dependent, but the role of fluids are still poorly understood. Results from Duan et al. (2016) state that “D-Type” elements (depleted relative to host rock) are typically mobile, and “R-Type" elements (enriched relative to host rock) are typically immobile in fault systems, with most trace elements behaving as R-Type, except for Ba and Sr as these are particularly sensitive to fluid-rock interactions (Janssen et al., 2014; Duan et al., 2016). The results from this study indicate a similar trend, implying that there is trace and major element mobility along the fault zone. Like the petrographic results from the Camp Lake and Offset faults, the whole rock geochemical signature varies throughout the fault zones. When examining bivariate diagrams comparing a typical major element oxide and trace elements to TiO_2, it is apparent that there are two distinct trends or groups, corresponding to lithology, the tonalites and the gabbronorite groups (Figure 4.28). Major element oxides (Figure 4.28) show a wider spread than the trace elements observed in Figure 4.28 when compared to TiO_2, however both show a relatively similar trend. The fault core samples from the bivariate plots are often outliers, indicating that there is likely some form of remobilization of both trace and major elements within the fault core and damage zone.

Chapter 6: Conclusions

This thesis focused on the deformation conditions, kinematics, and geochemical trends surrounding the Camp Lake and Offset faults at the Lac des Iles mine. While examining these themes, research into the mechanics behind fault zone architecture and development was conducted. The main findings of this study are:

1) The Camp Lake and Offset faults both show evidence for reverse shear sense kinematics. The Camp Lake shows evidence multiple generations of faulting in the fault gouge.
2) The deformation conditions were likely accelerated or influenced by chlorite growth during alteration and metamorphism. Three generations of chlorite growths were observed, a pre-faulting, syn-faulting, and post-faulting generation each with their own temperature of formation. Chlorite likely reduced the coefficient of friction which along with fluid pressure, likely facilitated faulting along the Camp Lake and Offset faults.
3) Mafic lithologies in this study (gabbronorites) develop a less wide damage zone compared to the felsic lithologies (tonalites). Fracture density also decays at a faster rate from the fault core in tonalites than in gabbronorites. Felsic lithologies are more brittle in nature, develop fractures at a faster rate than mafic lithologies when subject to the stresses associated with the faulting processes.
4) The damage zone of the logged drill holes display both the geochemical and petrographic apices of alteration. As fluids move across the fault zone, the high degree of fracturing in the damage zone focusses fluid, which in turn, alters the surrounding rocks.

Chapter 7: References

Bain, W. M., Hollings, P., Djon, L. M., Brzozowski, M. J., Layton-Matthews, D., & Dobosz, A. (2023). The geology, geochemistry, and magmatic evolution of the Legris Lake mafic–ultramafic complex, Ontario, Canada. *Mineralium Deposita*. https://doi.org/10.1007/s00126-023-01183-x

Barnes, S.-J., & Gomwe, T. S. (2011). Chapter 13 The Pd Deposits of the Lac des Iles Complex, Northwestern Ontario. *Economic Geology*, *17*, 351–370.

Battaglia, S., Leoni, L., & Sartori, F. (2004). The Kübler Index in Late Diagenetic To Low-grade Metamorphic Pelites: A Critical Comparison Of Data From 10 Å and 5 Å Peaks. *Clays and Clay Minerals*, *52*(1), 85–105. https://doi.org/10.1346/CCMN.2004.0520109

Behnsen, J., & Faulkner, D. R. (2012). The effect of mineralogy and effective normal stress on frictional strength of sheet silicates. *Journal of Structural Geology*, *42*, 49–61. https://doi.org/10.1016/j.jsg.2012.06.015

Billi, A., Salvini, F., & Storti, F. (2003). The damage zone-fault core transition in carbonate rocks: implications for fault growth, structure and permeability. *Journal of Structural Geology*, *25*(11), 1779–1794. https://doi.org/10.1016/S0191-8141(03)00037-3

Blackburn, C. E., Johns, G. W., Ayer, J., & Davis, D. W. (1991). Wabigoon Subprovince. *Geology of Ontario*, *4*, 303–381.

Blenkinsop, T. G., & Rutter, E. H. (1986). Cataclastic deformation of quartzite in the moine thrust zone. In *Journal of Structural Geology* (Vol. 8, pp. 669–681).

Boudreau, A., Djon, L., Tchalikian, A., & Corkery, J. (2014). The Lac Des Iles Palladium Deposit, Ontario, Canada part I. The effect of variable alteration on the Offset Zone. *Mineralium Deposita*, *49*(5), 625–654. https://doi.org/10.1007/s00126-014-0510-y

Bourdelle, F., & Cathelineau, M. (2015). Low-temperature chlorite geothermometry: a graphical representation based on a T–R2+ –Si diagram. *European Journal of Mineralogy*, *27*(5), 617–626. https://doi.org/10.1127/ejm/2015/0027-2467

Bradbury, K. K., Davis, C. R., Shervais, J. W., Janecke, S. U., & Evans, J. P. (2015). Composition, Alteration, and Texture of Fault-Related Rocks from Safod Core and Surface Outcrop Analogs: Evidence for Deformation Processes and Fluid-Rock Interactions. *Pure and Applied Geophysics*, *172*(5), 1053–1078. https://doi.org/10.1007/s00024-014-0896-6

Braden, Z., & Behr, W. M. (2021). Weakening Mechanisms in a Basalt-Hosted Subduction Megathrust Fault Segment, Southern Alaska. *Journal of Geophysical Research: Solid Earth*, *126*(9), e2021JB022039. https://doi.org/10.1029/2021JB022039

Brown, W. L., & Macaudiére, J. (1984). Microfracturing in relation to atomic structure of plagioclase from a deformed meta-anorthosite. *Journal of Structural Geology*, *6*(5), 579–586. https://doi.org/10.1016/0191-8141(84)90067-1

Brügmann, G. E., Reischmann, T., Naldrett, A. J., & Sutcliffe, R. H. (1996). Roots of an Archean volcanic arc complex: the Lac des Iles area in Ontario, Canada.

Byerlee, J. (1978). Friction of rocks. *Pure and Applied Geophysics*, *116*(4), 615–626. https://doi.org/10.1007/BF00876528

Caine, J. S., & Forster, C. B. (1999). Fault zone architecture and fluid flow: Insights from field data and numerical modeling. In W. C. Haneberg, P. S. Mozley, J. C. Moore, & L. B.

Goodwin (Eds.), *Geophysical Monograph Series* (Vol. 113, pp. 101–127). Washington, D. C.: American Geophysical Union. https://doi.org/10.1029/GM113p0101
Caine, J. S., Evans, J. P., & Forster, C. B. (1996). Fault zone architecture and permeability structure. *Geology*, *24*(11), 1025. https://doi.org/10.1130/0091-7613(1996)024<1025:FZAAPS>2.3.CO;2
Card, K. D. (1990). A review of the Superior Province of the Canadian Shield, a product of Archean accretion. *Precambrian Research*, *48*(1–2), 99–156. https://doi.org/10.1016/0301-9268(90)90059-Y
Card, K. D., & Ciesielski, A. (1986). Subdivisions of the Superior Province of the Canadian Shield. *Geoscience Canada*. Retrieved from https://journals.lib.unb.ca/index.php/GC/article/view/3439
Cathelineau, M. (1988). Cation site occupancy in chlorites and illites as a function of temperature. *Clay Minerals*, *23*(4), 471–485. https://doi.org/10.1180/claymin.1988.023.4.13
Cheng, N., Shi, M., Hou, Q., Wang, J., & Pan, J. (2022). The impact of tectonic stress chemistry on mineralization processes: A review. *Solid Earth Sciences*, *7*(2), 151–166. https://doi.org/10.1016/j.sesci.2021.11.002
Chester, F. M., Evans, J. P., & Biegel, R. L. (1993). Internal structure and weakening mechanisms of the San Andreas Fault. *Journal of Geophysical Research: Solid Earth*, *98*(B1), 771–786. https://doi.org/10.1029/92JB01866
Coulomb, C. A. (1776). Essai sur une application des regles de maximis et minimis quelques problemes de statique, relatits a l'architecture. *Memoires de Mathematique de l'Academie Royale de Science*, *7*, 343–387.
De Caritat, P., Hutcheon, I., & Walshe, J. L. (1993). Chlorite Geothermometry: A Review. *Clays and Clay Minerals*, *41*(2), 219–239. https://doi.org/10.1346/CCMN.1993.0410210
Djon, M. L., Peck, D. C., Olivo, G. R., Miller, J. D., & Joy, B. (2018). Contrasting Styles of Pd-Rich Magmatic Sulfide Mineralization in the Lac des Iles Intrusive Complex, Ontario, Canada. *Economic Geology*, *113*(3), 741–767. https://doi.org/10.5382/econgeo.2018.4568
Dorsey, M. T., Rockwell, T. K., Girty, G. H., Ostermeijer, G. A., Browning, J., Mitchell, T. M., & Fletcher, J. M. (2021). Evidence of hydrothermal fluid circulation driving elemental mass redistribution in an active fault zone. *Journal of Structural Geology*, *144*, 104269. https://doi.org/10.1016/j.jsg.2020.104269
Duan, Q., Yang, X., Ma, S., Chen, J., & Chen, J. (2016). Fluid–rock interactions in seismic faults: Implications from the structures and mineralogical and geochemical compositions of drilling cores from the rupture of the 2008 Wenchuan earthquake, China. *Tectonophysics*, *666*, 260–280. https://doi.org/10.1016/j.tecto.2015.11.008
Duran, C. J., Barnes, S.-J., & Corkery, J. T. (2016). Geology, petrography, geochemistry, and genesis of sulfide-rich pods in the Lac des Iles palladium deposits, western Ontario, Canada. *Mineralium Deposita*, *51*(4), 509–532. https://doi.org/10.1007/s00126-015-0622-z
Evans, J. P. (1990). Thickness-displacement relationships for fault zones. *Journal of Structural Geology*, *12*(8), 1061–1065. https://doi.org/10.1016/0191-8141(90)90101-4
Faulkner, D. R., Jackson, C. A. L., Lunn, R. J., Schlische, R. W., Shipton, Z. K., Wibberley, C. A. J., & Withjack, M. O. (2010). A review of recent developments concerning the

structure, mechanics and fluid flow properties of fault zones. *Journal of Structural Geology*, *32*(11), 1557–1575. https://doi.org/10.1016/j.jsg.2010.06.009
Fumerton, S. L. (1982). Redefinition of the Quetico Fault near Atikokan, Ontario. *Canadian Journal of Earth Sciences*, *19*(1), 222–224. https://doi.org/10.1139/e82-015
Goddard, J. V., & Evans, J. P. (1995). Chemical changes and fluid-rock interaction in faults of crystalline thrust sheets, northwestern Wyoming, U.S.A. *Journal of Structural Geology*, *17*(4), 533–547. https://doi.org/10.1016/0191-8141(94)00068-B
He, C., Wang, Z., & Yao, W. (2007). Frictional sliding of gabbro gouge under hydrothermal conditions. *Tectonophysics*, *445*(3–4), 353–362. https://doi.org/10.1016/j.tecto.2007.09.008
Higgins, M. (1971). *Cataclastic Rocks* (Geological Survey Professional Paper No. 0687) (p. 97). United States Geological Survey.
Hinchey, J. G., Hattori, K. H., & Lavigne, M. J. (2005). Geology, Petrology, and Controls on PGE Mineralization of the Southern Roby and Twilight Zones, Lac des Iles Mine, Canada. *Economic Geology*, *100*, 43–61.
Implats. (2022). *Regional & Local Geological Setting Overview*.
Implats. (2024). *Impala Canada Fact Sheet*. https://implats-ir.co.za/results/2024/annual-results-2024/pdf/MRR-2024.pdf
Isaacs, A. J. (2005). Characterizing Deformation, Damage Parameters, and Clay Composition in Fault Zones: Insights from the Chelungpu Thrust, Taiwan, and Mozumi Right Lateral Fault, Japan.
Jamison, W., & Stearns, D. (1982, December). *Tectonic Deformation of Wingate Sandston, Colorado National Monument*. AAPG Bulletin.
Janssen, C., Wirth, R., Wenk, H.-R., Morales, L., Naumann, R., Kienast, M., et al. (2014). Faulting processes in active faults – Evidences from TCDP and SAFOD drill core samples. *Journal of Structural Geology*, *65*, 100–116. https://doi.org/10.1016/j.jsg.2014.04.004
Jonsson, J. (2023, April). *Petrogenesis of mineralized horizons in the Offset and Creek zones, Lac des Iles Complex, N. Ontario*. Lakehead University, Ontario.
Kehlenbeck, M. M. (1976). Nature of the Quetico–Wabigoon boundary in the de Courcey – Smiley Lakes area, northwestern Ontario. *Canadian Journal of Earth Sciences*, *13*(6), 737–748. https://doi.org/10.1139/e76-078
Keren, T. T., & Kirkpatrick, J. D. (2016). The damage is done: Low fault friction recorded in the damage zone of the shallow Japan Trench décollement. *Journal of Geophysical Research: Solid Earth*, *121*(5), 3804–3824. https://doi.org/10.1002/2015JB012311
Kisch, H. J. (1987). Correlation between indicators of very low-grade metamorphism. In *Low Temperature Metamorphism* (pp. 227–300). Glasgow: Blackie and Son Ltd.
Knipe, R. J. (1989). Deformation mechanisms — recognition from natural tectonites. *Journal of Structural Geology*, *11*(1), 127–146. https://doi.org/10.1016/0191-8141(89)90039-4
Lavigne, M. J., & Michaud, M. J. (2001). Geology of North American Palladium Ltd.'s Roby Zone Deposit, Lac des Iles. *Exploration and Mining Geology*, *10*(1–2), 1–17. https://doi.org/10.2113/10.1-2.1
Lavigne, M. J., Michaud, M. J., & Rickard, J. (2005, August). Exploration For Platinum Group Elements. Retrieved May 15, 2023, from https://www.mineralogicalassociation.ca/wordpress/wp-content/uploads/2022/08/Exploration_for_Platinum_Group_Elements.pdf

Logan, J. M., Dengo, C. A., Higgs, N. G., & Wang, Z. Z. (1992). Chapter 2 Fabrics of Experimental Fault Zones: Their Development and Relationship to Mechanical Behavior. In *International Geophysics* (Vol. 51, pp. 33–67). Elsevier. https://doi.org/10.1016/S0074-6142(08)62814-4

Ma, S., Zeng, L., Tian, H., Shi, X., Wu, W., Yang, S., et al. (2023). Fault damage zone and its effect on deep shale gas: Insights from 3D seismic interpretation in the southern Sichuan Basin, China. *Journal of Structural Geology*, *170*, 104848. https://doi.org/10.1016/j.jsg.2023.104848

Masuda, K., Arai, T., & Takahashi, M. (2019). Effects of frictional properties of quartz and feldspar in the crust on the depth extent of the seismogenic zone. *Progress in Earth and Planetary Science*, *6*(1), 50. https://doi.org/10.1186/s40645-019-0299-5

Maxwell, J., & Benson, D. (2020). 20000018567: 2018 Exploration Geophysics (UAV-borne Magnetic Survey) Assessment Report on the East Mine Block Project, Lac des Iles Mine.

McLennan, S., & Taylor, S. R. (1979). Rare earth element mobility associated with uranium mineralisation. *Nature*, *282*.

Mitchell, T. M., & Faulkner, D. R. (2012). Towards quantifying the matrix permeability of fault damage zones in low porosity rocks. *Earth and Planetary Science Letters*, *339–340*, 24–31. https://doi.org/10.1016/j.epsl.2012.05.014

Nimis, P., Tesalina, S. G., Omenetto, P., Tartarotti, P., & Lerouge, C. (2004). Phyllosilicate minerals in the hydrothermal mafic?ultramafic-hosted massive-sulfide deposit of Ivanovka (southern Urals): comparison with modern ocean seafloor analogues. *Contributions to Mineralogy and Petrology*, *147*(3), 363–383. https://doi.org/10.1007/s00410-004-0565-3

Olgaard, D. L., & Brace, W. F. (1983). The microstructure of gouge from a mining-induced seismic shear zone. *International Journal of Rock Mechanics and Mining Sciences & Geomechanics Abstracts*, *20*(1), 11–19. https://doi.org/10.1016/0148-9062(83)91610-8

Peck, D., & Djon, M. L. (2020). *The Lac des Iles Palladium Deposits* (Internal) (p. 193).

Peck, D. C., decharte, D., Penna, D., Roney, C., Young, B., Duinker, R., & Houdeh, B. (2015). NI 43-101 Technical Report for Lac des Iles Mine, Ontario Incorporating a Preliminary Economic Assessment of the Mine Expansion Plan.

Percival, & Easton. (2007). *Geology of the Canadian Shield in Ontario: An Update* (No. 5511) (p. 5511). https://doi.org/10.4095/223891

Percival, & Williams. (1989). Late Archean Quetico accretionary complex, Superior province, Canada. *Geology*, *17*(1), 23. https://doi.org/10.1130/0091-7613(1989)017<0023:LAQACS>2.3.CO;2

Percival, J. (2007). Geology and Metallogeny of the Superior Province, Canada. In *Geological Association of Canada, Mineral Deposits Division, Special Publication* (Vol. 5, pp. 903–928).

Percival, J., Skulski, T., Sanborn-Barrie, M., Stott, G., Leclair, A., Corkery, T., & Boily, M. (2012). *Geology and tectonic evolution of the Superior Province, Canada; in Tectonic Styles in Canada: The Lithoprobe Perspective.*

Percival, J. A., Sanborn-Barrie, M., Skulski, T., Stott, G. M., Helmstaedt, H., & White, D. J. (2006). Tectonic evolution of the western Superior Province from NATMAP and Lithoprobe studies. *Canadian Journal of Earth Sciences*, *43*(7), 1085–1117. https://doi.org/10.1139/e06-062

Pettigrew, N. T., & Hattori, K. H. (2001). Geology of the Palladium-rich Legris Lake Mafic-Ultramafic Complex, Western Wabigoon Subprovince, Northwestern Ontario. *Exploration and Mining Geology*, *10*(1–2), 35–49. https://doi.org/10.2113/10.1-2.35

Phillips, N. J., Belzer, B., French, M. E., Rowe, C. D., & Ujiie, K. (2020). Frictional Strengths of Subduction Thrust Rocks in the Region of Shallow Slow Earthquakes. *Journal of Geophysical Research: Solid Earth*, *125*(3), e2019JB018888. https://doi.org/10.1029/2019JB018888

Poppe, L. J., Paskevich, V. F., Hatheway, J. C., & Blackwood, D. S. (2001). *A Laboratory Manual for X-Ray Powder Diffraction* (Open-File Report No. 01–041). United States Geological Survey. Retrieved from http://pubs.usgs.gov/openfile/of01-041/index.htm

Rankin, L. R. (2013). *Structural controls on emplacement and deformation of PGE mineralized mafic and ultramafic intruions*.

Sánchez-Roa, C., Faulkner, D. R., Boulton, C., Jimenez-Millan, J., & Nieto, F. (2017). How phyllosilicate mineral structure affects fault strength in Mg-rich fault systems. *Geophysical Research Letters*, *44*(11), 5457–5467. https://doi.org/10.1002/2017GL073055

Savage, H. M., & Brodsky, E. E. (2011). Collateral damage: Evolution with displacement of fracture distribution and secondary fault strands in fault damage zones. *Journal of Geophysical Research*, *116*(B3), B03405. https://doi.org/10.1029/2010JB007665

Savage, H. M., Shreedharan, S., Fagereng, Å., Morgan, J. K., Meneghini, F., Wang, M., et al. (2021). Asymmetric Brittle Deformation at the Pāpaku Fault, Hikurangi Subduction Margin, NZ, IODP Expedition 375. *Geochemistry, Geophysics, Geosystems*, *22*(8), e2021GC009662. https://doi.org/10.1029/2021GC009662

Sawyer, E. W. (1983). The structural history of a part of the Archaean Quetico Metasedimentary Belt, superior province, Canada. *Precambrian Research*, *22*(3–4), 271–294. https://doi.org/10.1016/0301-9268(83)90052-9

Schleicher, A. M., Van Der Pluijm, B. A., & Warr, L. N. (2012). Chlorite-smectite clay minerals and fault behavior: New evidence from the San Andreas Fault Observatory at Depth (SAFOD) core. *Lithosphere*, *4*(3), 209–220. https://doi.org/10.1130/L158.1

Sheldon, H. A., & Micklethwaite, S. (2007). Damage and permeability around faults: Implications for mineralization. *Geology*, *35*(10), 903. https://doi.org/10.1130/G23860A.1

Smith, W. D. (2023). *Camp Lake Zone Report*.

Smith, W. D., Fay, L., Mungall, J. E., Far, M. S., & Djon, L. (2024). Olivine compositions reveal an andesitic parent magma for the Archean palladium-mineralized Lac des Iles Complex of Ontario, Canada. *Mineralium Deposita*. https://doi.org/10.1007/s00126-024-01257-4

Somarin, A. K., Kissin, S. A., Heerema, D. D., & Bihari, D. J. (2009). Hydrothermal Alteration, Fluid Inclusion and Stable Isotope Studies of the North Roby Zone, Lac des Iles PGE Mine, Ontario, Canada. *Resource Geology*, *59*(2), 107–120. https://doi.org/10.1111/j.1751-3928.2009.00084.x

Stone, D. (2010). *Precambrian Geology of the Central Wabigoon Subprovince Area, Northwestern Ontario* (Open File Report No. 5422). Ontario: Ontario Geological Survey.

Stone, D., Lavigne, M. J., Schnieders, B., Scott, J., & Wagner, D. (2003). *Summary of Field Work* (Open File Report No. 6120) (pp. 138–162). Ontario Geological Survey.

Stott, G. M., Corkery, M. T., Percival, J. A., Simard, M., & Goutier, J. (2010). *A Revised Terrane Subdivision of the Superior Province* (Open File Report No. 6260) (pp. 20–1 to 20–10). Ontario Geological Survey.

Sun, S., & McDonough, W. (1989). Chemical and isotopic systematics of ocean basalts: Implications for mantle composition and processes, in Magmatism in the Ocean Basins. *Geol. Soc. Spec. Publ.*, *423*, 13–345.

Sutcliffe, R. H. (1986). Geological and Geophysical Studies in the Lac des Iles Area, District of Thunder Bay.

Sutcliffe, R. H. (1989). Magma mixing in late Archean tonalitic and mafic rocks of the Lac des Iles area, western Superior province. *Precambrian Research*, *44*(2), 81–101. https://doi.org/10.1016/0301-9268(89)90077-6

Sutcliffe, R. H., Sweeny, J. M., & Edgar, A. D. (1989). The Lac des Iles Complex, Ontario: petrology and platinum-group-elements mineralization in an Archean mafic intrusion. *Canadian Journal of Earth Sciences*, *26*(7), 1408–1427. https://doi.org/10.1139/e89-120

Tesei, T., Collettini, C., Carpenter, B. M., Viti, C., & Marone, C. (2012). Frictional strength and healing behavior of phyllosilicate-rich faults. *Journal of Geophysical Research: Solid Earth*, *117*(B9), 2012JB009204. https://doi.org/10.1029/2012JB009204

Thomas, M. Y., Mitchell, T. M., & Bhat, H. S. (Eds.). (2017). *Fault zone dynamic processes: evolution of fault properties during seismic rupture*. Hoboken, New Jersey : Washington, D.C: John Wiley & Sons, Inc. ; American Geophysical Union.

Thurston, P. C. (1991). Archean Geology of Ontario: Introduction. *Geology of Ontario*, *4*, 73–78.

Tomlinson, K. Y., Davis, D. W., Stone, D., & Hart, T. R. (2003). U–Pb age and Nd isotopic evidence for Archean terrane development and crustal recycling in the south-central Wabigoon subprovince, Canada. *Contributions to Mineralogy and Petrology*, *144*(6), 684–702. https://doi.org/10.1007/s00410-002-0423-0

Tomlinson, K. Y., Stott, G. M., Percival, J. A., & Stone, D. (2004). Basement terrane correlations and crustal recycling in the western Superior Province: Nd isotopic character of granitoid and felsic volcanic rocks in the Wabigoon subprovince, N. Ontario, Canada. *Precambrian Research*, *132*(3), 245–274. https://doi.org/10.1016/j.precamres.2003.12.017

Vektore. (2021, January). *Camp Lake Project Pre-Field Stage Report*. Internal, Impala Canada.

Volpe, G. (2023). *Structural and frictional properties of phyllosilicate-rich faults and implications for their seismogenic potential*. Sapienza Università di Roma.

Watkinson, D. H., & Dunning, G. (1979). Geology and platinum-group mineralization, Lac-des-Iles complex, northwestern Ontario. *Can. Mineral.*, *17*, 453–462.

Wiewióra, A., & Weiss, Z. (1990). Crystallochemical classifications of phyllosilicates based on the unified system of projection of chemical composition: II. The chlorite group. *Clay Minerals*, *25*(1), 83–92. https://doi.org/10.1180/claymin.1990.025.1.09

Williams, H. R. (1991). Quetico Subprovince. *Geology of Ontario*, *4*, 73–78.

Woodward, N. B., Wojtal, S., Paul, J. B., & Zadins, Z. Z. (1988). Partitioning of Deformation within Several External Thrust Zones of the Appalachian Orogen. *The Journal of Geology*, *96*(3), 351–361.

Yang, T., Chou, Y.-M., Ferré, E. C., Dekkers, M. J., Chen, J., Yeh, E.-C., & Tanikawa, W. (2020). Faulting Processes Unveiled by Magnetic Properties of Fault Rocks. *Reviews of Geophysics*, *58*(4), e2019RG000690. https://doi.org/10.1029/2019RG000690

Yongliang, X., & Yusheng, Z. (1991). The mobility of rare-earth elements during hydrothermal activity: A review. *Chinese Journal of Geochemistry*, *10*(4), 295–306. https://doi.org/10.1007/BF02841090

Zane, A., & Weiss, Z. (1998). A procedure for classifying rock-forming chlorites based on microprobe data. *Rendiconti Lincei*, *9*(1), 51–56. https://doi.org/10.1007/BF02904455

Zang, W., & Fyfe, W. S. (1995). Chloritization of the hydrothermally altered bedrock at the Igarape Bahia gold deposit, Carajas, Brazil.

Appendix One: Drill Hole Logs

21-503

0 - 45.5 m	Mafic Dike	Mafic dike with intermixed felsic dikes and brecciated gabbro.
45.5 - 58.3 m	Gabbronorite	Variably textured gabbro, variable (weak) alteration.
58.3 - 63.92 m	Mafic Dike	Fine grained mafic dike.
63.92 - 72 m	Gabbronorite	Variably textured gabbro, variable (weak) alteration.
72 - 74.1 m	Felsic Dike	Coarse grained.
74.1 - 107.75 m	Gabbronorite	Variably textured gabbronorite, brecciated and altered, felsic dikes present which are sheared and altered.
107.65 - 109 m	Felsic Dike	Strongly altered felsic dike.
109 - 331 m	Gabbronorite	Alteration increases down section from weak to moderately altered. Coarse to fine grained gabbronorite.
331 - 367.7 m	Norite	Weakly altered norite. Medium grained.
367.7 - 370.15 m	Felsic Dike	Strongly altered felsic dike.
370.15 - 377.85 m	Gabbronorite	Moderately altered.
377.85 - 379.7 m	Intermediate Dike	Strongly altered dike.
379.7 - 427.8 m	Gabbronorite	Damage zone, extremely altered gabbronorite.
427.8 - 431.5 m	Intermediate Dike	Strongly altered.
431.5 - 519.6 m	Gabbronorite	Damage zone. Extremely altered gabbronorite. Variable grain size. Sheared and fractured.

519.6 - 526 m	Fault	Camp Lake Fault
526 - 636.2 m	Tonalite	Strongly altered and fractured tonalite. Damage zone. Moderately foliated.
636.2 - 638.85 m	Intermediate Dike	Strongly altered. Healed fractures.
638.85 - 679 m	Tonalite	Moderately altered. Strongly foliated.
679 - 687 m	Mafic Dike	Fine grained, fratured.

21-700

486 - 537 m	Diorite	Quartz diorite. Coarse grained. Foliated. Weakly altered, with increased alteration at end of interval.
537 - 542.12 m	Mafic Dike	Moderately altered.
542.12 - 578.3 m	Tonalite	Moderately/Variably altered. Foliated.
578.3 - 580 m	Intermediate Dike	Fine grained
580 - 640.9 m	Diorite	Quartz diorite. Coarse grained. Foliated. Weakly altered.
640.9 - 786.6 m	Tonalite	Strongly altered tonalite. Fractured and sheared with small (< 30cm) felsic and mafic dikes.
786.6 - 788.4 m	Fault	Camp Lake Fault
788.4 - 1300m (EOH)	Gabbronorite	Gabbronorite to norite interval. Variable from medium to coarse grained. Alteration is strong and pervasive from fault until ~850 m, where it changes to moderate and localized alteration.

22-750

0 - 86 m	Norite	Weakly altered. Somewhat variable between Norite and Gabbro.
86 - 163 m	Gabbronorite	Weak but variably altered. Alteration occurs in patches. Medium grained.
163 - 169.5 m	Diorite	Moderately altered. Coarse grained.
169 - 181.5 m	Gabbronorite	Moderately altered. Medium grained.
181.5 - 183.25 m	Intermediate Dike	Moderately altered. Fine grained.
183.25 - 207.6 m	Gabbronorite	Moderately/Variably altered. Medium grained. Healed fractures.
207.6 - 209.9 m	Intermediate Dike	Strongly altered. Fine grained.
212.05 - 216 m	Fault	Camp Lake Fault
216 - 217.3 m	Gabbronorite	Strongly altered, fractured.
217.3 - 248.1 m	Tonalite	Strongly altered and fractured. Healed fractures with sericite and epidote.
248.1 - 252.5 m	Felsic Dike	Altered, coarse grained.
252.5 - 262.68 m	Tonalite	Strongly altered, medium grained. Healed fractures.
262.68 - 268.64 m	Felsic Dike	Altered, coarse grained.
268.64 - 315.1 m	Tonalite	Moderately altered. Foliated.
315.1 - 317.6 m	Intermediate Dike	Altered. Fine grained.
317.6 - 327.9 m	Tonalite	Moderately altered. Foliated.
327.9 - 451.1 m	Gabbronorite	Weakly altered. Minor fracturing.

22-905

497.90 - 533.66 m	Gabbronorite	Variably altered. Weak with local moderate alteration by sericite. Medium grained.
533.66 - 537.94 m	Mafic Dike	Fine grained. Weakly altered.
537.94 - 709.45 m	Gabbronorite	Moderately altered with patches of locally weak alteration/"fresh" textured. Medium grained.
709.45 - 729.3 m	Tonalite	Tonalite blip/Large felsic dike. Medium to coarse grained.
729.3 - 753.7 m	Gabbronorite	Beginning of stronger alteration zone. Increased fractures, some healed with clay alteration.
753.7 - 754 m	Fault	Camp Lake Fault
754 - 801 m (EOH)	Tonalite	Highly altered and fractured. Damage zone.

18-602

0 - 20.14 m	Mafic Dike	Fine grained.
20.14 - 58.68 m	Gabbronorite	Medium grained. Weakly altered.
58.68 - 65.04 m	Mafic Dike	Fine grained.
65.04 - 107.1 m	Gabbronorite	Medium grained. Weakly altered.
107.1 - 141.8 m	Norite	Medium grained. Weakly altered.
141.8 - 189.95 m	Gabbronorite	Medium grained. Weakly altered.
189.95 - 192.1 m	Mafic dike	Fine grained.
192.1 - 286.7 m	Gabbronorite	Moderate to strong alteration. Moderate amount of fractures that are healed.
286.7 - 290.15 m	Fault	Offset Fault
290.15 - 587.48 m (EOH)	Gabbronorite	Moderate to strong alteration. Moderate amount of fractures that are healed for damage zone. Weak alteration after damage zone with minor fracturing.

21-600

0 - 3.2 m	Mafic Dike	Fine grained.
3.2 - 53.7 m	Tonalite	Medium grained. Weakly altered with local moderate alteration
53.7 - 61.03 m	Mafic Dike	Fine grained.
61.03 - 70.7 m	Tonalite	Highly altered and fractured, moderately sheared.
70.7 - 73.74	Fault	Offset Fault
73.74 - 149.73 m	Gabbronorite	Variably altered. Highly altered within ~40 m of fault. Brecciated and fractured. Some healed fractures. Medium to coarse grained.
149.73 - 152.9 m	Mafic Dike	Highly altered and sheared. Fine grained.
152.9 - 170 m	Gabbronorite	Variably altered, moderate to weak alteration. Medium to coarse grained.

21-603

0 - 5.96 m	Mafic Dike	Fine grained.
5.96 - 24.29 m	Tonalite	Medium grained. Weakly altered.
24.29 -26.02 m	Mafic Dike	Fine grained.
26.02 - 34.77 m	Tonalite	Variably altered. Foliated. Medium grained.
34.77 - 38.54 m	Mafic Dike	Fine grained.
38.54 - 119 m	Tonalite	Highly altered and fractured with moderate shearing.
119 - 122 m	Fault	Offset Fault
122 - 273 m	Gabbronorite	Strong alteration for first ~30 m. Moderate amount of fracturing. Alteration changes to moderate/weak once out of damage zone.

22-682

0 - 2.85 m	Mafic Dike	Fine grained.
2.85 - 34.27 m	Tonalite	Medium grained. Variably altered. Strongly foliated.
34.27 - 35.81 m	Mafic Dike	Fine grained.
35.81 - 38.44 m	Tonalite	Variably altered. Foliated. Medium grained.
38.44 - 39.5 m	Mafic Dike	Fine grained.
39.5 - 65.4 m	Tonalite	Highly altered and fractured in damage zone.
65.4 - 66 m	Fault	Offset Fault
66 - 80.3 m	Gabbronorite	Strong alteration and fractured. Fine to coarse grained. Damage zone.
80.3 - 82.73 m	Intermediate Dike	Fine grained, weakly altered.
82.73 - 152.76 m	Gabbronorite	Moderate pervasive alteration. Small inclusions of mafic dikes. Fracturing that has been healed. Fine to coarse grained.
152.76 - 153.9 m	Mafic Dike	Fine grained.
153.9 - 159.7 m	Gabbronorite	Moderately altered. Medium grained.
159.7 - 161.3 m	Mafic Dike	Fine grained.
161.3 - 216.65 m	Gabbronorite	Moderately altered. Typically meduim to coarse grained. Minor amount of fracturing.

Appendix Two: Geochemical Data

Sample Number	*JPCL01*	*JPCL02*	*JPCL03*	*JPCL04*	*JPCL05*	*JPCL06*	*JPCL07*	*JPCL08*
Sample Meterage	1	25	50	75	81	101	110	121
SiO_2 %	49.7	51.5	50.6	50.6	49.6	57.9	51.1	50.8
Al_2O_3 %	14.1	14.6	13.8	12.4	12.65	15.45	15.2	11.55
Fe_2O_3 %	8.38	10.15	8.84	9.88	9.43	6.77	8.2	10.55
CaO %	7.96	9.24	8.22	7.72	7.92	8.11	8.29	6.71
MgO %	13.35	11.55	14.05	15.55	14.5	6.15	11.7	14.9
Na_2O %	1.35	1.92	1.46	0.98	1.38	3.35	1.72	1.22
K_2O %	0.31	0.48	0.21	0.32	0.5	0.84	0.71	0.44
Cr_2O_3 %	0.064	0.038	0.063	0.071	0.068	0.024	0.053	0.059
TiO_2 %	0.1	0.13	0.09	0.1	0.11	0.33	0.1	0.11
MnO %	0.14	0.17	0.15	0.16	0.16	0.1	0.14	0.17
P_2O_5 %	0.005	0.005	0.01	0.01	0.005	0.09	0.01	0.005
SrO %	0.02	0.02	0.02	0.01	0.01	0.06	0.02	0.01
BaO %	0.01	0.01	0.005	0.01	0.01	0.02	0.01	0.01
LOI %	3.53	1.82	1.51	3.85	4.06	2.71	3.88	3.77
Total %	99.01	101.63	99.02	101.66	100.4	101.9	101.13	100.3
C %	0.04	0.15	0.17	0.09	0.07	0.2	0.24	0.08
S %	0.04	0.19	0.07	0.06	0.04	0.25	0.08	0.06
Ba ppm	51.5	84.5	47.9	74.5	82.8	209	109	94.9
Ce ppm	1.5	2.7	3	4.5	2.2	28.4	3	2.2
Cr ppm	493	308	507	565	535	207	415	473
Cs ppm	2.55	2.24	2.04	2.01	2.11	2.6	2.13	1.84
Dy ppm	0.37	0.51	0.37	0.46	0.39	0.95	0.35	0.34
Er ppm	0.3	0.33	0.33	0.32	0.29	0.5	0.29	0.31
Eu ppm	0.16	0.21	0.17	0.11	0.13	0.74	0.17	0.13
Ga ppm	10.4	12.6	10.3	9.4	9.8	15.9	11	9.3
Gd ppm	0.27	0.42	0.31	0.34	0.29	1.43	0.32	0.26
Ge ppm	1.4	1.3	1.4	1.4	1.5	1.1	1.2	1.5
Hf ppm	0.1	0.16	0.11	0.16	0.14	1.83	0.39	0.21
Ho ppm	0.1	0.12	0.09	0.1	0.09	0.17	0.1	0.08
La ppm	0.9	1.4	3	4.7	1.2	13.9	2.1	1.2
Lu ppm	0.06	0.06	0.06	0.05	0.06	0.07	0.07	0.05
Nb ppm	0.025	0.12	0.025	0.11	0.16	2.23	0.23	0.28
Nd ppm	0.8	1.3	1	1.2	0.9	13.7	1.1	0.8
Pr ppm	0.18	0.31	0.24	0.31	0.23	3.42	0.26	0.26
Rb ppm	10.4	15.9	5.9	8.5	16.4	28.5	22.5	14.1
Sm ppm	0.17	0.31	0.24	0.2	0.26	2.46	0.25	0.27
Sn ppm	0.25	0.25	0.25	0.25	0.25	0.25	0.25	0.25
Sr ppm	151.5	198.5	171.5	118.5	132	543	182	119.5
Ta ppm	0.05	0.05	0.05	0.05	0.05	0.05	0.05	0.05

Tb ppm	0.06	0.07	0.05	0.08	0.06	0.16	0.06	0.05
Th ppm	0.025	0.08	0.09	0.16	0.09	2.79	0.24	0.27
Tm ppm	0.04	0.06	0.06	0.04	0.05	0.07	0.06	0.05
U ppm	0.025	0.07	0.025	0.1	0.06	1.02	0.08	0.11
V ppm	93	141	125	151	108	104	95	119
W ppm	0.25	13.2	6.1	4.3	0.25	0.25	0.25	0.25
Y ppm	2.5	3.3	2.8	3.1	2.3	5	2.7	2.3
Yb ppm	0.28	0.41	0.32	0.38	0.33	0.48	0.29	0.34
Zr ppm	4	5	4	6	5	76	15	7
As ppm	0.05	0.3	0.05	0.05	0.05	0.05	0.2	0.1
Bi ppm	0.05	0.03	0.01	0.05	0.01	0.11	0.01	0.03
Hg ppm	0.0025	0.0025	0.0025	0.0025	0.0025	0.0025	0.0025	0.0025
In ppm	0.0025	0.0025	0.0025	0.0025	0.0025	0.005	0.0025	0.0025
Re ppm	0.0005	0.001	0.0005	0.0005	0.0005	0.0005	0.0005	0.0005
Sb ppm	0.025	0.025	0.025	0.025	0.025	0.025	0.025	0.025
Se ppm	0.3	0.8	0.2	0.2	0.2	0.3	0.4	0.4
Te ppm	0.01	0.09	0.03	0.05	0.005	0.04	0.02	0.1
Tl ppm	0.01	0.07	0.03	0.01	0.01	0.03	0.02	0.04
Ag ppm	0.25	0.25	0.25	0.25	0.25	0.25	0.25	0.25
Cd ppm	0.25	0.25	0.25	0.25	0.25	0.25	0.25	0.25
Co ppm	65	71	70	75	70	36	60	79
Cu ppm	102	353	112	118	138	196	163	261
Li ppm	20	10	10	10	20	20	20	10
Mo ppm	0.5	0.5	0.5	0.5	0.5	0.5	0.5	0.5
Ni ppm	375	465	398	422	436	135	370	540
Pb ppm	1	18	3	1	1	1	6	1
Sc ppm	20	28	30	31	28	21	22	32
Zn ppm	58	142	60	63	62	49	83	67
Sample Number	JPCL09	JPCL10	JPCL11	JPCL12	JPCL13	JPCL14	JPCL15	JPCL16
Sample Meterage	131	141	151	161	174	180	187	192
SiO_2 %	50.4	51	50.6	51.1	49.2	49.6	50.5	37.7
Al_2O_3 %	11.25	12.55	13.05	13.8	10.85	18.75	8.54	5.38
Fe_2O_3 %	10.85	10.3	9.82	9.25	10.7	7.06	13.15	11.7
CaO %	7.1	7.9	7.68	6.89	8.7	8.78	6.57	9.08
MgO %	15.8	15.2	14.75	12.9	14.5	9.81	17.55	22
Na_2O %	1.01	1.23	1.32	1.91	0.99	2.28	0.5	0.01
K_2O %	0.32	0.16	0.24	0.44	0.31	0.75	0.17	0.01
Cr_2O_3 %	0.056	0.055	0.055	0.045	0.055	0.04	0.066	0.025
TiO_2 %	0.11	0.13	0.11	0.12	0.15	0.1	0.17	0.06
MnO %	0.18	0.17	0.17	0.16	0.18	0.11	0.21	0.06
P_2O_5 %	0.01	0.02	0.01	0.01	0.005	0.005	0.005	0.005

SrO %	0.01	0.01	0.01	0.02	0.01	0.03	0.005	0.005
BaO %	0.01	0.005	0.01	0.01	0.01	0.02	0.005	0.005
LOI %	3.98	1.36	2.21	3.71	3.35	3.36	3.93	12.3
Total %	101.09	100.09	100.04	100.37	99.01	100.69	101.36	98.33
C %	0.05	0.21	0.21	0.08	0.05	0.04	0.03	2.06
S %	0.14	0.05	0.04	0.04	0.35	0.12	0.09	0.09
Ba ppm	0.25	39.6	58.3	113	60.9	194.5	28.2	2.2
Ce ppm	0.3	3.1	2.6	3.5	2	2.3	1.6	1.3
Cr ppm	2.5	412	405	341	416	302	482	196
Cs ppm	0.005	1.43	1.91	2.05	1.37	2.67	1.24	0.2
Dy ppm	0.025	0.46	0.37	0.38	0.56	0.26	0.45	0.28
Er ppm	0.015	0.32	0.24	0.31	0.39	0.23	0.39	0.18
Eu ppm	0.01	0.13	0.11	0.12	0.16	0.18	0.13	0.07
Ga ppm	0.05	10.2	10.7	11.6	9.1	12.4	8.7	4
Gd ppm	0.025	0.3	0.24	0.38	0.4	0.22	0.39	0.2
Ge ppm	0.25	1.7	1.4	1.4	1.6	1.2	1.7	1.3
Hf ppm	0.025	0.17	0.2	0.27	0.21	0.12	0.18	0.14
Ho ppm	0.005	0.09	0.08	0.11	0.12	0.06	0.11	0.07
La ppm	0.2	1.5	1.3	1.6	0.9	1.1	0.7	0.6
Lu ppm	0.005	0.07	0.04	0.07	0.07	0.05	0.06	0.02
Nb ppm	0.025	0.26	0.19	0.65	0.12	0.11	0.15	0.13
Nd ppm	0.2	1.4	0.9	1.4	1.1	0.9	0.9	0.6
Pr ppm	0.04	0.37	0.31	0.41	0.28	0.28	0.22	0.15
Rb ppm	0.1	3.7	7.1	16.9	10	26.3	4.9	0.1
Sm ppm	0.06	0.3	0.27	0.26	0.29	0.18	0.25	0.14
Sn ppm	0.25	0.25	0.25	0.25	0.25	0.25	0.25	0.25
Sr ppm	0.2	132	135.5	192	107.5	289	45.9	13.8
Ta ppm	0.05	0.05	0.05	0.1	0.05	0.05	0.05	0.05
Tb ppm	0.005	0.07	0.05	0.05	0.06	0.05	0.07	0.04
Th ppm	0.06	0.16	0.15	0.59	0.11	0.08	0.08	0.28
Tm ppm	0.01	0.05	0.05	0.05	0.06	0.03	0.06	0.03
U ppm	0.025	0.25	0.06	0.25	0.05	0.025	0.06	0.08
V ppm	2.5	126	117	117	167	94	183	68
W ppm	0.25	1.9	1	0.8	3.1	1.8	1.5	0.5
Y ppm	0.5	2.8	2.2	2.6	3.1	1.8	3.2	1.9
Yb ppm	0.015	0.28	0.31	0.32	0.37	0.18	0.39	0.17
Zr ppm	0.5	11	6	10	7	4	7	5
As ppm	0.05	0.1	0.05	0.1	0.05	0.1	0.05	0.2
Bi ppm	0.03	0.03	0.02	0.05	0.08	0.34	0.13	0.04
Hg ppm	0.0025	0.0025	0.0025	0.0025	0.0025	0.0025	0.0025	0.0025
In ppm	0.0025	0.0025	0.0025	0.0025	0.0025	0.0025	0.0025	0.008
Re ppm	0.0005	0.0005	0.0005	0.0005	0.001	0.0005	0.0005	0.0005

Sb ppm	0.025	0.025	0.025	0.025	0.025	0.025	0.025	0.025
Se ppm	1.2	0.5	0.2	0.2	1.5	1.1	0.4	0.1
Te ppm	0.18	0.17	0.1	0.14	0.21	0.64	0.06	0.08
Tl ppm	0.01	0.02	0.02	0.01	0.04	0.02	0.01	0.01
Ag ppm	0.25	0.25	0.25	0.25	0.25	0.25	0.25	0.25
Cd ppm	0.25	0.25	0.25	0.25	0.25	0.25	0.25	0.25
Co ppm	87	82	74	66	83	54	90	132
Cu ppm	419	277	147	161	444	443	145	48
Li ppm	20	10	10	20	10	20	20	5
Mo ppm	0.5	0.5	0.5	0.5	0.5	0.5	0.5	0.5
Ni ppm	709	583	485	496	642	611	537	1540
Pb ppm	1	1	1	7	5	1	1	1
Sc ppm	36	32	33	24	38	15	41	21
Zn ppm	64	65	62	84	64	51	79	53
Sample Number	JPCL17	JPCL18	JPCL19	JPCL20	JPCL21	JPCL22	JPCL23	JPCL24
Sample Meterage	197	202	203.75	204.75	205.75	206.75	207.75	208.85
SiO_2 %	50.6	51.5	50.6	51.5	51.4	51.2	65.6	56.6
Al_2O_3 %	4.9	10.4	9.88	9.98	10.25	10.35	16.45	13.95
Fe_2O_3 %	14.5	10.85	10.75	11.15	10.9	10.95	3.41	6.92
CaO %	4.03	6.5	5.99	6.36	6.23	5.85	4.94	5.77
MgO %	21.4	17.4	17.7	18.05	17.85	17.7	1.47	8.89
Na_2O %	0.15	1.07	0.97	0.93	0.97	0.98	5.82	3.86
K_2O %	0.05	0.31	0.35	0.35	0.39	0.62	0.55	0.49
Cr_2O_3 %	0.084	0.074	0.074	0.077	0.076	0.076	0.001	0.032
TiO_2 %	0.19	0.13	0.13	0.13	0.13	0.13	0.53	0.38
MnO %	0.23	0.2	0.2	0.19	0.19	0.19	0.04	0.1
P_2O_5 %	0.01	0.01	0.01	0.005	0.01	0.005	0.21	0.18
SrO %	0.005	0.01	0.01	0.01	0.01	0.01	0.09	0.06
BaO %	0.005	0.01	0.01	0.01	0.01	0.02	0.06	0.03
LOI %	3.61	2.16	3.35	1.18	1.93	1.97	2.03	3.19
Total %	99.75	100.62	100.02	99.92	100.35	100.05	101.2	100.45
C %	0.05	0.14	0.14	0.1	0.09	0.08	0.08	0.05
S %	0.06	0.04	0.04	0.04	0.04	0.04	0.22	0.17
Ba ppm	4.6	70.8	68.8	70.5	89	151	509	306
Ce ppm	1.9	2.5	2.2	2.1	2.1	2.1	88.6	63.5
Cr ppm	623	553	551	569	566	569	13	243
Cs ppm	0.76	2.14	2.13	1.5	2.23	2.31	0.82	1.36
Dy ppm	0.48	0.44	0.46	0.49	0.45	0.46	1.57	1.11
Er ppm	0.46	0.38	0.31	0.31	0.33	0.4	0.66	0.59
Eu ppm	0.09	0.16	0.13	0.15	0.13	0.12	1.2	1
Ga ppm	6.7	9.1	8.5	9.1	8.9	9.3	21.6	15.6

Gd ppm	0.35	0.33	0.32	0.38	0.34	0.31	3.07	2.45
Ge ppm	1.9	1.7	1.6	1.9	1.6	1.6	0.9	1.1
Hf ppm	0.21	0.24	0.21	0.2	0.2	0.21	4.52	2.41
Ho ppm	0.12	0.12	0.1	0.1	0.11	0.11	0.26	0.2
La ppm	0.9	1.2	1	1	1	1	42.9	29.4
Lu ppm	0.07	0.08	0.08	0.07	0.06	0.07	0.08	0.09
Nb ppm	0.21	0.19	0.12	0.12	0.15	0.22	5.78	3.76
Nd ppm	1	1.1	1.1	0.9	1	1.1	37.4	28.1
Pr ppm	0.27	0.31	0.27	0.28	0.27	0.26	10.3	7.49
Rb ppm	0.8	9.4	11.2	10	12.5	19.7	16.6	16.3
Sm ppm	0.3	0.23	0.23	0.24	0.21	0.37	5.35	4.22
Sn ppm	0.25	0.25	0.25	0.25	0.25	0.25	0.8	0.6
Sr ppm	6.8	118	89.1	107	105.5	106.5	762	506
Ta ppm	0.05	0.05	0.05	0.05	0.05	0.05	0.3	0.2
Tb ppm	0.07	0.07	0.05	0.05	0.07	0.06	0.32	0.27
Th ppm	0.12	0.1	0.13	0.13	0.13	0.15	8.96	5.29
Tm ppm	0.07	0.06	0.05	0.07	0.05	0.06	0.09	0.07
U ppm	0.05	0.025	0.025	0.08	0.06	0.06	2.49	1.35
V ppm	202	143	148	149	149	147	62	95
W ppm	1	0.7	0.8	1.3	0.9	1.1	0.7	0.7
Y ppm	3.4	3	2.8	2.9	2.9	2.6	7.4	5.6
Yb ppm	0.45	0.38	0.37	0.42	0.35	0.34	0.49	0.47
Zr ppm	9	7	6	6	7	6	177	96
As ppm	0.1	0.05	0.2	0.05	0.1	0.1	0.2	0.05
Bi ppm	0.02	0.01	0.01	0.01	0.02	0.01	0.02	0.04
Hg ppm	0.0025	0.0025	0.0025	0.0025	0.0025	0.0025	0.0025	0.0025
In ppm	0.0025	0.0025	0.0025	0.0025	0.0025	0.0025	0.005	0.005
Re ppm	0.0005	0.0005	0.0005	0.0005	0.0005	0.0005	0.0005	0.0005
Sb ppm	0.025	0.025	0.025	0.025	0.025	0.025	0.025	0.025
Se ppm	0.2	0.1	0.1	0.1	0.3	0.1	0.1	0.2
Te ppm	0.12	0.05	0.03	0.04	0.1	0.05	0.005	0.02
Tl ppm	0.01	0.01	0.01	0.01	0.02	0.02	0.01	0.01
Ag ppm	0.25	0.25	0.25	0.25	0.25	0.25	0.25	0.25
Cd ppm	0.25	0.25	0.25	0.25	0.25	0.25	0.25	0.25
Co ppm	107	81	82	84	80	83	9	41
Cu ppm	170	69	49	54	68	76	42	44
Li ppm	10	30	30	20	20	30	10	30
Mo ppm	0.5	0.5	0.5	0.5	0.5	0.5	0.5	0.5
Ni ppm	717	524	516	524	512	528	12	231
Pb ppm	1	1	1	1	1	1	5	2
Sc ppm	45	38	39	39	38	39	5	19
Zn ppm	97	74	73	71	71	74	46	56

Sample Number	JPCL25	JPCL26	JPCL27	JPCL28	JPCL29	JPCL30	JPCL31	JPCL32
Sample Meterage	209.75	210.75	211.75	214.75	215.75	216.75	217.75	219.75
SiO_2 %	48	49.2	50.7	52	52.2	50.5	58	65.7
Al_2O_3 %	9.96	9.8	9.33	16.1	15.75	15.45	21.8	18.05
Fe_2O_3 %	10.25	10.35	10.5	8.82	9.06	9.05	3.73	2.75
CaO %	4.61	4.14	5.49	7.64	7.74	8.39	6.42	4.56
MgO %	17.85	17.85	17.95	8.63	9.35	9.25	3	1.78
Na_2O %	1.34	1.28	0.87	3.22	2.71	2.51	5.36	5.87
K_2O %	0.47	0.43	0.19	0.36	0.62	0.66	0.68	0.5
Cr_2O_3 %	0.079	0.075	0.074	0.018	0.018	0.026	0.004	0.001
TiO_2 %	0.12	0.12	0.12	0.16	0.16	0.15	0.1	0.13
MnO %	0.16	0.16	0.19	0.13	0.14	0.15	0.05	0.03
P_2O_5 %	0.005	0.005	0.01	0.02	0.01	0.02	0.03	0.03
SrO %	0.005	0.005	<0.01	0.06	0.04	0.04	0.08	0.06
BaO %	0.01	0.01	<0.01	0.01	0.01	0.01	0.02	0.01
LOI %	5.64	5.42	5.24	3.23	3.38	3.78	2.15	1.66
Total %	98.49	98.84	100.66	100.4	101.19	99.99	101.42	101.13
C %	0.2	0.14	0.05	0.02	0.09	0.23	0.02	0.01
S %	0.04	0.05	0.01	0.29	0.14	0.03	0.01	0.01
Ba ppm	77.3	68.1	20.7	78.1	126	135	169	104
Ce ppm	3.1	2.7	3.3	7.6	5.4	5.4	4.4	11.2
Cr ppm	589	566	555	138	146	199	33	17
Cs ppm	3.21	2.91	2.63	1.52	2.06	2.09	2.05	1.18
Dy ppm	0.4	0.33	0.51	0.84	0.81	0.88	0.26	0.28
Er ppm	0.34	0.33	0.35	0.51	0.51	0.52	0.14	0.12
Eu ppm	0.17	0.13	0.09	0.37	0.29	0.34	0.57	0.65
Ga ppm	9.1	8.6	8.6	15.7	15	15.7	25.6	22.3
Gd ppm	0.34	0.32	0.35	0.73	0.76	0.86	0.21	0.6
Ge ppm	1.4	1.4	1.6	1.7	1.5	1.5	1.2	0.9
Hf ppm	0.22	0.21	0.28	0.43	0.43	0.43	0.34	0.63
Ho ppm	0.12	0.1	0.13	0.17	0.18	0.2	0.05	0.05
La ppm	1.6	1.4	1.9	4	2.4	2.5	2.9	9.2
Lu ppm	0.07	0.06	0.06	0.07	0.09	0.08	0.03	0.02
Nb ppm	0.19	0.17	0.61	0.47	0.27	0.19	0.25	0.24
Nd ppm	1.1	1	1.4	3.2	3	3.1	1.5	4.4
Pr ppm	0.35	0.3	0.34	0.8	0.67	0.72	0.41	1.07
Rb ppm	17.8	16.5	6.4	12	21.7	22.4	20.7	17.8
Sm ppm	0.29	0.24	0.25	0.79	0.73	0.76	0.22	0.58
Sn ppm	0.25	0.25	0.25	0.25	0.25	0.25	0.25	0.25
Sr ppm	38.5	34.6	16.6	518	396	344	714	492
Ta ppm	0.05	0.05	0.1	0.05	0.05	0.05	0.05	0.05

Tb ppm	0.05	0.06	0.06	0.12	0.13	0.14	0.04	0.06
Th ppm	0.2	0.17	2.16	0.36	0.14	0.11	0.11	0.08
Tm ppm	0.05	0.04	0.06	0.07	0.08	0.08	0.02	0.02
U ppm	0.1	0.08	0.6	0.1	0.05	0.05	0.07	0.07
V ppm	143	137	147	136	133	144	33	28
W ppm	0.7	0.6	1.7	3.4	2.3	21.4	1.1	1
Y ppm	2.9	2.6	3.5	4.6	4.8	5.2	1.4	1.2
Yb ppm	0.34	0.29	0.35	0.46	0.53	0.56	0.16	0.12
Zr ppm	7	8	10	15	18	16	15	28
As ppm	0.2	0.05	<0.1	0.4	0.2	0.05	0.2	0.05
Bi ppm	0.03	0.04	0.14	0.3	0.11	0.05	0.06	0.05
Hg ppm	0.0025	0.0025	<0.005	0.0025	0.0025	0.0025	0.0025	0.0025
In ppm	0.005	0.0025	<0.005	0.005	0.0025	0.0025	0.0025	0.0025
Re ppm	0.0005	0.0005	<0.001	0.0005	0.0005	0.0005	0.0005	0.0005
Sb ppm	0.025	0.025	<0.05	0.025	0.025	0.025	0.025	0.025
Se ppm	0.1	0.3	0.2	0.5	0.2	0.1	0.1	0.1
Te ppm	0.02	0.04	0.04	0.03	0.06	0.04	0.005	0.01
Tl ppm	0.02	0.02	<0.02	0.01	0.01	0.01	0.01	0.01
Ag ppm	0.25	0.25	<0.5	0.25	0.25	0.25	0.25	0.25
Cd ppm	0.25	0.25	<0.5	0.25	0.25	0.25	0.25	0.25
Co ppm	82	80	75	55	56	54	17	9
Cu ppm	82	96	20	68	130	37	1	1
Li ppm	80	80	70	30	40	40	20	20
Mo ppm	0.5	0.5	<1	0.5	0.5	0.5	0.5	0.5
Ni ppm	536	528	490	235	228	234	45	11
Pb ppm	1	1	1	1	1	1	1	1
Sc ppm	40	38	35	23	26	25	5	3
Zn ppm	78	78	79	62	73	79	35	21
Sample Number	JPCL33	JPCL34	JPCL35	JPCL36	JPCL37	JPCL38	JPCL39	JPCL40
Sample Meterage	220.75	221.75	222.75	223.75	230	235	240	245
SiO_2 %	64.2	65.3	66	68	65	69.7	72.2	68.6
Al_2O_3 %	18.55	18.15	17.9	17.55	18.65	16	14.85	15.9
Fe_2O_3 %	2.69	2.45	2.6	2.16	2.57	2.65	3.04	3.19
CaO %	4.59	3.78	4.2	3.91	4.37	1.87	2.08	3.13
MgO %	1.69	1.72	1.52	1.26	1.48	1.65	1.49	1.66
Na_2O %	5.71	5.58	5.18	5.32	5.41	6.28	5.79	5.24
K_2O %	0.69	0.84	0.86	0.66	0.84	0.69	0.51	1
Cr_2O_3 %	0.001	0.001	0.002	0.001	0.002	0.001	0.001	0.003
TiO_2 %	0.14	0.12	0.1	0.14	0.15	0.21	0.13	0.18
MnO %	0.03	0.03	0.03	0.03	0.03	0.02	0.03	0.04
P_2O_5 %	0.04	0.02	0.02	0.02	0.03	0.03	0.03	0.03

SrO %	0.06	0.06	0.06	0.06	0.06	0.03	0.04	0.04
BaO %	0.01	0.02	0.02	0.02	0.02	0.01	0.01	0.03
LOI %	1.76	1.82	1.8	1.35	1.62	1.65	1.42	1.85
Total %	100.16	99.89	100.29	100.48	100.23	100.79	101.62	100.89
C %	0.02	0.02	0.02	0.04	0.05	0.02	0.01	0.08
S %	0.01	0.01	0.01	0.03	0.14	0.07	0.24	0.09
Ba ppm	143	159.5	167	175	210	110	104	298
Ce ppm	4.9	4.5	4.8	6.3	6.3	14.5	13	20.9
Cr ppm	18	19	19	17	23	15	20	30
Cs ppm	1.86	3.1	2.64	1.47	1.95	1.13	0.92	1.68
Dy ppm	0.22	0.18	0.18	0.41	0.26	0.2	0.4	0.69
Er ppm	0.11	0.08	0.11	0.32	0.11	0.1	0.22	0.32
Eu ppm	0.49	0.47	0.52	0.42	0.47	0.53	0.58	0.65
Ga ppm	21.5	20.8	21.6	19.8	21	18.8	17.5	20.3
Gd ppm	0.39	0.22	0.23	0.48	0.46	0.4	0.59	0.98
Ge ppm	0.9	0.8	0.8	0.7	0.6	0.6	0.7	1
Hf ppm	0.71	0.63	0.75	1.1	1.57	1.36	1.42	1.46
Ho ppm	0.03	0.03	0.04	0.09	0.06	0.04	0.08	0.11
La ppm	3.7	3.1	3.4	3.7	3.8	8.9	6.9	11.1
Lu ppm	0.01	0.02	0.02	0.04	0.02	0.01	0.03	0.04
Nb ppm	0.38	0.29	0.21	1.83	0.63	0.62	5.41	1.92
Nd ppm	2.2	1.6	1.9	2.6	2.5	4.6	4.5	7.5
Pr ppm	0.53	0.5	0.45	0.68	0.66	1.33	1.31	2.17
Rb ppm	23.2	28.7	26.9	23.5	27.1	28.9	17.4	27.1
Sm ppm	0.36	0.33	0.28	0.59	0.42	0.51	0.67	1.28
Sn ppm	0.25	0.25	0.25	0.25	0.25	0.25	0.25	0.25
Sr ppm	547	522	520	493	559	267	337	322
Ta ppm	0.05	0.05	0.05	0.2	0.1	0.05	0.1	0.05
Tb ppm	0.04	0.03	0.03	0.07	0.04	0.04	0.09	0.1
Th ppm	0.08	0.09	0.1	0.79	0.4	0.55	0.88	1.66
Tm ppm	0.02	0.02	0.01	0.04	0.03	0.01	0.04	0.05
U ppm	0.07	0.08	0.08	0.97	0.33	0.23	0.3	0.45
V ppm	27	24	23	24	33	36	40	51
W ppm	1.6	15.4	1.5	3.4	2.5	1.7	16.6	1.6
Y ppm	1.2	0.9	0.9	2.8	1.5	1.2	2	2.8
Yb ppm	0.07	0.05	0.08	0.26	0.12	0.08	0.19	0.27
Zr ppm	28	31	34	41	68	53	61	53
As ppm	0.1	0.05	0.1	0.05	0.2	0.05	0.2	0.1
Bi ppm	0.03	0.02	0.03	0.03	0.08	0.15	0.58	0.47
Hg ppm	0.0025	0.0025	0.0025	0.0025	0.0025	0.0025	0.0025	0.0025
In ppm	0.0025	0.0025	0.0025	0.0025	0.0025	0.0025	0.0025	0.006
Re ppm	0.0005	0.0005	0.0005	0.0005	0.0005	0.0005	0.0005	0.001

Sb ppm	0.025	0.025	0.025	0.025	0.025	0.025	0.025	0.025
Se ppm	0.1	0.1	0.1	0.1	0.2	0.1	0.3	0.1
Te ppm	0.01	0.005	0.005	0.01	0.03	0.03	0.32	0.24
Tl ppm	0.01	0.01	0.01	0.01	0.01	0.01	0.01	0.01
Ag ppm	0.25	0.25	0.25	0.25	0.25	0.25	0.25	0.25
Cd ppm	0.25	0.25	0.25	0.25	0.25	0.25	0.25	0.25
Co ppm	9	8	8	8	9	7	11	7
Cu ppm	1	1	1	56	35	6	8	8
Li ppm	20	30	20	20	20	30	30	20
Mo ppm	0.5	0.5	0.5	0.5	0.5	0.5	0.5	0.5
Ni ppm	11	11	10	8	9	5	12	22
Pb ppm	1	1	1	5	2	1	1	1
Sc ppm	3	3	3	3	3	3	3	6
Zn ppm	24	28	29	38	33	22	22	36
Sample Number	JPCL41	JPCL42	JPCL43	JPCL44	JPCL45	JPCL46	JPCL47	JPCL48
Sample Meterage	255	265	275	285	295	305	315	340
SiO_2 %	71.8	74.9	69	69.8	69	71.1	67.2	51.1
Al_2O_3 %	15.15	13.65	15.85	15.85	15.2	15	16.75	16.15
Fe_2O_3 %	2.68	1.84	2.46	3.71	4.65	2.35	4	8.31
CaO %	2.78	3.44	3.41	4.41	2.7	1.75	4.78	10.35
MgO %	0.97	0.44	1.04	1.1	1.64	1.66	1.71	8.08
Na_2O %	5.09	4.2	5.22	4.6	4.99	5.79	4.66	2.45
K_2O %	0.75	0.85	0.78	0.38	0.93	0.5	0.59	0.25
Cr_2O_3 %	0.001	0.001	0.001	0.001	0.002	0.001	0.002	0.003
TiO_2 %	0.19	0.08	0.21	0.3	0.39	0.15	0.33	0.13
MnO %	0.03	0.02	0.03	0.03	0.03	0.03	0.04	0.13
P_2O_5 %	0.02	0.02	0.05	0.06	0.16	0.02	0.06	0.005
SrO %	0.03	0.03	0.04	0.05	0.04	0.03	0.05	0.03
BaO %	0.03	0.03	0.03	0.03	0.03	0.01	0.03	0.01
LOI %	1.15	0.57	1.19	0.88	2.05	1.57	0.83	2.14
Total %	100.67	100.07	99.31	101.2	101.81	99.96	101.03	99.13
C %	0.03	0.04	0.04	0.1	0.08	0.02	0.06	0.11
S %	0.09	0.09	0.03	0.04	0.21	0.08	0.14	0.06
Ba ppm	265	301	242	238	311	100.5	312	70.8
Ce ppm	22.4	16.7	13.7	21.5	29.7	10.7	12.7	5.1
Cr ppm	17	17	17	22	25	12	25	36
Cs ppm	1.26	0.77	1.29	0.76	1.48	1.08	2.38	1.18
Dy ppm	0.35	0.34	0.44	0.47	0.82	0.24	0.41	0.82
Er ppm	0.12	0.12	0.18	0.21	0.48	0.08	0.18	0.5
Eu ppm	0.71	0.52	0.52	0.87	0.75	0.58	0.53	0.27
Ga ppm	20	18.6	19.4	19.6	18.8	17.4	19.7	13.2

Gd ppm	0.56	0.45	0.73	0.74	1.53	0.4	0.62	0.8
Ge ppm	0.8	0.8	0.8	0.8	0.7	0.7	0.8	1.2
Hf ppm	1.54	0.97	2.1	2.18	3.49	1.36	1.22	0.4
Ho ppm	0.06	0.05	0.09	0.08	0.18	0.04	0.07	0.18
La ppm	13.7	10.1	7.4	12.6	15.2	6.7	7.3	2.4
Lu ppm	0.03	0.01	0.04	0.03	0.06	0.01	0.04	0.07
Nb ppm	1.37	1.48	1.96	1.02	2.51	0.45	1.4	0.24
Nd ppm	6.1	5.1	5.1	7.3	12.4	3.5	4.8	2.9
Pr ppm	2.06	1.63	1.43	2.12	3.06	0.99	1.28	0.62
Rb ppm	19.1	13.4	19.6	7.8	20.9	14.8	12.8	5.7
Sm ppm	0.85	0.71	0.93	1.2	1.91	0.46	0.68	0.65
Sn ppm	0.25	0.25	0.25	0.25	0.25	0.25	0.25	0.25
Sr ppm	311	281	398	364	310	253	447	224
Ta ppm	0.05	0.05	0.1	0.1	0.2	0.05	0.1	0.05
Tb ppm	0.05	0.06	0.08	0.1	0.21	0.06	0.06	0.13
Th ppm	1.03	0.88	1.13	0.72	1.18	0.71	0.5	0.17
Tm ppm	0.02	0.02	0.03	0.02	0.07	0.01	0.02	0.08
U ppm	0.23	0.21	0.33	0.23	0.52	0.23	0.19	0.07
V ppm	32	16	27	44	54	25	45	132
W ppm	1.4	1.1	1.1	0.9	1.8	1	0.8	0.7
Y ppm	1.4	1.2	2.3	2.2	4.7	1.3	1.8	4.8
Yb ppm	0.13	0.07	0.17	0.25	0.45	0.09	0.17	0.49
Zr ppm	63	37	86	90	153	54	49	13
As ppm	0.1	0.2	0.2	0.1	0.1	0.1	0.1	0.1
Bi ppm	0.11	0.53	0.03	0.01	0.3	0.07	0.05	0.06
Hg ppm	0.0025	0.0025	0.0025	0.0025	0.0025	0.0025	0.0025	0.0025
In ppm	0.0025	0.0025	0.0025	0.0025	0.0025	0.0025	0.0025	0.0025
Re ppm	0.001	0.0005	0.0005	0.0005	0.0005	0.0005	0.0005	0.0005
Sb ppm	0.025	0.025	0.025	0.025	0.025	0.025	0.025	0.025
Se ppm	0.1	0.1	0.1	0.1	0.2	0.1	0.1	0.2
Te ppm	0.05	0.31	0.01	0.01	0.06	0.04	0.03	0.06
Tl ppm	0.01	0.03	0.01	0.03	0.02	0.01	0.05	0.01
Ag ppm	0.25	0.25	0.25	0.25	0.25	0.25	0.25	0.25
Cd ppm	0.25	0.25	0.25	0.25	0.25	0.25	0.25	0.25
Co ppm	7	4	7	9	11	6	12	55
Cu ppm	35	9	18	18	85	6	24	152
Li ppm	20	10	10	10	20	40	10	10
Mo ppm	0.5	0.5	0.5	0.5	1	0.5	0.5	0.5
Ni ppm	2	4	6	6	10	4	13	249
Pb ppm	1	5	2	3	1	1	1	1
Sc ppm	3	1	4	3	6	3	7	31
Zn ppm	42	39	39	67	55	29	55	65

Sample Number	JPCL49	JPCL50	JPCL51	JPOFF01	JPOFF02	JPOFF03	JPOFF04	JPOFF05
Sample Meterage	365	390	415	7.5	30.5	50.5	75.5	85.5
SiO_2 %	48	48.8	50.7	71.7	70.8	65.3	72.9	71.5
Al_2O_3 %	21.6	21.5	18.5	14.85	15.4	16.5	15.1	15.45
Fe_2O_3 %	4.65	5.36	8.35	3.13	2.39	3.92	1.95	2.65
CaO %	11.2	11.55	10.65	3.81	3.66	4.36	3.75	3.53
MgO %	8	7.74	7.18	0.83	0.62	1.32	0.7	0.71
Na_2O %	1.54	1.76	2.03	4.39	4.8	4.67	4.77	4.9
K_2O %	0.43	0.19	0.22	0.51	0.51	0.57	0.43	0.57
Cr_2O_3 %	0.031	0.019	0.012	0.001	0.001	0.001	0.001	0.001
TiO_2 %	0.08	0.12	0.14	0.25	0.23	0.39	0.31	0.25
MnO %	0.07	0.08	0.11	0.03	0.02	0.04	0.01	0.01
P_2O_5 %	0.005	0.005	0.01	0.05	0.03	0.09	0.02	0.02
SrO %	0.02	0.02	0.03	0.04	0.05	0.04	0.06	0.05
BaO %	0.01	0.005	0.01	0.05	0.04	0.05	0.03	0.04
LOI %	2.95	2.74	2.55	0.32	0.3	1.02	0.35	0.45
Total %	98.58	99.88	100.49	99.96	98.85	98.27	100.38	100.13
C %	0.07	0.06	0.12	0.04	0.03	0.04	0.02	0.02
S %	0.01	0.05	0.72	0.03	0.01	0.27	0.01	0.09
Ba ppm	75.5	43.6	48.2	481	418	484	253	341
Ce ppm	2.1	2.5	3.9	44.5	37.9	55.3	36.9	11.8
Cr ppm	247	158	99	14	10	16	16	12
Cs ppm	2.55	1.76	1.36	3.32	2.34	2.52	4.06	2.46
Dy ppm	0.34	0.52	0.57	0.94	0.34	1.22	0.37	0.18
Er ppm	0.24	0.32	0.4	0.39	0.17	0.57	0.21	0.17
Eu ppm	0.15	0.18	0.26	0.96	0.81	0.91	0.78	0.54
Ga ppm	11.4	12.4	14.4	18.6	18.5	21.1	17.5	18.4
Gd ppm	0.24	0.37	0.63	1.27	0.76	2.09	0.75	0.33
Ge ppm	1	1.2	1.1	0.9	0.7	0.7	0.7	0.6
Hf ppm	0.22	0.28	0.32	2.37	3.27	4.78	3.08	1.88
Ho ppm	0.09	0.09	0.13	0.18	0.05	0.22	0.07	0.04
La ppm	1.1	1.2	1.9	26.2	22.9	31.5	21.9	7.8
Lu ppm	0.04	0.05	0.05	0.07	0.04	0.08	0.03	0.02
Nb ppm	0.23	0.27	0.2	1.95	0.99	3.92	2.32	1.09
Nd ppm	1	1.1	2.1	14.4	11.9	19.4	11.6	3.8
Pr ppm	0.23	0.31	0.46	4.38	3.67	5.75	3.61	1.16
Rb ppm	15.4	7.1	7.8	12.6	5.6	8	10.7	9.3
Sm ppm	0.22	0.33	0.46	2.01	1.45	3	1.32	0.45
Sn ppm	0.25	0.25	0.25	0.25	0.25	0.25	0.25	0.25
Sr ppm	185	193.5	224	380	488	403	510	437
Ta ppm	0.05	0.05	0.05	0.05	0.05	0.05	0.05	0.05

Tb ppm	0.05	0.07	0.12	0.16	0.05	0.23	0.06	0.04
Th ppm	0.25	0.17	0.19	2.65	1.98	3.55	2.5	0.35
Tm ppm	0.03	0.05	0.06	0.05	0.03	0.07	0.03	0.03
U ppm	0.14	0.08	0.08	0.16	0.26	0.21	0.17	0.11
V ppm	66	85	124	39	25	50	33	32
W ppm	0.9	1.1	1.7	0.8	1	1.2	2	15.3
Y ppm	2.4	2.5	4	4.1	1.8	5.6	2	1.3
Yb ppm	0.23	0.33	0.39	0.44	0.24	0.5	0.2	0.18
Zr ppm	10	9	9	95	129	217	123	72
As ppm	0.1	0.05	2.5	0.05	0.05	0.05	0.05	0.05
Bi ppm	0.69	0.03	0.09	0.01	0.01	0.23	0.02	0.05
Hg ppm	0.0025	0.0025	0.0025	0.0025	0.0025	0.0025	0.0025	0.0025
In ppm	0.0025	0.0025	0.0025	0.005	0.0025	0.0025	0.0025	0.0025
Re ppm	0.0005	0.0005	0.002	0.0005	0.0005	0.0005	0.0005	0.0005
Sb ppm	0.025	0.025	0.025	0.025	0.025	0.025	0.025	0.025
Se ppm	0.2	0.2	2.4	0.1	0.1	0.1	0.1	0.1
Te ppm	0.07	0.06	0.1	0.005	0.005	0.16	0.005	0.01
Tl ppm	0.01	0.01	0.01	0.05	0.02	0.03	0.04	0.03
Ag ppm	0.25	0.25	0.6	0.25	0.25	0.25	0.25	0.25
Cd ppm	0.25	0.25	0.25	0.25	0.25	0.25	0.25	0.25
Co ppm	35	38	69	7	4	13	5	10
Cu ppm	10	27	763	22	3	218	1	56
Li ppm	10	10	10	10	10	10	20	10
Mo ppm	0.5	0.5	0.5	1	0.5	0.5	0.5	0.5
Ni ppm	264	246	327	5	2	7	2	1
Pb ppm	1	1	1	2	3	3	1	1
Sc ppm	14	14	21	6	2	9	2	3
Zn ppm	27	29	40	45	36	44	16	21
Sample Number	JPOFF06	JPOFF07	JPOFF08	JPOFF09	JPOFF10	JPOFF11	JPOFF12	JPOFF13
Sample Meterage	95.5	105.5	110.5	112	113	114	115	116.5
SiO_2 %	71.9	78.2	69.9	68.6	67.8	73.7	65.6	71.5
Al_2O_3 %	14.85	12.85	15.9	15.7	16.05	14.65	17.5	16.3
Fe_2O_3 %	2.65	1.32	2.79	3.04	3.5	1.65	3.85	2.08
CaO %	3.62	1.4	3.45	3.46	3.55	2.08	4.68	2.68
MgO %	0.86	0.41	1.2	1.14	1.52	0.55	1.34	0.75
Na_2O %	4.5	5.27	5.74	5.1	5.08	5.87	4.74	5.82
K_2O %	0.59	0.62	0.58	0.95	0.85	1.02	0.98	0.82
Cr_2O_3 %	0.001	0.001	0.002	0.002	0.002	0.001	0.002	0.001
TiO_2 %	0.35	0.06	0.29	0.35	0.38	0.16	0.35	0.21
MnO %	0.02	0.01	0.02	0.03	0.04	0.02	0.04	0.02
P_2O_5 %	0.02	0.01	0.06	0.08	0.1	0.04	0.05	0.03

SrO %	0.05	0.02	0.03	0.04	0.05	0.03	0.05	0.03
BaO %	0.04	0.03	0.01	0.03	0.03	0.02	0.02	0.02
LOI %	0.45	0.88	1.76	1.26	1.68	0.7	1.84	1.28
Total %	99.9	101.08	101.73	99.78	100.63	100.49	101.04	101.54
C %	0.04	0.03	0.15	0.03	0.12	0.03	0.11	0.07
S %	0.05	0.06	0.1	0.04	0.08	0.08	0.11	0.07
Ba ppm	426	291	112.5	246	271	187.5	225	224
Ce ppm	32.7	18.5	14.3	17.2	29.2	13.9	17.7	18.6
Cr ppm	13	14	17	19	22	14	21	5
Cs ppm	2.81	1.69	1.87	2.77	2.75	1.54	3.22	2.52
Dy ppm	0.39	0.21	0.25	0.42	0.79	1.22	0.54	0.61
Er ppm	0.17	0.11	0.12	0.2	0.38	0.69	0.35	0.35
Eu ppm	0.69	0.52	0.53	0.63	0.63	0.33	0.79	0.5
Ga ppm	18.2	14.3	16.4	18.9	18.9	19.9	24.5	17
Gd ppm	0.6	0.39	0.51	0.76	1.3	1.47	0.76	0.77
Ge ppm	0.7	0.6	0.6	0.7	0.7	1	1.1	0.5
Hf ppm	3.47	1.33	1.54	2.79	3.69	2.51	3.73	1.36
Ho ppm	0.05	0.04	0.04	0.06	0.13	0.24	0.11	0.11
La ppm	19.9	12.5	8.7	9.7	17.1	7.2	10.3	12.4
Lu ppm	0.03	0.02	0.02	0.03	0.06	0.09	0.05	0.05
Nb ppm	3.53	0.96	1.92	7.11	7.33	9	4.06	3.24
Nd ppm	10.2	5	5.2	7.3	10.4	6.1	6.8	6.2
Pr ppm	3.2	1.6	1.4	1.9	3	1.68	1.84	1.83
Rb ppm	7.4	18	21.4	31.1	29.6	35.2	34.7	30.4
Sm ppm	1.08	0.53	0.75	1.11	1.49	1.4	1.04	0.87
Sn ppm	0.25	0.25	0.25	0.25	0.25	0.25	0.25	0.25
Sr ppm	476	222	233	377	417	243	468	263
Ta ppm	0.05	0.05	0.05	0.05	0.1	0.8	0.1	0.1
Tb ppm	0.05	0.04	0.06	0.08	0.13	0.22	0.09	0.08
Th ppm	1.7	0.48	0.36	0.79	1.56	2.61	1.05	1.16
Tm ppm	0.02	0.01	0.01	0.03	0.05	0.09	0.04	0.04
U ppm	0.22	0.27	0.11	0.06	0.51	3.49	0.6	0.93
V ppm	30	7	36	45	45	20	54	52
W ppm	3.1	1	2.8	1.7	2.3	1.4	3.3	3.9
Y ppm	1.9	1.3	1.5	2.1	4.2	7.7	3.2	3.7
Yb ppm	0.22	0.11	0.14	0.22	0.39	0.67	0.31	0.31
Zr ppm	146	44	73	123	164	76	162	52
As ppm	0.05	0.05	0.05	0.05	0.05	0.05	0.1	0.05
Bi ppm	0.02	0.02	0.04	0.04	0.05	0.09	0.1	0.05
Hg ppm	0.0025	0.0025	0.0025	0.0025	0.0025	0.0025	0.0025	0.0025
In ppm	0.0025	0.0025	0.0025	0.0025	0.0025	0.0025	0.005	0.005
Re ppm	0.0005	0.0005	0.0005	0.0005	0.001	0.0005	0.0005	0.0005

Sb ppm	0.025	0.025	0.025	0.025	0.025	0.025	0.025	0.025
Se ppm	0.1	0.1	0.2	0.1	0.1	0.1	0.1	0.1
Te ppm	0.005	0.005	0.005	0.005	0.005	0.01	0.02	0.005
Tl ppm	0.03	0.01	0.01	0.01	0.01	0.01	0.01	0.01
Ag ppm	0.25	0.25	0.25	0.25	0.25	0.25	0.25	0.25
Cd ppm	0.25	0.25	0.25	0.25	0.25	0.25	0.25	0.25
Co ppm	7	2	7	7	10	4	10	4
Cu ppm	4	21	10	6	14	7	29	30
Li ppm	10	10	10	10	10	10	10	10
Mo ppm	0.5	0.5	0.5	0.5	0.5	0.5	0.5	0.5
Ni ppm	5	0.5	10	9	10	4	8	0.5
Pb ppm	1	1	1	1	1	6	1	1
Sc ppm	1	1	3	4	5	3	5	2
Zn ppm	36	10	23	25	33	10	29	17
Sample Number	JPOFF14	JPOFF15	JPOFF16	JPOFF17	JPOFF18	JPOFF19	JPOFF20	JPOFF21
Sample Meterage	117	118	119	121	123	124	125	126
SiO_2 %	71.3	70.7	42.2	50.2	50.5	49.2	48.9	48.7
Al_2O_3 %	16.3	16.35	14.85	17.05	16.25	21.9	18.05	9.4
Fe_2O_3 %	2.29	2.55	8.31	7.8	7.64	3.73	5.95	11.05
CaO %	2.89	2.94	17.2	5.33	6.31	9.79	10	7.04
MgO %	0.86	1.08	9.1	8.91	11.4	5.73	9.12	16.55
Na_2O %	5.49	5.72	0.6	4.88	1.95	2.73	1.82	0.57
K_2O %	0.73	0.48	0.09	0.53	1.62	2.37	1.91	0.3
Cr_2O_3 %	0.001	0.001	0.092	0.034	0.038	0.022	0.042	0.059
TiO_2 %	0.24	0.25	0.41	0.28	0.09	0.07	0.09	0.13
MnO %	0.02	0.02	0.12	0.1	0.13	0.07	0.11	0.19
P_2O_5 %	0.03	0.04	0.29	0.18	0.01	0.02	0.01	0.005
SrO %	0.04	0.04	0.06	0.02	0.02	0.03	0.02	0.005
BaO %	0.04	0.02	0.005	0.01	0.03	0.04	0.03	0.005
LOI %	1.26	1.22	6.88	5.12	3.83	3.86	3.33	4.07
Total %	101.49	101.41	100.2	100.44	99.82	99.56	99.38	98.06
C %	0.06	0.04	0.91	0.52	0.09	0.26	0.16	0.04
S %	0.23	0.3	0.28	0.53	0.07	0.03	0.13	0.38
Ba ppm	415	183.5	19.2	92.9	315	426	300	44.3
Ce ppm	16.6	22.6	81	48.2	4.4	3.7	3	3.3
Cr ppm	6	6	729	269	310	189	321	496
Cs ppm	2.89	2.32	1.86	2.97	5.95	10.05	8.31	3.35
Dy ppm	0.14	0.39	2.78	1.65	0.43	0.31	0.47	0.53
Er ppm	0.14	0.27	1.13	0.86	0.31	0.18	0.34	0.46
Eu ppm	0.56	0.61	2.02	1.27	0.18	0.22	0.17	0.12
Ga ppm	18.6	18	21.7	12.1	10.7	14	10.7	8.3

Gd ppm	0.38	0.62	5.11	2.98	0.35	0.32	0.39	0.4
Ge ppm	0.6	0.6	2.3	1.1	1.2	1.2	1.1	1.5
Hf ppm	2.01	2.09	2.27	1.3	0.26	0.32	0.21	0.3
Ho ppm	0.03	0.09	0.47	0.29	0.1	0.07	0.09	0.13
La ppm	10.7	14.4	38.8	20.3	2.3	2.1	1.5	1.6
Lu ppm	0.03	0.04	0.12	0.12	0.05	0.05	0.04	0.08
Nb ppm	1.13	2.87	5.07	2.69	0.39	0.41	0.21	0.31
Nd ppm	5.4	7.1	41.5	25.9	1.9	1.4	1.6	1.6
Pr ppm	1.58	2.22	10.35	6.27	0.5	0.4	0.36	0.38
Rb ppm	24.5	17.2	2	23.2	71.7	102	72	15.4
Sm ppm	0.55	0.88	7.47	4.35	0.4	0.29	0.4	0.31
Sn ppm	0.25	0.25	0.8	0.25	0.25	0.25	0.25	0.25
Sr ppm	411	417	586	183	204	316	203	40.5
Ta ppm	0.05	0.1	0.05	0.05	0.4	0.05	0.05	0.05
Tb ppm	0.03	0.08	0.59	0.36	0.07	0.04	0.08	0.09
Th ppm	0.35	1	2.47	1.57	0.54	0.64	0.13	0.32
Tm ppm	0.02	0.04	0.15	0.11	0.05	0.03	0.05	0.07
U ppm	0.18	0.77	0.91	0.71	0.15	0.17	0.08	0.16
V ppm	28	28	165	122	92	61	94	139
W ppm	3.4	1.3	7.6	1.5	4.2	0.25	0.25	0.25
Y ppm	1.1	2.7	13.3	8.4	2.6	2	2.6	3.4
Yb ppm	0.12	0.26	0.86	0.66	0.31	0.23	0.33	0.48
Zr ppm	82	83	101	52	9	12	6	10
As ppm	0.1	0.1	0.2	0.05	0.05	0.1	0.2	0.6
Bi ppm	0.22	0.63	1.38	1.46	0.31	1.24	0.22	0.09
Hg ppm	0.0025	0.0025	0.0025	0.0025	0.0025	0.0025	0.0025	0.0025
In ppm	0.011	0.0025	0.017	0.009	0.005	0.0025	0.0025	0.006
Re ppm	0.0005	0.0005	0.001	0.001	0.0005	0.001	0.0005	0.001
Sb ppm	0.025	0.025	0.025	0.025	0.025	0.025	0.025	0.025
Se ppm	0.3	0.2	0.4	0.5	0.8	0.2	1.3	3.5
Te ppm	0.03	0.09	0.25	0.64	0.2	2.9	0.26	0.4
Tl ppm	0.01	0.01	0.01	0.02	0.03	0.04	0.03	0.03
Ag ppm	0.25	0.25	0.25	0.25	0.25	0.25	0.25	0.25
Cd ppm	0.25	0.25	0.25	0.25	0.25	0.25	0.25	0.25
Co ppm	7	8	39	52	60	23	54	102
Cu ppm	53	49	38	65	447	110	245	915
Li ppm	10	10	70	60	30	20	20	30
Mo ppm	0.5	0.5	0.5	1	0.5	0.5	0.5	0.5
Ni ppm	2	1	217	324	567	353	849	1365
Pb ppm	1	1	2	1	1	1	1	1
Sc ppm	2	3	19	17	15	10	23	32
Zn ppm	16	17	58	67	56	32	43	69

Sample Number	JPOFF22	JPOFF23	JPOFF24	JPOFF25	JPOFF26	JPOFF27	JPOFF28	JPOFF29
Sample Meterage	127	128	129	130	132	136.5	141.5	146.5
SiO_2 %	48.7	49.4	49.2	62.7	48.3	49.4	49.6	49.5
Al_2O_3 %	11.4	9.71	9.56	17.4	18.15	17.75	10.85	15.8
Fe_2O_3 %	9.76	10.45	10.3	4.56	6.58	6.74	10.15	7.71
CaO %	7.27	7.82	7.18	5.73	9.52	10.65	7.85	9.69
MgO %	15.1	16.4	17.25	4.45	10.4	10.55	16.25	11
Na_2O %	0.92	0.62	0.43	4.07	1.56	1.45	0.58	1.74
K_2O %	0.46	0.31	0.26	0.64	1.12	0.78	0.39	0.58
Cr_2O_3 %	0.055	0.063	0.067	0.015	0.04	0.042	0.06	0.038
TiO_2 %	0.11	0.14	0.11	0.25	0.08	0.09	0.11	0.1
MnO %	0.17	0.18	0.18	0.06	0.11	0.11	0.17	0.13
P_2O_5 %	0.01	0.02	0.01	0.08	0.005	0.01	0.01	0.01
SrO %	0.01	0.005	0.005	0.04	0.02	0.02	0.01	0.02
BaO %	0.01	0.01	0.005	0.03	0.02	0.02	0.01	0.01
LOI %	4.07	3.95	4.3	1.96	3.46	3.12	4	2.9
Total %	98.05	99.07	98.85	101.99	99.36	100.73	100.04	99.23
C %	0.04	0.07	0.05	0.08	0.06	0.08	0.05	0.08
S %	0.15	0.15	0.09	0.07	0.17	0.09	0.18	0.15
Ba ppm	85.8	51.2	39.6	262	216	142	55	105.5
Ce ppm	2.1	3	2.8	27.8	2.3	2.8	1.6	2.5
Cr ppm	450	506	556	129	330	337	473	295
Cs ppm	3.04	3.08	2.92	5.58	6.87	3.37	2.7	4.24
Dy ppm	0.49	0.65	0.46	1	0.34	0.41	0.41	0.42
Er ppm	0.39	0.48	0.38	0.57	0.31	0.27	0.31	0.28
Eu ppm	0.16	0.16	0.13	0.51	0.17	0.17	0.12	0.2
Ga ppm	9.8	8.6	8	16.3	11	10.4	7.8	10.9
Gd ppm	0.3	0.49	0.4	1.25	0.33	0.35	0.33	0.39
Ge ppm	1.4	1.6	1.6	1.3	1.1	1.1	1.5	1.3
Hf ppm	0.17	0.33	0.19	3.22	0.18	0.15	0.12	0.16
Ho ppm	0.12	0.16	0.11	0.22	0.08	0.11	0.09	0.09
La ppm	1.1	1.3	1.5	16	1.1	1.9	0.7	1.3
Lu ppm	0.06	0.07	0.07	0.12	0.04	0.05	0.05	0.05
Nb ppm	0.25	0.42	0.12	3.99	0.11	0.07	0.06	0.11
Nd ppm	1	1.8	1.3	9.4	1	1.2	0.9	1.3
Pr ppm	0.26	0.38	0.37	2.85	0.29	0.31	0.2	0.33
Rb ppm	21.1	14.8	12.9	23.9	41.3	29.8	17.5	22.1
Sm ppm	0.24	0.46	0.31	1.66	0.31	0.24	0.29	0.3
Sn ppm	0.25	0.25	0.25	0.5	0.25	0.25	0.25	0.25
Sr ppm	79.8	54.2	31	345	187.5	168	59.6	175.5
Ta ppm	0.05	0.05	0.05	0.2	0.05	0.05	0.05	0.05

Tb ppm	0.08	0.11	0.08	0.16	0.06	0.07	0.07	0.07
Th ppm	0.38	0.17	0.14	4.05	0.21	0.1	0.07	0.12
Tm ppm	0.06	0.08	0.07	0.09	0.05	0.05	0.06	0.05
U ppm	0.16	0.11	0.07	1.17	0.1	0.05	0.025	0.05
V ppm	123	141	128	67	86	110	123	102
W ppm	0.25	0.25	0.25	0.8	0.25	0.8	0.25	0.25
Y ppm	3	3.9	3.3	5.6	2.3	2.7	2.7	2.6
Yb ppm	0.36	0.48	0.4	0.56	0.34	0.32	0.39	0.37
Zr ppm	6	14	6	118	6	5	4	5
As ppm	0.1	0.1	0.2	0.2	0.2	0.05	0.3	0.5
Bi ppm	0.17	0.13	0.1	0.13	0.2	0.06	0.06	0.1
Hg ppm	0.0025	0.0025	0.0025	0.0025	0.0025	0.0025	0.015	0.0025
In ppm	0.005	0.005	0.005	0.006	0.0025	0.0025	0.0025	0.0025
Re ppm	0.0005	0.001	0.0005	0.0005	0.001	0.0005	0.001	0.001
Sb ppm	0.025	0.1	0.025	0.025	0.025	0.025	0.13	0.09
Se ppm	1.1	1.4	0.8	0.2	1.6	0.5	0.8	1.4
Te ppm	0.16	0.33	0.34	0.36	0.59	0.24	0.3	0.25
Tl ppm	0.02	0.02	0.02	0.06	0.03	0.03	0.03	0.02
Ag ppm	0.25	0.25	0.25	0.25	0.25	0.25	0.25	0.25
Cd ppm	0.25	0.25	0.25	0.25	0.25	0.25	0.25	0.25
Co ppm	79	90	83	23	55	53	84	72
Cu ppm	859	449	362	194	587	309	405	288
Li ppm	40	30	30	20	30	20	20	20
Mo ppm	0.5	0.5	0.5	0.5	0.5	0.5	0.5	0.5
Ni ppm	841	1055	849	230	855	524	751	886
Pb ppm	1	1	1	5	7	1	9	2
Sc ppm	28	35	32	11	17	21	35	23
Zn ppm	66	84	75	38	48	41	98	47
Sample Number	JPOFF30	JPOFF31	JPOFF32	JPOFF33	JPOFF34	JPOFF35	JPOFF36	JPOFF37
Sample Meterage	172	182	192	202	213	222	247	272
SiO_2 %	48.7	49	49.3	48.6	49.4	50.5	51.1	51.3
Al_2O_3 %	14.45	18	18.65	21.8	19.4	18.2	17.7	15.9
Fe_2O_3 %	8.63	7.93	7.39	4.86	7.38	7.14	6.91	7.96
CaO %	9.44	9.89	10.2	11.1	10.15	10.3	9.67	10.25
MgO %	12.65	8.54	7.98	7.03	7.8	9.28	8.99	7.89
Na_2O %	1.26	2.02	2.22	2.09	2.15	1.86	2.27	2.37
K_2O %	0.22	0.25	0.57	0.48	0.17	0.2	0.36	0.28
Cr_2O_3 %	0.051	0.026	0.025	0.02	0.019	0.031	0.025	0.002
TiO_2 %	0.1	0.09	0.1	0.07	0.09	0.11	0.16	0.15
MnO %	0.14	0.11	0.11	0.08	0.1	0.11	0.11	0.13
P_2O_5 %	0.005	0.01	0.01	0.02	0.01	0.01	0.02	0.005

SrO %	0.01	0.02	0.02	0.02	0.03	0.02	0.02	0.02
BaO %	0.005	0.01	0.01	0.01	0.01	0.01	0.01	0.01
LOI %	2.88	2.39	2.91	3.28	2.42	2.44	2.25	2.52
Total %	98.53	98.29	99.5	99.46	99.13	100.21	99.6	98.78
C %	0.21	0.13	0.19	0.22	0.13	0.15	0.08	0.26
S %	0.18	0.43	0.26	0.02	0.57	0.1	0.04	0.08
Ba ppm	46.3	73.1	125	79	67	58.1	97.4	80.7
Ce ppm	2.2	2.4	2.7	3.2	2.8	3.5	5.6	8.3
Cr ppm	420	224	201	177	163	253	202	24
Cs ppm	2.71	2.29	2.7	3.53	1.43	1.47	2.03	1.62
Dy ppm	0.46	0.42	0.38	0.36	0.31	0.51	0.66	0.9
Er ppm	0.3	0.28	0.27	0.22	0.28	0.3	0.33	0.61
Eu ppm	0.17	0.22	0.21	0.21	0.27	0.22	0.29	0.32
Ga ppm	10.1	14.3	13	13.4	14.4	12.2	12.4	14.3
Gd ppm	0.36	0.32	0.4	0.29	0.35	0.39	0.61	0.95
Ge ppm	1.4	1.1	1.1	1.2	1	1.3	1.2	1.4
Hf ppm	0.18	0.16	0.16	0.21	0.17	0.26	0.38	0.61
Ho ppm	0.1	0.08	0.07	0.07	0.08	0.1	0.13	0.23
La ppm	1.2	1.3	1.4	1.7	1.5	1.8	3	5.9
Lu ppm	0.06	0.05	0.04	0.04	0.04	0.06	0.06	0.09
Nb ppm	0.11	0.025	0.1	0.53	0.14	0.36	0.5	0.66
Nd ppm	1.1	1.2	1.3	1.4	1.2	1.6	2.5	3.9
Pr ppm	0.25	0.28	0.31	0.35	0.32	0.41	0.67	0.9
Rb ppm	8	8.6	19.9	21.2	5	4.4	9.1	6.4
Sm ppm	0.23	0.23	0.37	0.32	0.31	0.33	0.53	0.7
Sn ppm	0.25	0.25	0.25	0.25	0.25	0.25	0.25	0.25
Sr ppm	140.5	226	223	238	248	188.5	205	181
Ta ppm	0.05	0.05	0.05	0.05	0.05	0.05	0.05	0.05
Tb ppm	0.07	0.05	0.07	0.06	0.06	0.08	0.1	0.17
Th ppm	0.08	0.06	0.09	0.18	0.11	0.22	0.27	0.4
Tm ppm	0.05	0.04	0.04	0.04	0.04	0.05	0.06	0.11
U ppm	0.025	0.025	0.025	0.16	0.025	0.11	0.1	0.42
V ppm	124	105	89	64	85	102	101	190
W ppm	2.9	0.25	0.25	0.25	0.25	0.25	0.25	2.7
Y ppm	2.6	2.5	2.2	2.1	1.9	2.6	3.4	6
Yb ppm	0.35	0.26	0.28	0.21	0.25	0.35	0.36	0.53
Zr ppm	6	5	6	7	7	10	16	20
As ppm	0.2	0.1	0.4	0.1	0.7	0.3	0.1	0.3
Bi ppm	0.08	0.16	0.1	0.08	0.26	0.06	0.02	0.14
Hg ppm	0.0025	0.0025	0.0025	0.0025	0.0025	0.0025	0.0025	0.0025
In ppm	0.0025	0.007	0.005	0.0025	0.008	0.0025	0.0025	0.006
Re ppm	0.001	0.001	0.001	0.0005	0.001	0.001	0.0005	0.0005

Sb ppm	0.025	0.025	0.025	0.025	0.025	0.025	0.025	0.07
Se ppm	1.8	4.1	2.7	0.1	4.6	0.9	0.1	0.6
Te ppm	0.49	1.38	0.66	0.18	1.42	0.52	0.11	0.34
Tl ppm	0.06	0.12	0.06	0.03	0.03	0.01	0.01	0.01
Ag ppm	0.25	0.5	0.25	0.25	0.5	0.25	0.25	0.25
Cd ppm	0.25	0.25	0.25	0.25	0.25	0.25	0.25	0.25
Co ppm	70	68	58	36	70	53	46	52
Cu ppm	495	1470	883	37	1750	367	111	275
Li ppm	10	10	10	20	10	10	10	10
Mo ppm	0.5	0.5	0.5	0.5	0.5	0.5	0.5	1
Ni ppm	822	1425	1100	361	1430	705	327	354
Pb ppm	1	1	1	1	1	1	1	6
Sc ppm	26	17	17	13	18	19	20	33
Zn ppm	52	51	59	36	46	46	47	63

Appendix Three: Chlorite Analysis Data

Sample #	*21-700-02-01-S1*	*21-700-02-01-S1*	*21-700-02-01-S2*	*21-700-02-01-S2*	*21-700-02-01-S2*	*21-700-02-01-S3*	*21-700-02-01-S4*
SiO2	34.04	39.89	34.25	33.83	33.79	31.98	34.20
TiO2	0.01	0.02	0.03	0.02	0.02	0.00	0.00
Al2O3	24.24	20.38	23.51	22.28	23.65	19.90	24.06
Cr2O3	0.02	0.00	0.03	0.01	0.02	0.02	0.03
Fe2O3	6.26	10.10	6.05	4.94	5.79	3.93	6.58
FeO	4.01	0.18	3.50	4.48	3.98	7.34	3.70
MnO	0.14	0.09	0.17	0.22	0.13	0.17	0.13
MgO	21.55	20.30	22.22	24.07	22.36	22.45	21.02
CaO	0.29	0.24	0.34	0.28	0.27	0.51	0.26
Na2O	0.02	0.04	0.12	0.03	0.07	0.03	0.00
K2O	0.35	0.25	0.28	0.13	0.24	0.05	0.46
*H2O**	13.01	13.23	12.98	12.94	12.94	12.20	12.93
Total	103.95	104.72	103.47	103.23	103.26	98.57	103.34
Si	6.17	7.05	6.22	6.19	6.16	6.22	6.23
Al iv	1.83	0.95	1.78	1.81	1.84	1.78	1.77
Al vi	3.44	3.41	3.34	3.06	3.33	2.83	3.49
Ti	0.00	0.00	0.00	0.00	0.00	0.00	0.00
Cr	0.00	0.00	0.00	0.00	0.00	0.00	0.00
Fe3+	0.85	1.34	0.83	0.68	0.80	0.57	0.90
Fe2+	0.61	0.03	0.53	0.69	0.61	1.19	0.56
Mn	0.02	0.01	0.03	0.03	0.02	0.03	0.02
Mg	5.82	5.35	6.02	6.57	6.08	6.51	5.71
Ca	0.06	0.05	0.07	0.05	0.05	0.11	0.05
Na	0.01	0.03	0.08	0.02	0.05	0.02	0.00
K	0.16	0.11	0.13	0.06	0.11	0.03	0.21
*OH**	16.00	16.00	16.00	16.00	16.00	16.00	16.00
Total	34.99	34.33	35.03	35.16	35.05	35.28	34.94

Oxidized	no	no	no	no	no	yes	no
Fe/Fe+Mg	0.201	0.204	0.184	0.172	0.187	0.214	0.204

Sample #	*21-700-02-01-S4*	*21-700-02-01-S4*	*21-700-02-01-S4*	*21-700-02-01-S4*	*21-700-02-01-S5*	*21-700-02-01-S5*	*21-700-02-01-S5*
SiO_2	31.08	33.88	34.14	33.11	12.93	29.79	33.23
TiO_2	0.02	0.02	0.01	0.01	0.00	0.01	0.00
Al_2O_3	22.34	23.81	24.17	22.95	9.80	20.98	22.91
Cr_2O_3	0.02	0.03	0.02	0.01	0.04	0.05	0.04
Fe_2O_3	3.61	5.73	6.43	4.80	0.00	2.39	4.90
FeO	5.45	3.88	3.30	5.81	9.56	7.78	5.22
MnO	0.14	0.16	0.09	0.15	0.20	0.17	0.16
MgO	21.54	22.89	21.67	22.85	25.11	23.69	23.17
CaO	3.33	0.26	0.32	0.33	0.38	0.40	0.41
Na_2O	0.03	0.03	0.02	0.04	0.06	0.04	0.04
K_2O	0.18	0.20	0.35	0.21	0.11	0.08	0.11
H_2O*	12.41	13.03	12.99	12.85	7.66	12.08	12.88
Total	100.15	103.91	103.51	103.13	65.85	97.45	103.09
Si	5.94	6.14	6.20	6.10	3.76	5.87	6.11
Al^{iv}	2.06	1.86	1.80	1.90	3.62	2.13	1.89
Al^{vi}	3.03	3.31	3.46	3.15	0.00	2.78	3.14
Ti	0.00	0.00	0.00	0.00	0.00	0.00	0.00
Cr	0.00	0.00	0.00	0.00	0.01	0.01	0.01
Fe^{3+}	0.52	0.78	0.88	0.67	0.00	0.35	0.68
Fe^{2+}	0.87	0.59	0.50	0.89	4.34	1.28	0.80
Mn	0.02	0.03	0.01	0.02	0.05	0.03	0.02
Mg	6.14	6.19	5.86	6.28	10.87	6.96	6.35
Ca	0.68	0.05	0.06	0.07	0.12	0.09	0.08
Na	0.02	0.02	0.01	0.03	0.07	0.03	0.03
K	0.09	0.09	0.16	0.10	0.08	0.04	0.05
*OH**	16.00	16.00	16.00	16.00	16.00	16.00	16.00

Total	35.38	35.05	34.96	35.20	38.91	35.58	35.17
Oxidized	yes	no	no	no	yes	yes	no
Fe/Fe+Mg	0.185	0.181	0.191	0.199	0.285	0.190	0.189

Sample #	*21-700-02-01-S6*	*21-700-02-01-S6*	*21-700-02-01-S6*	*21-700-02-01-S7*	*21-700-02-01-S7*	*21-700-02-01-S7*	*21-700-02-01-S8*
SiO_2	30.53	33.19	32.26	34.32	32.40	32.95	33.39
TiO_2	0.01	0.02	0.01	0.02	0.00	0.02	0.00
Al_2O_3	21.23	23.17	21.63	23.88	22.43	22.13	23.42
Cr_2O_3	0.02	0.02	0.03	0.02	0.02	0.02	0.03
Fe_2O_3	2.89	4.94	3.23	6.40	4.61	4.40	5.19
FeO	6.87	5.34	8.23	2.72	6.26	5.48	4.60
MnO	0.13	0.13	0.17	0.16	0.15	0.19	0.12
MgO	22.37	23.17	24.28	22.29	22.48	23.90	23.12
CaO	2.63	0.26	0.31	0.24	0.27	0.25	0.31
Na_2O	0.02	0.03	0.03	0.04	0.00	0.03	0.04
K_2O	0.07	0.14	0.05	0.28	0.14	0.11	0.17
H_2O*	12.24	12.90	12.75	13.01	12.61	12.78	12.94
Total	99.02	103.31	102.99	103.37	101.34	102.25	103.32
Si	5.94	6.09	6.02	6.22	6.09	6.12	6.11
Al^{iv}	2.06	1.91	1.98	1.78	1.91	1.88	1.89
Al^{vi}	2.84	3.17	2.81	3.41	3.12	3.01	3.22
Ti	0.00	0.00	0.00	0.00	0.00	0.00	0.00
Cr	0.00	0.00	0.01	0.00	0.00	0.00	0.00
Fe^{3+}	0.42	0.68	0.45	0.87	0.65	0.61	0.71
Fe^{2+}	1.12	0.82	1.28	0.41	0.98	0.85	0.70
Mn	0.02	0.02	0.03	0.02	0.02	0.03	0.02
Mg	6.48	6.34	6.75	6.02	6.30	6.61	6.30
Ca	0.55	0.05	0.06	0.05	0.06	0.05	0.06

Na	0.01	0.02	0.02	0.03	0.00	0.02	0.03
K	0.03	0.07	0.03	0.13	0.07	0.05	0.08
*OH**	16.00	16.00	16.00	16.00	16.00	16.00	16.00
Total	35.48	35.17	35.44	34.96	35.20	35.25	35.14
Oxidized	yes	no	yes	no	no	no	no
Fe/Fe+Mg	0.192	0.192	0.205	0.176	0.206	0.181	0.184

Sample #	*21-700-02-01-S8*	*21-700-02-01-S9*	*21-700-02-01-S9*	*21-700-02-01-S9*	*21-700-02-01-S9*	*21-700-02-01-S10*	*21-700-02-01-S10*
SiO_2	32.12	32.11	34.01	33.29	32.64	31.61	33.55
TiO_2	0.03	0.02	0.00	0.00	0.00	0.02	0.02
Al_2O_3	22.52	22.90	24.26	22.38	23.30	22.26	22.39
Cr_2O_3	0.03	0.01	0.03	0.02	0.01	0.02	0.03
Fe_2O_3	3.70	4.26	6.24	4.67	4.96	3.40	4.75
FeO	6.90	5.81	3.57	4.82	4.90	7.83	4.87
MnO	0.13	0.11	0.14	0.20	0.12	0.19	0.15
MgO	24.11	23.39	21.67	23.92	22.46	23.21	24.13
CaO	0.23	0.19	0.25	0.26	0.24	0.87	0.25
Na_2O	0.02	0.05	0.03	0.06	0.09	0.03	0.01
K_2O	0.06	0.09	0.43	0.11	0.24	0.03	0.14
H_2O*	12.77	12.69	12.99	12.84	12.71	12.63	12.92
Total	102.62	101.62	103.62	102.56	101.62	102.11	103.22
Si	5.98	6.00	6.17	6.14	6.08	5.95	6.15
Al^{iv}	2.02	2.00	1.83	1.86	1.92	2.05	1.85
Al^{vi}	2.96	3.11	3.45	3.06	3.26	2.93	3.05
Ti	0.00	0.00	0.00	0.00	0.00	0.00	0.00
Cr	0.00	0.00	0.00	0.00	0.00	0.00	0.00
Fe^{3+}	0.52	0.60	0.85	0.65	0.69	0.48	0.65
Fe^{2+}	1.07	0.91	0.54	0.74	0.76	1.23	0.75
Mn	0.02	0.02	0.02	0.03	0.02	0.03	0.02

Mg	6.69	6.52	5.86	6.58	6.23	6.51	6.59
Ca	0.05	0.04	0.05	0.05	0.05	0.18	0.05
Na	0.01	0.03	0.02	0.04	0.07	0.02	0.00
K	0.03	0.04	0.20	0.05	0.11	0.02	0.07
*OH**	16.00	16.00	16.00	16.00	16.00	16.00	16.00
Total	35.36	35.27	35.00	35.21	35.19	35.40	35.19
Oxidized	yes	no	no	no	no	yes	no
Fe/Fe+Mg	0.192	0.188	0.192	0.175	0.190	0.208	0.175

Sample #	*21-700-02-01-S11*	*21-700-02-01-S11*	*21-700-02-02-S1*	*21-700-02-02-S1*	*21-700-02-02-S2*	*21-700-02-02-S2*	*21-700-02-02-S2*
SiO_2	32.75	31.56	32.47	30.28	31.43	30.97	28.12
TiO_2	0.02	0.00	0.01	0.05	0.15	0.04	0.02
Al_2O_3	22.70	21.18	19.53	21.16	21.31	21.53	19.49
Cr_2O_3	0.02	0.02	0.02	0.01	0.02	0.02	0.03
Fe_2O_3	4.56	3.01	2.84	2.11	2.67	2.45	2.27
FeO	6.32	8.52	7.14	10.96	9.60	10.40	9.53
MnO	0.15	0.13	0.25	0.17	0.20	0.18	0.20
MgO	22.77	23.89	25.64	23.18	23.94	23.48	21.03
CaO	0.61	0.29	0.27	0.59	0.51	0.45	0.57
Na_2O	0.02	0.03	0.03	0.01	0.01	0.02	0.02
K_2O	0.09	0.03	0.01	0.00	0.04	0.04	0.03
H_2O*	12.78	12.51	12.54	12.35	12.61	12.53	11.36
Total	102.81	101.17	100.76	100.88	102.48	102.12	92.68
Si	6.07	6.00	6.16	5.85	5.93	5.89	5.90
Al^{iv}	1.93	2.00	1.84	2.15	2.07	2.11	2.10
Al^{vi}	3.09	2.79	2.57	2.69	2.71	2.74	2.75
Ti	0.00	0.00	0.00	0.01	0.02	0.01	0.00
Cr	0.00	0.00	0.00	0.00	0.00	0.00	0.01
Fe^{3+}	0.64	0.43	0.41	0.31	0.38	0.35	0.36

Fe^{2+}	0.98	1.36	1.13	1.77	1.52	1.65	1.67
Mn	0.02	0.02	0.04	0.03	0.03	0.03	0.04
Mg	6.29	6.77	7.26	6.68	6.74	6.65	6.57
Ca	0.12	0.06	0.06	0.12	0.10	0.09	0.13
Na	0.02	0.02	0.02	0.01	0.00	0.02	0.02
K	0.04	0.02	0.00	0.00	0.02	0.02	0.01
*OH**	16.00	16.00	16.00	16.00	16.00	16.00	16.00
Total	35.21	35.47	35.49	35.61	35.53	35.57	35.56
Oxidized	no	yes	yes	yes	yes	yes	yes
Fe/Fe+Mg	0.204	0.209	0.175	0.237	0.219	0.232	0.236

Sample #	*21-700-02-02-S3*	*21-700-02-02-S3*	*21-700-02-02-S4*	*21-700-02-02-S4*	*21-700-02-02-S5*	*21-700-02-02-S5*	*21-700-02-02-S6*
SiO_2	31.17	31.36	31.54	31.40	30.93	32.53	25.28
TiO_2	0.00	0.02	0.01	0.02	0.04	0.43	0.05
Al_2O_3	21.91	22.18	21.44	21.49	21.86	19.71	16.76
Cr_2O_3	0.02	0.03	0.03	0.05	0.05	0.05	0.04
Fe_2O_3	2.49	2.67	2.48	2.62	2.22	3.77	2.60
FeO	9.57	9.35	9.25	9.68	10.47	7.90	6.75
MnO	0.21	0.18	0.16	0.19	0.19	0.17	0.16
MgO	24.21	24.15	24.14	23.84	23.71	20.75	18.28
CaO	0.34	0.35	1.06	0.47	0.81	1.61	0.88
Na_2O	0.03	0.02	0.04	0.04	0.06	0.65	0.03
K_2O	0.01	0.04	0.03	0.04	0.01	0.02	0.00
H_2O*	12.65	12.71	12.68	12.61	12.63	12.29	9.96
Total	102.61	103.07	102.87	102.45	102.97	99.90	80.79
Si	5.87	5.87	5.93	5.93	5.84	6.26	6.03
Al^{iv}	2.13	2.13	2.07	2.07	2.16	1.74	1.97
Al^{vi}	2.77	2.81	2.71	2.75	2.73	2.79	2.79
Ti	0.00	0.00	0.00	0.00	0.00	0.06	0.01
Cr	0.00	0.00	0.01	0.01	0.01	0.01	0.01

Fe^{3+}	0.35	0.38	0.35	0.37	0.31	0.55	0.47
Fe^{2+}	1.51	1.46	1.45	1.53	1.65	1.27	1.35
Mn	0.03	0.03	0.03	0.03	0.03	0.03	0.03
Mg	6.80	6.75	6.76	6.71	6.67	5.95	6.51
Ca	0.07	0.07	0.21	0.10	0.16	0.33	0.22
Na	0.02	0.01	0.03	0.03	0.04	0.49	0.03
K	0.00	0.02	0.01	0.02	0.00	0.01	0.00
*OH**	16.00	16.00	16.00	16.00	16.00	16.00	16.00
Total	35.56	35.53	35.57	35.54	35.62	35.48	35.42
Oxidized	yes	yes	yes	yes	yes	yes	yes
Fe/Fe+Mg	0.215	0.214	0.211	0.221	0.228	0.234	0.218

Sample #	*21-700-02-02-S6*	*21-700-02-02-S6*	*21-700-02-02-S6*	*21-700-02-02-S7*	*21-700-02-02-S7*	*21-700-02-02-S8*	*21-700-02-02-S9*
SiO_2	30.64	30.81	30.85	30.80	32.03	29.94	31.00
TiO_2	0.02	0.03	0.00	0.01	0.00	7.04	0.17
Al_2O_3	21.78	21.72	21.98	21.35	22.44	16.62	21.57
Cr_2O_3	0.03	0.03	0.02	0.05	0.03	0.04	0.04
Fe_2O_3	2.03	1.93	2.08	1.83	3.69	6.71	2.38
FeO	11.04	11.23	11.17	10.36	7.19	3.28	10.29
MnO	0.18	0.17	0.17	0.20	0.14	0.16	0.19
MgO	24.00	24.15	23.93	24.85	23.57	16.18	23.99
CaO	0.37	0.38	0.37	0.34	0.48	7.50	0.51
Na_2O	0.00	0.01	0.01	0.00	0.02	0.00	0.00
K_2O	0.02	0.03	0.04	0.03	0.11	0.00	0.02
H_2O*	12.59	12.64	12.66	12.60	12.71	11.99	12.62
Total	102.67	103.14	103.28	102.41	102.41	99.45	102.74
Si	5.81	5.82	5.81	5.84	5.98	5.88	5.86
Al^{iv}	2.19	2.18	2.19	2.16	2.02	2.12	2.14

Al^{vi}	2.70	2.68	2.72	2.63	2.97	1.80	2.69
Ti	0.00	0.00	0.00	0.00	0.00	1.04	0.02
Cr	0.00	0.00	0.00	0.01	0.00	0.01	0.01
Fe^{3+}	0.29	0.27	0.30	0.26	0.52	0.99	0.34
Fe^{2+}	1.75	1.77	1.76	1.64	1.12	0.54	1.63
Mn	0.03	0.03	0.03	0.03	0.02	0.03	0.03
Mg	6.78	6.80	6.72	7.02	6.56	4.74	6.76
Ca	0.08	0.08	0.08	0.07	0.10	1.58	0.10
Na	0.00	0.01	0.00	0.00	0.01	0.00	0.00
K	0.01	0.02	0.02	0.01	0.05	0.00	0.01
*OH**	16.00	16.00	16.00	16.00	16.00	16.00	16.00
Total	35.63	35.66	35.63	35.67	35.37	34.72	35.56
Oxidized	yes	yes	yes	yes	yes	no	yes
Fe/Fe+Mg	0.231	0.231	0.234	0.213	0.200	0.244	0.225

Sample #	*21-700-02-02-S9*	*21-700-02-02-S9*	*21-700-02-02-S10*	*21-700-02-02-S10*	*21-700-02-02-S10*	*21-700-02-02-S10*	*21-700-02-03-S1*
SiO_2	31.01	30.71	31.97	31.09	30.86	30.58	31.13
TiO_2	0.02	0.00	0.04	0.03	0.13	0.07	0.05
Al_2O_3	21.72	21.61	21.61	21.43	21.34	21.30	21.90
Cr_2O_3	0.04	0.05	0.05	0.02	0.03	0.04	0.04
Fe_2O_3	2.11	2.28	2.89	2.36	2.46	1.80	2.30
FeO	10.71	10.14	9.51	10.29	10.25	11.02	10.75
MnO	0.20	0.22	0.20	0.20	0.16	0.21	0.21
MgO	24.08	23.89	23.91	24.04	23.60	24.25	23.82
CaO	0.57	0.34	0.30	0.35	0.42	0.41	0.41
Na_2O	0.02	0.00	0.00	0.00	0.00	0.03	0.02
K_2O	0.02	0.02	0.18	0.02	0.02	0.01	0.07
H_2O*	12.66	12.51	12.73	12.59	12.50	12.54	12.68
Total	103.16	101.78	103.40	102.41	101.77	102.25	103.40

Si	5.84	5.85	5.97	5.89	5.89	5.82	5.85
Al iv	2.16	2.15	2.03	2.11	2.11	2.18	2.15
Al vi	2.70	2.73	2.77	2.70	2.71	2.63	2.73
Ti	0.00	0.00	0.01	0.00	0.02	0.01	0.01
Cr	0.01	0.01	0.01	0.00	0.00	0.01	0.01
Fe^{3+}	0.30	0.33	0.41	0.34	0.35	0.26	0.33
Fe^{2+}	1.69	1.62	1.49	1.63	1.64	1.75	1.69
Mn	0.03	0.04	0.03	0.03	0.03	0.03	0.03
Mg	6.76	6.79	6.66	6.79	6.71	6.88	6.67
Ca	0.12	0.07	0.06	0.07	0.09	0.08	0.08
Na	0.02	0.00	0.00	0.00	0.00	0.02	0.02
K	0.01	0.01	0.09	0.01	0.01	0.01	0.03
*OH**	16.00	16.00	16.00	16.00	16.00	16.00	16.00
Total	35.63	35.59	35.52	35.57	35.56	35.68	35.60
Oxidized	yes	yes	yes	yes	yes	yes	yes
Fe/Fe+Mg	0.227	0.223	0.221	0.225	0.229	0.226	0.232

Sample #	*21-700-02-03-S1*	*21-700-02-03-S2*	*21-700-02-03-S2*	*21-700-02-03-S2*	*21-700-02-03-S3*	*21-700-02-03-S3*	*21-700-02-03-S3*
SiO_2	30.80	31.68	31.11	31.44	31.23	30.85	30.73
TiO_2	0.01	0.00	0.00	0.01	0.05	0.01	0.78
Al_2O_3	21.47	21.90	21.76	21.71	21.64	21.82	21.25
Cr_2O_3	0.04	0.03	0.04	0.04	0.04	0.05	0.02
Fe_2O_3	1.84	3.04	2.74	2.81	2.49	1.98	2.98
FeO	11.10	9.22	9.69	9.78	10.90	11.06	9.63
MnO	0.20	0.17	0.22	0.19	0.20	0.20	0.20
MgO	24.38	23.72	23.45	23.59	23.52	24.21	22.52
CaO	0.37	0.28	0.31	0.29	0.40	0.37	1.17
Na_2O	0.00	0.02	0.02	0.03	0.02	0.02	0.01
K_2O	0.05	0.03	0.04	0.03	0.00	0.01	0.03
H_2O*	12.61	12.67	12.54	12.62	12.64	12.66	12.47

Total	102.87	102.76	101.90	102.54	103.13	103.24	101.77
Si	5.83	5.95	5.91	5.93	5.89	5.82	5.87
Al ^{iv}	2.17	2.05	2.09	2.07	2.11	2.18	2.13
Al ^{vi}	2.64	2.83	2.81	2.79	2.73	2.69	2.68
Ti	0.00	0.00	0.00	0.00	0.01	0.00	0.11
Cr	0.01	0.00	0.01	0.01	0.01	0.01	0.00
Fe^{3+}	0.26	0.43	0.39	0.40	0.35	0.28	0.43
Fe^{2+}	1.76	1.45	1.54	1.54	1.72	1.74	1.54
Mn	0.03	0.03	0.04	0.03	0.03	0.03	0.03
Mg	6.88	6.64	6.64	6.63	6.61	6.80	6.41
Ca	0.07	0.06	0.06	0.06	0.08	0.07	0.24
Na	0.00	0.02	0.02	0.02	0.01	0.02	0.01
K	0.02	0.01	0.02	0.01	0.00	0.00	0.01
*OH**	16.00	16.00	16.00	16.00	16.00	16.00	16.00
Total	35.67	35.46	35.52	35.51	35.56	35.65	35.46
Oxidized	yes	yes	yes	yes	yes	yes	yes
Fe/Fe+Mg	0.227	0.220	0.225	0.226	0.239	0.229	0.235

Sample #	*21-700-02-03-S4*	*21-700-02-03-S4*	*21-700-02-03-S5*	*21-700-02-03-S5*	*21-700-02-03-S5*	*21-700-02-03-S6*	*21-700-02-03-S7*
SiO_2	30.88	30.56	33.55	31.08	30.57	28.57	31.27
TiO_2	0.02	0.02	0.00	0.41	0.00	1.61	0.05
Al_2O_3	21.78	21.46	20.23	20.75	21.19	18.01	21.28
Cr_2O_3	0.03	0.04	0.00	0.02	0.02	0.16	0.05
Fe_2O_3	2.22	1.87	3.53	2.38	1.61	1.35	2.23
FeO	10.43	11.41	5.49	11.26	10.92	14.31	9.82
MnO	0.21	0.17	0.21	0.19	0.18	0.19	0.18
MgO	24.00	23.84	26.04	23.11	24.97	21.23	24.52
CaO	0.34	0.59	0.25	0.71	0.17	1.44	0.72

Na_2O	0.03	0.00	0.02	0.02	0.00	0.02	0.00
K_2O	0.03	0.02	0.14	0.09	0.00	0.01	0.01
H_2O*	12.60	12.54	12.80	12.52	12.55	11.82	12.65
Total	102.56	102.51	102.25	102.55	102.18	98.73	102.78
Si	5.84	5.82	6.22	5.92	5.82	5.78	5.90
Al^{iv}	2.16	2.18	1.78	2.08	2.18	2.22	2.10
Al^{vi}	2.73	2.65	2.69	2.60	2.59	2.08	2.65
Ti	0.00	0.00	0.00	0.06	0.00	0.25	0.01
Cr	0.00	0.01	0.00	0.00	0.00	0.03	0.01
Fe^{3+}	0.32	0.27	0.49	0.34	0.23	0.21	0.32
Fe^{2+}	1.65	1.82	0.85	1.79	1.74	2.42	1.55
Mn	0.03	0.03	0.03	0.03	0.03	0.03	0.03
Mg	6.77	6.76	7.20	6.56	7.08	6.40	6.89
Ca	0.07	0.12	0.05	0.14	0.03	0.31	0.15
Na	0.02	0.00	0.01	0.02	0.00	0.01	0.00
K	0.01	0.01	0.07	0.04	0.00	0.01	0.00
*OH**	16.00	16.00	16.00	16.00	16.00	16.00	16.00
Total	35.61	35.66	35.40	35.59	35.71	35.74	35.60
Oxidized	yes	yes	yes	yes	yes	yes	yes
Fe/Fe+Mg	0.225	0.235	0.157	0.245	0.217	0.291	0.213

Sample #	*21-700-02-03-S7*	*21-700-02-03-S7*	*21-700-02-03-S8*	*21-700-02-03-S8*	*21-700-02-03-S9*	*21-700-02-03-S9*	*21-700-02-03-S10*
SiO_2	31.48	31.21	29.23	28.54	30.74	30.68	31.00
TiO_2	0.00	0.06	0.05	0.05	0.01	0.03	0.01
Al_2O_3	22.23	21.36	20.38	19.50	21.58	21.74	21.72
Cr_2O_3	0.06	0.04	0.04	0.05	0.03	0.02	0.03
Fe_2O_3	2.95	2.40	2.28	2.86	2.11	1.81	2.16
FeO	8.64	10.01	9.11	8.22	10.81	11.35	10.71
MnO	0.15	0.20	0.18	0.18	0.18	0.22	0.16

MgO	24.13	24.15	22.24	20.97	23.88	24.23	24.17
CaO	0.34	0.39	0.76	0.60	0.33	0.37	0.33
Na_2O	0.01	0.01	0.10	0.00	0.04	0.02	0.02
K_2O	0.03	0.02	0.01	0.00	0.01	0.02	0.03
*H_2O**	12.70	12.60	11.83	11.38	12.55	12.63	12.64
Total	102.71	102.45	96.20	92.36	102.27	103.12	102.98
Si	5.90	5.90	5.88	5.97	5.84	5.80	5.85
Al^{iv}	2.10	2.10	2.12	2.03	2.16	2.20	2.15
Al^{vi}	2.85	2.70	2.75	2.82	2.71	2.66	2.70
Ti	0.00	0.01	0.01	0.01	0.00	0.00	0.00
Cr	0.01	0.01	0.01	0.01	0.00	0.00	0.01
Fe^{3+}	0.42	0.34	0.35	0.45	0.30	0.26	0.31
Fe^{2+}	1.35	1.58	1.53	1.44	1.72	1.79	1.69
Mn	0.02	0.03	0.03	0.03	0.03	0.04	0.03
Mg	6.74	6.81	6.67	6.54	6.77	6.83	6.80
Ca	0.07	0.08	0.16	0.14	0.07	0.08	0.07
Na	0.01	0.01	0.08	0.00	0.03	0.01	0.01
K	0.01	0.01	0.00	0.00	0.01	0.01	0.01
*OH**	16.00	16.00	16.00	16.00	16.00	16.00	16.00
Total	35.48	35.57	35.59	35.43	35.63	35.68	35.62
Oxidized	yes	yes	yes	yes	yes	yes	yes
Fe/Fe+Mg	0.208	0.220	0.220	0.224	0.230	0.231	0.227

Sample #	*21-700-02-03-S10*	*21-700-02-03-S10*	*22-905-11-01-S5*	*22-905-11-01-S5*	*22-905-11-01-S5*	*22-905-11-01-S6*	*22-905-11-01-S6*
SiO_2	31.04	30.65	30.89	33.32	31.16	28.88	29.33
TiO_2	0.04	0.03	0.02	0.00	0.01	0.04	0.03
Al_2O_3	22.21	21.50	20.12	17.90	19.76	22.02	22.11
Cr_2O_3	0.01	0.02	0.07	0.11	0.08	0.03	0.01
Fe_2O_3	2.69	1.95	2.11	2.52	1.91	1.37	1.59

FeO	9.40	10.93	8.93	6.22	8.95	11.26	10.66
MnO	0.19	0.16	0.23	0.16	0.29	0.26	0.24
MgO	23.68	24.16	25.04	27.43	25.54	23.82	24.14
CaO	0.36	0.32	0.13	0.26	0.18	0.07	0.06
Na_2O	0.02	0.01	0.00	0.02	0.01	0.00	0.00
K_2O	0.10	0.02	0.01	0.05	0.03	0.00	0.00
H_2O*	12.61	12.55	12.35	12.58	12.41	12.25	12.35
Total	102.35	102.29	99.90	100.58	100.32	99.99	100.53
Si	5.86	5.83	5.97	6.31	5.99	5.63	5.67
Al^{iv}	2.14	2.17	2.03	1.69	2.01	2.37	2.33
Al^{vi}	2.84	2.67	2.57	2.33	2.50	2.71	2.73
Ti	0.01	0.00	0.00	0.00	0.00	0.01	0.00
Cr	0.00	0.00	0.01	0.02	0.01	0.00	0.00
Fe^{3+}	0.38	0.28	0.31	0.36	0.28	0.20	0.23
Fe^{2+}	1.48	1.74	1.44	0.98	1.44	1.84	1.72
Mn	0.03	0.03	0.04	0.03	0.05	0.04	0.04
Mg	6.66	6.85	7.21	7.74	7.32	6.93	6.96
Ca	0.07	0.07	0.03	0.05	0.04	0.02	0.01
Na	0.01	0.01	0.00	0.02	0.00	0.00	0.00
K	0.05	0.01	0.00	0.02	0.02	0.00	0.00
*OH**	16.00	16.00	16.00	16.00	16.00	16.00	16.00
Total	35.54	35.65	35.61	35.55	35.65	35.75	35.71
Oxidized	yes	yes	yes	yes	yes	yes	yes
Fe/Fe+Mg	0.219	0.227	0.195	0.148	0.190	0.227	0.219

Sample #	*22-905-11-01-S7*	*22-905-11-01-S7*	*22-905-11-01-S10*	*22-905-11-01-S10*	*22-905-11-01-S14*	*22-905-11-01-S14*	*22-905-11-02-S1*
SiO_2	30.48	31.72	29.70	32.00	33.06	32.95	33.41
TiO_2	0.01	0.00	0.00	0.03	0.00	0.05	0.00
Al_2O_3	20.54	19.51	21.46	19.52	18.08	18.70	17.91

Cr_2O_3	0.01	0.02	0.01	0.03	0.12	0.11	0.09
Fe_2O_3	1.90	1.96	1.52	2.31	2.50	2.46	2.19
FeO	10.15	9.54	10.60	8.49	6.96	7.41	6.83
MnO	0.27	0.25	0.27	0.28	0.18	0.22	0.21
MgO	24.34	25.57	24.48	25.65	26.84	26.72	27.92
CaO	0.24	0.24	0.13	0.26	0.42	0.35	0.28
Na_2O	0.01	0.02	0.00	0.01	0.00	0.02	0.04
K_2O	0.02	0.02	0.00	0.02	0.01	0.01	0.00
H_2O*	12.34	12.51	12.35	12.53	12.55	12.65	12.69
Total	100.30	101.36	100.51	101.14	100.72	101.64	101.58
Si	5.90	6.05	5.74	6.09	6.28	6.21	6.28
Al^{iv}	2.10	1.95	2.26	1.91	1.72	1.79	1.72
Al^{vi}	2.60	2.46	2.65	2.50	2.35	2.39	2.27
Ti	0.00	0.00	0.00	0.00	0.00	0.01	0.00
Cr	0.00	0.00	0.00	0.00	0.02	0.02	0.01
Fe^{3+}	0.28	0.28	0.22	0.33	0.36	0.35	0.31
Fe^{2+}	1.64	1.52	1.71	1.35	1.10	1.17	1.07
Mn	0.04	0.04	0.04	0.04	0.03	0.04	0.03
Mg	7.02	7.27	7.06	7.28	7.59	7.51	7.82
Ca	0.05	0.05	0.03	0.05	0.08	0.07	0.06
Na	0.01	0.01	0.00	0.01	0.00	0.01	0.03
K	0.01	0.01	0.00	0.01	0.01	0.00	0.00
*OH**	16.00	16.00	16.00	16.00	16.00	16.00	16.00
Total	35.66	35.65	35.72	35.58	35.54	35.56	35.61
Oxidized	yes	yes	yes	yes	yes	yes	yes
Fe/Fe+Mg	0.215	0.199	0.215	0.188	0.161	0.168	0.150

Sample #	*22-905-11-02-S1*	*22-905-11-02-S1*	*22-905-11-02-S1*	*22-905-11-02-S1*	*22-905-11-02-S2*	*22-905-11-02-S2*	*22-905-11-02-S2*
SiO_2	33.36	29.27	28.73	32.09	32.55	28.81	29.22
TiO_2	0.00	0.00	0.05	0.01	0.04	0.04	0.00

Al_2O_3	17.94	22.61	22.93	19.13	17.88	22.96	22.71
Cr_2O_3	0.10	0.03	0.03	0.06	0.09	0.02	0.02
Fe_2O_3	1.96	1.30	1.14	1.51	1.89	0.88	1.37
FeO	6.81	11.91	12.62	7.69	7.39	12.86	11.94
MnO	0.17	0.25	0.28	0.20	0.25	0.29	0.25
MgO	28.47	24.10	23.62	28.04	27.53	24.17	23.87
CaO	0.25	0.06	0.05	0.18	0.24	0.02	0.09
Na_2O	0.03	0.00	0.00	0.02	0.00	0.00	0.00
K_2O	0.01	0.00	0.00	0.00	0.02	0.00	0.00
H_2O*	12.73	12.48	12.42	12.66	12.51	12.51	12.47
Total	101.85	102.01	101.88	101.59	100.39	102.57	101.95
Si	6.25	5.61	5.53	6.05	6.21	5.51	5.60
Al^{iv}	1.75	2.39	2.47	1.95	1.79	2.49	2.40
Al^{vi}	2.24	2.73	2.75	2.32	2.25	2.70	2.75
Ti	0.00	0.00	0.01	0.00	0.01	0.01	0.00
Cr	0.02	0.00	0.01	0.01	0.01	0.00	0.00
Fe^{3+}	0.28	0.19	0.17	0.21	0.27	0.13	0.20
Fe^{2+}	1.07	1.91	2.03	1.21	1.18	2.06	1.91
Mn	0.03	0.04	0.05	0.03	0.04	0.05	0.04
Mg	7.95	6.88	6.78	7.89	7.83	6.89	6.82
Ca	0.05	0.01	0.01	0.04	0.05	0.01	0.02
Na	0.03	0.00	0.00	0.02	0.00	0.00	0.00
K	0.00	0.00	0.00	0.00	0.01	0.00	0.00
*OH**	16.00	16.00	16.00	16.00	16.00	16.00	16.00
Total	35.65	35.76	35.79	35.73	35.66	35.84	35.75
Oxidized	yes	yes	yes	yes	yes	yes	yes
Fe/Fe+Mg	0.145	0.233	0.245	0.153	0.156	0.241	0.236

Sample #	*22-905-11-02-S2*	*22-905-11-02-S3*	*22-905-11-02-S3*	*22-905-11-02-S3*	*22-905-11-02-S4*	*22-905-11-02-S4*	*22-905-11-02-S4*
SiO_2	33.38	33.25	32.97	32.43	33.20	32.84	32.55
TiO_2	0.00	0.03	0.00	0.00	0.01	0.01	0.00
Al_2O_3	18.63	17.43	17.60	18.09	17.62	17.89	18.32
Cr_2O_3	0.10	0.04	0.05	0.05	0.16	0.13	0.11
Fe_2O_3	2.19	1.81	1.79	1.61	1.83	1.95	1.85
FeO	7.11	7.16	6.93	7.23	6.91	7.09	7.53
MnO	0.21	0.19	0.17	0.21	0.17	0.22	0.22
MgO	27.99	28.41	28.35	28.19	28.63	27.78	27.48
CaO	0.28	0.25	0.21	0.23	0.21	0.24	0.28
Na_2O	0.00	0.01	0.02	0.00	0.01	0.03	0.04
K_2O	0.01	0.05	0.02	0.02	0.00	0.03	0.02
H_2O*	12.82	12.64	12.59	12.56	12.67	12.57	12.58
Total	102.70	101.27	100.70	100.62	101.41	100.77	100.99
Si	6.21	6.28	6.25	6.17	6.25	6.23	6.18
Al^{iv}	1.79	1.72	1.75	1.83	1.75	1.77	1.82
Al^{vi}	2.32	2.18	2.21	2.24	2.18	2.25	2.29
Ti	0.00	0.00	0.00	0.00	0.00	0.00	0.00
Cr	0.02	0.01	0.01	0.01	0.02	0.02	0.02
Fe^{3+}	0.31	0.26	0.26	0.23	0.26	0.28	0.26
Fe^{2+}	1.11	1.13	1.10	1.15	1.09	1.13	1.19
Mn	0.03	0.03	0.03	0.03	0.03	0.03	0.04
Mg	7.76	8.00	8.02	7.99	8.04	7.86	7.77
Ca	0.06	0.05	0.04	0.05	0.04	0.05	0.06
Na	0.00	0.00	0.02	0.00	0.00	0.02	0.03
K	0.01	0.02	0.01	0.01	0.00	0.01	0.01
*OH**	16.00	16.00	16.00	16.00	16.00	16.00	16.00
Total	35.61	35.68	35.68	35.71	35.67	35.65	35.67
Oxidized	yes	yes	yes	yes	yes	yes	yes
Fe/Fe+Mg	0.154	0.148	0.145	0.147	0.144	0.151	0.158

Sample #	*22-905-11-02-S4*	*22-905-11-02-S5*	*22-905-11-02-S5*	*22-905-11-02-S5*	*22-905-11-02-S5*	*22-905-11-02-S5*	*22-905-11-02-S6*
SiO_2	33.05	33.15	29.47	32.02	28.22	32.90	32.23
TiO_2	0.00	0.03	0.02	0.00	0.00	0.00	0.00
Al_2O_3	18.15	17.74	22.13	18.11	22.55	18.00	18.31
Cr_2O_3	0.13	0.16	0.07	0.09	0.01	0.10	0.14
Fe_2O_3	1.92	1.53	1.50	1.36	1.03	2.09	1.40
FeO	6.85	7.53	11.05	7.94	12.11	6.86	8.04
MnO	0.19	0.22	0.29	0.21	0.27	0.20	0.22
MgO	28.18	28.76	24.17	27.89	23.52	27.78	28.11
CaO	0.30	0.23	0.13	0.21	0.05	0.28	0.18
Na_2O	0.04	0.05	0.00	0.02	0.00	0.00	0.00
K_2O	0.02	0.01	0.00	0.02	0.00	0.00	0.00
H_2O*	12.68	12.74	12.42	12.49	12.21	12.59	12.60
Total	101.50	102.14	101.25	100.36	99.98	100.80	101.24
Si	6.22	6.22	5.67	6.12	5.53	6.24	6.11
Al^{iv}	1.78	1.78	2.33	1.88	2.47	1.76	1.89
Al^{vi}	2.26	2.15	2.71	2.22	2.75	2.28	2.22
Ti	0.00	0.00	0.00	0.00	0.00	0.00	0.00
Cr	0.02	0.02	0.01	0.01	0.00	0.02	0.02
Fe^{3+}	0.27	0.22	0.22	0.20	0.15	0.30	0.20
Fe^{2+}	1.08	1.18	1.78	1.27	1.98	1.09	1.28
Mn	0.03	0.03	0.05	0.03	0.04	0.03	0.04
Mg	7.90	8.04	6.93	7.95	6.87	7.85	7.95
Ca	0.06	0.05	0.03	0.04	0.01	0.06	0.04
Na	0.03	0.03	0.00	0.02	0.00	0.00	0.00
K	0.01	0.01	0.00	0.01	0.00	0.00	0.00
*OH**	16.00	16.00	16.00	16.00	16.00	16.00	16.00
Total	35.66	35.74	35.72	35.76	35.81	35.62	35.74
Oxidized	yes	yes	yes	yes	yes	yes	yes

Fe/Fe+Mg	0.146	0.148	0.224	0.156	0.237	0.150	0.157

Sample #	*22-905-11-02-S6*	*22-905-11-02-S8*	*22-905-11-02-S8*	*22-905-11-02-S10*	*22-905-11-02-S11*	*22-905-11-02-S11*	*22-905-11-02-S11*
SiO_2	29.03	29.11	32.97	27.43	32.43	32.31	32.74
TiO_2	0.00	0.01	0.00	0.08	0.00	0.03	0.01
Al_2O_3	21.95	21.69	17.92	23.23	18.51	18.10	18.51
Cr_2O_3	0.03	0.07	0.09	0.01	0.03	0.01	0.03
Fe_2O_3	1.11	1.18	1.84	0.80	1.74	1.34	1.82
FeO	11.43	11.85	6.77	16.09	7.26	7.21	6.75
MnO	0.21	0.26	0.21	0.18	0.19	0.18	0.18
MgO	24.45	24.08	28.48	21.31	27.93	28.72	28.39
CaO	0.07	0.03	0.21	0.01	0.21	0.20	0.22
Na_2O	0.00	0.00	0.01	0.00	0.02	0.01	0.00
K_2O	0.00	0.00	0.00	0.00	0.02	0.02	0.03
H_2O*	12.34	12.30	12.65	12.17	12.60	12.59	12.68
Total	100.62	100.57	101.14	101.29	100.92	100.72	101.35
Si	5.63	5.66	6.22	5.40	6.15	6.14	6.16
Al^{iv}	2.37	2.34	1.78	2.60	1.85	1.86	1.84
Al^{vi}	2.66	2.64	2.23	2.79	2.30	2.20	2.29
Ti	0.00	0.00	0.00	0.01	0.00	0.00	0.00
Cr	0.01	0.01	0.01	0.00	0.00	0.00	0.00
Fe^{3+}	0.16	0.17	0.26	0.12	0.25	0.19	0.26
Fe^{2+}	1.85	1.93	1.07	2.65	1.15	1.15	1.06
Mn	0.03	0.04	0.03	0.03	0.03	0.03	0.03
Mg	7.07	6.98	8.01	6.25	7.89	8.13	7.97
Ca	0.01	0.01	0.04	0.00	0.04	0.04	0.04
Na	0.00	0.00	0.00	0.00	0.02	0.01	0.00
K	0.00	0.00	0.00	0.00	0.01	0.01	0.01
*OH**	16.00	16.00	16.00	16.00	16.00	16.00	16.00

Total	35.79	35.78	35.67	35.85	35.69	35.76	35.67
Oxidized	yes	yes	yes	yes	yes	yes	yes
Fe/Fe+Mg	0.222	0.231	0.142	0.307	0.151	0.141	0.142

Sample #	*22-905-11-02-S12*	*22-905-11-02-S12*	*22-905-11-02-S12*	*22-905-11-02-S12*	*22-905-11-03-S1*	*22-905-11-03-S1*	*22-905-11-03-S2*
SiO_2	28.92	29.11	32.41	30.52	32.32	32.71	30.56
TiO_2	0.01	0.00	0.00	0.02	0.00	0.00	0.04
Al_2O_3	22.77	22.95	18.92	20.33	19.31	18.15	20.81
Cr_2O_3	0.01	0.08	0.11	0.09	0.10	0.11	0.09
Fe_2O_3	1.09	1.29	1.68	1.50	2.06	1.98	1.65
FeO	12.54	11.81	7.95	9.85	7.76	6.92	9.86
MnO	0.21	0.23	0.18	0.23	0.20	0.16	0.26
MgO	23.94	24.09	27.73	25.57	26.97	27.75	25.38
CaO	0.06	0.05	0.20	0.18	0.26	0.27	0.16
Na_2O	0.00	0.01	0.04	0.00	0.01	0.02	0.00
K_2O	0.00	0.00	0.01	0.00	0.01	0.03	0.00
H_2O*	12.45	12.50	12.68	12.42	12.64	12.57	12.49
Total	102.00	102.10	101.90	100.70	101.63	100.67	101.28
Si	5.56	5.57	6.10	5.87	6.10	6.21	5.84
Al^{iv}	2.44	2.43	1.90	2.13	1.90	1.79	2.16
Al^{vi}	2.72	2.76	2.32	2.50	2.42	2.29	2.56
Ti	0.00	0.00	0.00	0.00	0.00	0.00	0.01
Cr	0.00	0.01	0.02	0.01	0.01	0.02	0.01
Fe^{3+}	0.16	0.19	0.24	0.22	0.29	0.28	0.24
Fe^{2+}	2.01	1.89	1.25	1.58	1.22	1.10	1.58
Mn	0.03	0.04	0.03	0.04	0.03	0.03	0.04
Mg	6.86	6.87	7.78	7.33	7.59	7.85	7.24
Ca	0.01	0.01	0.04	0.04	0.05	0.05	0.03
Na	0.00	0.01	0.03	0.00	0.01	0.02	0.00

K	0.00	0.00	0.01	0.00	0.00	0.01	0.00
*OH**	16.00	16.00	16.00	16.00	16.00	16.00	16.00
Total	35.80	35.77	35.71	35.72	35.63	35.65	35.70
Oxidized	yes	yes	yes	yes	yes	yes	yes
Fe/Fe+Mg	0.241	0.232	0.161	0.197	0.167	0.150	0.200

Sample #	*22-905-11-03-S2*	*22-905-11-03-S2*	*22-905-11-03-S3*	*22-905-11-03-S3*	*22-905-11-03-S3*	*22-905-11-03-S4*	*22-905-11-03-S4*
SiO_2	33.03	31.88	33.21	33.06	32.05	33.01	33.05
TiO_2	0.01	0.01	0.00	0.00	0.00	0.00	0.00
Al_2O_3	18.22	19.42	17.62	18.16	19.35	18.20	18.36
Cr_2O_3	0.10	0.11	0.11	0.13	0.07	0.09	0.08
Fe_2O_3	2.03	2.03	1.87	2.16	2.04	1.94	2.07
FeO	7.20	8.44	6.77	6.79	7.97	6.94	7.43
MnO	0.22	0.21	0.15	0.20	0.17	0.18	0.22
MgO	27.86	26.24	28.55	27.69	26.66	28.11	27.68
CaO	0.31	0.23	0.25	0.30	0.23	0.23	0.26
Na_2O	0.00	0.02	0.00	0.03	0.00	0.03	0.00
K_2O	0.00	0.00	0.03	0.02	0.03	0.04	0.01
H_2O*	12.68	12.54	12.66	12.64	12.57	12.67	12.69
Total	101.68	101.14	101.23	101.19	101.14	101.43	101.86
Si	6.22	6.06	6.26	6.24	6.08	6.22	6.21
Al^{iv}	1.78	1.94	1.74	1.76	1.92	1.78	1.79
Al^{vi}	2.28	2.44	2.20	2.30	2.43	2.28	2.30
Ti	0.00	0.00	0.00	0.00	0.00	0.00	0.00
Cr	0.02	0.02	0.02	0.02	0.01	0.01	0.01
Fe^{3+}	0.29	0.29	0.27	0.31	0.29	0.27	0.29
Fe^{2+}	1.13	1.34	1.07	1.07	1.26	1.09	1.17
Mn	0.03	0.03	0.02	0.03	0.03	0.03	0.03
Mg	7.82	7.44	8.02	7.79	7.54	7.89	7.76
Ca	0.06	0.05	0.05	0.06	0.05	0.05	0.05

Na	0.00	0.01	0.00	0.02	0.00	0.02	0.00
K	0.00	0.00	0.01	0.01	0.01	0.02	0.01
*OH**	16.00	16.00	16.00	16.00	16.00	16.00	16.00
Total	35.63	35.63	35.66	35.62	35.63	35.66	35.63
Oxidized	yes	yes	yes	yes	yes	yes	yes
Fe/Fe+Mg	0.154	0.180	0.142	0.150	0.171	0.148	0.159

Sample #	*22-905-11-03-S5*	*22-905-11-03-S5*	*22-905-11-03-S6*	*22-905-11-03-S6*	*22-905-11-03-S6*	*22-905-11-03-S6*	*22-905-11-03-S7*
SiO_2	32.91	32.96	31.38	28.93	32.88	33.27	32.29
TiO_2	0.01	0.01	0.03	0.02	0.00	0.01	0.00
Al_2O_3	18.80	18.62	19.78	22.22	18.29	18.99	18.63
Cr_2O_3	0.09	0.08	0.07	0.08	0.07	0.08	0.05
Fe_2O_3	2.23	2.04	2.08	1.22	1.84	2.68	2.00
FeO	6.80	6.61	9.93	11.39	6.88	6.56	8.15
MnO	0.24	0.18	0.22	0.21	0.19	0.24	0.21
MgO	27.52	28.09	24.88	24.17	28.20	27.00	26.66
CaO	0.30	0.28	0.29	0.12	0.31	0.39	0.32
Na_2O	0.02	0.02	0.00	0.00	0.04	0.00	0.02
K_2O	0.03	0.03	0.01	0.00	0.01	0.04	0.01
H_2O*	12.69	12.71	12.45	12.34	12.67	12.73	12.52
Total	101.63	101.64	101.13	100.69	101.39	101.98	100.86
Si	6.18	6.19	6.01	5.61	6.19	6.22	6.15
Al^{iv}	1.82	1.81	1.99	2.39	1.81	1.78	1.85
Al^{vi}	2.37	2.33	2.51	2.70	2.28	2.44	2.36
Ti	0.00	0.00	0.00	0.00	0.00	0.00	0.00
Cr	0.01	0.01	0.01	0.01	0.01	0.01	0.01
Fe^{3+}	0.31	0.29	0.30	0.18	0.26	0.38	0.29
Fe^{2+}	1.07	1.04	1.59	1.85	1.08	1.03	1.30

Mn	0.04	0.03	0.04	0.03	0.03	0.04	0.03
Mg	7.71	7.86	7.11	6.98	7.92	7.53	7.57
Ca	0.06	0.06	0.06	0.02	0.06	0.08	0.07
Na	0.01	0.01	0.00	0.00	0.03	0.00	0.01
K	0.01	0.02	0.00	0.00	0.00	0.02	0.00
*OH**	16.00	16.00	16.00	16.00	16.00	16.00	16.00
Total	35.61	35.64	35.62	35.78	35.68	35.52	35.64
Oxidized	yes	yes	yes	yes	yes	yes	yes
Fe/Fe+Mg	0.152	0.144	0.210	0.225	0.145	0.157	0.173

Sample #	*22-905-11-03-S7*	*22-905-11-03-S7*	*22-905-11-03-S8*	*22-905-11-03-S8*	*22-905-11-03-S10*	*22-905-11-03-S10*	*22-905-11-03-S10*
SiO_2	32.54	33.44	32.84	33.03	33.07	33.23	29.28
TiO_2	0.03	0.00	0.00	0.03	0.01	0.03	0.00
Al_2O_3	18.85	18.19	18.42	18.40	18.59	17.91	21.31
Cr_2O_3	0.04	0.07	0.06	0.07	0.08	0.08	0.06
Fe_2O_3	2.16	2.31	1.96	1.73	2.36	2.40	1.28
FeO	7.46	6.60	6.76	7.23	6.88	6.49	10.90
MnO	0.17	0.19	0.21	0.19	0.21	0.20	0.25
MgO	27.00	27.96	28.00	28.51	27.31	27.54	24.44
CaO	0.34	0.31	0.29	0.29	0.33	0.35	0.10
Na_2O	0.02	0.00	0.03	0.02	0.02	0.00	0.00
K_2O	0.00	0.01	0.01	0.02	0.01	0.00	0.00
H_2O*	12.60	12.73	12.65	12.77	12.67	12.60	12.26
Total	101.22	101.81	101.24	102.29	101.52	100.82	99.87
Si	6.16	6.27	6.19	6.18	6.22	6.29	5.71
Al^{iv}	1.84	1.73	1.81	1.82	1.78	1.71	2.29
Al^{vi}	2.39	2.31	2.31	2.25	2.37	2.31	2.62
Ti	0.00	0.00	0.00	0.00	0.00	0.00	0.00
Cr	0.01	0.01	0.01	0.01	0.01	0.01	0.01

Fe^{3+}	0.31	0.33	0.28	0.24	0.33	0.34	0.19
Fe^{2+}	1.18	1.03	1.07	1.13	1.08	1.03	1.78
Mn	0.03	0.03	0.03	0.03	0.03	0.03	0.04
Mg	7.62	7.81	7.87	7.95	7.66	7.77	7.10
Ca	0.07	0.06	0.06	0.06	0.07	0.07	0.02
Na	0.01	0.00	0.02	0.01	0.02	0.00	0.00
K	0.00	0.00	0.01	0.01	0.00	0.00	0.00
*OH**	16.00	16.00	16.00	16.00	16.00	16.00	16.00
Total	35.61	35.58	35.65	35.70	35.58	35.56	35.76
Oxidized	yes	yes	yes	yes	yes	yes	yes
Fe/Fe+Mg	0.163	0.148	0.146	0.147	0.156	0.150	0.217

Sample #	*22-905-11-03-S12*	*22-905-11-04-01*	*22-905-11-04-01*	*22-905-11-04-01*	*22-905-11-04-01*	*22-905-11-04-02*	*22-905-11-04-02*
SiO_2	31.66	33.14	32.83	32.68	32.25	30.91	31.57
TiO_2	0.00	0.03	0.00	0.00	0.01	0.01	0.00
Al_2O_3	20.15	18.65	18.55	18.67	19.04	18.54	17.41
Cr_2O_3	0.08	0.05	0.06	0.03	0.05	0.06	0.05
Fe_2O_3	1.98	2.39	1.88	1.83	1.62	1.85	1.51
FeO	8.66	6.76	6.78	7.28	7.51	7.10	6.88
MnO	0.26	0.19	0.17	0.17	0.18	0.21	0.19
MgO	26.07	27.53	28.34	27.94	28.06	26.35	27.50
CaO	0.26	0.28	0.25	0.30	0.23	0.20	0.25
Na_2O	0.02	0.00	0.00	0.03	0.00	0.00	0.04
K_2O	0.01	0.00	0.00	0.00	0.00	0.00	0.01
H_2O*	12.61	12.71	12.70	12.68	12.68	12.14	12.19
Total	101.75	101.73	101.57	101.60	101.63	97.37	97.60
Si	5.99	6.22	6.17	6.15	6.08	6.08	6.18
Al^{iv}	2.01	1.78	1.83	1.85	1.92	1.92	1.82
Al^{vi}	2.51	2.37	2.30	2.31	2.32	2.40	2.22

Ti	0.00	0.00	0.00	0.00	0.00	0.00	0.00
Cr	0.01	0.01	0.01	0.01	0.01	0.01	0.01
Fe^{3+}	0.28	0.34	0.27	0.26	0.23	0.27	0.22
Fe^{2+}	1.37	1.06	1.07	1.15	1.18	1.17	1.13
Mn	0.04	0.03	0.03	0.03	0.03	0.03	0.03
Mg	7.36	7.70	7.94	7.84	7.88	7.72	8.03
Ca	0.05	0.06	0.05	0.06	0.05	0.04	0.05
Na	0.02	0.00	0.00	0.02	0.00	0.00	0.03
K	0.00	0.00	0.00	0.00	0.00	0.00	0.01
*OH**	16.00	16.00	16.00	16.00	16.00	16.00	16.00
Total	35.65	35.57	35.66	35.68	35.70	35.65	35.72
Oxidized	yes	yes	yes	yes	yes	yes	yes
Fe/Fe+Mg	0.184	0.154	0.144	0.152	0.152	0.157	0.144

Sample #	*22-905-11-04-02*	*22-905-11-04-04*	*22-905-11-04-05*	*22-905-11-04-05*	*22-905-11-04-05*	*22-905-11-04-06*	*22-905-11-04-06*
SiO_2	30.58	32.88	31.36	32.10	32.13	32.73	32.44
TiO_2	0.04	0.02	0.01	0.00	0.00	0.00	0.06
Al_2O_3	16.75	18.32	18.25	17.71	17.95	18.30	17.73
Cr_2O_3	0.05	0.02	0.05	0.06	0.04	0.01	0.02
Fe_2O_3	1.92	2.26	2.27	2.32	1.96	2.02	1.80
FeO	5.83	7.32	7.12	6.21	6.65	7.16	7.36
MnO	0.17	0.17	0.19	0.18	0.22	0.21	0.13
MgO	26.14	27.09	25.70	26.71	27.35	27.57	27.62
CaO	0.24	0.38	0.29	0.27	0.30	0.29	0.28
Na_2O	0.01	0.00	0.00	0.02	0.00	0.00	0.03
K_2O	0.02	0.01	0.00	0.00	0.01	0.03	0.00
H_2O*	11.70	12.59	12.12	12.23	12.37	12.59	12.46
Total	93.44	101.07	97.38	97.81	98.98	100.89	99.94
Si	6.23	6.23	6.17	6.26	6.20	6.20	6.21
Al^{iv}	1.77	1.77	1.83	1.74	1.80	1.80	1.79

Al^{vi}	2.28	2.34	2.42	2.35	2.30	2.31	2.24
Ti	0.01	0.00	0.00	0.00	0.00	0.00	0.01
Cr	0.01	0.00	0.01	0.01	0.01	0.00	0.00
Fe^{3+}	0.30	0.32	0.34	0.34	0.28	0.29	0.26
Fe^{2+}	0.99	1.16	1.17	1.01	1.07	1.13	1.18
Mn	0.03	0.03	0.03	0.03	0.04	0.03	0.02
Mg	7.94	7.65	7.53	7.76	7.87	7.79	7.89
Ca	0.05	0.08	0.06	0.06	0.06	0.06	0.06
Na	0.01	0.00	0.00	0.01	0.00	0.00	0.02
K	0.01	0.01	0.00	0.00	0.00	0.02	0.00
*OH**	16.00	16.00	16.00	16.00	16.00	16.00	16.00
Total	35.63	35.59	35.57	35.57	35.64	35.64	35.68
Oxidized	yes	yes	yes	yes	yes	yes	yes
Fe/Fe+Mg	0.140	0.162	0.167	0.148	0.147	0.154	0.154

Sample #	*22-905-11-04-06*	*22-905-11-04-07*	*22-905-11-04-08*	*22-905-11-04-08*	*22-905-11-04-09*	*22-905-11-04-09*	*22-905-11-04-10*
SiO_2	28.64	32.95	32.56	33.06	33.17	32.87	32.78
TiO_2	0.00	0.01	0.01	0.00	0.03	0.02	0.03
Al_2O_3	22.19	18.85	18.76	18.79	18.69	18.29	18.61
Cr_2O_3	0.00	0.02	0.04	0.03	0.03	0.04	0.03
Fe_2O_3	0.99	2.13	1.94	2.78	2.29	2.11	2.06
FeO	11.69	7.33	7.57	6.61	6.68	6.93	7.41
MnO	0.22	0.20	0.20	0.19	0.16	0.17	0.18
MgO	24.23	27.50	27.46	26.53	27.76	27.67	27.48
CaO	0.06	0.35	0.25	0.41	0.30	0.28	0.30
Na_2O	0.00	0.02	0.02	0.01	0.01	0.02	0.02
K_2O	0.00	0.01	0.01	0.00	0.03	0.01	0.01
H_2O*	12.28	12.73	12.64	12.61	12.73	12.61	12.65

Total	100.30	102.11	101.44	101.02	101.89	101.01	101.54
Si	5.58	6.18	6.15	6.25	6.21	6.22	6.18
Al ^{iv}	2.42	1.82	1.85	1.75	1.79	1.78	1.82
Al ^{vi}	2.68	2.36	2.34	2.46	2.36	2.32	2.34
Ti	0.00	0.00	0.00	0.00	0.00	0.00	0.00
Cr	0.00	0.00	0.01	0.00	0.01	0.01	0.00
Fe^{3+}	0.15	0.30	0.28	0.40	0.32	0.30	0.29
Fe^{2+}	1.90	1.15	1.20	1.04	1.05	1.10	1.17
Mn	0.04	0.03	0.03	0.03	0.03	0.03	0.03
Mg	7.03	7.68	7.73	7.47	7.75	7.80	7.72
Ca	0.01	0.07	0.05	0.08	0.06	0.06	0.06
Na	0.00	0.02	0.02	0.01	0.01	0.01	0.01
K	0.00	0.01	0.00	0.00	0.01	0.00	0.00
*OH**	16.00	16.00	16.00	16.00	16.00	16.00	16.00
Total	35.82	35.62	35.65	35.50	35.59	35.62	35.63
Oxidized	yes	yes	yes	yes	yes	yes	yes
Fe/Fe+Mg	0.226	0.159	0.160	0.162	0.150	0.152	0.159

Sample #	*22-905-11-04-11*	*22-905-11-04-11*	*22-905-11-04-11*	*22-905-11-04-11*	*22-905-11-04-11*	*22-905-11-04-12*	*22-905-11-04-12*
SiO_2	33.22	33.56	33.69	33.10	32.58	33.25	33.31
TiO_2	0.00	0.02	0.03	0.00	0.00	0.00	0.00
Al_2O_3	18.10	18.28	18.08	18.47	19.31	18.23	17.95
Cr_2O_3	0.08	0.06	0.06	0.04	0.08	0.05	0.04
Fe_2O_3	2.12	2.37	2.31	2.42	2.35	2.37	2.16
FeO	7.13	6.97	6.56	6.76	7.13	6.34	6.37
MnO	0.20	0.18	0.17	0.15	0.22	0.18	0.20
MgO	27.87	27.68	28.23	27.37	26.84	27.83	28.16
CaO	0.27	0.31	0.26	0.30	0.35	0.27	0.30

Na_2O	0.01	0.04	0.01	0.00	0.01	0.00	0.03
K_2O	0.00	0.01	0.01	0.00	0.02	0.00	0.01
H_2O*	12.69	12.76	12.78	12.65	12.65	12.66	12.67
Total	101.69	102.22	102.18	101.27	101.54	101.18	101.19
Si	6.25	6.27	6.28	6.24	6.14	6.26	6.27
Al^{iv}	1.75	1.73	1.72	1.76	1.86	1.74	1.73
Al^{vi}	2.28	2.32	2.28	2.37	2.45	2.33	2.28
Ti	0.00	0.00	0.00	0.00	0.00	0.00	0.00
Cr	0.01	0.01	0.01	0.01	0.01	0.01	0.01
Fe^{3+}	0.30	0.33	0.32	0.34	0.33	0.34	0.31
Fe^{2+}	1.12	1.09	1.02	1.07	1.12	1.00	1.00
Mn	0.03	0.03	0.03	0.02	0.03	0.03	0.03
Mg	7.81	7.71	7.85	7.69	7.54	7.81	7.90
Ca	0.05	0.06	0.05	0.06	0.07	0.05	0.06
Na	0.01	0.03	0.01	0.00	0.01	0.00	0.02
K	0.00	0.00	0.00	0.00	0.01	0.00	0.00
*OH**	16.00	16.00	16.00	16.00	16.00	16.00	16.00
Total	35.62	35.58	35.59	35.56	35.58	35.57	35.62
Oxidized	yes	yes	yes	yes	yes	yes	yes
Fe/Fe+Mg	0.154	0.156	0.147	0.155	0.162	0.146	0.142

Sample #	*22-905-11-04-13*	*22-905-11-04-13*	*22-905-11-04-14*	*22-905-11-04-14*	*22-905-11-04-14*	*22-905-11-04-14*	*22-905-11-04-15*
SiO_2	33.38	32.74	33.29	33.02	33.19	30.15	33.43
TiO_2	0.01	0.03	0.00	0.01	0.03	0.00	0.01
Al_2O_3	18.32	18.95	17.73	18.01	18.40	20.85	18.35
Cr_2O_3	0.04	0.06	0.05	0.06	0.06	0.06	0.05
Fe_2O_3	2.65	2.27	2.27	2.03	2.35	1.42	2.45
FeO	6.20	7.14	6.61	6.81	7.03	10.90	6.57

MnO	0.24	0.20	0.18	0.20	0.20	0.21	0.20
MgO	27.26	27.25	27.80	28.03	27.35	24.94	27.69
CaO	0.39	0.23	0.27	0.23	0.25	0.09	0.25
Na_2O	0.00	0.01	0.02	0.01	0.04	0.00	0.01
K_2O	0.02	0.01	0.00	0.01	0.01	0.00	0.00
*H_2O**	12.65	12.66	12.60	12.63	12.67	12.41	12.72
Total	101.16	101.54	100.83	101.05	101.56	101.02	101.73
Si	6.29	6.17	6.30	6.24	6.24	5.81	6.27
Al^{iv}	1.71	1.83	1.70	1.76	1.76	2.19	1.73
Al^{vi}	2.38	2.40	2.28	2.27	2.35	2.56	2.35
Ti	0.00	0.00	0.00	0.00	0.00	0.00	0.00
Cr	0.01	0.01	0.01	0.01	0.01	0.01	0.01
Fe^{3+}	0.38	0.32	0.32	0.29	0.33	0.21	0.35
Fe^{2+}	0.98	1.12	1.05	1.08	1.11	1.76	1.03
Mn	0.04	0.03	0.03	0.03	0.03	0.03	0.03
Mg	7.65	7.65	7.84	7.89	7.67	7.16	7.74
Ca	0.08	0.05	0.05	0.05	0.05	0.02	0.05
Na	0.00	0.01	0.01	0.01	0.03	0.00	0.01
K	0.01	0.00	0.00	0.01	0.00	0.00	0.00
*OH**	16.00	16.00	16.00	16.00	16.00	16.00	16.00
Total	35.52	35.59	35.59	35.63	35.58	35.74	35.56
Oxidized	yes	yes	yes	yes	yes	yes	yes
Fe/Fe+Mg	0.150	0.159	0.149	0.147	0.158	0.215	0.151

Sample #	*22-905-11-04-15*	*22-905-11-04-15*	*21-700-13-01-S1*	*21-700-13-01-S2*	*21-700-13-01-S2*	*21-700-13-01-S3*	*21-700-13-01-S3*
SiO_2	29.55	32.90	30.22	33.75	28.90	33.74	33.60
TiO_2	0.00	0.03	0.00	0.02	0.01	0.02	0.00
Al_2O_3	22.03	18.65	20.35	18.60	19.74	17.15	17.11

Cr_2O_3	0.06	0.04	0.05	0.07	0.06	0.12	0.08
Fe_2O_3	1.19	2.36	1.26	3.02	0.91	1.75	1.59
FeO	11.01	6.59	12.15	7.08	12.10	7.56	7.44
MnO	0.23	0.21	0.22	0.12	0.17	0.10	0.07
MgO	25.02	27.29	24.56	26.45	23.97	28.93	29.18
CaO	0.07	0.33	0.09	0.33	0.09	0.20	0.19
Na_2O	0.00	0.03	0.01	0.00	0.00	0.00	0.02
K_2O	0.00	0.01	0.00	0.04	0.00	0.01	0.00
H_2O*	12.49	12.63	12.38	12.73	11.96	12.77	12.74
Total	101.64	101.06	101.28	102.20	97.91	102.34	102.03
Si	5.66	6.21	5.84	6.31	5.78	6.31	6.30
Al^{iv}	2.34	1.79	2.16	1.69	2.22	1.69	1.70
Al^{vi}	2.64	2.39	2.49	2.44	2.45	2.11	2.09
Ti	0.00	0.00	0.00	0.00	0.00	0.00	0.00
Cr	0.01	0.01	0.01	0.01	0.01	0.02	0.01
Fe^{3+}	0.17	0.33	0.18	0.42	0.14	0.25	0.22
Fe^{2+}	1.76	1.04	1.96	1.11	2.02	1.18	1.17
Mn	0.04	0.03	0.04	0.02	0.03	0.02	0.01
Mg	7.14	7.68	7.07	7.37	7.15	8.07	8.15
Ca	0.01	0.07	0.02	0.07	0.02	0.04	0.04
Na	0.00	0.02	0.01	0.00	0.00	0.00	0.01
K	0.00	0.01	0.00	0.02	0.00	0.00	0.00
*OH**	16.00	16.00	16.00	16.00	16.00	16.00	16.00
Total	35.78	35.58	35.77	35.46	35.82	35.68	35.72
Oxidized	yes	yes	yes	yes	yes	yes	yes
Fe/Fe+Mg	0.213	0.152	0.233	0.172	0.232	0.150	0.146

Sample #	*21-700-13-01-S3*	*21-700-13-01-S4*	*21-700-13-01-S4*	*21-700-13-01-S5*	*21-700-13-01-S5*	*21-700-13-01-S5*	*21-700-13-01-S6*

SiO_2	33.84	30.61	30.24	33.43	28.88	29.96	34.41
TiO_2	0.01	0.00	0.00	0.03	0.00	0.01	0.00
Al_2O_3	16.82	20.41	20.78	17.46	22.77	21.19	16.82
Cr_2O_3	0.14	0.08	0.11	0.08	0.02	0.04	0.08
Fe_2O_3	1.91	1.09	1.88	1.73	0.89	1.21	2.01
FeO	7.06	11.52	10.78	7.52	14.39	11.69	6.63
MnO	0.06	0.19	0.21	0.09	0.20	0.22	0.08
MgO	28.87	25.73	24.05	28.73	23.35	24.86	29.46
CaO	0.22	0.07	0.06	0.21	0.02	0.08	0.23
Na_2O	0.00	0.01	0.00	0.00	0.00	0.00	0.00
K_2O	0.01	0.00	0.00	0.02	0.00	0.00	0.01
H_2O*	12.70	12.55	12.33	12.73	12.49	12.46	12.84
Total	101.64	102.26	100.45	102.02	103.01	101.71	102.56
Si	6.36	5.84	5.86	6.27	5.54	5.75	6.39
Al^{iv}	1.64	2.16	2.14	1.73	2.46	2.25	1.61
Al^{vi}	2.10	2.44	2.62	2.15	2.69	2.56	2.10
Ti	0.00	0.00	0.00	0.00	0.00	0.00	0.00
Cr	0.02	0.01	0.02	0.01	0.00	0.01	0.01
Fe^{3+}	0.27	0.16	0.27	0.24	0.13	0.18	0.28
Fe^{2+}	1.11	1.84	1.75	1.18	2.31	1.88	1.03
Mn	0.01	0.03	0.03	0.01	0.03	0.04	0.01
Mg	8.09	7.31	6.94	8.03	6.67	7.11	8.16
Ca	0.04	0.01	0.01	0.04	0.00	0.02	0.04
Na	0.00	0.01	0.00	0.00	0.00	0.00	0.00
K	0.01	0.00	0.00	0.01	0.00	0.00	0.00
*OH**	16.00	16.00	16.00	16.00	16.00	16.00	16.00
Total	35.65	35.80	35.65	35.69	35.84	35.78	35.64
Oxidized	yes	yes	yes	yes	yes	yes	yes
Fe/Fe+Mg	0.146	0.214	0.225	0.150	0.267	0.224	0.138

Sample #	*21-700-13-01-S6*	*21-700-13-01-S6*	*21-700-13-01-S7*	*21-700-13-01-S8*	*21-700-13-01-S8*	*21-700-13-01-S9*	*21-700-13-01-S9*
SiO_2	30.47	32.99	28.51	33.89	29.86	31.06	30.88
TiO_2	0.01	0.00	0.04	0.00	0.02	0.02	0.00
Al_2O_3	20.28	16.76	21.46	17.05	20.67	21.85	22.00
Cr_2O_3	0.07	0.08	0.06	0.14	0.08	0.06	0.06
Fe_2O_3	1.46	1.95	1.03	1.78	0.44	1.66	1.32
FeO	10.43	7.26	14.05	7.37	13.20	10.48	11.05
MnO	0.22	0.11	0.20	0.07	0.16	0.18	0.20
MgO	25.30	27.79	22.61	29.00	25.59	25.81	26.10
CaO	0.10	0.22	0.03	0.29	0.09	0.03	0.03
Na_2O	0.00	0.00	0.00	0.02	0.00	0.00	0.00
K_2O	0.00	0.01	0.00	0.00	0.00	0.00	0.00
H_2O*	12.40	12.42	12.12	12.78	12.52	12.81	12.86
Total	100.73	99.60	100.11	102.40	102.64	103.97	104.50
Si	5.87	6.34	5.62	6.33	5.71	5.79	5.74
Al^{iv}	2.13	1.66	2.38	1.67	2.29	2.21	2.26
Al^{vi}	2.50	2.15	2.63	2.10	2.38	2.61	2.58
Ti	0.00	0.00	0.01	0.00	0.00	0.00	0.00
Cr	0.01	0.01	0.01	0.02	0.01	0.01	0.01
Fe^{3+}	0.21	0.28	0.15	0.25	0.06	0.23	0.18
Fe^{2+}	1.68	1.17	2.32	1.15	2.11	1.63	1.72
Mn	0.04	0.02	0.03	0.01	0.03	0.03	0.03
Mg	7.27	7.96	6.65	8.07	7.30	7.18	7.24
Ca	0.02	0.04	0.01	0.06	0.02	0.01	0.01
Na	0.00	0.00	0.00	0.02	0.00	0.00	0.00
K	0.00	0.01	0.00	0.00	0.00	0.00	0.00
*OH**	16.00	16.00	16.00	16.00	16.00	16.00	16.00
Total	35.73	35.64	35.81	35.68	35.92	35.70	35.77
Oxidized	yes	yes	yes	yes	yes	yes	yes

Fe/Fe+Mg	0.207	0.154	0.271	0.148	0.230	0.207	0.208

Sample #	*21-700-13-01-S10*	*21-700-13-01-S10*	*21-700-13-01-S11*	*21-700-13-01-S11*	*21-700-13-02-S3*	*21-700-13-02-S5*	*21-700-13-02-S6*
SiO_2	30.61	31.04	34.02	34.09	30.10	33.82	34.01
TiO_2	0.01	0.00	0.00	0.03	0.01	0.01	0.01
Al_2O_3	21.73	21.84	17.19	17.22	21.27	16.85	16.95
Cr_2O_3	0.03	0.04	0.10	0.13	0.16	0.08	0.10
Fe_2O_3	1.75	1.94	1.61	1.78	1.37	1.77	1.78
FeO	11.71	11.30	7.57	7.31	11.41	6.98	6.81
MnO	0.20	0.15	0.05	0.08	0.19	0.09	0.08
MgO	24.37	24.67	29.52	29.37	24.78	29.22	29.38
CaO	0.10	0.08	0.18	0.22	0.13	0.24	0.25
Na_2O	0.00	0.00	0.02	0.00	0.01	0.00	0.04
K_2O	0.00	0.00	0.00	0.01	0.00	0.00	0.01
H_2O*	12.63	12.73	12.88	12.88	12.49	12.73	12.79
Total	103.14	103.78	103.15	103.15	101.93	101.79	102.21
Si	5.79	5.82	6.31	6.32	5.76	6.34	6.35
Al^{iv}	2.21	2.18	1.69	1.68	2.24	1.66	1.65
Al^{vi}	2.65	2.67	2.08	2.10	2.57	2.09	2.09
Ti	0.00	0.00	0.00	0.00	0.00	0.00	0.00
Cr	0.00	0.01	0.02	0.02	0.02	0.01	0.01
Fe^{3+}	0.25	0.27	0.22	0.25	0.20	0.25	0.25
Fe^{2+}	1.85	1.77	1.17	1.13	1.83	1.10	1.06
Mn	0.03	0.02	0.01	0.01	0.03	0.01	0.01
Mg	6.87	6.89	8.16	8.12	7.07	8.17	8.17
Ca	0.02	0.02	0.04	0.04	0.03	0.05	0.05
Na	0.00	0.00	0.02	0.00	0.01	0.00	0.03
K	0.00	0.00	0.00	0.00	0.00	0.00	0.00
*OH**	16.00	16.00	16.00	16.00	16.00	16.00	16.00

Total	35.68	35.65	35.72	35.68	35.75	35.68	35.69
Oxidized	yes	yes	yes	yes	yes	yes	yes
Fe/Fe+Mg	0.234	0.229	0.146	0.146	0.222	0.141	0.138

Sample #	*21-700-13-02-S7*	*21-700-13-02-S8*	*21-700-13-02-S9*	*21-700-13-02-S10*	*21-700-13-02-S12*	*21-700-13-03-S5*	*21-700-13-03-S6*
SiO_2	29.31	33.55	30.24	33.87	30.03	28.41	27.89
TiO_2	0.03	0.12	0.00	0.00	0.01	0.01	0.02
Al_2O_3	22.07	17.36	20.61	16.78	21.70	22.66	23.53
Cr_2O_3	0.06	0.11	0.06	0.10	0.14	0.03	0.02
Fe_2O_3	1.13	1.94	1.28	1.86	1.48	0.99	0.94
FeO	12.68	7.29	11.36	6.94	11.39	13.03	13.78
MnO	0.21	0.05	0.20	0.07	0.19	0.24	0.21
MgO	24.01	28.52	25.05	29.07	24.64	23.29	22.69
CaO	0.10	0.33	0.08	0.25	0.04	0.12	0.09
Na_2O	0.00	0.00	0.00	0.00	0.00	0.00	0.00
K_2O	0.00	0.00	0.00	0.00	0.00	0.00	0.00
H_2O*	12.45	12.73	12.42	12.71	12.52	12.31	12.31
Total	102.04	102.02	101.29	101.66	102.14	101.10	101.48
Si	5.63	6.29	5.82	6.36	5.73	5.52	5.42
Al^{iv}	2.37	1.71	2.18	1.64	2.27	2.48	2.58
Al^{vi}	2.65	2.15	2.51	2.09	2.63	2.73	2.82
Ti	0.00	0.02	0.00	0.00	0.00	0.00	0.00
Cr	0.01	0.02	0.01	0.01	0.02	0.00	0.00
Fe^{3+}	0.16	0.27	0.19	0.26	0.21	0.15	0.14
Fe^{2+}	2.04	1.14	1.83	1.09	1.82	2.12	2.24
Mn	0.03	0.01	0.03	0.01	0.03	0.04	0.03
Mg	6.88	7.97	7.19	8.14	7.01	6.75	6.57
Ca	0.02	0.07	0.02	0.05	0.01	0.03	0.02
Na	0.00	0.00	0.00	0.00	0.00	0.00	0.00

K	0.00	0.00	0.00	0.00	0.00	0.00	0.00
*OH**	16.00	16.00	16.00	16.00	16.00	16.00	16.00
Total	35.79	35.65	35.76	35.66	35.73	35.82	35.83
Oxidized	yes	yes	yes	yes	yes	yes	yes
Fe/Fe+Mg	0.243	0.151	0.219	0.143	0.225	0.251	0.266

Sample #	*21-700-13-03-S7*	*21-700-13-03-S8*	*21-700-13-03-S8*	*21-700-13-03-S9*	*21-700-13-03-S11*	*21-700-13-03-S12*	*21-700-13-03-S14*
SiO_2	28.80	28.39	28.51	30.54	30.89	29.72	28.62
TiO_2	0.01	0.03	0.04	0.00	0.03	0.01	0.04
Al_2O_3	22.60	23.16	23.17	20.41	20.71	20.83	22.87
Cr_2O_3	0.04	0.02	0.01	0.05	0.06	0.08	0.00
Fe_2O_3	1.42	1.08	1.14	1.30	1.39	1.28	1.38
FeO	12.40	13.78	13.70	10.81	11.11	11.53	13.08
MnO	0.23	0.19	0.19	0.27	0.25	0.20	0.21
MgO	23.06	22.83	22.87	25.49	25.60	24.47	22.67
CaO	0.12	0.07	0.06	0.13	0.10	0.10	0.10
Na_2O	0.00	0.00	0.00	0.00	0.00	0.00	0.00
K_2O	0.00	0.00	0.00	0.00	0.00	0.00	0.00
H_2O*	12.31	12.37	12.39	12.47	12.62	12.31	12.32
Total	100.98	101.91	102.08	101.49	102.75	100.53	101.29
Si	5.59	5.49	5.50	5.85	5.85	5.77	5.55
Al^{iv}	2.41	2.51	2.50	2.15	2.15	2.23	2.45
Al^{vi}	2.78	2.78	2.79	2.48	2.49	2.55	2.80
Ti	0.00	0.00	0.01	0.00	0.00	0.00	0.01
Cr	0.01	0.00	0.00	0.01	0.01	0.01	0.00
Fe^{3+}	0.21	0.16	0.17	0.19	0.20	0.19	0.20
Fe^{2+}	2.01	2.23	2.21	1.73	1.76	1.87	2.12
Mn	0.04	0.03	0.03	0.04	0.04	0.03	0.04
Mg	6.67	6.58	6.58	7.28	7.23	7.08	6.56

Ca	0.03	0.01	0.01	0.03	0.02	0.02	0.02
Na	0.00	0.00	0.00	0.00	0.00	0.00	0.00
K	0.00	0.00	0.00	0.00	0.00	0.00	0.00
*OH**	16.00	16.00	16.00	16.00	16.00	16.00	16.00
Total	35.74	35.80	35.79	35.76	35.75	35.76	35.74
Oxidized	yes	yes	yes	yes	yes	yes	yes
Fe/Fe+Mg	0.250	0.266	0.265	0.209	0.213	0.225	0.262

Sample #	*21-700-13-03-S15*	*21-700-13-03-S16*	*21-700-13-03-S17*	*21-700-13-03-S18*	*21-700-18-01-S2*	*21-700-18-01-S4*	*21-700-18-01-S6*
SiO_2	28.72	28.86	28.70	28.85	28.75	28.03	28.47
TiO_2	0.02	0.01	0.05	0.00	0.10	0.08	0.11
Al_2O_3	22.95	22.98	21.69	21.75	21.90	22.57	22.49
Cr_2O_3	0.04	0.04	0.04	0.05	0.40	0.25	0.27
Fe_2O_3	1.30	1.22	1.27	1.23	1.27	0.59	0.91
FeO	12.46	12.83	13.71	12.95	12.93	14.34	13.68
MnO	0.22	0.22	0.19	0.19	0.11	0.12	0.17
MgO	23.15	23.39	22.50	23.15	22.91	23.25	23.26
CaO	0.15	0.13	0.03	0.04	0.21	0.03	0.02
Na_2O	0.04	0.00	0.00	0.00	0.04	0.00	0.00
K_2O	0.00	0.00	0.00	0.00	0.02	0.01	0.04
H_2O*	12.37	12.44	12.17	12.22	12.26	12.30	12.35
Total	101.44	102.13	100.34	100.43	100.89	101.58	101.77
Si	5.55	5.54	5.64	5.64	5.60	5.46	5.51
Al^{iv}	2.45	2.46	2.36	2.36	2.40	2.54	2.49
Al^{vi}	2.79	2.77	2.68	2.67	2.65	2.64	2.66
Ti	0.00	0.00	0.01	0.00	0.02	0.01	0.02
Cr	0.01	0.01	0.01	0.01	0.06	0.04	0.04
Fe^{3+}	0.19	0.18	0.19	0.18	0.19	0.09	0.13
Fe^{2+}	2.01	2.06	2.25	2.12	2.11	2.34	2.22

Mn	0.04	0.04	0.03	0.03	0.02	0.02	0.03
Mg	6.67	6.70	6.59	6.75	6.66	6.75	6.72
Ca	0.03	0.03	0.01	0.01	0.04	0.01	0.00
Na	0.03	0.00	0.00	0.00	0.03	0.00	0.00
K	0.00	0.00	0.00	0.00	0.01	0.01	0.02
*OH**	16.00	16.00	16.00	16.00	16.00	16.00	16.00
Total	35.77	35.78	35.76	35.77	35.78	35.89	35.84
Oxidized	yes	yes	yes	yes	yes	yes	yes
Fe/Fe+Mg	0.248	0.250	0.270	0.254	0.256	0.264	0.259

Sample #	*21-700-18-01-S11*	*21-700-18-01-S15*	*21-700-18-01-S16*	*21-700-18-01-S17*	*21-700-18-01-S18*	*21-700-18-01-S19*	*21-700-18-01-S19*
SiO_2	27.80	27.94	28.28	27.84	28.25	28.23	28.31
TiO_2	0.09	0.10	0.05	0.07	0.09	0.07	0.07
Al_2O_3	22.50	22.36	22.30	22.82	22.65	22.08	22.13
Cr_2O_3	0.19	0.02	0.02	0.01	0.01	0.02	0.02
Fe_2O_3	0.55	0.58	0.61	0.50	0.70	0.42	0.69
FeO	14.08	14.15	14.12	14.88	14.47	14.74	13.89
MnO	0.14	0.12	0.16	0.15	0.12	0.13	0.15
MgO	23.25	23.26	23.45	22.95	23.15	23.48	23.48
CaO	0.06	0.02	0.02	0.00	0.02	0.01	0.00
Na_2O	0.00	0.01	0.00	0.00	0.00	0.00	0.00
K_2O	0.01	0.00	0.03	0.03	0.02	0.02	0.00
H_2O*	12.23	12.22	12.29	12.28	12.33	12.28	12.26
Total	100.90	100.76	101.32	101.54	101.81	101.48	100.98
Si	5.44	5.48	5.51	5.43	5.48	5.51	5.53
Al^{iv}	2.56	2.52	2.49	2.57	2.52	2.49	2.47
Al^{vi}	2.65	2.65	2.64	2.69	2.68	2.59	2.63
Ti	0.01	0.01	0.01	0.01	0.01	0.01	0.01
Cr	0.03	0.00	0.00	0.00	0.00	0.00	0.00

Fe^{3+}	0.08	0.08	0.09	0.07	0.10	0.06	0.10
Fe^{2+}	2.31	2.32	2.30	2.43	2.35	2.40	2.27
Mn	0.02	0.02	0.03	0.03	0.02	0.02	0.02
Mg	6.79	6.80	6.81	6.67	6.70	6.83	6.83
Ca	0.01	0.00	0.00	0.00	0.00	0.00	0.00
Na	0.00	0.00	0.00	0.00	0.00	0.00	0.00
K	0.00	0.00	0.01	0.01	0.01	0.01	0.00
*OH**	16.00	16.00	16.00	16.00	16.00	16.00	16.00
Total	35.90	35.89	35.89	35.91	35.87	35.92	35.87
Oxidized	yes	yes	yes	yes	yes	yes	yes
Fe/Fe+Mg	0.260	0.261	0.260	0.272	0.268	0.265	0.257

Sample #	*21-700-18-02-S1*	*21-700-18-02-S4*	*21-700-18-02-S5*	*21-700-18-02-S6*	*21-700-18-02-S7*	*21-700-18-02-S8*	*21-700-18-02-S9*
SiO_2	28.61	28.36	27.60	27.67	28.02	28.04	28.03
TiO_2	0.06	0.46	0.09	0.03	0.07	0.06	0.05
Al_2O_3	21.51	22.17	23.04	23.48	22.39	22.53	22.43
Cr_2O_3	0.06	0.09	0.03	0.00	0.02	0.01	0.14
Fe_2O_3	0.61	0.88	0.55	0.48	0.52	0.38	0.76
FeO	13.77	14.22	14.43	14.39	14.30	14.32	13.55
MnO	0.12	0.14	0.13	0.15	0.10	0.13	0.12
MgO	23.82	22.90	22.81	23.26	23.35	23.75	23.20
CaO	0.04	0.33	0.01	0.01	0.01	0.01	0.03
Na_2O	0.00	0.00	0.00	0.00	0.00	0.00	0.00
K_2O	0.04	0.04	0.09	0.00	0.03	0.00	0.04
H_2O*	12.25	12.33	12.23	12.34	12.25	12.32	12.22
Total	100.88	101.93	101.00	101.81	101.08	101.54	100.56
Si	5.59	5.50	5.40	5.37	5.48	5.45	5.49
Al^{iv}	2.41	2.50	2.60	2.63	2.52	2.55	2.51
Al^{vi}	2.55	2.59	2.73	2.75	2.64	2.63	2.68
Ti	0.01	0.07	0.01	0.00	0.01	0.01	0.01

Cr	0.01	0.01	0.00	0.00	0.00	0.00	0.02
Fe^{3+}	0.09	0.13	0.08	0.07	0.08	0.06	0.11
Fe^{2+}	2.25	2.31	2.36	2.34	2.34	2.33	2.22
Mn	0.02	0.02	0.02	0.02	0.02	0.02	0.02
Mg	6.94	6.63	6.66	6.73	6.80	6.89	6.78
Ca	0.01	0.07	0.00	0.00	0.00	0.00	0.01
Na	0.00	0.00	0.00	0.00	0.00	0.00	0.00
K	0.02	0.02	0.04	0.00	0.01	0.00	0.02
*OH**	16.00	16.00	16.00	16.00	16.00	16.00	16.00
Total	35.89	35.84	35.91	35.91	35.91	35.93	35.86
Oxidized	yes	yes	yes	yes	yes	yes	yes
Fe/Fe+Mg	0.252	0.269	0.268	0.263	0.262	0.257	0.256

Sample #	*21-700-18-02-S10*	*21-700-18-02-S11*	*21-700-18-02-S14*	*21-700-18-02-S15*	*21-700-18-02-S16*	*21-700-18-02-S17*	*21-700-18-02-S18*
SiO_2	27.95	28.06	28.67	28.19	28.10	28.02	27.96
TiO_2	0.07	0.09	0.12	0.07	0.09	0.06	0.05
Al_2O_3	22.62	22.50	21.96	22.26	22.38	22.53	22.64
Cr_2O_3	0.03	0.08	0.09	0.05	0.05	0.01	0.01
Fe_2O_3	0.75	0.54	0.73	0.75	0.52	0.27	0.48
FeO	13.74	14.13	14.01	13.90	14.26	14.74	14.33
MnO	0.13	0.13	0.13	0.09	0.14	0.16	0.11
MgO	23.10	23.47	23.36	23.21	23.52	23.72	23.39
CaO	0.01	0.02	0.01	0.06	0.01	0.00	0.02
Na_2O	0.00	0.00	0.00	0.00	0.00	0.00	0.00
K_2O	0.03	0.03	0.17	0.01	0.00	0.00	0.03
*H_2O**	12.22	12.29	12.32	12.24	12.29	12.34	12.28
Total	100.64	101.34	101.57	100.83	101.37	101.84	101.31
Si	5.47	5.47	5.57	5.51	5.48	5.45	5.45
Al^{iv}	2.53	2.53	2.43	2.49	2.52	2.55	2.55

Al^{vi}	2.71	2.64	2.61	2.66	2.62	2.61	2.66
Ti	0.01	0.01	0.02	0.01	0.01	0.01	0.01
Cr	0.01	0.01	0.01	0.01	0.01	0.00	0.00
Fe^{3+}	0.11	0.08	0.11	0.11	0.08	0.04	0.07
Fe^{2+}	2.25	2.30	2.28	2.27	2.32	2.39	2.34
Mn	0.02	0.02	0.02	0.01	0.02	0.03	0.02
Mg	6.75	6.82	6.76	6.77	6.83	6.87	6.80
Ca	0.00	0.00	0.00	0.01	0.00	0.00	0.00
Na	0.00	0.00	0.00	0.00	0.00	0.00	0.00
K	0.01	0.01	0.08	0.01	0.00	0.00	0.01
*OH**	16.00	16.00	16.00	16.00	16.00	16.00	16.00
Total	35.87	35.90	35.89	35.86	35.90	35.95	35.92
Oxidized	yes	yes	yes	yes	yes	yes	yes
Fe/Fe+Mg	0.259	0.259	0.261	0.261	0.260	0.262	0.262

Sample #	*21-700-18-03-S1*	*21-700-18-03-S1*	*21-700-18-03-S2*	*21-700-18-03-S3*	*21-700-18-03-S5*	*21-700-18-03-S6*	*21-700-18-03-S10*
SiO_2	27.97	28.25	27.94	28.03	27.77	27.83	27.78
TiO_2	0.07	0.09	0.08	0.08	0.03	0.08	0.11
Al_2O_3	22.27	22.09	22.70	22.62	22.62	22.44	22.77
Cr_2O_3	0.02	0.05	0.03	0.03	0.00	0.13	0.04
Fe_2O_3	0.37	0.41	0.55	0.64	0.52	0.39	0.42
FeO	14.50	14.28	14.25	13.83	14.16	14.44	14.82
MnO	0.13	0.16	0.13	0.11	0.16	0.18	0.14
MgO	23.50	23.73	23.34	23.37	23.23	23.40	23.01
CaO	0.01	0.03	0.02	0.03	0.01	0.04	0.02
Na_2O	0.00	0.00	0.00	0.00	0.00	0.00	0.00
K_2O	0.02	0.05	0.00	0.04	0.00	0.00	0.09
H_2O*	12.25	12.30	12.29	12.27	12.21	12.26	12.27
Total	101.11	101.43	101.34	101.05	100.71	101.19	101.48

Si	5.47	5.50	5.45	5.47	5.45	5.44	5.42
Al ^{iv}	2.53	2.50	2.55	2.53	2.55	2.56	2.58
Al ^{vi}	2.61	2.58	2.67	2.68	2.68	2.62	2.67
Ti	0.01	0.01	0.01	0.01	0.00	0.01	0.02
Cr	0.00	0.01	0.01	0.00	0.00	0.02	0.01
Fe^{3+}	0.05	0.06	0.08	0.09	0.08	0.06	0.06
Fe^{2+}	2.37	2.33	2.32	2.26	2.32	2.36	2.42
Mn	0.02	0.03	0.02	0.02	0.03	0.03	0.02
Mg	6.85	6.89	6.78	6.80	6.79	6.82	6.69
Ca	0.00	0.01	0.00	0.01	0.00	0.01	0.00
Na	0.00	0.00	0.00	0.00	0.00	0.00	0.00
K	0.01	0.02	0.00	0.02	0.00	0.00	0.05
*OH**	16.00	16.00	16.00	16.00	16.00	16.00	16.00
Total	35.94	35.93	35.90	35.89	35.90	35.93	35.94
Oxidized	yes	yes	yes	yes	yes	yes	yes
Fe/Fe+Mg	0.262	0.257	0.262	0.257	0.261	0.262	0.270

Sample #	*21-700-18-03-S13*	*21-700-18-03-S15*	*21-700-18-03-S17*	*21-700-18-03-S17*	*22-750-28-02-G1*	*22-750-28-02-G1*	*22-750-28-02-G1*
SiO_2	28.25	28.27	28.06	28.18	27.65	27.69	27.62
TiO_2	0.07	0.08	0.09	0.08	0.02	0.05	0.03
Al_2O_3	22.36	22.26	22.47	22.62	23.02	22.96	22.74
Cr_2O_3	0.12	0.08	0.06	0.06	0.14	0.09	0.16
Fe_2O_3	0.60	0.56	0.51	0.42	0.57	0.60	0.76
FeO	14.08	14.23	14.01	14.52	11.95	12.33	11.86
MnO	0.13	0.10	0.13	0.17	0.25	0.19	0.23
MgO	23.31	23.34	23.46	23.49	24.19	24.04	23.73
CaO	0.04	0.03	0.01	0.01	0.13	0.09	0.10
Na_2O	0.00	0.00	0.00	0.00	0.00	0.00	0.01
K_2O	0.12	0.12	0.10	0.10	0.00	0.00	0.00

H_2O*	12.29	12.29	12.28	12.36	12.25	12.25	12.15
Total	101.38	101.37	101.17	102.01	100.17	100.28	99.39
Si	5.50	5.51	5.47	5.46	5.40	5.41	5.44
Al^{iv}	2.50	2.49	2.53	2.54	2.60	2.59	2.56
Al^{vi}	2.64	2.63	2.65	2.64	2.72	2.71	2.73
Ti	0.01	0.01	0.01	0.01	0.00	0.01	0.00
Cr	0.02	0.01	0.01	0.01	0.02	0.01	0.02
Fe^{3+}	0.09	0.08	0.08	0.06	0.08	0.09	0.11
Fe^{2+}	2.29	2.32	2.29	2.35	1.95	2.02	1.95
Mn	0.02	0.02	0.02	0.03	0.04	0.03	0.04
Mg	6.77	6.78	6.82	6.79	7.05	7.01	6.97
Ca	0.01	0.01	0.00	0.00	0.03	0.02	0.02
Na	0.00	0.00	0.00	0.00	0.00	0.00	0.01
K	0.06	0.06	0.05	0.05	0.00	0.00	0.00
*OH**	16.00	16.00	16.00	16.00	16.00	16.00	16.00
Total	35.91	35.92	35.92	35.94	35.89	35.88	35.86
Oxidized	yes	yes	yes	yes	yes	yes	yes
Fe/Fe+Mg	0.260	0.262	0.257	0.263	0.224	0.231	0.229

Sample #	*22-750-28-02-G1*	*22-750-28-02-G1*	*22-750-28-02-G1*	*22-750-28-02-G2*	*22-750-28-02-G2*	*22-750-28-02-G2*	*22-750-28-02-G2*
SiO_2	27.65	27.75	28.47	28.05	28.08	28.16	27.71
TiO_2	0.04	0.04	0.04	0.03	0.05	0.00	0.00
Al_2O_3	23.14	23.10	22.94	21.88	22.40	22.88	22.03
Cr_2O_3	0.11	0.10	0.17	0.00	0.01	0.00	0.00
Fe_2O_3	0.49	0.71	1.27	0.52	0.61	0.62	0.64
FeO	12.48	12.20	11.30	11.94	11.97	12.24	11.77
MnO	0.21	0.21	0.18	0.19	0.21	0.19	0.22
MgO	24.03	23.78	22.63	24.52	24.54	24.46	23.97
CaO	0.17	0.29	1.86	0.06	0.04	0.02	0.05
Na_2O	0.01	0.01	0.00	0.02	0.00	0.00	0.02

K_2O	0.00	0.00	0.00	0.00	0.00	0.00	0.00
H_2O*	12.28	12.27	12.34	12.16	12.26	12.34	12.05
Total	100.62	100.43	101.18	99.36	100.14	100.89	98.45
Si	5.39	5.42	5.52	5.52	5.49	5.46	5.51
Al^{iv}	2.61	2.58	2.48	2.48	2.51	2.54	2.49
Al^{vi}	2.72	2.74	2.77	2.61	2.65	2.70	2.67
Ti	0.01	0.01	0.01	0.00	0.01	0.00	0.00
Cr	0.02	0.02	0.03	0.00	0.00	0.00	0.00
Fe^{3+}	0.07	0.10	0.18	0.08	0.09	0.09	0.10
Fe^{2+}	2.04	1.99	1.83	1.97	1.96	1.99	1.96
Mn	0.03	0.04	0.03	0.03	0.03	0.03	0.04
Mg	6.99	6.92	6.54	7.20	7.15	7.07	7.10
Ca	0.04	0.06	0.39	0.01	0.01	0.00	0.01
Na	0.01	0.00	0.00	0.01	0.00	0.00	0.01
K	0.00	0.00	0.00	0.00	0.00	0.00	0.00
*OH**	16.00	16.00	16.00	16.00	16.00	16.00	16.00
Total	35.91	35.87	35.76	35.90	35.88	35.88	35.88
Oxidized	yes	yes	yes	yes	yes	yes	yes
Fe/Fe+Mg	0.232	0.232	0.236	0.221	0.222	0.227	0.224

Sample #	*22-750-28-02-G3*	*22-750-28-02-G3*	*22-750-28-02-G3*	*22-750-28-02-G3*	*22-750-28-02-G3*	*22-750-28-02-G4*	*22-750-28-02-G4*
SiO_2	28.50	28.69	29.26	29.39	28.84	28.54	29.76
TiO_2	0.03	0.03	0.00	0.01	0.02	0.01	0.03
Al_2O_3	21.87	22.38	21.31	21.39	22.30	22.16	21.64
Cr_2O_3	0.01	0.01	0.01	0.00	0.00	0.02	0.02
Fe_2O_3	0.64	0.83	0.72	0.79	1.02	0.95	1.17
FeO	12.00	11.58	11.47	11.25	11.77	11.22	10.95
MnO	0.19	0.26	0.21	0.22	0.20	0.21	0.21

MgO	24.87	24.78	25.47	25.51	24.40	24.51	25.36
CaO	0.01	0.03	0.03	0.06	0.03	0.10	0.07
Na_2O	0.00	0.00	0.00	0.02	0.00	0.00	0.00
K_2O	0.00	0.00	0.00	0.00	0.00	0.00	0.00
*H_2O**	12.29	12.38	12.38	12.41	12.36	12.27	12.50
Total	100.35	100.96	100.83	101.04	100.92	99.99	101.69
Si	5.56	5.55	5.66	5.67	5.58	5.57	5.69
Al^{iv}	2.44	2.45	2.34	2.33	2.42	2.43	2.31
Al^{vi}	2.59	2.66	2.53	2.54	2.68	2.67	2.59
Ti	0.00	0.00	0.00	0.00	0.00	0.00	0.00
Cr	0.00	0.00	0.00	0.00	0.00	0.00	0.00
Fe^{3+}	0.09	0.12	0.10	0.11	0.15	0.14	0.17
Fe^{2+}	1.96	1.87	1.86	1.81	1.90	1.83	1.75
Mn	0.03	0.04	0.03	0.04	0.03	0.03	0.03
Mg	7.23	7.14	7.34	7.33	7.04	7.13	7.23
Ca	0.00	0.01	0.01	0.01	0.01	0.02	0.02
Na	0.00	0.00	0.00	0.01	0.00	0.00	0.00
K	0.00	0.00	0.00	0.00	0.00	0.00	0.00
*OH**	16.00	16.00	16.00	16.00	16.00	16.00	16.00
Total	35.87	35.85	35.86	35.86	35.81	35.82	35.78
Oxidized	yes	yes	yes	yes	yes	yes	yes
Fe/Fe+Mg	0.221	0.218	0.211	0.208	0.226	0.216	0.210

Sample #	*22-750-28-02-G4*	*22-750-28-02-G4*	*22-750-28-02-G4*	*22-750-28-02-G4*	*22-750-28-02-G4*	*22-750-28-02-G4*	*22-750-28-02-G4*
SiO_2	28.38	28.48	28.40	28.49	28.68	28.53	29.81
TiO_2	0.02	0.04	0.05	0.01	0.04	0.02	0.02
Al_2O_3	22.39	21.92	22.30	22.05	22.08	22.07	21.73
Cr_2O_3	0.05	0.04	0.02	0.03	0.03	0.03	0.03

Fe_2O_3	0.75	0.53	0.54	0.89	0.62	0.79	0.99
FeO	11.75	11.66	12.14	11.38	11.91	11.41	11.30
MnO	0.24	0.21	0.17	0.22	0.18	0.18	0.22
MgO	24.60	25.11	24.84	24.31	25.04	24.73	25.56
CaO	0.05	0.07	0.05	0.26	0.06	0.11	0.07
Na_2O	0.00	0.00	0.01	0.02	0.00	0.00	0.01
K_2O	0.00	0.00	0.00	0.00	0.00	0.00	0.00
H_2O*	12.31	12.31	12.34	12.24	12.38	12.28	12.56
Total	100.51	100.36	100.85	99.88	101.02	100.14	102.28
Si	5.52	5.54	5.51	5.57	5.55	5.56	5.68
Al^{iv}	2.48	2.46	2.49	2.43	2.45	2.44	2.32
Al^{vi}	2.66	2.58	2.62	2.66	2.59	2.64	2.57
Ti	0.00	0.01	0.01	0.00	0.01	0.00	0.00
Cr	0.01	0.01	0.00	0.00	0.00	0.00	0.00
Fe^{3+}	0.11	0.08	0.08	0.13	0.09	0.12	0.14
Fe^{2+}	1.91	1.90	1.97	1.86	1.93	1.86	1.80
Mn	0.04	0.03	0.03	0.04	0.03	0.03	0.04
Mg	7.13	7.28	7.18	7.08	7.22	7.18	7.26
Ca	0.01	0.02	0.01	0.05	0.01	0.02	0.01
Na	0.00	0.00	0.01	0.01	0.00	0.00	0.01
K	0.00	0.00	0.00	0.00	0.00	0.00	0.00
*OH**	16.00	16.00	16.00	16.00	16.00	16.00	16.00
Total	35.85	35.90	35.90	35.84	35.88	35.85	35.82
Oxidized	yes	yes	yes	yes	yes	yes	yes
Fe/Fe+Mg	0.221	0.213	0.222	0.219	0.218	0.216	0.211

Sample #	*22-750-28-02-G4*	*22-750-28-02-G4*	*22-750-28-02-G4*	*22-750-28-02-G4*	*22-750-28-02-G4*	*22-750-28-02-G4*	*22-750-28-02-G4*
SiO_2	28.58	28.59	28.79	28.66	28.79	28.39	29.11

TiO_2	0.00	0.02	0.01	0.02	0.00	0.02	0.00
Al_2O_3	22.47	21.78	22.33	22.16	22.11	22.03	21.55
Cr_2O_3	0.05	0.04	0.01	0.03	0.03	0.03	0.03
Fe_2O_3	0.61	0.58	0.83	0.74	0.58	0.22	0.69
FeO	11.99	12.07	11.46	11.87	12.13	12.55	11.36
MnO	0.25	0.25	0.19	0.18	0.22	0.25	0.19
MgO	24.91	24.78	24.65	24.72	25.07	25.18	25.37
CaO	0.05	0.09	0.39	0.07	0.07	0.06	0.07
Na_2O	0.01	0.02	0.01	0.01	0.00	0.01	0.04
K_2O	0.00	0.00	0.00	0.00	0.00	0.00	0.00
H_2O*	12.41	12.30	12.39	12.35	12.41	12.36	12.37
Total	101.32	100.49	101.07	100.80	101.42	101.09	100.76
Si	5.52	5.57	5.56	5.56	5.55	5.51	5.63
Al^{iv}	2.48	2.43	2.44	2.44	2.45	2.49	2.37
Al^{vi}	2.64	2.58	2.66	2.63	2.59	2.55	2.56
Ti	0.00	0.00	0.00	0.00	0.00	0.00	0.00
Cr	0.01	0.01	0.00	0.00	0.00	0.00	0.00
Fe^{3+}	0.09	0.08	0.12	0.11	0.08	0.03	0.10
Fe^{2+}	1.93	1.97	1.85	1.92	1.96	2.04	1.84
Mn	0.04	0.04	0.03	0.03	0.04	0.04	0.03
Mg	7.17	7.19	7.10	7.14	7.21	7.28	7.32
Ca	0.01	0.02	0.08	0.02	0.02	0.01	0.01
Na	0.01	0.01	0.01	0.01	0.00	0.01	0.03
K	0.00	0.00	0.00	0.00	0.00	0.00	0.00
*OH**	16.00	16.00	16.00	16.00	16.00	16.00	16.00
Total	35.89	35.89	35.85	35.86	35.89	35.96	35.88
Oxidized	yes	yes	yes	yes	yes	yes	yes
Fe/Fe+Mg	0.220	0.222	0.217	0.222	0.221	0.221	0.209

Sample #	*22-750-28-02-G4*	*22-750-28-02-G5*	*22-750-28-02-G5*	*22-750-28-02-G5*	*22-750-28-02-G5*	*22-750-28-02-G5*	*22-750-28-01-S1*
SiO_2	28.30	27.80	27.61	28.08	27.81	27.89	28.08
TiO_2	0.00	0.01	0.02	0.02	0.03	0.01	0.01
Al_2O_3	22.31	22.77	22.62	23.02	23.09	23.19	22.68
Cr_2O_3	0.05	0.03	0.01	0.04	0.07	0.02	0.04
Fe_2O_3	0.66	0.56	0.00	0.80	0.48	0.98	0.48
FeO	11.84	12.21	12.30	11.73	12.31	11.61	11.78
MnO	0.23	0.19	0.17	0.18	0.21	0.20	0.21
MgO	24.54	23.82	24.22	23.81	24.20	22.82	24.85
CaO	0.06	0.41	0.17	0.55	0.16	1.25	0.05
Na_2O	0.02	0.03	0.45	0.04	0.04	0.03	0.02
K_2O	0.00	0.03	0.23	0.00	0.01	0.00	0.00
H_2O*	12.28	12.22	12.21	12.30	12.31	12.23	12.32
Total	100.26	100.07	100.00	100.56	100.71	100.24	100.51
Si	5.52	5.45	5.39	5.46	5.41	5.45	5.46
Al^{iv}	2.48	2.55	2.61	2.54	2.59	2.55	2.54
Al^{vi}	2.65	2.71	2.62	2.75	2.71	2.81	2.66
Ti	0.00	0.00	0.00	0.00	0.00	0.00	0.00
Cr	0.01	0.00	0.00	0.01	0.01	0.00	0.01
Fe^{3+}	0.10	0.08	0.00	0.12	0.07	0.14	0.07
Fe^{2+}	1.93	2.00	2.08	1.91	2.00	1.90	1.92
Mn	0.04	0.03	0.03	0.03	0.03	0.03	0.03
Mg	7.13	6.95	7.05	6.91	7.02	6.65	7.20
Ca	0.01	0.09	0.03	0.12	0.03	0.26	0.01
Na	0.01	0.02	0.34	0.03	0.03	0.02	0.02
K	0.00	0.01	0.12	0.00	0.00	0.00	0.00
*OH**	16.00	16.00	16.00	16.00	16.00	16.00	16.00
Total	35.88	35.91	36.27	35.86	35.92	35.83	35.92
Oxidized	yes	yes	yes	yes	yes	yes	yes
Fe/Fe+Mg	0.221	0.230	0.228	0.227	0.228	0.235	0.216

Sample #	*22-750-28-01-S1*	*22-750-28-01-S1*	*22-750-28-01-S1*	*22-750-28-01-S1*	*22-750-28-01-S1*	*22-750-28-01-S2*	*22-750-28-01-S2*
SiO_2	28.30	27.97	30.92	28.02	29.44	28.85	28.83
TiO_2	0.04	0.02	0.03	0.05	0.02	0.04	0.04
Al_2O_3	22.87	22.93	21.41	23.08	22.23	22.39	22.37
Cr_2O_3	0.05	0.07	0.05	0.02	0.03	0.00	0.00
Fe_2O_3	0.63	0.23	1.76	0.63	1.02	0.63	0.76
FeO	11.90	12.22	10.46	11.48	11.51	11.58	11.86
MnO	0.23	0.20	0.18	0.21	0.18	0.23	0.19
MgO	24.83	25.01	24.52	24.40	24.76	25.35	24.98
CaO	0.03	0.05	0.99	0.07	0.38	0.04	0.03
Na_2O	0.00	0.05	0.05	0.09	0.05	0.02	0.00
K_2O	0.00	0.01	0.02	0.05	0.00	0.00	0.00
H_2O*	12.40	12.38	12.65	12.32	12.52	12.47	12.44
Total	101.26	101.14	103.01	100.42	102.12	101.58	101.47
Si	5.46	5.41	5.83	5.44	5.62	5.54	5.55
Al^{iv}	2.54	2.59	2.17	2.56	2.38	2.46	2.45
Al^{vi}	2.68	2.65	2.62	2.74	2.64	2.62	2.63
Ti	0.01	0.00	0.00	0.01	0.00	0.01	0.01
Cr	0.01	0.01	0.01	0.00	0.00	0.00	0.00
Fe^{3+}	0.09	0.03	0.25	0.09	0.15	0.09	0.11
Fe^{2+}	1.92	1.98	1.65	1.86	1.84	1.86	1.91
Mn	0.04	0.03	0.03	0.03	0.03	0.04	0.03
Mg	7.15	7.21	6.90	7.07	7.05	7.26	7.17
Ca	0.01	0.01	0.20	0.01	0.08	0.01	0.01
Na	0.00	0.04	0.04	0.07	0.03	0.01	0.00
K	0.00	0.01	0.01	0.03	0.00	0.00	0.00
*OH**	16.00	16.00	16.00	16.00	16.00	16.00	16.00
Total	35.88	35.97	35.70	35.92	35.82	35.89	35.86
Oxidized	yes	yes	yes	yes	yes	yes	yes

Fe/Fe+Mg	0.220	0.218	0.216	0.217	0.220	0.212	0.220

Sample #	*22-750-28-01-S2*	*22-750-28-01-S2*	*22-750-28-01-S2*	*22-750-28-01-S2*	*22-750-28-01-S2*	*22-750-28-01-S2*	*22-750-28-01-S2*
SiO_2	28.66	27.59	27.65	28.48	27.66	28.21	27.91
TiO_2	0.07	0.02	0.03	0.01	0.01	0.04	0.00
Al_2O_3	22.25	23.53	23.39	22.12	23.65	22.85	22.62
Cr_2O_3	0.00	0.03	0.02	0.01	0.19	0.01	0.00
Fe_2O_3	0.35	0.19	0.26	0.50	0.28	0.50	0.31
FeO	12.39	13.26	12.76	12.13	12.99	12.01	12.39
MnO	0.20	0.25	0.21	0.21	0.20	0.20	0.20
MgO	25.21	24.37	24.41	24.99	24.51	24.84	24.62
CaO	0.03	0.03	0.06	0.02	0.02	0.03	0.06
Na_2O	0.05	0.02	0.05	0.00	0.00	0.04	0.03
K_2O	0.03	0.00	0.01	0.00	0.00	0.00	0.01
H_2O*	12.44	12.39	12.36	12.34	12.43	12.38	12.28
Total	101.65	101.67	101.21	100.80	101.92	101.10	100.41
Si	5.52	5.34	5.36	5.53	5.33	5.46	5.45
Al^{iv}	2.48	2.66	2.64	2.47	2.67	2.54	2.55
Al^{vi}	2.57	2.71	2.71	2.60	2.71	2.67	2.65
Ti	0.01	0.00	0.00	0.00	0.00	0.01	0.00
Cr	0.00	0.00	0.00	0.00	0.03	0.00	0.00
Fe^{3+}	0.05	0.03	0.04	0.07	0.04	0.07	0.05
Fe^{2+}	2.00	2.15	2.07	1.97	2.09	1.94	2.02
Mn	0.03	0.04	0.04	0.03	0.03	0.03	0.03
Mg	7.24	7.03	7.05	7.23	7.04	7.16	7.16
Ca	0.01	0.01	0.01	0.00	0.00	0.01	0.01
Na	0.03	0.02	0.03	0.00	0.00	0.03	0.02
K	0.01	0.00	0.00	0.00	0.00	0.00	0.01

*OH**	16.00	16.00	16.00	16.00	16.00	16.00	16.00
Total	35.95	35.97	35.97	35.91	35.95	35.92	35.95
Oxidized	yes	yes	yes	yes	yes	yes	yes
Fe/Fe+Mg	0.220	0.236	0.230	0.220	0.233	0.220	0.224

Sample #	*22-750-28-01-S2*	*22-750-28-01-S3*	*22-750-28-01-S3*	*22-750-28-01-S3*	*22-750-28-01-S3*	*22-750-28-01-S3*	*22-750-28-01-S3*
SiO_2	28.20	28.52	27.97	28.65	28.74	29.01	28.34
TiO_2	0.04	0.08	0.06	0.02	0.07	0.04	0.05
Al_2O_3	22.70	22.43	22.42	22.72	22.98	22.79	22.62
Cr_2O_3	0.02	0.04	0.06	0.01	0.07	0.04	0.06
Fe_2O_3	0.47	0.64	0.33	0.70	0.54	1.43	0.83
FeO	11.81	11.56	11.93	11.67	11.88	10.76	11.26
MnO	0.25	0.23	0.22	0.22	0.17	0.18	0.22
MgO	24.90	24.97	24.90	24.77	25.28	22.95	23.95
CaO	0.04	0.13	0.11	0.13	0.19	1.78	0.80
Na_2O	0.04	0.01	0.02	0.05	0.03	0.02	0.05
K_2O	0.00	0.01	0.01	0.03	0.01	0.02	0.01
H_2O*	12.36	12.39	12.28	12.43	12.57	12.41	12.31
Total	100.84	101.01	100.30	101.41	102.53	101.44	100.49
Si	5.46	5.51	5.46	5.51	5.48	5.59	5.51
Al^{iv}	2.54	2.49	2.54	2.49	2.52	2.41	2.49
Al^{vi}	2.66	2.63	2.62	2.68	2.64	2.78	2.71
Ti	0.01	0.01	0.01	0.00	0.01	0.01	0.01
Cr	0.00	0.01	0.01	0.00	0.01	0.01	0.01
Fe^{3+}	0.07	0.09	0.05	0.10	0.08	0.21	0.12
Fe^{2+}	1.91	1.87	1.95	1.88	1.89	1.73	1.83
Mn	0.04	0.04	0.04	0.04	0.03	0.03	0.04
Mg	7.19	7.19	7.24	7.11	7.18	6.59	6.94

Ca	0.01	0.03	0.02	0.03	0.04	0.37	0.17
Na	0.03	0.01	0.02	0.04	0.02	0.01	0.04
K	0.00	0.01	0.01	0.01	0.01	0.01	0.01
*OH**	16.00	16.00	16.00	16.00	16.00	16.00	16.00
Total	35.93	35.89	35.95	35.89	35.91	35.75	35.86
Oxidized	yes	yes	yes	yes	yes	yes	yes
Fe/Fe+Mg	0.216	0.214	0.216	0.218	0.215	0.228	0.220

Sample #	*22-750-28-01-S4*	*22-750-28-01-S4*	*22-750-28-01-S4*	*22-750-28-01-S4*	*22-750-28-01-S4*	*22-750-28-01-S4*	*22-750-28-01-S4*
SiO_2	28.44	28.17	33.20	29.08	28.74	29.27	28.27
TiO_2	0.02	0.03	0.02	0.03	0.04	0.01	0.00
Al_2O_3	22.51	23.03	16.41	22.34	22.61	22.55	23.26
Cr_2O_3	0.03	0.04	0.01	0.03	0.00	0.05	0.03
Fe_2O_3	0.42	0.52	1.75	0.82	0.81	1.05	0.54
FeO	11.89	11.92	10.05	11.97	11.84	11.45	12.02
MnO	0.20	0.23	0.24	0.17	0.19	0.19	0.22
MgO	25.19	24.84	23.93	24.88	24.74	24.78	24.88
CaO	0.05	0.03	4.10	0.29	0.11	0.34	0.08
Na_2O	0.03	0.02	0.02	0.00	0.00	0.00	0.00
K_2O	0.01	0.00	0.00	0.00	0.01	0.00	0.00
H_2O*	12.41	12.40	12.46	12.50	12.44	12.53	12.46
Total	101.21	101.23	102.18	102.08	101.51	102.23	101.76
Si	5.49	5.44	6.36	5.57	5.53	5.59	5.43
Al^{iv}	2.51	2.56	1.64	2.43	2.47	2.41	2.57
Al^{vi}	2.62	2.69	2.08	2.62	2.67	2.67	2.71
Ti	0.00	0.00	0.00	0.00	0.01	0.00	0.00
Cr	0.00	0.01	0.00	0.00	0.00	0.01	0.01
Fe^{3+}	0.06	0.08	0.25	0.12	0.12	0.15	0.08

Fe^{2+}	1.92	1.93	1.61	1.92	1.91	1.83	1.93
Mn	0.03	0.04	0.04	0.03	0.03	0.03	0.04
Mg	7.25	7.15	6.84	7.10	7.10	7.05	7.13
Ca	0.01	0.01	0.84	0.06	0.02	0.07	0.02
Na	0.02	0.02	0.01	0.00	0.00	0.00	0.00
K	0.01	0.00	0.00	0.00	0.01	0.00	0.00
*OH**	16.00	16.00	16.00	16.00	16.00	16.00	16.00
Total	35.93	35.91	35.68	35.84	35.85	35.81	35.90
Oxidized	yes	yes	yes	yes	yes	yes	yes
Fe/Fe+Mg	0.215	0.219	0.214	0.223	0.222	0.219	0.220

Sample #	*22-750-28-03-S1*	*22-750-28-03-S1*	*22-750-28-03-S1*	*22-750-28-03-S1*	*22-750-28-03-S1*	*22-750-28-03-S1*	*22-750-28-03-S1*
SiO_2	28.55	28.47	28.39	28.50	28.29	28.59	27.98
TiO_2	0.00	0.02	0.02	0.01	0.00	0.03	0.05
Al_2O_3	22.79	22.77	22.75	23.00	23.01	22.54	23.26
Cr_2O_3	0.01	0.02	0.00	0.01	0.03	0.01	0.08
Fe_2O_3	0.62	0.57	0.52	0.59	0.63	0.72	0.41
FeO	11.32	11.38	11.50	11.53	11.19	11.00	11.74
MnO	0.19	0.26	0.25	0.23	0.20	0.19	0.25
MgO	25.39	25.39	25.33	25.31	25.20	25.32	25.16
CaO	0.02	0.02	0.02	0.03	0.02	0.04	0.02
Na_2O	0.00	0.00	0.00	0.00	0.00	0.00	0.00
K_2O	0.00	0.00	0.00	0.00	0.00	0.00	0.00
H_2O*	12.45	12.44	12.42	12.48	12.41	12.40	12.43
Total	101.33	101.33	101.20	101.68	100.96	100.83	101.37
Si	5.49	5.48	5.47	5.47	5.46	5.52	5.39
Al^{iv}	2.51	2.52	2.53	2.53	2.54	2.48	2.61
Al^{vi}	2.66	2.65	2.65	2.68	2.70	2.66	2.68

Ti	0.00	0.00	0.00	0.00	0.00	0.00	0.01
Cr	0.00	0.00	0.00	0.00	0.01	0.00	0.01
Fe^{3+}	0.09	0.08	0.08	0.09	0.09	0.10	0.06
Fe^{2+}	1.82	1.83	1.85	1.85	1.81	1.78	1.89
Mn	0.03	0.04	0.04	0.04	0.03	0.03	0.04
Mg	7.28	7.29	7.28	7.24	7.25	7.29	7.23
Ca	0.00	0.00	0.00	0.01	0.00	0.01	0.00
Na	0.00	0.00	0.00	0.00	0.00	0.00	0.00
K	0.00	0.00	0.00	0.00	0.00	0.00	0.00
*OH**	16.00	16.00	16.00	16.00	16.00	16.00	16.00
Total	35.88	35.89	35.90	35.89	35.88	35.87	35.92
Oxidized	yes	yes	yes	yes	yes	yes	yes
Fe/Fe+Mg	0.208	0.208	0.210	0.211	0.207	0.205	0.213

Sample #	*22-750-28-03-S1*	*22-750-28-03-S1*	*22-750-28-03-S1*	*22-750-28-03-S1*	*22-750-28-03-S1*	*22-750-28-03-S2*	*22-750-28-03-S2*
SiO_2	28.47	29.19	28.29	28.33	28.40	28.85	29.01
TiO_2	0.03	0.02	0.01	0.05	0.05	0.02	0.01
Al_2O_3	22.70	21.48	22.69	22.96	23.11	22.10	22.28
Cr_2O_3	0.01	0.07	0.58	0.11	0.01	0.00	0.01
Fe_2O_3	0.63	0.46	0.51	0.60	0.38	0.39	0.69
FeO	11.20	11.42	11.44	11.55	12.09	11.87	11.34
MnO	0.22	0.21	0.22	0.25	0.24	0.21	0.27
MgO	25.39	25.94	25.29	25.02	25.37	25.65	25.49
CaO	0.03	0.03	0.07	0.03	0.01	0.08	0.05
Na_2O	0.00	0.00	0.00	0.04	0.01	0.02	0.00
K_2O	0.00	0.07	0.00	0.00	0.00	0.00	0.00
H_2O*	12.42	12.44	12.45	12.43	12.52	12.47	12.48
Total	101.05	101.32	101.53	101.36	102.20	101.64	101.63

Si	5.49	5.62	5.44	5.46	5.43	5.55	5.56
Al iv	2.51	2.38	2.56	2.54	2.57	2.45	2.44
Al vi	2.66	2.50	2.60	2.68	2.65	2.56	2.61
Ti	0.00	0.00	0.00	0.01	0.01	0.00	0.00
Cr	0.00	0.01	0.09	0.02	0.00	0.00	0.00
Fe^{3+}	0.09	0.07	0.07	0.09	0.05	0.06	0.10
Fe^{2+}	1.81	1.84	1.84	1.86	1.93	1.91	1.82
Mn	0.04	0.03	0.04	0.04	0.04	0.03	0.04
Mg	7.30	7.44	7.25	7.18	7.24	7.35	7.29
Ca	0.01	0.01	0.02	0.01	0.00	0.02	0.01
Na	0.00	0.00	0.00	0.03	0.01	0.01	0.00
K	0.00	0.03	0.00	0.00	0.00	0.00	0.00
*OH**	16.00	16.00	16.00	16.00	16.00	16.00	16.00
Total	35.88	35.92	35.91	35.90	35.93	35.93	35.87
Oxidized	yes	yes	yes	yes	yes	yes	yes
Fe/Fe+Mg	0.206	0.204	0.209	0.213	0.216	0.211	0.208

Sample #	*22-750-28-03-S2*	*22-750-28-03-S2*	*22-750-28-03-S2*	*22-750-28-03-S2*	*22-750-28-03-S2*	*22-750-28-03-S2*	*22-750-28-03-S2*
SiO_2	28.62	29.36	29.31	28.64	28.32	28.65	35.34
TiO_2	0.03	0.02	0.02	0.04	0.02	0.01	0.02
Al_2O_3	22.58	21.89	21.68	22.50	22.91	22.40	19.93
Cr_2O_3	0.01	0.00	0.00	0.01	0.00	0.01	0.01
Fe_2O_3	0.45	0.51	0.27	0.39	0.40	0.49	5.44
FeO	11.74	11.21	11.93	11.79	11.68	11.62	6.28
MnO	0.26	0.24	0.21	0.20	0.23	0.19	0.21
MgO	25.49	26.21	26.22	25.66	25.29	25.55	23.43
CaO	0.05	0.06	0.06	0.06	0.08	0.09	0.06
Na_2O	0.00	0.01	0.05	0.00	0.03	0.00	0.02

K_2O	0.00	0.01	0.00	0.00	0.01	0.00	0.00
H_2O*	12.48	12.56	12.55	12.49	12.44	12.45	12.89
Total	101.70	102.08	102.29	101.77	101.40	101.43	103.63
Si	5.50	5.60	5.60	5.50	5.45	5.51	6.49
Al^{iv}	2.50	2.40	2.40	2.50	2.55	2.49	1.51
Al^{vi}	2.61	2.53	2.48	2.59	2.66	2.60	2.86
Ti	0.00	0.00	0.00	0.01	0.00	0.00	0.00
Cr	0.00	0.00	0.00	0.00	0.00	0.00	0.00
Fe^{3+}	0.06	0.07	0.04	0.06	0.06	0.07	0.75
Fe^{2+}	1.89	1.79	1.90	1.89	1.88	1.87	0.96
Mn	0.04	0.04	0.03	0.03	0.04	0.03	0.03
Mg	7.30	7.45	7.46	7.34	7.26	7.33	6.41
Ca	0.01	0.01	0.01	0.01	0.02	0.02	0.01
Na	0.00	0.01	0.03	0.00	0.03	0.00	0.01
K	0.00	0.00	0.00	0.00	0.00	0.00	0.00
*OH**	16.00	16.00	16.00	16.00	16.00	16.00	16.00
Total	35.92	35.91	35.96	35.92	35.94	35.90	35.04
Oxidized	yes	yes	yes	yes	yes	yes	no
Fe/Fe+Mg	0.211	0.200	0.207	0.210	0.211	0.209	0.211

Sample #	*22-750-28-03-S2*	*22-750-28-03-S2*	*22-750-28-03-S3*	*22-750-28-03-S3*	*22-750-28-03-S3*	*22-750-28-03-S3*	*22-750-28-03-S3*
SiO_2	29.31	28.39	29.09	28.51	29.23	28.74	28.88
TiO_2	0.00	0.04	0.00	0.04	0.02	0.01	0.00
Al_2O_3	21.87	22.39	22.76	22.38	21.77	22.41	22.07
Cr_2O_3	0.00	0.00	0.00	0.00	0.01	0.01	0.00
Fe_2O_3	0.49	0.35	1.18	0.39	0.55	0.66	0.48
FeO	11.62	11.82	11.05	11.53	11.53	11.34	11.40
MnO	0.24	0.20	0.21	0.25	0.24	0.22	0.22

MgO	26.00	25.52	24.71	25.65	25.75	25.39	25.80
CaO	0.07	0.02	0.08	0.06	0.13	0.07	0.10
Na_2O	0.01	0.00	0.01	0.00	0.01	0.00	0.00
K_2O	0.00	0.00	0.00	0.00	0.00	0.00	0.00
*H_2O**	12.54	12.40	12.47	12.43	12.49	12.44	12.46
Total	102.13	101.11	101.53	101.21	101.72	101.26	101.38
Si	5.60	5.49	5.58	5.50	5.61	5.53	5.56
Al^{iv}	2.40	2.51	2.42	2.50	2.39	2.47	2.44
Al^{vi}	2.53	2.59	2.73	2.59	2.53	2.63	2.56
Ti	0.00	0.01	0.00	0.01	0.00	0.00	0.00
Cr	0.00	0.00	0.00	0.00	0.00	0.00	0.00
Fe^{3+}	0.07	0.05	0.17	0.06	0.08	0.10	0.07
Fe^{2+}	1.86	1.91	1.77	1.86	1.85	1.83	1.83
Mn	0.04	0.03	0.03	0.04	0.04	0.04	0.04
Mg	7.40	7.35	7.06	7.37	7.36	7.29	7.40
Ca	0.01	0.01	0.02	0.01	0.03	0.01	0.02
Na	0.00	0.00	0.00	0.00	0.01	0.00	0.00
K	0.00	0.00	0.00	0.00	0.00	0.00	0.00
*OH**	16.00	16.00	16.00	16.00	16.00	16.00	16.00
Total	35.91	35.93	35.79	35.92	35.90	35.87	35.90
Oxidized	yes	yes	yes	yes	yes	yes	yes
Fe/Fe+Mg	0.207	0.211	0.216	0.206	0.208	0.209	0.205

Sample #	*22-750-28-03-S3*	*22-750-28-03-S3*	*22-750-28-03-S3*	*22-750-28-03-S3*	*22-750-28-03-S4*	*22-750-28-03-S4*	*22-750-28-03-S4*
SiO_2	28.10	28.74	28.39	28.79	28.96	28.33	28.68
TiO_2	0.02	0.00	0.00	0.01	0.00	0.05	0.00
Al_2O_3	23.22	23.49	21.64	22.72	21.43	22.52	22.01
Cr_2O_3	0.00	0.01	0.00	0.02	0.00	0.02	0.01

Fe_2O_3	0.49	1.28	1.55	1.23	0.37	0.48	0.30
FeO	11.40	11.59	10.27	11.88	11.57	11.64	11.53
MnO	0.21	0.22	0.17	0.17	0.24	0.22	0.20
MgO	25.21	23.95	23.35	23.82	25.87	25.25	25.83
CaO	0.09	0.05	0.10	0.04	0.06	0.11	0.08
Na_2O	0.00	0.02	0.01	0.02	0.00	0.00	0.02
K_2O	0.00	0.00	0.01	0.00	0.00	0.00	0.00
H_2O*	12.42	12.47	11.98	12.37	12.38	12.38	12.41
Total	101.14	101.81	97.47	101.05	100.87	100.97	101.05
Si	5.42	5.51	5.66	5.57	5.60	5.48	5.54
Al^{iv}	2.58	2.49	2.34	2.43	2.40	2.52	2.46
Al^{vi}	2.70	2.83	2.77	2.76	2.50	2.62	2.55
Ti	0.00	0.00	0.00	0.00	0.00	0.01	0.00
Cr	0.00	0.00	0.00	0.00	0.00	0.00	0.00
Fe^{3+}	0.07	0.18	0.23	0.18	0.05	0.07	0.04
Fe^{2+}	1.84	1.86	1.71	1.92	1.87	1.88	1.86
Mn	0.03	0.04	0.03	0.03	0.04	0.04	0.03
Mg	7.25	6.84	6.94	6.86	7.46	7.28	7.43
Ca	0.02	0.01	0.02	0.01	0.01	0.02	0.02
Na	0.00	0.02	0.01	0.02	0.00	0.00	0.01
K	0.00	0.00	0.00	0.00	0.00	0.00	0.00
*OH**	16.00	16.00	16.00	16.00	16.00	16.00	16.00
Total	35.91	35.77	35.71	35.78	35.93	35.90	35.95
Oxidized	yes	yes	yes	yes	yes	yes	yes
Fe/Fe+Mg	0.209	0.230	0.219	0.234	0.205	0.212	0.204

Sample #	*22-750-28-03-S4*	*22-750-28-03-S4*	*22-750-28-03-S4*	*22-750-28-03-S4*	*22-750-28-03-S4*	*22-750-28-03-S4*	*22-750-28-04-S1*
SiO_2	28.75	28.48	28.71	29.40	29.20	29.37	27.74

TiO_2	0.03	0.02	0.04	0.02	0.02	0.00	0.00
Al_2O_3	22.26	22.32	21.78	20.87	21.71	22.25	23.05
Cr_2O_3	0.03	0.02	0.00	0.00	0.00	0.02	0.01
Fe_2O_3	0.39	0.20	0.38	0.93	0.81	0.82	0.29
FeO	11.52	11.65	11.37	10.55	11.32	11.40	12.38
MnO	0.20	0.25	0.25	0.21	0.19	0.22	0.21
MgO	25.83	25.87	25.80	25.46	25.30	25.46	24.78
CaO	0.10	0.08	0.11	0.14	0.11	0.17	0.02
Na_2O	0.00	0.02	0.00	0.00	0.01	0.00	0.00
K_2O	0.00	0.00	0.00	0.00	0.00	0.00	0.01
H_2O*	12.48	12.44	12.38	12.30	12.41	12.56	12.33
Total	101.57	101.33	100.78	99.87	101.08	102.26	100.80
Si	5.52	5.49	5.56	5.72	5.63	5.60	5.39
Al^{iv}	2.48	2.51	2.44	2.28	2.37	2.40	2.61
Al^{vi}	2.57	2.56	2.53	2.52	2.58	2.61	2.68
Ti	0.00	0.00	0.01	0.00	0.00	0.00	0.00
Cr	0.00	0.00	0.00	0.00	0.00	0.00	0.00
Fe^{3+}	0.06	0.03	0.06	0.14	0.12	0.12	0.04
Fe^{2+}	1.85	1.88	1.84	1.72	1.83	1.82	2.01
Mn	0.03	0.04	0.04	0.03	0.03	0.04	0.04
Mg	7.40	7.43	7.44	7.39	7.27	7.23	7.18
Ca	0.02	0.02	0.02	0.03	0.02	0.03	0.00
Na	0.00	0.01	0.00	0.00	0.01	0.00	0.00
K	0.00	0.00	0.00	0.00	0.00	0.00	0.01
*OH**	16.00	16.00	16.00	16.00	16.00	16.00	16.00
Total	35.93	35.97	35.93	35.83	35.85	35.85	35.94
Oxidized	yes	yes	yes	yes	yes	yes	yes
Fe/Fe+Mg	0.205	0.204	0.203	0.201	0.211	0.211	0.223

Sample #	*22-750-28-04-S1*	*22-750-28-04-S1*	*22-750-28-04-S1*	*22-750-28-04-S2*	*22-750-28-04-S2*	*22-750-28-04-S2*	*22-750-28-04-S3*
SiO_2	28.00	28.17	27.77	28.23	27.79	27.59	28.23
TiO_2	0.02	0.01	0.04	0.00	0.03	0.01	0.04
Al_2O_3	22.78	22.61	23.06	22.85	23.27	23.05	22.62
Cr_2O_3	0.01	0.01	0.02	0.00	0.01	0.08	0.01
Fe_2O_3	0.46	0.50	0.31	0.45	0.23	0.21	0.32
FeO	11.97	11.95	12.37	11.97	12.82	12.50	12.32
MnO	0.19	0.22	0.26	0.23	0.21	0.27	0.23
MgO	24.82	24.92	24.74	25.06	24.55	24.50	24.99
CaO	0.01	0.03	0.01	0.03	0.02	0.04	0.03
Na_2O	0.00	0.00	0.00	0.00	0.00	0.05	0.00
K_2O	0.01	0.00	0.00	0.00	0.09	0.01	0.07
H_2O*	12.32	12.34	12.34	12.40	12.38	12.29	12.39
Total	100.58	100.72	100.90	101.20	101.41	100.61	101.24
Si	5.44	5.47	5.39	5.45	5.38	5.38	5.46
Al^{iv}	2.56	2.53	2.61	2.55	2.62	2.62	2.54
Al^{vi}	2.67	2.65	2.67	2.66	2.69	2.68	2.62
Ti	0.00	0.00	0.01	0.00	0.00	0.00	0.01
Cr	0.00	0.00	0.00	0.00	0.00	0.01	0.00
Fe^{3+}	0.07	0.07	0.05	0.07	0.03	0.03	0.05
Fe^{2+}	1.95	1.94	2.01	1.93	2.07	2.04	1.99
Mn	0.03	0.04	0.04	0.04	0.04	0.05	0.04
Mg	7.19	7.21	7.16	7.22	7.08	7.12	7.20
Ca	0.00	0.01	0.00	0.01	0.00	0.01	0.01
Na	0.00	0.00	0.00	0.00	0.00	0.04	0.00
K	0.00	0.00	0.00	0.00	0.04	0.00	0.03
*OH**	16.00	16.00	16.00	16.00	16.00	16.00	16.00
Total	35.92	35.90	35.94	35.91	35.97	35.98	35.95
Oxidized	yes	yes	yes	yes	yes	yes	yes
Fe/Fe+Mg	0.219	0.218	0.223	0.217	0.229	0.225	0.221

Sample #	*22-750-28-04-S3*	*22-750-28-04-S3*	*22-750-28-04-S4*	*22-750-28-04-S4*	*22-750-28-04-S4*	*22-750-28-04-S5*	*22-750-28-04-S5*
SiO_2	28.03	28.12	28.54	28.25	29.18	29.23	28.28
TiO_2	0.01	0.00	0.02	0.02	0.01	0.03	0.02
Al_2O_3	22.66	22.91	22.23	22.61	21.24	20.97	22.59
Cr_2O_3	0.02	0.00	0.00	0.01	0.00	0.00	0.02
Fe_2O_3	0.28	0.26	0.39	0.33	0.54	0.51	0.42
FeO	12.48	12.37	12.33	12.08	11.34	11.52	11.93
MnO	0.21	0.21	0.22	0.24	0.22	0.20	0.22
MgO	24.98	25.10	25.17	25.28	25.93	25.72	25.13
CaO	0.02	0.02	0.04	0.03	0.02	0.16	0.10
Na_2O	0.00	0.02	0.00	0.00	0.00	0.01	0.00
K_2O	0.00	0.00	0.01	0.00	0.00	0.00	0.00
H_2O*	12.35	12.41	12.40	12.40	12.39	12.36	12.39
Total	101.01	101.42	101.35	101.24	100.83	100.70	101.09
Si	5.44	5.43	5.51	5.46	5.64	5.66	5.47
Al^{iv}	2.56	2.57	2.49	2.54	2.36	2.34	2.53
Al^{vi}	2.62	2.65	2.58	2.61	2.49	2.46	2.63
Ti	0.00	0.00	0.00	0.00	0.00	0.00	0.00
Cr	0.00	0.00	0.00	0.00	0.00	0.00	0.00
Fe^{3+}	0.04	0.04	0.06	0.05	0.08	0.07	0.06
Fe^{2+}	2.03	2.00	1.99	1.95	1.83	1.87	1.93
Mn	0.03	0.03	0.04	0.04	0.04	0.03	0.04
Mg	7.23	7.22	7.25	7.28	7.47	7.43	7.25
Ca	0.00	0.00	0.01	0.01	0.00	0.03	0.02
Na	0.00	0.02	0.00	0.00	0.00	0.01	0.00
K	0.00	0.00	0.00	0.00	0.00	0.00	0.00
*OH**	16.00	16.00	16.00	16.00	16.00	16.00	16.00
Total	35.94	35.96	35.93	35.94	35.89	35.91	35.92
Oxidized	yes	yes	yes	yes	yes	yes	yes

Fe/Fe+Mg	0.222	0.220	0.220	0.215	0.204	0.207	0.215

Sample #	*22-750-28-04-S7*	*22-750-28-04-S7*	*22-750-28-04-S7*	*22-750-28-04-S7*	*22-750-28-04-S7*	*22-750-28-04-S8*	*22-750-28-04-S8*
SiO_2	27.73	28.08	28.03	28.31	28.15	28.14	28.36
TiO_2	0.01	0.04	0.01	0.03	0.05	0.02	0.00
Al_2O_3	23.31	22.99	23.16	22.80	23.41	23.35	22.72
Cr_2O_3	0.00	0.00	0.03	0.01	0.02	0.00	0.00
Fe_2O_3	0.27	0.35	0.47	0.38	0.49	0.44	0.26
FeO	12.41	12.32	12.18	12.50	12.07	12.54	12.55
MnO	0.21	0.22	0.24	0.22	0.24	0.21	0.21
MgO	24.80	24.93	24.68	25.11	24.87	24.78	25.33
CaO	0.04	0.04	0.05	0.00	0.18	0.02	0.03
Na_2O	0.00	0.01	0.02	0.00	0.00	0.00	0.00
K_2O	0.00	0.00	0.00	0.00	0.00	0.01	0.00
H_2O*	12.37	12.41	12.39	12.45	12.48	12.47	12.46
Total	101.15	101.40	101.25	101.76	101.94	101.96	101.88
Si	5.37	5.42	5.42	5.45	5.40	5.41	5.45
Al^{iv}	2.63	2.58	2.58	2.55	2.60	2.59	2.55
Al^{vi}	2.70	2.66	2.70	2.63	2.71	2.70	2.61
Ti	0.00	0.01	0.00	0.00	0.01	0.00	0.00
Cr	0.00	0.00	0.00	0.00	0.00	0.00	0.00
Fe^{3+}	0.04	0.05	0.07	0.06	0.07	0.06	0.04
Fe^{2+}	2.01	1.99	1.97	2.01	1.94	2.02	2.02
Mn	0.03	0.04	0.04	0.04	0.04	0.03	0.03
Mg	7.16	7.18	7.11	7.21	7.12	7.10	7.26
Ca	0.01	0.01	0.01	0.00	0.04	0.00	0.01
Na	0.00	0.01	0.01	0.00	0.00	0.00	0.00
K	0.00	0.00	0.00	0.00	0.00	0.01	0.00

*OH**	16.00	16.00	16.00	16.00	16.00	16.00	16.00
Total	35.95	35.94	35.92	35.92	35.91	35.92	35.95
Oxidized	yes	yes	yes	yes	yes	yes	yes
Fe/Fe+Mg	0.223	0.221	0.223	0.223	0.220	0.226	0.221

Sample #	*22-750-28-04-S9*	*22-750-28-04-S9*	*22-750-28-04-S9*	*22-750-28-04-S10*	*22-750-28-05-S01*	*22-750-28-05-S01*	*22-750-28-05-S02*
SiO_2	28.23	27.57	27.93	27.98	27.87	27.70	27.82
TiO_2	0.05	0.02	0.03	0.03	0.02	0.03	0.05
Al_2O_3	23.02	23.41	23.10	23.21	22.89	22.44	23.01
Cr_2O_3	0.00	0.02	0.01	0.02	0.02	0.02	0.00
Fe_2O_3	0.32	0.24	0.43	0.38	0.52	0.41	0.30
FeO	12.62	12.50	12.23	12.50	12.38	12.21	13.04
MnO	0.24	0.27	0.21	0.27	0.24	0.27	0.21
MgO	24.99	24.30	24.68	24.66	24.28	24.35	24.46
CaO	0.06	0.05	0.04	0.06	0.05	0.07	0.05
Na_2O	0.01	0.10	0.01	0.01	0.01	0.01	0.00
K_2O	0.00	0.02	0.00	0.00	0.00	0.00	0.00
H_2O*	12.47	12.32	12.36	12.41	12.29	12.19	12.35
Total	102.00	100.82	101.03	101.53	100.57	99.69	101.29
Si	5.43	5.36	5.41	5.40	5.43	5.45	5.40
Al^{iv}	2.57	2.64	2.59	2.60	2.57	2.55	2.60
Al^{vi}	2.65	2.73	2.69	2.69	2.70	2.65	2.66
Ti	0.01	0.00	0.00	0.00	0.00	0.00	0.01
Cr	0.00	0.00	0.00	0.00	0.00	0.00	0.00
Fe^{3+}	0.05	0.04	0.06	0.05	0.08	0.06	0.04
Fe^{2+}	2.03	2.03	1.98	2.02	2.02	2.01	2.12
Mn	0.04	0.04	0.03	0.04	0.04	0.05	0.03
Mg	7.16	7.04	7.13	7.10	7.05	7.14	7.07
Ca	0.01	0.01	0.01	0.01	0.01	0.02	0.01

Na	0.01	0.08	0.01	0.01	0.00	0.00	0.00
K	0.00	0.01	0.00	0.00	0.00	0.00	0.00
*OH**	16.00	16.00	16.00	16.00	16.00	16.00	16.00
Total	35.94	35.99	35.92	35.93	35.90	35.92	35.94
Oxidized	yes	yes	yes	yes	yes	yes	yes
Fe/Fe+Mg	0.225	0.227	0.223	0.226	0.229	0.225	0.234

Sample #	*22-750-28-05-S02*	*22-750-28-05-S02*	*22-750-28-05-S02*	*22-750-28-05-S03*	*22-750-28-05-S03*	*22-750-28-05-S03*	*22-750-28-05-S03*
SiO_2	28.84	28.24	28.15	28.66	28.73	28.62	29.05
TiO_2	0.02	0.00	0.02	0.01	0.02	0.00	0.01
Al_2O_3	22.70	22.98	22.92	23.04	22.60	23.10	22.14
Cr_2O_3	0.01	0.01	0.00	0.01	0.04	0.01	0.10
Fe_2O_3	1.16	0.72	0.60	1.11	0.84	1.23	0.99
FeO	11.61	12.21	12.52	11.77	11.62	11.77	11.34
MnO	0.22	0.25	0.25	0.19	0.20	0.23	0.24
MgO	24.26	24.35	24.39	23.71	24.64	23.77	24.74
CaO	0.05	0.07	0.07	0.32	0.15	0.10	0.12
Na_2O	0.00	0.00	0.00	0.06	0.03	0.00	0.01
K_2O	0.00	0.00	0.00	0.02	0.01	0.00	0.01
H_2O*	12.41	12.37	12.37	12.39	12.42	12.39	12.41
Total	101.26	101.16	101.26	101.28	101.30	101.22	101.16
Si	5.56	5.47	5.45	5.53	5.54	5.52	5.60
Al^{iv}	2.44	2.53	2.55	2.47	2.46	2.48	2.40
Al^{vi}	2.73	2.72	2.69	2.78	2.68	2.80	2.65
Ti	0.00	0.00	0.00	0.00	0.00	0.00	0.00
Cr	0.00	0.00	0.00	0.00	0.01	0.00	0.01
Fe^{3+}	0.17	0.10	0.09	0.16	0.12	0.18	0.14
Fe^{2+}	1.87	1.98	2.03	1.90	1.87	1.90	1.83
Mn	0.04	0.04	0.04	0.03	0.03	0.04	0.04

Mg	6.97	7.02	7.04	6.82	7.08	6.84	7.11
Ca	0.01	0.01	0.01	0.07	0.03	0.02	0.03
Na	0.00	0.00	0.00	0.04	0.02	0.00	0.01
K	0.00	0.00	0.00	0.01	0.00	0.00	0.00
*OH**	16.00	16.00	16.00	16.00	16.00	16.00	16.00
Total	35.78	35.86	35.88	35.82	35.86	35.78	35.82
Oxidized	yes	yes	yes	yes	yes	yes	yes
Fe/Fe+Mg	0.226	0.228	0.231	0.232	0.220	0.233	0.217

Sample #	*22-750-28-05-S03*	*22-750-28-05-S03*	*22-750-28-05-S03*	*22-750-28-05-S04*	*22-750-28-05-S04*	*22-750-28-05-S04*	*22-750-28-05-S05*
SiO_2	27.11	27.38	27.53	27.48	27.64	28.25	27.74
TiO_2	0.07	0.03	0.04	0.00	0.01	0.04	0.03
Al_2O_3	23.64	23.50	23.45	23.22	23.33	22.85	22.86
Cr_2O_3	0.02	0.01	0.00	0.06	0.02	0.04	0.00
Fe_2O_3	0.34	0.22	0.29	0.56	0.49	0.51	0.27
FeO	13.31	13.93	13.16	12.42	12.87	12.63	13.44
MnO	0.23	0.24	0.23	0.25	0.24	0.24	0.25
MgO	23.52	23.71	24.06	23.84	23.91	24.58	24.10
CaO	0.06	0.06	0.07	0.10	0.05	0.04	0.07
Na_2O	0.02	0.01	0.02	0.00	0.01	0.00	0.01
K_2O	0.01	0.00	0.01	0.01	0.00	0.00	0.00
H_2O*	12.24	12.32	12.33	12.23	12.30	12.41	12.30
Total	100.57	101.41	101.18	100.14	100.87	101.58	101.03
Si	5.31	5.33	5.35	5.38	5.38	5.45	5.41
Al^{iv}	2.69	2.67	2.65	2.62	2.62	2.55	2.59
Al^{vi}	2.77	2.72	2.73	2.75	2.74	2.66	2.66
Ti	0.01	0.00	0.01	0.00	0.00	0.01	0.00
Cr	0.00	0.00	0.00	0.01	0.00	0.01	0.00
Fe^{3+}	0.05	0.03	0.04	0.08	0.07	0.07	0.04

Fe^{2+}	2.18	2.27	2.14	2.03	2.10	2.04	2.19
Mn	0.04	0.04	0.04	0.04	0.04	0.04	0.04
Mg	6.86	6.88	6.97	6.96	6.94	7.08	7.00
Ca	0.01	0.01	0.01	0.02	0.01	0.01	0.01
Na	0.01	0.01	0.02	0.00	0.01	0.00	0.01
K	0.01	0.00	0.00	0.00	0.00	0.00	0.00
*OH**	16.00	16.00	16.00	16.00	16.00	16.00	16.00
Total	35.94	35.96	35.95	35.89	35.91	35.91	35.95
Oxidized	yes	yes	yes	yes	yes	yes	yes
Fe/Fe+Mg	0.245	0.251	0.238	0.233	0.238	0.230	0.242

Sample #	*22-750-28-05-S05*	*22-750-28-05-S06*	*22-750-28-05-S06*	*22-750-28-05-S07*	*22-750-28-05-S07*	*22-750-28-05-S07*	*22-750-28-05-S07*
SiO_2	28.16	28.41	28.65	28.07	27.50	28.22	27.60
TiO_2	0.02	0.04	0.00	0.03	0.01	0.00	0.05
Al_2O_3	21.64	22.61	22.53	22.94	23.40	22.59	23.57
Cr_2O_3	0.01	0.03	0.07	0.06	0.07	0.04	0.03
Fe_2O_3	0.75	0.77	0.90	0.29	0.23	0.86	0.51
FeO	11.95	12.05	11.86	13.13	13.29	12.00	12.91
MnO	0.22	0.24	0.20	0.28	0.24	0.20	0.23
MgO	23.85	24.40	24.49	24.68	24.11	24.10	23.88
CaO	0.09	0.08	0.09	0.01	0.02	0.03	0.02
Na_2O	0.04	0.00	0.00	0.00	0.01	0.00	0.02
K_2O	0.03	0.00	0.00	0.00	0.02	0.00	0.00
H_2O*	12.09	12.35	12.38	12.43	12.33	12.27	12.34
Total	98.86	100.96	101.14	101.90	101.24	100.27	101.16
Si	5.58	5.51	5.54	5.42	5.34	5.51	5.36
Al^{iv}	2.42	2.49	2.46	2.58	2.66	2.49	2.64
Al^{vi}	2.64	2.68	2.68	2.64	2.71	2.71	2.76
Ti	0.00	0.01	0.00	0.00	0.00	0.00	0.01

Cr	0.00	0.00	0.01	0.01	0.01	0.01	0.00
Fe^{3+}	0.11	0.11	0.13	0.04	0.03	0.13	0.07
Fe^{2+}	1.98	1.95	1.92	2.12	2.16	1.96	2.10
Mn	0.04	0.04	0.03	0.05	0.04	0.03	0.04
Mg	7.04	7.05	7.06	7.10	6.99	7.01	6.91
Ca	0.02	0.02	0.02	0.00	0.00	0.01	0.00
Na	0.03	0.00	0.00	0.00	0.01	0.00	0.02
K	0.02	0.00	0.00	0.00	0.01	0.00	0.00
*OH**	16.00	16.00	16.00	16.00	16.00	16.00	16.00
Total	35.87	35.86	35.83	35.94	35.96	35.84	35.91
Oxidized	yes	yes	yes	yes	yes	yes	yes
Fe/Fe+Mg	0.229	0.227	0.225	0.233	0.239	0.229	0.239

Sample #	*22-750-28-05-S09*	*22-750-28-05-S09*	*22-750-28-05-S09*	*22-750-28-05-S13*	*22-750-28-05-S13*	*22-750-28-05-S14*	*22-750-28-05-S14*
SiO_2	28.09	27.88	28.07	27.69	27.35	28.09	27.60
TiO_2	0.02	0.01	0.03	0.01	0.05	0.00	0.03
Al_2O_3	23.20	23.15	23.20	23.69	23.94	23.08	24.35
Cr_2O_3	0.01	0.01	0.01	0.00	0.00	0.00	0.01
Fe_2O_3	0.49	0.38	0.70	0.35	0.37	0.96	0.55
FeO	12.53	12.98	12.29	12.82	13.43	11.80	12.74
MnO	0.22	0.22	0.23	0.22	0.22	0.26	0.23
MgO	24.57	24.26	24.02	24.42	23.80	23.85	24.06
CaO	0.11	0.12	0.30	0.01	0.01	0.06	0.02
Na_2O	0.00	0.01	0.01	0.01	0.00	0.00	0.01
K_2O	0.00	0.00	0.00	0.00	0.00	0.00	0.00
*H_2O**	12.42	12.36	12.37	12.41	12.36	12.28	12.46
Total	101.64	101.37	101.21	101.63	101.52	100.34	102.06
Si	5.42	5.40	5.44	5.35	5.30	5.47	5.30
Al^{iv}	2.58	2.60	2.56	2.65	2.70	2.53	2.70

Al^{vi}	2.70	2.70	2.74	2.74	2.78	2.79	2.83
Ti	0.00	0.00	0.00	0.00	0.01	0.00	0.00
Cr	0.00	0.00	0.00	0.00	0.00	0.00	0.00
Fe^{3+}	0.07	0.06	0.10	0.05	0.05	0.14	0.08
Fe^{2+}	2.02	2.10	1.99	2.07	2.18	1.92	2.05
Mn	0.04	0.04	0.04	0.04	0.04	0.04	0.04
Mg	7.06	7.01	6.93	7.03	6.88	6.93	6.89
Ca	0.02	0.02	0.06	0.00	0.00	0.01	0.00
Na	0.00	0.01	0.01	0.01	0.00	0.00	0.01
K	0.00	0.00	0.00	0.00	0.00	0.00	0.00
*OH**	16.00	16.00	16.00	16.00	16.00	16.00	16.00
Total	35.90	35.93	35.87	35.94	35.93	35.82	35.90
Oxidized	yes	yes	yes	yes	yes	yes	yes
Fe/Fe+Mg	0.229	0.236	0.232	0.232	0.245	0.229	0.236

Sample #	*22-750-28-05-S14*	*22-750-28-05-S14*	*22-750-28-05-S15*	*22-750-28-05-S15*	*22-750-28-05-S15*	*22-750-28-05-S15*	*21-503-08-01-S1*
SiO_2	27.67	27.62	27.88	27.68	27.77	28.27	27.07
TiO_2	0.04	0.03	0.05	0.02	0.03	0.01	0.10
Al_2O_3	23.65	23.72	23.44	24.04	23.48	23.30	22.20
Cr_2O_3	0.01	0.00	0.00	0.00	0.00	0.01	0.00
Fe_2O_3	0.41	0.41	0.57	0.46	0.38	0.55	0.00
FeO	12.86	12.89	12.50	13.02	12.94	12.49	20.47
MnO	0.26	0.22	0.24	0.22	0.23	0.25	0.23
MgO	24.12	24.23	24.20	24.14	24.25	24.61	20.05
CaO	0.04	0.01	0.04	0.02	0.03	0.06	0.04
Na_2O	0.04	0.00	0.01	0.00	0.03	0.01	0.00
K_2O	0.00	0.00	0.00	0.00	0.00	0.00	0.02
H_2O*	12.38	12.39	12.38	12.45	12.39	12.47	12.06
Total	101.48	101.52	101.31	102.04	101.51	102.03	102.23

Si	5.35	5.34	5.39	5.33	5.37	5.43	5.38
Al iv	2.65	2.66	2.61	2.67	2.63	2.57	2.62
Al vi	2.75	2.76	2.75	2.79	2.73	2.71	2.59
Ti	0.01	0.00	0.01	0.00	0.00	0.00	0.01
Cr	0.00	0.00	0.00	0.00	0.00	0.00	0.00
Fe^{3+}	0.06	0.06	0.08	0.07	0.06	0.08	0.00
Fe^{2+}	2.08	2.08	2.02	2.10	2.09	2.01	3.41
Mn	0.04	0.04	0.04	0.04	0.04	0.04	0.04
Mg	6.95	6.98	6.98	6.93	6.99	7.04	5.94
Ca	0.01	0.00	0.01	0.00	0.01	0.01	0.01
Na	0.03	0.00	0.01	0.00	0.02	0.01	0.00
K	0.00	0.00	0.00	0.00	0.00	0.00	0.01
*OH**	16.00	16.00	16.00	16.00	16.00	16.00	16.00
Total	35.94	35.92	35.90	35.92	35.94	35.90	36.01
Oxidized	yes	yes	yes	yes	yes	yes	yes
Fe/Fe+Mg	0.235	0.235	0.232	0.238	0.235	0.228	0.364

Sample #	*21-503-08-01-S1*	*21-503-08-01-S1*	*21-503-08-01-S1*	*21-503-08-01-S2*	*21-503-08-01-S2*	*21-503-08-01-S2*	*21-503-08-01-S2*
SiO_2	26.46	26.27	26.90	26.62	26.75	26.85	26.82
TiO_2	0.00	0.05	0.04	0.00	0.04	0.06	0.04
Al_2O_3	23.03	22.91	22.55	22.89	22.34	22.22	22.68
Cr_2O_3	0.01	0.01	0.00	0.01	0.02	0.00	0.01
Fe_2O_3	0.00	0.00	0.00	0.14	0.07	0.01	0.20
FeO	20.61	22.20	19.95	19.83	20.88	21.59	20.47
MnO	0.25	0.26	0.21	0.24	0.20	0.20	0.20
MgO	19.60	18.49	20.39	19.73	19.29	19.13	19.47
CaO	0.00	0.01	0.01	0.00	0.01	0.00	0.00
Na_2O	0.02	0.03	0.00	0.01	0.00	0.01	0.00
K_2O	0.00	0.00	0.02	0.00	0.04	0.02	0.00
H_2O*	12.02	11.95	12.08	12.00	11.95	11.98	12.01

Total	101.98	102.18	102.14	101.46	101.59	102.09	101.89
Si	5.28	5.27	5.34	5.32	5.36	5.37	5.35
Al ^{iv}	2.72	2.73	2.66	2.68	2.64	2.63	2.65
Al ^{vi}	2.69	2.69	2.62	2.71	2.65	2.62	2.69
Ti	0.00	0.01	0.01	0.00	0.01	0.01	0.01
Cr	0.00	0.00	0.00	0.00	0.00	0.00	0.00
Fe^{3+}	0.00	0.00	0.00	0.02	0.01	0.00	0.03
Fe^{2+}	3.45	3.74	3.33	3.32	3.50	3.61	3.42
Mn	0.04	0.04	0.04	0.04	0.03	0.03	0.03
Mg	5.83	5.53	6.03	5.88	5.77	5.71	5.79
Ca	0.00	0.00	0.00	0.00	0.00	0.00	0.00
Na	0.02	0.02	0.00	0.01	0.00	0.01	0.00
K	0.00	0.00	0.01	0.00	0.02	0.01	0.00
*OH**	16.00	16.00	16.00	16.00	16.00	16.00	16.00
Total	36.02	36.03	36.03	35.97	35.99	36.00	35.96
Oxidized	yes	yes	yes	yes	yes	yes	yes
Fe/Fe+Mg	0.372	0.403	0.356	0.362	0.379	0.388	0.373

Sample #	*21-503-08-01-S2*	*21-503-08-01-S3*	*21-503-08-01-S3*	*21-503-08-01-S3*	*21-503-08-01-S4*	*21-503-08-01-S4*	*21-503-08-01-S4*
SiO_2	26.85	26.98	26.75	26.76	26.51	26.80	27.06
TiO_2	0.03	0.04	0.03	0.04	0.03	0.05	0.04
Al_2O_3	22.55	22.20	22.45	22.34	21.80	22.02	21.49
Cr_2O_3	0.01	0.00	0.00	0.01	0.04	0.01	0.00
Fe_2O_3	0.05	0.00	0.00	0.00	0.00	0.18	0.02
FeO	20.53	20.18	20.10	20.93	19.80	20.81	21.36
MnO	0.22	0.24	0.21	0.26	0.22	0.21	0.20
MgO	19.64	20.31	20.15	19.46	19.99	19.12	19.43
CaO	0.01	0.01	0.00	0.00	0.02	0.01	0.01
Na_2O	0.01	0.00	0.01	0.02	0.09	0.01	0.00

K_2O	0.03	0.00	0.01	0.00	0.00	0.00	0.00
H_2O*	12.02	12.05	12.02	11.98	11.85	11.90	11.92
Total	101.95	102.00	101.72	101.79	100.36	101.13	101.51
Si	5.35	5.37	5.34	5.36	5.36	5.40	5.44
Al^{iv}	2.65	2.63	2.66	2.64	2.64	2.60	2.56
Al^{vi}	2.66	2.58	2.62	2.63	2.56	2.63	2.54
Ti	0.01	0.01	0.00	0.01	0.00	0.01	0.01
Cr	0.00	0.00	0.00	0.00	0.01	0.00	0.00
Fe^{3+}	0.01	0.00	0.00	0.00	0.00	0.03	0.00
Fe^{2+}	3.42	3.37	3.37	3.51	3.39	3.51	3.59
Mn	0.04	0.04	0.04	0.04	0.04	0.04	0.03
Mg	5.84	6.03	5.99	5.81	6.02	5.74	5.83
Ca	0.00	0.00	0.00	0.00	0.00	0.00	0.00
Na	0.01	0.00	0.00	0.02	0.07	0.01	0.00
K	0.01	0.00	0.01	0.00	0.00	0.00	0.00
*OH**	16.00	16.00	16.00	16.00	16.00	16.00	16.00
Total	36.00	36.02	36.03	36.01	36.09	35.97	35.99
Oxidized	yes	yes	yes	yes	yes	yes	yes
Fe/Fe+Mg	0.370	0.359	0.360	0.376	0.360	0.381	0.382

Sample #	*21-503-08-01-S4*	*21-503-08-01-S4*	*21-503-08-01-S5*	*21-503-08-01-S5*	*21-503-08-01-S5*	*21-503-08-01-S5*	*21-503-08-01-S5*
SiO_2	26.68	26.99	26.63	26.82	26.98	26.45	27.01
TiO_2	0.03	0.02	0.04	0.01	0.06	0.03	0.07
Al_2O_3	21.77	21.71	22.28	22.08	22.08	22.41	21.97
Cr_2O_3	0.00	0.02	0.01	0.01	0.01	0.00	0.06
Fe_2O_3	0.00	0.00	0.00	0.12	0.26	0.00	0.16
FeO	20.51	21.57	20.52	20.75	20.67	20.41	19.60
MnO	0.23	0.23	0.21	0.24	0.23	0.23	0.23
MgO	19.63	19.31	20.13	19.10	19.27	19.61	20.15

CaO	0.01	0.01	0.01	0.03	0.01	0.00	0.01
Na_2O	0.00	0.00	0.02	0.05	0.00	0.03	0.00
K_2O	0.01	0.00	0.00	0.03	0.00	0.00	0.00
*H_2O**	11.87	11.95	12.00	11.90	11.95	11.92	11.97
Total	100.73	101.80	101.85	101.11	101.49	101.10	101.20
Si	5.39	5.42	5.31	5.40	5.41	5.32	5.41
Al^{iv}	2.61	2.58	2.69	2.60	2.59	2.68	2.59
Al^{vi}	2.58	2.56	2.56	2.65	2.64	2.64	2.60
Ti	0.00	0.00	0.01	0.00	0.01	0.00	0.01
Cr	0.00	0.00	0.00	0.00	0.00	0.00	0.01
Fe^{3+}	0.00	0.00	0.00	0.02	0.04	0.00	0.02
Fe^{2+}	3.48	3.63	3.47	3.50	3.47	3.45	3.28
Mn	0.04	0.04	0.04	0.04	0.04	0.04	0.04
Mg	5.91	5.78	5.99	5.74	5.76	5.88	6.02
Ca	0.00	0.00	0.00	0.01	0.00	0.00	0.00
Na	0.00	0.00	0.01	0.04	0.00	0.02	0.00
K	0.01	0.00	0.00	0.01	0.00	0.00	0.00
*OH**	16.00	16.00	16.00	16.00	16.00	16.00	16.00
Total	36.01	36.01	36.08	36.00	35.95	36.03	35.96
Oxidized	yes	yes	yes	yes	yes	yes	yes
Fe/Fe+Mg	0.370	0.386	0.367	0.380	0.378	0.370	0.355

Sample #	*21-503-08-01-S6*	*21-503-08-01-S6*	*21-503-08-01-S6*	*21-503-08-01-S6*	*21-503-08-01-S7*	*21-503-08-01-S7*	*21-503-08-01-S8*
SiO_2	26.84	26.71	26.71	26.87	27.08	27.46	26.59
TiO_2	0.07	0.10	0.05	0.04	0.03	0.06	0.04
Al_2O_3	22.35	22.24	22.11	22.11	21.82	21.17	22.99
Cr_2O_3	0.01	0.01	0.00	0.00	0.10	0.03	0.00
Fe_2O_3	0.00	0.00	0.00	0.00	0.02	0.13	0.00
FeO	20.54	20.45	20.51	21.16	20.76	20.94	20.51

MnO	0.21	0.26	0.24	0.26	0.22	0.22	0.20
MgO	19.84	19.74	19.98	19.81	19.67	19.60	19.73
CaO	0.01	0.01	0.01	0.01	0.01	0.02	0.00
Na_2O	0.00	0.02	0.00	0.00	0.03	0.03	0.00
K_2O	0.15	0.11	0.00	0.00	0.01	0.00	0.00
*H_2O**	12.02	11.97	11.97	12.02	11.98	11.95	12.04
Total	102.01	101.63	101.60	102.28	101.73	101.61	102.09
Si	5.35	5.34	5.35	5.35	5.42	5.51	5.30
Al^{iv}	2.65	2.66	2.65	2.65	2.58	2.49	2.70
Al^{vi}	2.61	2.59	2.57	2.55	2.57	2.51	2.69
Ti	0.01	0.01	0.01	0.01	0.01	0.01	0.01
Cr	0.00	0.00	0.00	0.00	0.02	0.00	0.00
Fe^{3+}	0.00	0.00	0.00	0.00	0.00	0.02	0.00
Fe^{2+}	3.44	3.45	3.46	3.56	3.48	3.51	3.42
Mn	0.04	0.04	0.04	0.04	0.04	0.04	0.03
Mg	5.90	5.89	5.96	5.89	5.87	5.86	5.86
Ca	0.00	0.00	0.00	0.00	0.00	0.01	0.00
Na	0.00	0.02	0.00	0.00	0.02	0.02	0.00
K	0.08	0.06	0.00	0.00	0.00	0.00	0.00
*OH**	16.00	16.00	16.00	16.00	16.00	16.00	16.00
Total	36.04	36.06	36.04	36.05	36.01	35.98	36.00
Oxidized	yes	yes	yes	yes	yes	yes	yes
Fe/Fe+Mg	0.369	0.369	0.367	0.377	0.372	0.376	0.369

Sample #	*21-503-08-01-S8*	*21-503-08-01-S8*	*21-503-08-01-S8*	*21-503-08-01-S8*	*21-503-08-01-S8*	*21-503-08-01-S9*	*21-503-08-01-S9*
SiO_2	26.46	26.76	26.46	26.80	27.03	26.86	26.88
TiO_2	0.02	0.02	0.01	0.04	0.00	0.01	0.03
Al_2O_3	22.85	22.35	22.62	22.50	21.84	22.40	22.25
Cr_2O_3	0.00	0.01	0.00	0.00	0.02	0.00	0.01

Fe_2O_3	0.06	0.03	0.00	0.00	0.00	0.02	0.00
FeO	20.62	20.47	21.55	20.78	20.82	20.20	20.61
MnO	0.25	0.24	0.29	0.22	0.21	0.21	0.22
MgO	19.30	19.60	19.14	19.86	20.02	20.03	19.91
CaO	0.02	0.00	0.00	0.01	0.01	0.00	0.01
Na_2O	0.00	0.00	0.01	0.00	0.00	0.00	0.00
K_2O	0.01	0.05	0.00	0.00	0.00	0.00	0.02
H_2O*	11.96	11.96	11.97	12.04	12.01	12.02	12.02
Total	101.53	101.48	102.04	102.24	101.95	101.73	101.94
Si	5.30	5.36	5.30	5.33	5.40	5.36	5.36
Al^{iv}	2.70	2.64	2.70	2.67	2.60	2.64	2.64
Al^{vi}	2.71	2.65	2.64	2.62	2.54	2.63	2.60
Ti	0.00	0.00	0.00	0.01	0.00	0.00	0.00
Cr	0.00	0.00	0.00	0.00	0.00	0.00	0.00
Fe^{3+}	0.01	0.00	0.00	0.00	0.00	0.00	0.00
Fe^{2+}	3.46	3.43	3.63	3.47	3.50	3.37	3.45
Mn	0.04	0.04	0.05	0.04	0.04	0.04	0.04
Mg	5.77	5.86	5.71	5.89	5.96	5.96	5.92
Ca	0.00	0.00	0.00	0.00	0.00	0.00	0.00
Na	0.00	0.00	0.00	0.00	0.00	0.00	0.00
K	0.01	0.02	0.00	0.00	0.00	0.00	0.01
*OH**	16.00	16.00	16.00	16.00	16.00	16.00	16.00
Total	35.99	36.00	36.04	36.02	36.03	35.99	36.01
Oxidized	yes	yes	yes	yes	yes	yes	yes
Fe/Fe+Mg	0.375	0.370	0.389	0.371	0.370	0.362	0.368

Sample #	*21-503-08-01-S9*	*21-503-08-01-s!0*	*21-503-08-01-S12*	*21-503-08-01-S12*	*21-503-08-01-S12*	*21-503-08-01-S12*	*21-503-08-02-S1*
SiO_2	26.74	27.57	26.87	26.57	26.82	26.86	26.77
TiO_2	0.03	0.05	0.03	0.01	0.05	0.04	0.00

Al_2O_3	21.99	21.37	22.23	20.68	22.47	22.23	21.96
Cr_2O_3	0.00	0.19	0.00	0.01	0.00	0.00	0.00
Fe_2O_3	0.00	0.38	0.02	0.00	0.00	0.00	0.00
FeO	21.26	20.40	20.16	19.20	20.70	20.87	21.50
MnO	0.22	0.22	0.23	0.18	0.23	0.21	0.22
MgO	19.18	19.23	20.01	19.53	19.85	19.86	19.33
CaO	0.02	0.32	0.01	0.04	0.00	0.00	0.02
Na_2O	0.04	0.04	0.00	0.13	0.00	0.03	0.00
K_2O	0.02	0.00	0.00	0.03	0.00	0.00	0.00
H_2O*	11.91	11.98	11.99	11.59	12.04	12.02	11.93
Total	101.41	101.75	101.53	97.96	102.15	102.09	101.67
Si	5.38	5.51	5.37	5.50	5.34	5.35	5.38
Al^{iv}	2.62	2.49	2.63	2.50	2.66	2.65	2.62
Al^{vi}	2.60	2.56	2.62	2.54	2.62	2.58	2.58
Ti	0.00	0.01	0.00	0.00	0.01	0.01	0.00
Cr	0.00	0.03	0.00	0.00	0.00	0.00	0.00
Fe^{3+}	0.00	0.06	0.00	0.00	0.00	0.00	0.00
Fe^{2+}	3.59	3.41	3.37	3.32	3.46	3.50	3.63
Mn	0.04	0.04	0.04	0.03	0.04	0.04	0.04
Mg	5.75	5.73	5.97	6.02	5.89	5.90	5.79
Ca	0.00	0.07	0.00	0.01	0.00	0.00	0.00
Na	0.04	0.03	0.00	0.10	0.00	0.03	0.00
K	0.01	0.00	0.00	0.01	0.00	0.00	0.00
*OH**	16.00	16.00	16.00	16.00	16.00	16.00	16.00
Total	36.03	35.94	35.99	36.05	36.01	36.04	36.02
Oxidized	yes	yes	yes	yes	yes	yes	yes
Fe/Fe+Mg	0.384	0.377	0.361	0.356	0.370	0.373	0.385

Sample #	*21-503-08-02-S1*	*21-503-08-02-S1*	*21-503-08-02-S1*	*21-503-08-02-S1*	*21-503-08-02-S2*	*21-503-08-02-S2*	*21-503-08-02-S2*
SiO_2	27.13	27.54	27.19	26.74	27.43	26.65	27.00

TiO_2	0.03	0.20	0.04	0.05	0.05	0.04	0.03
Al_2O_3	22.04	22.07	21.62	21.27	20.72	22.11	22.00
Cr_2O_3	0.00	0.01	0.02	0.00	0.00	0.01	0.01
Fe_2O_3	0.00	0.52	0.12	0.10	0.12	0.04	0.04
FeO	20.71	19.45	20.95	20.96	20.40	21.22	20.48
MnO	0.22	0.23	0.21	0.23	0.22	0.22	0.18
MgO	20.07	19.98	19.57	18.87	19.80	19.15	19.80
CaO	0.01	0.14	0.02	0.03	0.05	0.01	0.01
Na_2O	0.01	0.00	0.00	0.06	0.02	0.00	0.03
K_2O	0.01	0.00	0.00	0.00	0.00	0.00	0.00
H_2O*	12.05	12.09	11.96	11.75	11.86	11.90	11.98
Total	102.29	102.21	101.68	100.02	100.66	101.32	101.53
Si	5.39	5.46	5.45	5.46	5.54	5.37	5.41
Al^{iv}	2.61	2.54	2.55	2.54	2.46	2.63	2.59
Al^{vi}	2.56	2.61	2.56	2.57	2.48	2.62	2.60
Ti	0.00	0.03	0.01	0.01	0.01	0.01	0.00
Cr	0.00	0.00	0.00	0.00	0.00	0.00	0.00
Fe^{3+}	0.00	0.08	0.02	0.02	0.02	0.01	0.01
Fe^{2+}	3.46	3.22	3.51	3.58	3.45	3.58	3.43
Mn	0.04	0.04	0.04	0.04	0.04	0.04	0.03
Mg	5.95	5.90	5.85	5.74	5.97	5.75	5.91
Ca	0.00	0.03	0.00	0.01	0.01	0.00	0.00
Na	0.01	0.00	0.00	0.05	0.01	0.00	0.02
K	0.00	0.00	0.00	0.00	0.00	0.00	0.00
*OH**	16.00	16.00	16.00	16.00	16.00	16.00	16.00
Total	36.03	35.89	35.97	35.99	35.98	35.98	36.00
Oxidized	yes	yes	yes	yes	yes	yes	yes
Fe/Fe+Mg	0.368	0.359	0.376	0.385	0.368	0.384	0.368

Sample #	*21-503-08-02-S2*	*21-503-08-02-S2*	*21-503-08-02-S3*	*21-503-08-02-S3*	*21-503-08-02-S3*	*21-503-08-02-S3*	*21-503-08-02-S4*
SiO_2	27.03	27.02	26.82	26.92	27.11	26.88	27.18
TiO_2	0.03	0.06	0.04	0.04	0.06	0.04	0.06
Al_2O_3	21.86	21.85	22.33	22.22	22.37	22.34	21.41
Cr_2O_3	0.00	0.01	0.02	0.01	0.00	0.00	0.18
Fe_2O_3	0.00	0.06	0.15	0.00	0.02	0.23	0.01
FeO	20.29	20.88	19.95	20.55	20.48	20.40	20.82
MnO	0.23	0.27	0.23	0.26	0.23	0.20	0.22
MgO	20.15	19.52	19.71	19.97	20.01	19.53	19.74
CaO	0.03	0.02	0.00	0.00	0.02	0.00	0.02
Na_2O	0.01	0.01	0.01	0.00	0.02	0.00	0.02
K_2O	0.00	0.00	0.01	0.04	0.00	0.00	0.01
H_2O*	11.99	11.96	11.96	12.03	12.08	11.98	11.96
Total	101.59	101.64	101.24	102.03	102.40	101.55	101.61
Si	5.40	5.42	5.38	5.36	5.38	5.38	5.45
Al^{iv}	2.60	2.58	2.62	2.64	2.62	2.62	2.55
Al^{vi}	2.56	2.58	2.66	2.59	2.61	2.66	2.51
Ti	0.01	0.01	0.01	0.01	0.01	0.01	0.01
Cr	0.00	0.00	0.00	0.00	0.00	0.00	0.03
Fe^{3+}	0.00	0.01	0.02	0.00	0.00	0.03	0.00
Fe^{2+}	3.40	3.50	3.34	3.44	3.40	3.42	3.49
Mn	0.04	0.05	0.04	0.04	0.04	0.03	0.04
Mg	6.01	5.83	5.89	5.93	5.92	5.83	5.90
Ca	0.01	0.00	0.00	0.00	0.00	0.00	0.00
Na	0.01	0.01	0.01	0.00	0.02	0.00	0.01
K	0.00	0.00	0.01	0.02	0.00	0.00	0.01
*OH**	16.00	16.00	16.00	16.00	16.00	16.00	16.00
Total	36.02	35.99	35.98	36.03	36.00	35.95	36.01
Oxidized	yes	yes	yes	yes	yes	yes	yes
Fe/Fe+Mg	0.362	0.376	0.364	0.367	0.365	0.372	0.372

Sample #	*21-503-08-02-S4*	*21-503-08-02-S4*	*21-503-08-02-S5*	*21-503-08-02-S6*	*21-503-08-02-S6*	*21-503-08-02-S6*	*21-503-08-02-S6*
SiO_2	27.46	27.11	28.42	26.44	27.04	26.78	27.07
TiO_2	0.09	0.04	0.23	0.05	0.04	0.05	0.06
Al_2O_3	21.38	21.63	19.00	22.48	21.94	22.20	21.94
Cr_2O_3	0.23	0.18	0.15	0.06	0.02	0.08	0.04
Fe_2O_3	0.26	0.15	1.11	0.09	0.12	0.00	0.18
FeO	20.03	19.49	21.08	21.81	20.30	20.92	19.60
MnO	0.21	0.21	0.23	0.23	0.19	0.23	0.25
MgO	19.83	20.27	17.65	18.58	19.84	19.53	20.10
CaO	0.02	0.02	0.22	0.02	0.01	0.00	0.00
Na_2O	0.00	0.00	0.05	0.00	0.00	0.01	0.00
K_2O	0.09	0.00	0.06	0.00	0.00	0.00	0.00
H_2O*	11.98	11.95	11.67	11.91	11.97	11.98	11.97
Total	101.58	101.04	99.86	101.64	101.45	101.78	101.20
Si	5.49	5.44	5.82	5.33	5.42	5.36	5.42
Al^{iv}	2.51	2.56	2.18	2.67	2.58	2.64	2.58
Al^{vi}	2.54	2.55	2.42	2.67	2.60	2.60	2.60
Ti	0.01	0.01	0.03	0.01	0.01	0.01	0.01
Cr	0.04	0.03	0.02	0.01	0.00	0.01	0.01
Fe^{3+}	0.04	0.02	0.17	0.01	0.02	0.00	0.03
Fe^{2+}	3.35	3.27	3.61	3.67	3.40	3.51	3.28
Mn	0.04	0.04	0.04	0.04	0.03	0.04	0.04
Mg	5.91	6.06	5.39	5.58	5.92	5.83	6.00
Ca	0.00	0.00	0.05	0.00	0.00	0.00	0.00
Na	0.00	0.00	0.04	0.00	0.00	0.01	0.00
K	0.05	0.00	0.03	0.00	0.00	0.00	0.00
*OH**	16.00	16.00	16.00	16.00	16.00	16.00	16.00
Total	35.97	35.96	35.81	35.98	35.97	36.01	35.96
Oxidized	yes	yes	yes	yes	yes	yes	yes

Fe/Fe+Mg	0.364	0.352	0.412	0.398	0.366	0.376	0.356

Sample #	*21-503-08-02-S7*	*21-503-08-02-S7*	*21-503-08-02-S7*	*21-503-08-02-S7*	*21-503-08-02-S7*	*21-503-08-02-S7*	*21-503-08-02-S8*
SiO_2	26.72	26.65	26.98	27.53	27.13	26.32	27.56
TiO_2	0.02	0.05	0.00	0.14	0.07	0.07	0.12
Al_2O_3	22.62	22.18	22.07	21.85	22.57	22.60	21.19
Cr_2O_3	0.00	0.00	0.01	0.00	0.00	0.01	0.15
Fe_2O_3	0.04	0.00	0.00	0.24	0.27	0.00	0.27
FeO	20.32	21.03	21.09	20.31	19.40	22.32	20.30
MnO	0.22	0.24	0.24	0.19	0.21	0.23	0.17
MgO	19.75	19.40	19.39	19.72	20.12	18.32	19.76
CaO	0.01	0.02	0.03	0.01	0.01	0.02	0.04
Na_2O	0.01	0.03	0.04	0.00	0.02	0.02	0.00
K_2O	0.00	0.01	0.01	0.21	0.01	0.01	0.07
H_2O*	12.00	11.94	11.98	12.06	12.07	11.90	11.98
Total	101.70	101.55	101.83	102.24	101.88	101.82	101.60
Si	5.34	5.35	5.40	5.47	5.39	5.30	5.51
Al^{iv}	2.66	2.65	2.60	2.53	2.61	2.70	2.49
Al^{vi}	2.67	2.60	2.61	2.59	2.67	2.67	2.52
Ti	0.00	0.01	0.00	0.02	0.01	0.01	0.02
Cr	0.00	0.00	0.00	0.00	0.00	0.00	0.02
Fe^{3+}	0.01	0.00	0.00	0.04	0.04	0.00	0.04
Fe^{2+}	3.40	3.55	3.53	3.37	3.22	3.77	3.40
Mn	0.04	0.04	0.04	0.03	0.04	0.04	0.03
Mg	5.88	5.81	5.79	5.84	5.95	5.50	5.89
Ca	0.00	0.00	0.01	0.00	0.00	0.00	0.01
Na	0.01	0.03	0.03	0.00	0.01	0.02	0.00
K	0.00	0.01	0.00	0.11	0.00	0.00	0.04
*OH**	16.00	16.00	16.00	16.00	16.00	16.00	16.00

Total	35.99	36.04	36.02	35.99	35.95	36.01	35.96
Oxidized	yes	yes	yes	yes	yes	yes	yes
Fe/Fe+Mg	0.366	0.379	0.379	0.369	0.354	0.406	0.368

Sample #	*21-503-08-02-S8*	*21-503-08-02-S8*	*21-503-08-02-S9*	*21-503-08-02-S9*	*21-503-08-02-S9*	*21-503-08-03-S01*	*21-503-08-03-S01*
SiO_2	27.41	27.53	26.82	26.88	27.01	26.95	27.14
TiO_2	0.07	0.04	0.08	0.03	0.05	0.05	0.04
Al_2O_3	21.57	21.81	22.41	22.21	21.72	22.10	21.81
Cr_2O_3	0.04	0.03	0.00	0.00	0.00	0.00	0.02
Fe_2O_3	0.18	0.39	0.00	0.04	0.02	0.27	0.16
FeO	19.94	19.94	20.25	20.88	20.81	20.09	20.38
MnO	0.22	0.17	0.23	0.20	0.21	0.23	0.23
MgO	20.04	19.91	19.82	19.45	19.49	19.65	19.73
CaO	0.02	0.02	0.01	0.01	0.02	0.01	0.00
Na_2O	0.00	0.00	0.11	0.03	0.05	0.00	0.00
K_2O	0.06	0.00	0.06	0.00	0.01	0.00	0.00
H_2O*	12.00	12.04	12.01	11.97	11.93	11.95	11.97
Total	101.56	101.86	101.79	101.70	101.31	101.24	101.48
Si	5.48	5.48	5.35	5.38	5.43	5.41	5.44
Al^{iv}	2.52	2.52	2.65	2.62	2.57	2.59	2.56
Al^{vi}	2.56	2.60	2.62	2.63	2.58	2.64	2.59
Ti	0.01	0.01	0.01	0.00	0.01	0.01	0.01
Cr	0.01	0.01	0.00	0.00	0.00	0.00	0.00
Fe^{3+}	0.03	0.06	0.00	0.01	0.00	0.04	0.02
Fe^{2+}	3.33	3.32	3.40	3.50	3.50	3.37	3.41
Mn	0.04	0.03	0.04	0.03	0.04	0.04	0.04
Mg	5.97	5.91	5.89	5.81	5.84	5.88	5.89
Ca	0.00	0.00	0.00	0.00	0.00	0.00	0.00
Na	0.00	0.00	0.08	0.02	0.04	0.00	0.00

K	0.03	0.00	0.03	0.00	0.01	0.00	0.00
*OH**	16.00	16.00	16.00	16.00	16.00	16.00	16.00
Total	35.98	35.92	36.08	36.00	36.01	35.93	35.97
Oxidized	yes	yes	yes	yes	yes	yes	yes
Fe/Fe+Mg	0.360	0.364	0.366	0.376	0.375	0.367	0.369

Sample #	*21-503-08-03-S01*	*21-503-08-03-S01*	*21-503-08-03-S02*	*21-503-08-03-S02*	*21-503-08-03-S02*	*21-503-08-03-S02*	*21-503-08-03-S02*
SiO_2	27.18	27.21	26.17	26.95	26.36	26.33	26.93
TiO_2	0.05	0.03	0.05	0.01	0.05	0.02	0.06
Al_2O_3	21.78	21.70	21.53	21.67	22.19	22.66	21.78
Cr_2O_3	0.00	0.01	0.01	0.00	0.00	0.01	0.00
Fe_2O_3	0.23	0.27	0.38	0.02	0.04	0.21	0.16
FeO	20.39	20.37	19.53	21.22	21.04	21.59	20.74
MnO	0.22	0.22	0.19	0.20	0.22	0.28	0.25
MgO	19.57	19.48	18.53	19.28	18.94	18.21	19.27
CaO	0.00	0.01	0.04	0.01	0.01	0.01	0.02
Na_2O	0.02	0.00	0.04	0.03	0.00	0.01	0.00
K_2O	0.00	0.01	0.01	0.00	0.00	0.00	0.04
H_2O*	11.95	11.93	11.56	11.90	11.83	11.85	11.90
Total	101.38	101.25	98.04	101.28	100.68	101.19	101.13
Si	5.45	5.46	5.42	5.43	5.34	5.32	5.43
Al^{iv}	2.55	2.54	2.58	2.57	2.66	2.68	2.57
Al^{vi}	2.60	2.60	2.68	2.58	2.65	2.73	2.60
Ti	0.01	0.00	0.01	0.00	0.01	0.00	0.01
Cr	0.00	0.00	0.00	0.00	0.00	0.00	0.00
Fe^{3+}	0.03	0.04	0.06	0.00	0.01	0.03	0.02
Fe^{2+}	3.42	3.42	3.38	3.58	3.57	3.65	3.50
Mn	0.04	0.04	0.03	0.03	0.04	0.05	0.04
Mg	5.85	5.83	5.72	5.79	5.73	5.49	5.79

Ca	0.00	0.00	0.01	0.00	0.00	0.00	0.01
Na	0.02	0.00	0.04	0.02	0.00	0.00	0.00
K	0.00	0.01	0.01	0.00	0.00	0.00	0.02
*OH**	16.00	16.00	16.00	16.00	16.00	16.00	16.00
Total	35.96	35.95	35.94	36.00	35.99	35.96	35.97
Oxidized	yes	yes	yes	yes	yes	yes	yes
Fe/Fe+Mg	0.371	0.373	0.376	0.382	0.384	0.402	0.378

Sample #	*21-503-08-03-S02*	*21-503-08-03-S02*	*21-503-08-03-S05*	*21-503-08-03-S05*	*21-503-08-03-S05*	*21-503-08-03-S05*	*21-503-08-03-S06*
SiO_2	26.83	27.08	27.07	27.03	26.40	26.80	27.10
TiO_2	0.02	0.05	0.03	0.07	0.06	0.01	0.04
Al_2O_3	22.05	21.84	22.11	21.94	22.28	21.88	21.61
Cr_2O_3	0.02	0.00	0.00	0.00	0.00	0.01	0.00
Fe_2O_3	0.15	0.20	0.19	0.17	0.00	0.00	0.07
FeO	20.25	19.62	19.80	20.79	21.36	20.31	20.16
MnO	0.23	0.22	0.23	0.22	0.23	0.19	0.22
MgO	19.46	20.04	19.98	19.45	19.07	19.94	20.01
CaO	0.01	0.01	0.01	0.01	0.01	0.01	0.01
Na_2O	0.03	0.00	0.00	0.00	0.01	0.01	0.00
K_2O	0.00	0.00	0.00	0.00	0.00	0.00	0.00
H_2O*	11.90	11.95	11.99	11.96	11.89	11.92	11.94
Total	100.94	101.00	101.39	101.61	101.30	101.07	101.14
Si	5.40	5.43	5.41	5.42	5.32	5.39	5.44
Al^{iv}	2.60	2.57	2.59	2.58	2.68	2.61	2.56
Al^{vi}	2.64	2.60	2.63	2.60	2.62	2.58	2.56
Ti	0.00	0.01	0.00	0.01	0.01	0.00	0.01
Cr	0.00	0.00	0.00	0.00	0.00	0.00	0.00
Fe^{3+}	0.02	0.03	0.03	0.03	0.00	0.00	0.01
Fe^{2+}	3.41	3.29	3.31	3.48	3.62	3.43	3.39

Mn	0.04	0.04	0.04	0.04	0.04	0.03	0.04
Mg	5.84	5.99	5.96	5.81	5.73	5.98	5.99
Ca	0.00	0.00	0.00	0.00	0.00	0.00	0.00
Na	0.03	0.00	0.00	0.00	0.01	0.01	0.00
K	0.00	0.00	0.00	0.00	0.00	0.00	0.00
*OH**	16.00	16.00	16.00	16.00	16.00	16.00	16.00
Total	35.98	35.96	35.96	35.96	36.02	36.02	35.98
Oxidized	yes	yes	yes	yes	yes	yes	yes
Fe/Fe+Mg	0.370	0.357	0.359	0.377	0.387	0.364	0.362

Sample #	*21-503-08-03-S06*	*21-503-08-03-S06*	*21-503-08-03-S06*	*21-503-08-03-S07*	*21-503-08-03-S07*	*21-503-08-03-S07*	*21-503-08-03-S07*
SiO_2	27.13	26.91	26.77	26.63	27.02	26.81	26.97
TiO_2	0.04	0.07	0.03	0.03	0.02	0.03	0.01
Al_2O_3	21.41	21.70	22.13	22.00	21.85	21.53	21.88
Cr_2O_3	0.01	0.02	0.01	0.01	0.00	0.01	0.01
Fe_2O_3	0.00	0.21	0.13	0.10	0.11	0.22	0.16
FeO	20.66	19.70	20.33	19.94	19.95	19.84	19.91
MnO	0.21	0.24	0.18	0.22	0.23	0.20	0.22
MgO	19.84	19.84	19.50	19.65	20.03	19.46	19.81
CaO	0.01	0.01	0.00	0.01	0.00	0.00	0.00
Na_2O	0.02	0.00	0.01	0.01	0.00	0.02	0.00
K_2O	0.00	0.00	0.00	0.00	0.00	0.00	0.02
H_2O*	11.93	11.88	11.91	11.86	11.95	11.80	11.92
Total	101.25	100.55	101.00	100.42	101.14	99.92	100.90
Si	5.45	5.43	5.39	5.39	5.42	5.45	5.42
Al^{iv}	2.55	2.57	2.61	2.61	2.58	2.55	2.58
Al^{vi}	2.53	2.59	2.64	2.63	2.59	2.61	2.61
Ti	0.01	0.01	0.00	0.00	0.00	0.00	0.00
Cr	0.00	0.00	0.00	0.00	0.00	0.00	0.00

Fe^{3+}	0.00	0.03	0.02	0.01	0.02	0.03	0.02
Fe^{2+}	3.48	3.32	3.42	3.37	3.35	3.37	3.35
Mn	0.04	0.04	0.03	0.04	0.04	0.04	0.04
Mg	5.95	5.97	5.85	5.92	5.99	5.90	5.94
Ca	0.00	0.00	0.00	0.00	0.00	0.00	0.00
Na	0.02	0.00	0.01	0.00	0.00	0.01	0.00
K	0.00	0.00	0.00	0.00	0.00	0.00	0.01
*OH**	16.00	16.00	16.00	16.00	16.00	16.00	16.00
Total	36.01	35.95	35.98	35.98	35.97	35.96	35.97
Oxidized	yes	yes	yes	yes	yes	yes	yes
Fe/Fe+Mg	0.369	0.360	0.370	0.364	0.360	0.366	0.362

Sample #	*21-503-08-03-S08*	*21-503-08-03-S08*	*21-503-08-03-S09*	*21-503-08-03-S09*	*21-503-08-03-S09*	*21-503-08-03-S10*	*21-503-08-03-S10*
SiO_2	27.29	26.80	26.72	26.64	26.36	26.99	26.82
TiO_2	0.03	0.03	0.04	0.06	0.04	0.03	0.04
Al_2O_3	21.51	21.80	22.12	21.80	21.98	21.99	21.91
Cr_2O_3	0.01	0.00	0.00	0.02	0.00	0.00	0.03
Fe_2O_3	0.14	0.16	0.12	0.21	0.00	0.23	0.23
FeO	19.46	20.16	20.26	19.98	20.05	20.20	20.20
MnO	0.21	0.22	0.26	0.21	0.19	0.24	0.19
MgO	20.43	19.50	19.51	19.28	19.37	19.67	19.42
CaO	0.00	0.01	0.01	0.01	0.01	0.01	0.00
Na_2O	0.00	0.01	0.00	0.02	0.06	0.00	0.00
K_2O	0.00	0.00	0.00	0.01	0.00	0.00	0.00
H_2O*	11.96	11.86	11.91	11.80	11.78	11.95	11.87
Total	101.02	100.52	100.95	100.04	99.83	101.25	100.69
Si	5.47	5.42	5.38	5.41	5.37	5.42	5.41
Al^{iv}	2.53	2.58	2.62	2.59	2.63	2.58	2.59
Al^{vi}	2.55	2.62	2.64	2.63	2.64	2.62	2.63

Ti	0.00	0.00	0.01	0.01	0.01	0.00	0.01
Cr	0.00	0.00	0.00	0.00	0.00	0.00	0.00
Fe^{3+}	0.02	0.02	0.02	0.03	0.00	0.03	0.03
Fe^{2+}	3.26	3.41	3.41	3.39	3.41	3.39	3.41
Mn	0.04	0.04	0.04	0.04	0.03	0.04	0.03
Mg	6.11	5.88	5.86	5.84	5.88	5.89	5.85
Ca	0.00	0.00	0.00	0.00	0.00	0.00	0.00
Na	0.00	0.01	0.00	0.02	0.05	0.00	0.00
K	0.00	0.00	0.00	0.00	0.00	0.00	0.00
*OH**	16.00	16.00	16.00	16.00	16.00	16.00	16.00
Total	35.97	35.97	35.98	35.97	36.02	35.94	35.95
Oxidized	yes	yes	yes	yes	yes	yes	yes
Fe/Fe+Mg	0.350	0.369	0.369	0.370	0.367	0.368	0.371

Sample #	*21-503-08-03-S10*	*21-503-08-04-S01*	*21-503-08-04-S01*	*21-503-08-04-S01*	*21-503-08-04-S01*	*21-503-08-04-S01*	*21-503-08-04-S02*
SiO_2	26.97	26.92	27.15	26.93	26.68	26.75	26.86
TiO_2	0.04	0.01	0.04	0.04	0.06	0.04	0.03
Al_2O_3	21.62	22.12	22.26	22.00	22.39	22.45	22.31
Cr_2O_3	0.03	0.00	0.01	0.00	0.01	0.00	0.00
Fe_2O_3	0.12	0.19	0.09	0.18	0.00	0.00	0.00
FeO	20.49	19.63	20.01	19.97	20.19	20.76	20.69
MnO	0.22	0.21	0.19	0.21	0.21	0.20	0.23
MgO	19.56	19.88	20.15	19.81	19.90	19.72	19.73
CaO	0.00	0.00	0.00	0.00	0.00	0.00	0.01
Na_2O	0.01	0.00	0.00	0.00	0.00	0.02	0.03
K_2O	0.00	0.03	0.03	0.00	0.00	0.00	0.00
H_2O*	11.89	11.94	12.06	11.93	11.97	12.01	12.01
Total	100.93	100.91	101.99	101.03	101.42	101.94	101.90
Si	5.44	5.41	5.40	5.41	5.34	5.34	5.36

Al^{iv}	2.56	2.59	2.60	2.59	2.66	2.66	2.64
Al^{vi}	2.58	2.64	2.62	2.62	2.63	2.63	2.62
Ti	0.01	0.00	0.01	0.01	0.01	0.01	0.01
Cr	0.00	0.00	0.00	0.00	0.00	0.00	0.00
Fe^{3+}	0.02	0.03	0.01	0.03	0.00	0.00	0.00
Fe^{2+}	3.45	3.30	3.33	3.36	3.38	3.48	3.46
Mn	0.04	0.04	0.03	0.04	0.03	0.03	0.04
Mg	5.88	5.95	5.97	5.93	5.94	5.87	5.87
Ca	0.00	0.00	0.00	0.00	0.00	0.00	0.00
Na	0.01	0.00	0.00	0.00	0.00	0.01	0.02
K	0.00	0.01	0.01	0.00	0.00	0.00	0.00
*OH**	16.00	16.00	16.00	16.00	16.00	16.00	16.00
Total	35.98	35.96	35.99	35.96	36.00	36.02	36.02
Oxidized	yes	yes	yes	yes	yes	yes	yes
Fe/Fe+Mg	0.371	0.358	0.359	0.363	0.363	0.372	0.371

Sample #	*21-503-08-04-S02*	*21-503-08-04-S02*	*21-503-08-04-S03*	*21-503-08-04-S03*	*21-503-08-04-S03*	*21-503-08-04-S04*	*21-503-08-04-S04*
SiO_2	26.88	27.23	27.00	27.16	27.37	25.92	26.09
TiO_2	0.04	0.04	0.03	0.13	0.05	0.03	0.10
Al_2O_3	22.42	21.45	22.57	22.18	22.00	20.71	20.36
Cr_2O_3	0.02	0.01	0.01	0.02	0.01	0.11	0.17
Fe_2O_3	0.25	0.10	0.21	0.19	0.30	0.46	0.81
FeO	19.09	21.36	20.29	20.02	19.53	18.51	17.73
MnO	0.25	0.23	0.25	0.26	0.19	0.21	0.19
MgO	20.01	19.33	19.75	19.87	20.20	18.59	18.34
CaO	0.01	0.02	0.01	0.02	0.00	0.02	0.02
Na_2O	0.04	0.00	0.00	0.00	0.00	0.03	0.02
K_2O	0.00	0.02	0.00	0.09	0.00	0.00	0.03
H_2O*	11.97	11.94	12.05	12.04	12.04	11.34	11.27

Total	100.95	101.72	102.14	101.94	101.68	95.93	95.15
Si	5.38	5.47	5.37	5.41	5.45	5.47	5.54
Al ^{iv}	2.62	2.53	2.63	2.59	2.55	2.53	2.46
Al ^{vi}	2.68	2.54	2.66	2.62	2.61	2.64	2.65
Ti	0.01	0.01	0.01	0.02	0.01	0.01	0.02
Cr	0.00	0.00	0.00	0.00	0.00	0.02	0.03
Fe^{3+}	0.04	0.02	0.03	0.03	0.04	0.07	0.13
Fe^{2+}	3.20	3.59	3.37	3.33	3.25	3.27	3.15
Mn	0.04	0.04	0.04	0.04	0.03	0.04	0.03
Mg	5.97	5.78	5.86	5.90	5.99	5.85	5.80
Ca	0.00	0.00	0.00	0.00	0.00	0.00	0.00
Na	0.03	0.00	0.00	0.00	0.00	0.02	0.02
K	0.00	0.01	0.00	0.05	0.00	0.00	0.02
*OH**	16.00	16.00	16.00	16.00	16.00	16.00	16.00
Total	35.96	35.98	35.95	35.98	35.94	35.91	35.85
Oxidized	yes	yes	yes	yes	yes	yes	yes
Fe/Fe+Mg	0.351	0.384	0.368	0.363	0.355	0.364	0.361

Sample #	*21-503-08-04-S05*	*21-503-08-04-S05*	*21-503-08-04-S07*	*21-503-08-04-S07*	*21-503-08-04-S07*	*21-503-08-04-S08*	*21-503-08-04-S08*
SiO_2	26.94	29.22	27.09	27.19	26.98	27.05	27.06
TiO_2	0.04	0.13	0.06	0.02	0.08	0.07	0.04
Al_2O_3	22.00	20.84	21.99	21.95	21.98	22.34	22.42
Cr_2O_3	0.01	0.02	0.00	0.01	0.00	0.00	0.00
Fe_2O_3	0.06	1.38	0.12	0.00	0.00	0.00	0.12
FeO	19.84	18.86	19.92	20.04	20.55	20.61	20.15
MnO	0.21	0.19	0.21	0.22	0.23	0.21	0.24
MgO	19.93	19.54	20.16	20.46	20.10	19.92	19.78
CaO	0.01	0.02	0.00	0.00	0.00	0.00	0.00
Na_2O	0.04	0.00	0.00	0.00	0.00	0.03	0.01

K_2O	0.02	0.14	0.00	0.00	0.00	0.25	0.08
H_2O*	11.94	12.14	12.00	12.05	12.01	12.08	12.03
Total	101.04	102.45	101.51	101.92	101.89	102.55	101.92
Si	5.41	5.75	5.41	5.41	5.39	5.36	5.39
Al^{iv}	2.59	2.25	2.59	2.59	2.61	2.64	2.61
Al^{vi}	2.61	2.60	2.59	2.56	2.56	2.59	2.65
Ti	0.01	0.02	0.01	0.00	0.01	0.01	0.01
Cr	0.00	0.00	0.00	0.00	0.00	0.00	0.00
Fe^{3+}	0.01	0.21	0.02	0.00	0.00	0.00	0.02
Fe^{2+}	3.33	3.10	3.33	3.34	3.44	3.45	3.36
Mn	0.04	0.03	0.04	0.04	0.04	0.04	0.04
Mg	5.96	5.73	6.00	6.07	5.98	5.88	5.87
Ca	0.00	0.00	0.00	0.00	0.00	0.00	0.00
Na	0.03	0.00	0.00	0.00	0.00	0.02	0.01
K	0.01	0.07	0.00	0.00	0.00	0.12	0.04
*OH**	16.00	16.00	16.00	16.00	16.00	16.00	16.00
Total	36.00	35.76	35.97	36.01	36.01	36.11	36.00
Oxidized	yes	yes	yes	yes	yes	yes	yes
Fe/Fe+Mg	0.359	0.366	0.358	0.355	0.365	0.370	0.365

Sample #	*21-503-08-04-S09*	*21-503-08-04-S09*	*21-503-08-04-S09*	*21-503-08-05-S01*	*21-503-08-05-S01*	*21-503-08-05-S02*	*21-503-08-05-S02*
SiO_2	27.08	27.04	26.98	27.12	26.93	26.91	26.75
TiO_2	0.03	0.06	0.04	0.08	0.06	0.07	0.06
Al_2O_3	21.89	22.15	22.28	21.88	22.10	22.01	21.95
Cr_2O_3	0.01	0.00	0.02	0.04	0.01	0.01	0.00
Fe_2O_3	0.05	0.05	0.23	0.24	0.14	0.10	0.13
FeO	19.75	20.19	21.88	19.22	19.88	19.62	20.43
MnO	0.22	0.25	0.19	0.18	0.22	0.24	0.19
MgO	20.28	20.16	18.44	20.12	19.72	20.10	19.37

CaO	0.00	0.00	0.02	0.01	0.02	0.01	0.00
Na_2O	0.01	0.00	0.00	0.00	0.00	0.01	0.01
K_2O	0.00	0.00	0.18	0.09	0.10	0.00	0.03
*H_2O**	11.98	12.03	11.96	11.95	11.94	11.95	11.88
Total	101.28	101.88	102.18	100.91	101.12	101.01	100.78
Si	5.42	5.39	5.40	5.44	5.40	5.40	5.40
Al^{iv}	2.58	2.61	2.60	2.56	2.60	2.60	2.60
Al^{vi}	2.58	2.59	2.67	2.61	2.63	2.61	2.63
Ti	0.00	0.01	0.01	0.01	0.01	0.01	0.01
Cr	0.00	0.00	0.00	0.01	0.00	0.00	0.00
Fe^{3+}	0.01	0.01	0.03	0.04	0.02	0.02	0.02
Fe^{2+}	3.31	3.37	3.66	3.22	3.34	3.29	3.45
Mn	0.04	0.04	0.03	0.03	0.04	0.04	0.03
Mg	6.05	5.99	5.51	6.01	5.90	6.01	5.83
Ca	0.00	0.00	0.00	0.00	0.00	0.00	0.00
Na	0.01	0.00	0.00	0.00	0.00	0.01	0.01
K	0.00	0.00	0.09	0.05	0.05	0.00	0.01
*OH**	16.00	16.00	16.00	16.00	16.00	16.00	16.00
Total	35.99	35.98	35.98	35.96	35.99	35.98	35.98
Oxidized	yes	yes	yes	yes	yes	yes	yes
Fe/Fe+Mg	0.354	0.360	0.402	0.351	0.363	0.355	0.373

Sample #	*21-503-08-05-S02*	*21-503-08-05-S02*	*21-503-08-05-S02*	*21-503-08-05-S03*	*21-503-08-05-S03*	*21-503-08-05-S03*	*21-503-08-05-S04*
SiO_2	26.92	27.40	26.51	26.86	26.75	26.74	26.74
TiO_2	0.06	0.04	0.04	0.07	0.04	0.04	0.04
Al_2O_3	21.73	21.49	21.84	22.40	22.43	22.09	22.44
Cr_2O_3	0.01	0.01	0.02	0.07	0.07	0.03	0.01
Fe_2O_3	0.05	0.26	0.14	0.32	0.00	0.11	0.19
FeO	20.42	20.28	20.26	19.31	20.04	19.91	19.02

MnO	0.22	0.20	0.22	0.21	0.22	0.22	0.22
MgO	19.41	19.62	19.17	19.77	20.05	19.71	20.08
CaO	0.02	0.01	0.00	0.00	0.00	0.00	0.01
Na_2O	0.08	0.01	0.01	0.03	0.01	0.01	0.01
K_2O	0.04	0.06	0.00	0.00	0.00	0.01	0.01
*H_2O**	11.88	11.95	11.78	11.96	12.00	11.90	11.94
Total	100.83	101.33	100.00	100.99	101.60	100.77	100.71
Si	5.43	5.49	5.39	5.38	5.34	5.39	5.37
Al^{iv}	2.57	2.51	2.61	2.62	2.66	2.61	2.63
Al^{vi}	2.60	2.58	2.63	2.68	2.63	2.63	2.68
Ti	0.01	0.01	0.01	0.01	0.01	0.01	0.01
Cr	0.00	0.00	0.00	0.01	0.01	0.00	0.00
Fe^{3+}	0.01	0.04	0.02	0.05	0.00	0.02	0.03
Fe^{2+}	3.44	3.40	3.45	3.24	3.35	3.35	3.19
Mn	0.04	0.03	0.04	0.04	0.04	0.04	0.04
Mg	5.84	5.86	5.81	5.91	5.97	5.92	6.01
Ca	0.00	0.00	0.00	0.00	0.00	0.00	0.00
Na	0.06	0.01	0.01	0.02	0.01	0.01	0.01
K	0.02	0.03	0.00	0.00	0.00	0.00	0.00
*OH**	16.00	16.00	16.00	16.00	16.00	16.00	16.00
Total	36.02	35.96	35.98	35.95	36.00	35.99	35.97
Oxidized	yes	yes	yes	yes	yes	yes	yes
Fe/Fe+Mg	0.372	0.370	0.374	0.357	0.359	0.363	0.349

Sample #	*21-503-08-05-S04*	*21-503-08-05-S04*
SiO_2	26.65	26.96
TiO_2	0.02	0.03
Al_2O_3	21.84	22.00
Cr_2O_3	0.00	0.01

Fe_2O_3	0.23	0.14
FeO	20.00	19.45
MnO	0.22	0.22
MgO	19.30	20.07
CaO	0.00	0.01
Na_2O	0.00	0.02
K_2O	0.00	0.01
H_2O*	11.80	11.94
Total	100.05	100.85
Si	5.41	5.41
Al^{iv}	2.59	2.59
Al^{vi}	2.64	2.62
Ti	0.00	0.00
Cr	0.00	0.00
Fe^{3+}	0.03	0.02
Fe^{2+}	3.40	3.27
Mn	0.04	0.04
Mg	5.84	6.01
Ca	0.00	0.00
Na	0.00	0.01
K	0.00	0.00
*OH**	16.00	16.00
Total	35.96	35.98
Oxidized	yes	yes
Fe/Fe+Mg	0.370	0.354

Sample #	*test chlorite std 2*	*test chlorite std 3*	*test chlorite std 125*	*test chlorite std 125*	*test chlorite std 125*	*test chlorite std 4*	*test chlorite std 153*
SiO_2	24.27	24.62	24.51	24.64	24.49	24.62	24.34
TiO_2	0.10	0.06	0.07	0.08	0.09	0.10	0.06
Al_2O_3	22.50	22.45	22.73	22.78	22.78	22.69	22.87
Cr_2O_3	0.01	0.04	0.03	0.04	0.01	0.03	0.01
FeO	31.10	31.28	30.90	30.27	31.19	30.22	30.63
MnO	0.26	0.26	0.28	0.25	0.25	0.24	0.24
MgO	11.50	11.09	11.25	11.18	11.35	10.67	10.49
CaO	0.01	0.04	0.00	0.01	0.00	0.01	0.01
Na_2O	0.02	0.00	0.05	0.00	0.00	0.00	0.02
K_2O	0.00	0.00	0.00	0.00	0.00	0.00	0.00
O	0.00	0.00	0.00	0.00	0.00	0.00	0.00
H2O	10.50	10.50	10.50	10.50	10.50	10.50	10.50
TOTAL	100.24	100.28	100.32	99.73	100.60	99.09	99.18
Si CDL99	0.01	0.01	0.01	0.01	0.01	0.01	0.01
Ti CDL99	0.02	0.02	0.03	0.03	0.03	0.03	0.03
Al CDL99	0.01	0.01	0.01	0.01	0.01	0.01	0.01
Cr CDL99	0.01	0.01	0.01	0.01	0.01	0.01	0.01
Fe CDL99	0.04	0.03	0.04	0.04	0.04	0.03	0.04
Mn CDL99	0.02	0.03	0.02	0.02	0.03	0.03	0.02
Mg CDL99	0.01	0.01	0.01	0.01	0.01	0.02	0.02
Ca CDL99	0.01	0.01	0.01	0.01	0.01	0.01	0.01
Na CDL99	0.03	0.03	0.03	0.03	0.03	0.04	0.04
K CDL99	0.01	0.01	0.02	0.02	0.02	0.02	0.01

Sample #	*test chlorite std 153*	*test chlorite std 153*
SiO_2	24.28	24.64
TiO_2	0.07	0.06
Al_2O_3	23.56	23.19
Cr_2O_3	0.02	0.03
FeO	30.69	30.75
MnO	0.25	0.22
MgO	10.31	10.47
CaO	0.00	0.01
Na_2O	0.00	0.01
K_2O	0.00	0.00
O	0.00	0.00
H2O	10.50	10.50
TOTAL	99.69	99.88
Si CDL99	0.01	0.01
Ti CDL99	0.03	0.03
Al CDL99	0.01	0.01
Cr CDL99	0.01	0.01
Fe CDL99	0.04	0.04
Mn CDL99	0.02	0.02
Mg CDL99	0.02	0.02
Ca CDL99	0.01	0.01
Na CDL99	0.05	0.05
K CDL99	0.01	0.01

Appendix Four: Fault Core Thin Section Scans

JP001 PPL – Tonalite fault core

JP001 XPL

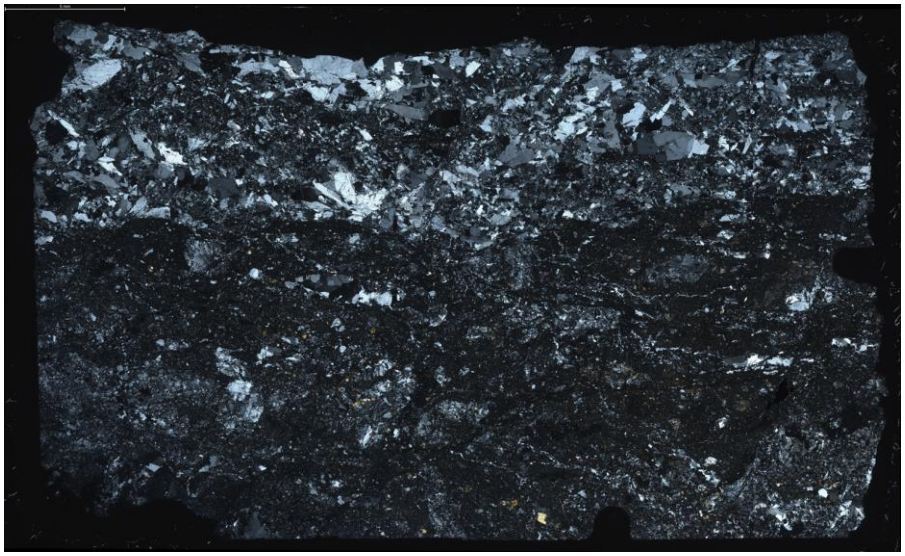

JP002A PPL – Gabbronorite fault core with tonalite inclusions

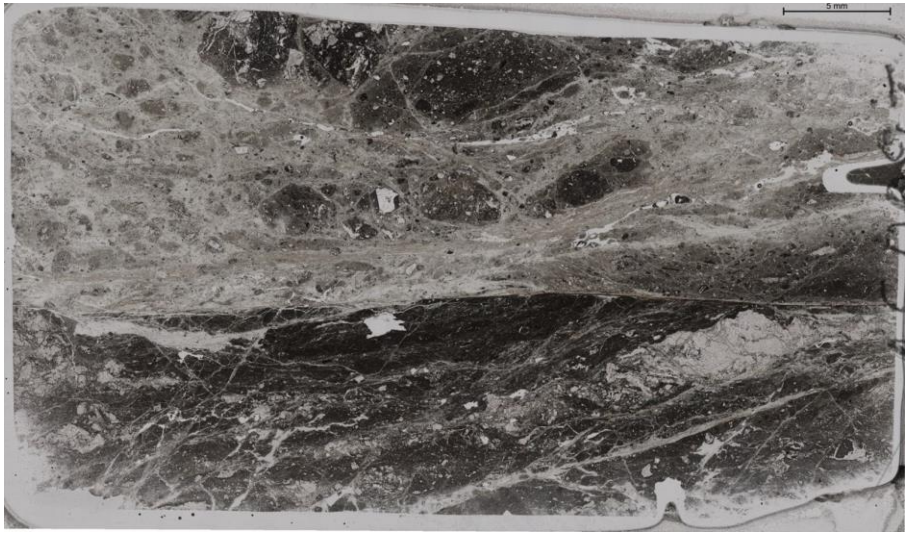

JP002A XPL

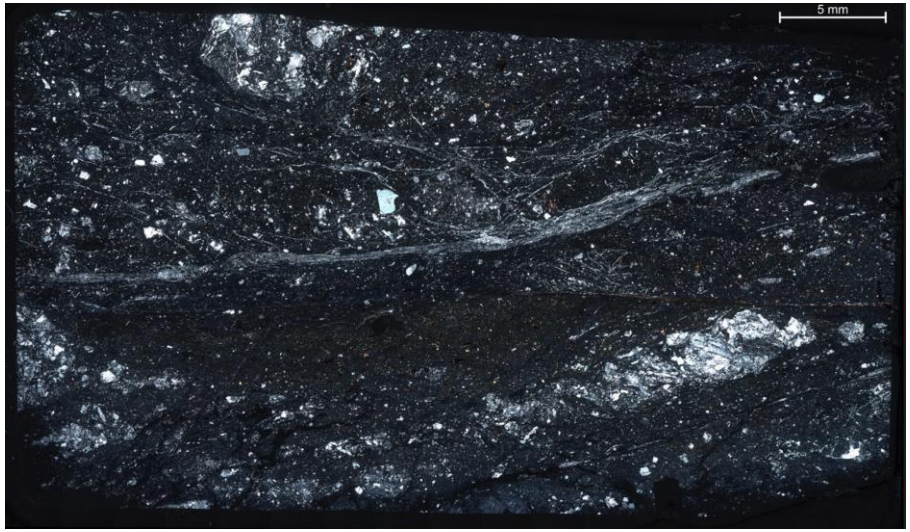

JP002B PPL – Gabbronorite fault core with tonalite inclusions

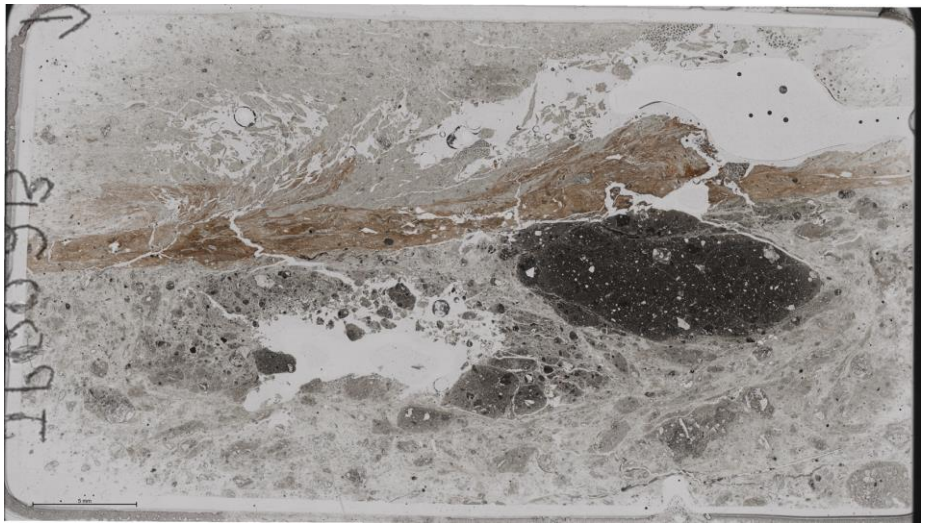

JP002B XPL

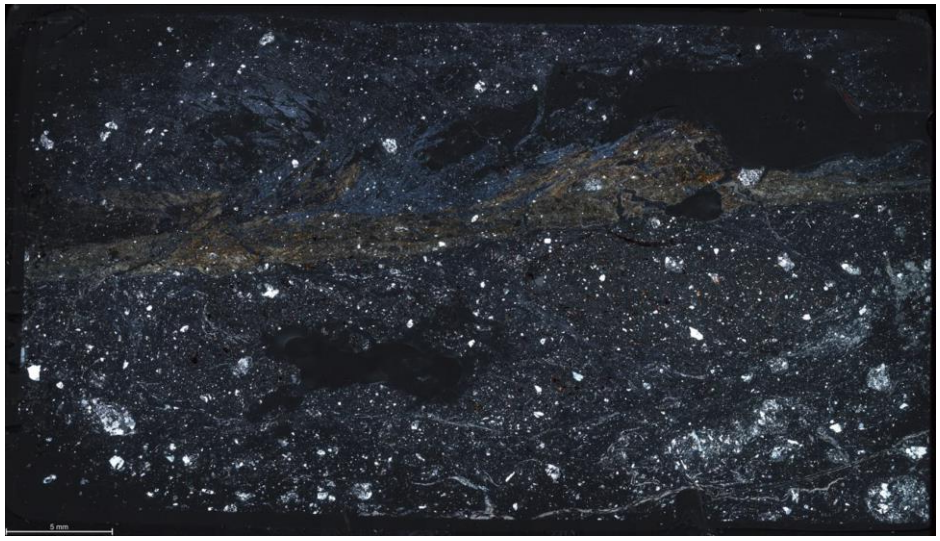

JP003 PPL – Gabbronorite fault core

JP003 XPL

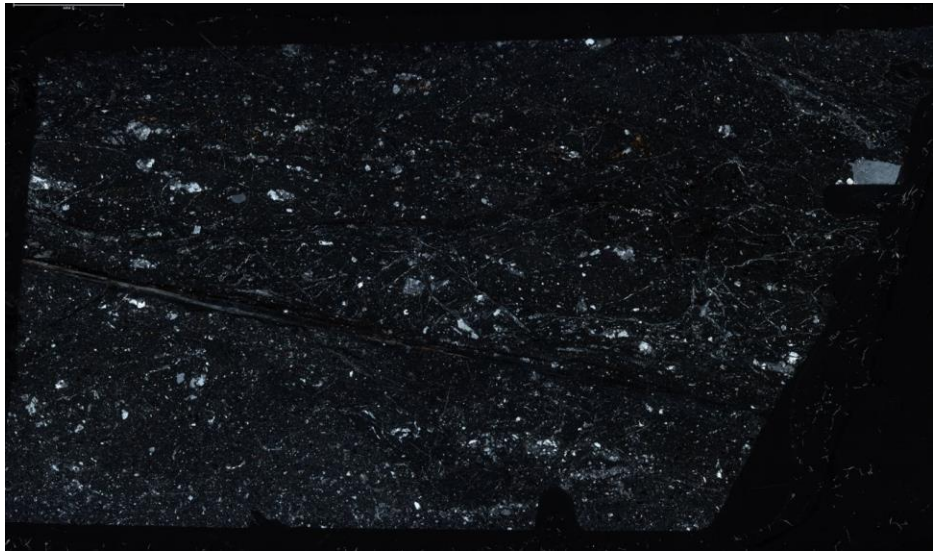

JP004 PPL – Gabbronorite fault core

JP004 XPL

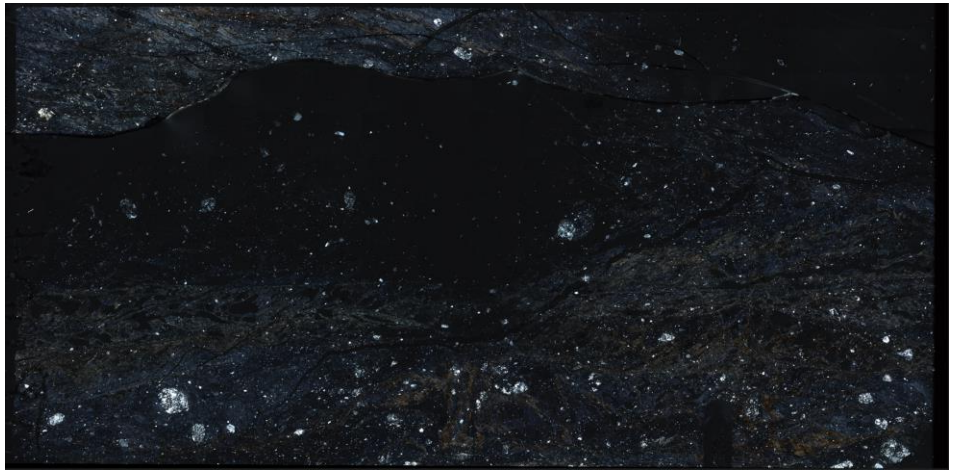

JP005 PPL – Tonalite and gabbronorite fault core with slip surface

JP005 XPL

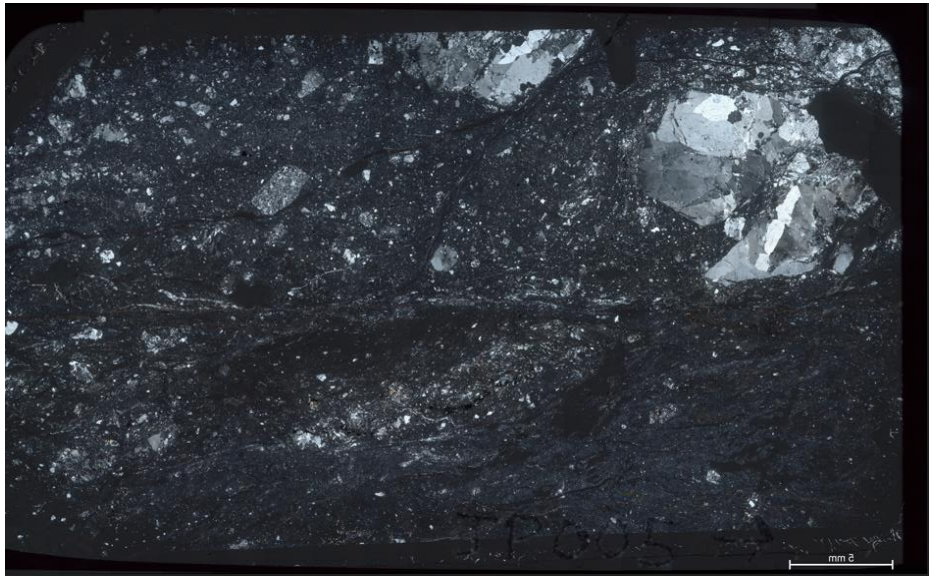

Appendix Five: Fracture Density Plots

22-750

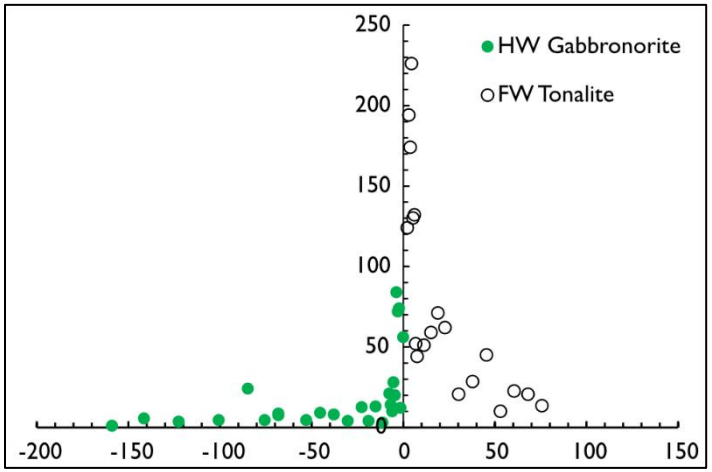

21-503

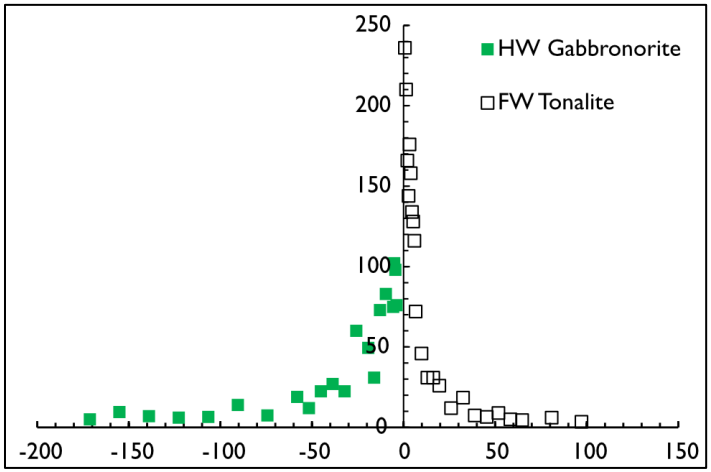

21-700

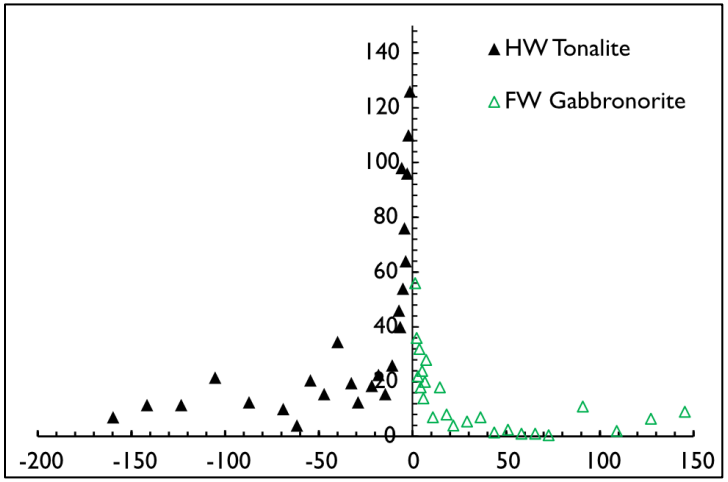

22-905

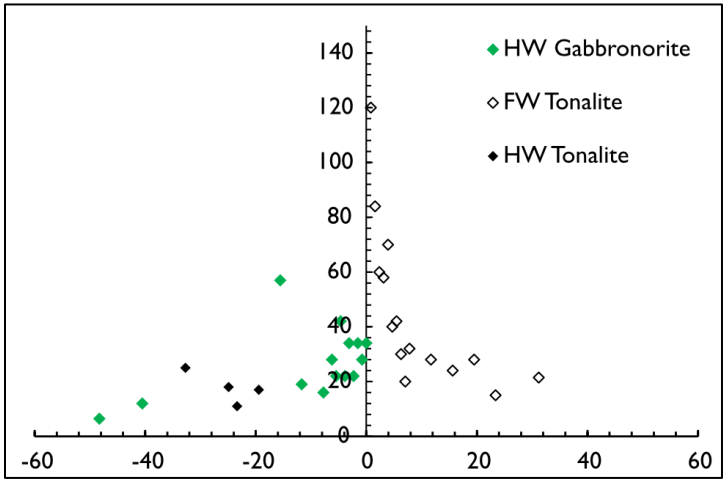

22-682

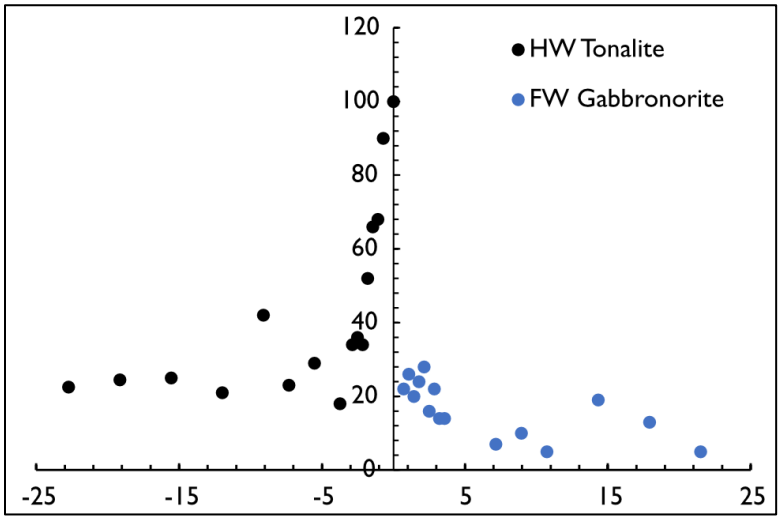

18-602

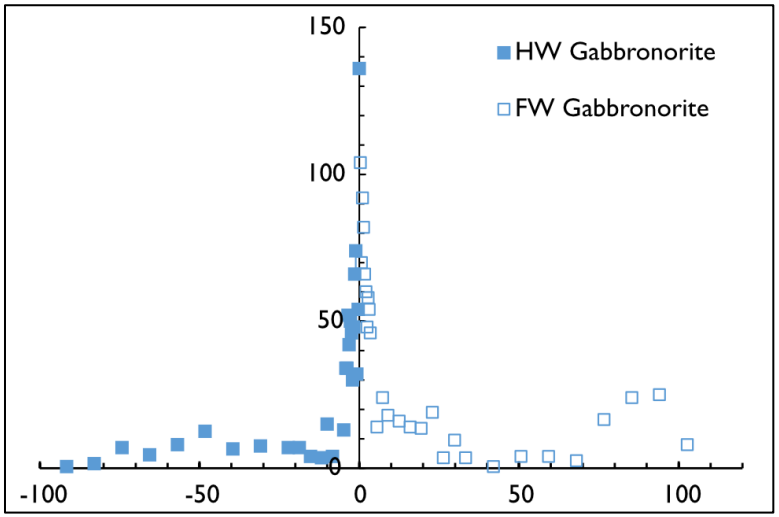

21-603

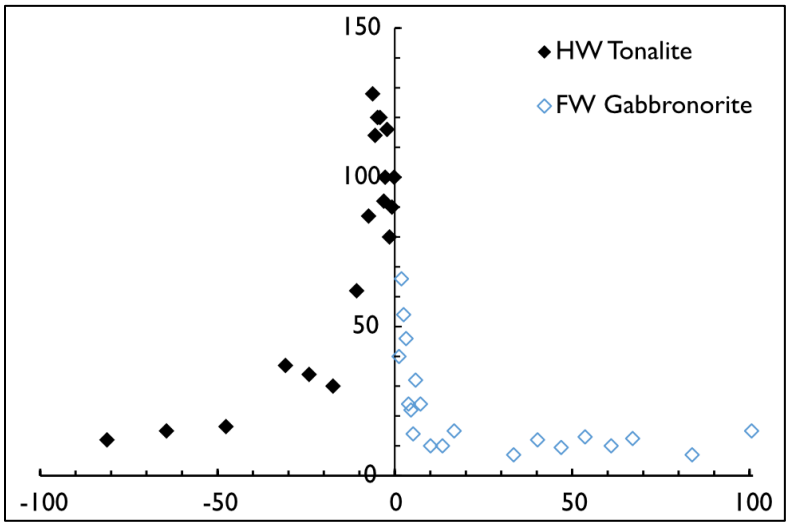

21-600

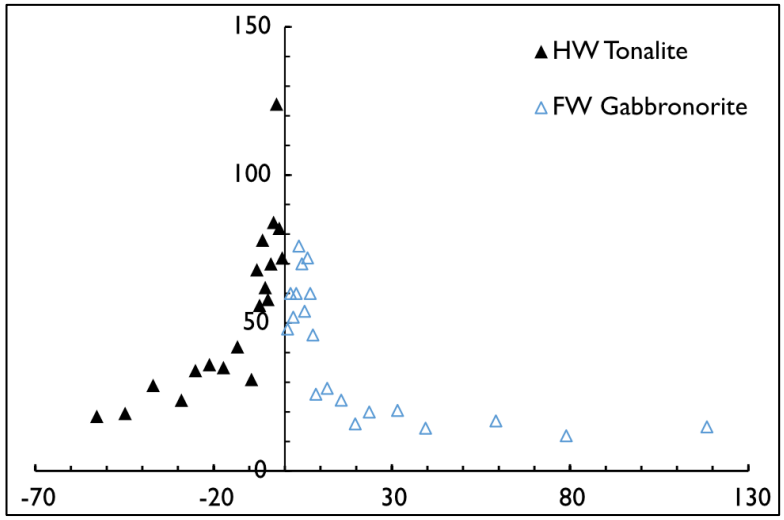

Appendix Six: Additional Geochemistry Plots

IUGS Plutonic Rock Classification QAP (Normative)

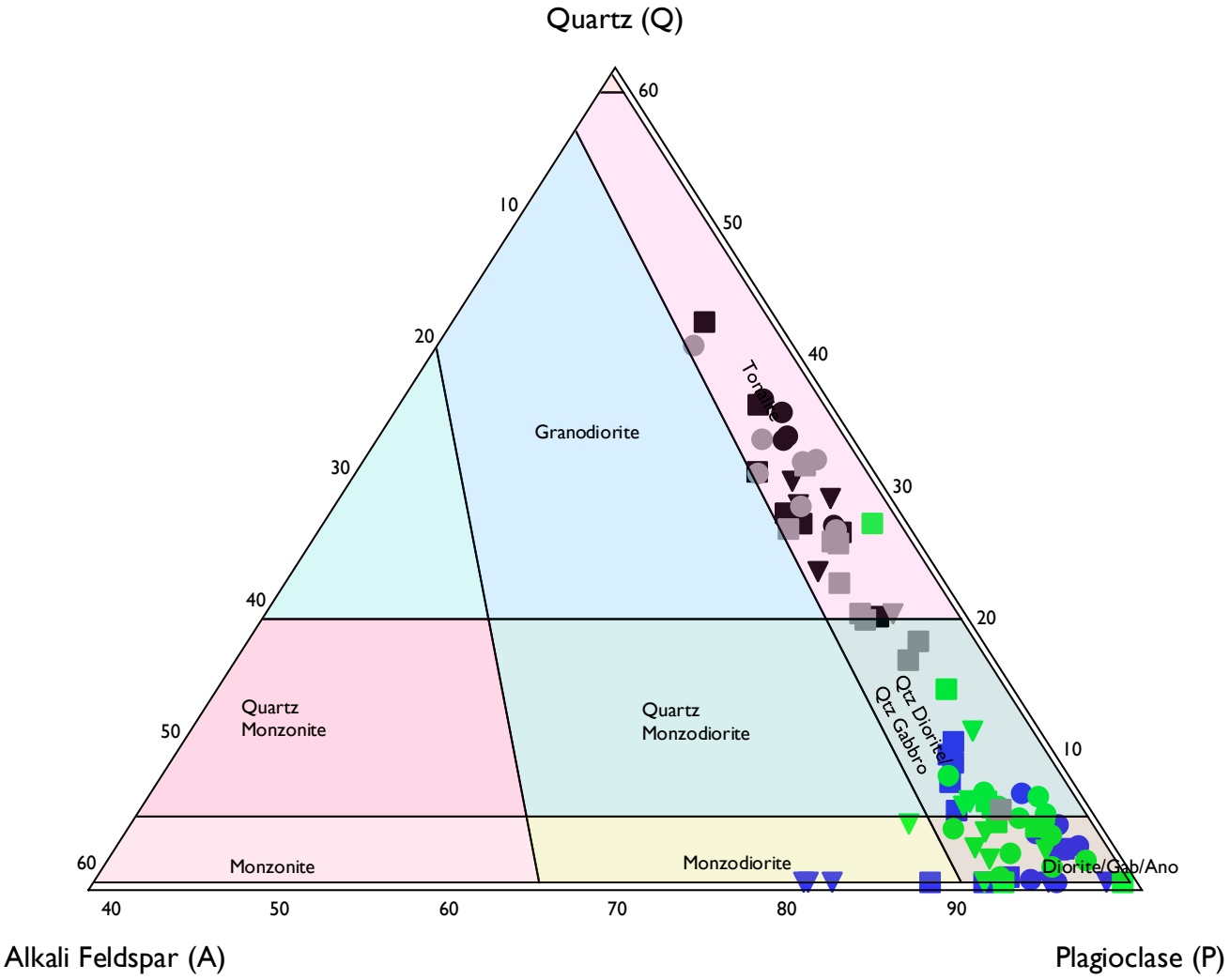

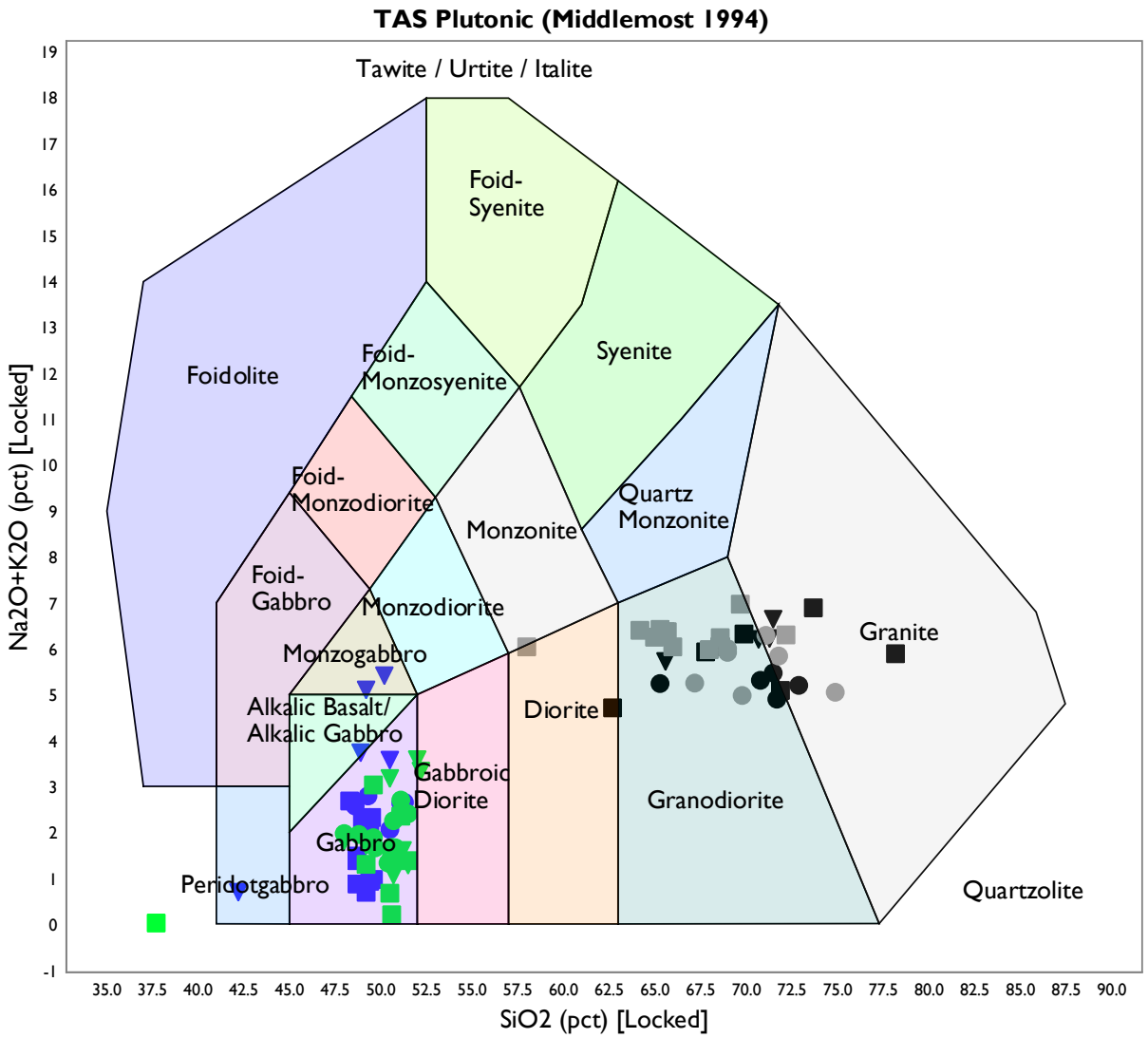
TAS Plutonic (Middlemost 1994)
Tawite / Urtite / Italite
Foid-
Syenite
Foidolite
Foid-
Monzosyenite
Syenite
Foid-
Monzodiorite
Monzonite
Quartz
Monzonite
Foid-
Gabbro
Monzodiorite
Granite
Monzogabbro
Alkalic Basalt/
Alkalic Gabbro
Diorite
Gabbroic
Diorite
Granodiorite
Gabbro
Peridotgabbro
Quartzolite
Na2O+K2O (pct) [Locked]
SiO2 (pct) [Locked]
19
18
17
16
15
14
13
12
11
10
9
8
7
6
5
4
3
2
1
0
-1
35.0 37.5 40.0 42.5 45.0 47.5 50.0 52.5 55.0 57.5 60.0 62.5 65.0 67.5 70.0 72.5 75.0 77.5 80.0 82.5 85.0 87.5 90.0